



8-2016

Hybrid Micellar Network Hydrogels of Thermosensitive Hydrophilic Triblock Copolymers and Thermosensitive Hairy Nanoparticles

Bin Hu

University of Tennessee, Knoxville, bhu6@vols.utk.edu

Follow this and additional works at: https://trace.tennessee.edu/utk_graddiss

 Part of the [Polymer Chemistry Commons](#)

Recommended Citation

Hu, Bin, "Hybrid Micellar Network Hydrogels of Thermosensitive Hydrophilic Triblock Copolymers and Thermosensitive Hairy Nanoparticles. " PhD diss., University of Tennessee, 2016.
https://trace.tennessee.edu/utk_graddiss/3927

This Dissertation is brought to you for free and open access by the Graduate School at TRACE: Tennessee Research and Creative Exchange. It has been accepted for inclusion in Doctoral Dissertations by an authorized administrator of TRACE: Tennessee Research and Creative Exchange. For more information, please contact trace@utk.edu.

To the Graduate Council:

I am submitting herewith a dissertation written by Bin Hu entitled "Hybrid Micellar Network Hydrogels of Thermosensitive Hydrophilic Triblock Copolymers and Thermosensitive Hairy Nanoparticles." I have examined the final electronic copy of this dissertation for form and content and recommend that it be accepted in partial fulfillment of the requirements for the degree of Doctor of Philosophy, with a major in Chemistry.

Bin Zhao, Major Professor

We have read this dissertation and recommend its acceptance:

Jimmy W. Mays, Michael D. Best, Zhanhu Guo

Accepted for the Council:

Carolyn R. Hodges

Vice Provost and Dean of the Graduate School

(Original signatures are on file with official student records.)

**Hybrid Micellar Network Hydrogels of Thermosensitive
Hydrophilic Triblock Copolymers and Thermosensitive
Hairy Nanoparticles**

A Dissertation Presented for the
Doctor of Philosophy
Degree
The University of Tennessee, Knoxville

Bin Hu
August 2016

Acknowledgements

First I would like to express my sincere gratitude to Professor Bin Zhao for your instructions, encouragement and support throughout my five years of graduate studies. With your guidance, I have learned the knowledge in the field of polymer chemistry and commanded the abilities to work more efficiently and professionally as a PhD student, and more importantly, I start thinking logically and critically as a scientist. These lessons I learned from you will be with me throughout my life.

I would like to thank Professor Jimmy Mays, Professor Michael Best, Professor Zhanhu Guo and Professor Wei He for serving on my committee and generously giving your time on the valuable comments and suggestions to my research. I have enjoyed meeting with each of you.

I would like to thank Professor Jeffrey Moore and Dr. Jun Li for the opportunity to collaborate on polymer-grafted silica nanoparticles that can be mechanochemically activated at heterogeneous interfaces. It was enjoyable to use our own knowledge to work with you to explore the unknown field.

I greatly thank the Department of Chemistry at the University of Tennessee and National Science Foundation for providing funding throughout my time in graduate school which has enabled this work to be accomplished. I would also like to thank Ed Wright from the BCMB Department for the use of the ultracentrifuge for the silica nanoparticle separation.

I would like to thank Professor Junlian Huang and Professor Guowei Wang who first introduced me to polymer chemistry and from whom I received my undergraduate training and guidance. And I would also like to thank Professor Mark Dadmun, Professor Alexei Sokolov and Professor Shanfeng Wang for further teaching me polymer chemistry in the graduate school.

I owe a huge debt to past group members Dr. Jonathan Horton, Dr. Jeremiah Woodcock and Dr. Naixiong Jin for your precious career advices and valuable suggestions on the interview when I was hunting for a job. Dr. Jonathan Horton also provided me a lot of useful advices and suggestions for the preparation of hairy silica nanoparticles with small sizes. I would also like to thank the other past and present group members for their friendship, help and advice. My thanks go to Dr. Xueguang Jiang, Dr. Chunhui Bao, Roger Wright, Daniel Henn, Sisi Jiang, Bryan Seymour, Jessica Holmes, Ethan Kent, Dr. Wenxin Fu, Dr. Chunhui Luo and Dr. Kewei Wang. I would also like to thank Dr. Jun Li, Dr. Qin hao Zhang, Dr. Shuangcheng Tang, Jun Zhang, Yang Chi, Wei Lu, Xinyi Lu, Hongbo Feng and Jinbo Dou for their friendship.

I would not be writing this without my family. I would like to thank my father Weimin Hu and my mother Zhilan Yang for their love, guidance and support. You provided me every tool I needed to succeed and always encouraged me and showed me the bright side of life. I would also like to thank my father-in-law Judong Jiang, my mother-in-law Yunnyu Zhu, my uncle Guorong Lu as well as my cousins Yingqiong Zhang, Jiwen Du, Xi Yang and Binghua Yang.

Finally and most importantly, I would like to thank my lab mate, my best friend and my wife Sisi. You consistently give me love, support and motivation and you have earned this as much as I have.

Abstract

Hybrid micellar network hydrogels, composed of thermosensitive hydrophilic triblock copolymers and thermosensitive polymer brush-grafted nanoparticles (hairy NPs), exhibit intriguing rheological properties. This dissertation work studies thermosensitive hybrid hydrogels with NPs positioned either inside or outside the core of block copolymer micelles.

Chapter 1 is an introduction. Chapter 2 examines the effect of NP's location on properties of hybrid hydrogels of a thermosensitive ABA triblock copolymer and hairy NPs. Two batches of thermoresponsive polymer brush-grafted silica NPs and an ABA triblock copolymer with thermosensitive outer blocks were prepared. When the lower critical solution temperature (LCST) of hairy NPs was similar to that of the ABA copolymer, the NPs were located in the core of micelles and both the sol-gel transition temperature ($T_{\text{sol-gel}}$) and dynamic storage modulus G' did not change much with increasing NP-to-polymer mass ratio. In contrast, when the LCST of hairy NPs was much higher, the NPs were located outside the micelles; $T_{\text{sol-gel}}$ increased slightly while G' decreased significantly with the increase of NP-to-polymer mass ratio. Chapter 3 presents a follow-up work to further study the LCST effect of hairy NPs on rheological properties of hybrid hydrogels which the NPs being initially outside the core of micelles. Four batches of hairy NPs with different LCSTs were synthesized and for all hybrid hydrogels, a significant increase in G' was observed from heating ramps around the LCST of hairy NPs.

Chapter 4 describes a study of hybrid hydrogels of a doubly thermosensitive hydrophilic ABC triblock copolymer and thermoresponsive hairy NPs. With the incorporation of hairy NPs having a LCST similar to that of the higher LCST C block of the ABC copolymer, the gelation efficiency was increased substantially. No such benefit was observed when the LCST of hairy NPs was much higher than that of the C block. Chapter 5 presents a method to synthesize polymer brush-grafted

mesoporous silica NPs (MSNs) with a silica NP size of 30-40 nm by “grafting from”. The hairy MSNs are an excellent candidate for the preparation of next generation hybrid hydrogels. Conclusions and future work are provided in Chapter 6.

Table of Contents

Chapter 1. Introduction	1
1.1. Introduction.....	2
1.1.1. Thermosensitive Polymers.....	2
1.1.2. Thermosensitive Block Copolymer Hydrogels	5
1.1.2.1. Gels Based on Jamming/Packing of Discrete Micelles of Thermosensitive Block Copolymers in Water	5
1.1.2.2. Physically Crosslinked Network Hydrogels of Thermosensitive Block Copolymers	8
1.1.2.3. Worm-Like Block Copolymer Micellar Hydrogels.....	12
1.1.3. Hybrid Hydrogels of Thermosensitive Block Copolymers and Nanoparticles	13
1.1.4. Polymer Brush-Grafted Nanoparticles	18
1.2. Dissertation Overview	22
1.3 References.....	26
Chapter 2. Hybrid Micellar Hydrogels of a Thermosensitive ABA Triblock Copolymer and Hairy Nanoparticles: Effect of Spatial Location of Hairy Nanoparticles on Gel Properties.....	31
Abstract.....	32
2.1. Introduction.....	34
2.2. Experimental Section.....	40
2.2.1. Materials	40
2.2.2. General Characterization	41
2.2.3. Preparation of ATRP Initiator-Functionalized Silica NPs (Initiator NPs)	42

2.2.4. Synthesis of Thermosensitive P(DEGMMA- <i>co</i> -DEGEMA- <i>co</i> -NBDMA) Brush Grafted Silica NPs (NP-D)	43
2.2.5. Synthesis of P(TEGMMA- <i>co</i> -NBDMA) Brush-Grafted Silica NPs (NP-T) ...	44
2.2.6. Synthesis of P(DEGMMA- <i>co</i> -DEGEMA- <i>co</i> -RhBMA)- <i>b</i> -PEO- <i>b</i> -P(DEGMMA- <i>co</i> -DEGEMA- <i>co</i> -RhBMA) (ABA-D)	46
2.2.7. Dynamic Light Scattering (DLS) Studies of Thermoresponsive Properties of Hairy NPs and ABA-D	46
2.2.8. Fluorescence Resonance Energy Transfer (FRET) Study of Aqueous Mixtures of Thermosensitive Hairy NPs and ABA-D	47
2.2.9. Rheology Studies of Hybrid Micellar Hydrogels of ABA-D and Thermosensitive Hairy NPs	47
2.3. Results and Discussion	49
2.3.1. Synthesis and Thermosensitive Property of P(DEGMMA- <i>co</i> -DEGEMA- <i>co</i> -NBDMA) Brush-Grafted 17 nm Silica NPs (NP-D)	49
2.3.2. Synthesis and Thermoresponsive Properties of P(TEGMMA- <i>co</i> -NBDMA) Brush-Grafted Silica NPs (NP-T)	52
2.3.3. Synthesis and Thermo-Induced Micellization of P(DEGMMA- <i>co</i> -DEGEMA- <i>co</i> -RhBMA)- <i>b</i> -PEO- <i>b</i> -P(DEGMMA- <i>co</i> -DEGEMA- <i>co</i> -RhBMA) (ABA-D) ..	52
2.3.4. FRET Study of Spatial Location of Thermosensitive Hairy NPs in Aqueous Mixtures of ABA-D and Hairy NPs	56
2.3.5. Rheological Studies of Hybrid Micellar Hydrogels of ABA-D and Thermosensitive Hairy NPs – Effects of Spatial Location of Hairy NPs and NP-to-Polymer Mass Ratio on Gel Properties	60

2.4. Conclusions.....	71
2.5. References.....	74
Appendix A.....	77
Chapter 3. Hybrid Micellar Network Hydrogels of Thermosensitive ABA Triblock Copolymer and Polymer Brush-Grafted Nanoparticles: Effect of LCST Transition of Polymer Brushes on Gel Property	
	121
Abstract.....	122
3.1. Introduction.....	123
3.2. Experimental Section.....	125
3.2.1. Materials	125
3.2.2. General Characterization	127
3.2.3. Synthesis of Thermosensitive ABA Triblock Copolymer P(DEGMMA-co-DEGEMA-co-RhBMA)-b-PEO-b-P(DEGMMA-co-DEGEMA-co-RhBMA) (ABA-N).....	128
3.2.4. Synthesis of Thermosensitive Polymer Brush-Grafted Silica Nanoparticles.....	128
3.2.5. DLS Studies of LCST Transitions of Thermosensitive Hairy NPs and ABA-N in Water	131
3.2.6. Fluorescence Spectroscopy Study of Aqueous Mixtures of Thermosensitive Hairy NPs and ABA-N.....	131
3.2.7. Rheology Studies of Aqueous Mixtures of ABA-N and Thermosensitive Hairy NPs	132
3.3. Results.....	133

3.3.1. Synthesis and Thermoresponsive Properties of ABA Triblock Copolymer P(DEGMMA-co-DEGEMA-co-RhBMA)-b-PEO-b-P(DEGEMA-co-DEGEMA-co-RhBMA) (ABA-N) and Thermosensitive Hairy NPs with Various LCST Transitions	133
3.3.2. Rheological Study of Aqueous Mixtures of ABA-N and NP-29 with a Polymer Concentration of 10 wt% and Various NP-to-Polymer Mass Ratios.	136
3.3.3. Rheological Study of Aqueous Mixtures of ABA-N and NP-34, -44, and -51 with a Polymer Concentration of 10 wt% and Various NP-to-Polymer Mass Ratios.....	141
3.3.4. Comparison of Hybrid Micellar Hydrogels of Four Hairy NP Samples.	144
3.4. Discussion	146
3.5. Conclusions.....	154
3.6. References.....	155
Appendix B	159
Chapter 4. Enhancing Gelation Efficiency of A Doubly Thermosensitive Hydrophilic Linear ABC Triblock Copolymer in Water by Thermoresponsive Hairy Nanoparticles.....	191
Abstract	192
4.1. Introduction.....	193
4.2. Experimental Section	197
4.2.1. Materials	197
4.2.2. General Characterization	200

4.2.3. Synthesis of Doubly Thermosensitive ABC Triblock Copolymer PDEGEMA- <i>b</i> -PDMAEMA- <i>b</i> -P(DEGMMA- <i>co</i> -RhBMA)	201
4.2.4. Quaternization Reaction of PDEGEMA- <i>b</i> -PDMAEMA- <i>b</i> -P(DEGMMA- <i>co</i> - RhBMA) with CH ₃ I to Yield PDEGEMA- <i>b</i> -poly(2- (methacryloyloxy)ethyltrimethylammonium iodide)- <i>b</i> -P(DEGMMA- <i>co</i> - RhBMA) (PDEGEMA- <i>b</i> -P(TMAEMA-I)- <i>b</i> -P(DEGMMA- <i>co</i> -RhBMA), ABC- Q).....	202
4.2.5. Synthesis of Thermosensitive Polymer Brush-Grafted Silica Nanoparticles	203
4.2.6. Dynamic Light Scattering Studies of LCST Transitions of Thermosensitive Hairy NPs NP-29.5 and PDEGEMA- <i>b</i> -P(TMAEMA-I)- <i>b</i> -P(DEGMMA- <i>co</i> - RhBMA) in Water	204
4.2.7. Fluorescence Spectroscopy Study of Aqueous Solutions of Thermosensitive Hairy NPs and PDEGEMA- <i>b</i> -P(TMAEMA-I)- <i>b</i> -P(DEGMMA- <i>co</i> - RhBMA).....	204
4.2.8. Rheological Measurements.....	205
4.3. Results.....	206
4.3.1. Synthesis and Thermoresponsive Properties of ABC Triblock Copolymer P(DEGEMA)- <i>b</i> -P(TMAEMA-I)- <i>b</i> -P(DEGMMA- <i>co</i> -RhBMA).....	206
4.3.2. Synthesis of Thermosensitive Hairy NPs with Different LCST Transitions..	212
4.3.3. Rheology Study of Hybrid 3-D Network Hydrogels of ABC-Q and NP-29.5 with a Polymer Concentration of 6 wt% and Various Polymer-to-NP Mass Ratios.....	214

4.3.4. Rheology Study of Hybrid Micellar Hydrogels of ABC-Q and NP-51 with a Polymer Concentration of 6 wt% and Various NP-to-Polymer Mass Ratios	218
4.4. Discussion	220
4.5. Conclusions.....	227
4.6. References.....	229
Appendix C	232
Chapter 5. Thermosensitive Polymer Brush-Grafted Mesoporous Silica Nanoparticles.....	250
Abstract.....	251
5.1. Introduction.....	252
5.2. Experimental Section	253
5.2.1. Materials	253
5.2.2. General Characterization	254
5.2.3. Synthesis of Mesoporous Silica Nanoparticles (MSNs) with Sizes of 30-40 nm.....	256
5.2.4. Synthesis of PDEGMMA-Grafted Mesoporous Silica Nanoparticles (PDEGMMA-MSNs)	257
5.3. Results and Discussion	258
5.3.1. Synthesis of Mesoporous Silica Nanoparticles (MSNs).....	258
5.3.2. Synthesis of PDEGMMA-Grafted Mesoporous Silica Nanoparticles (PDEGMMA-MSNs)	260
5.4. Conclusions.....	264
5.5. References.....	267

Chapter 6. Conclusions and Future Work	269
6.1. References.....	274
Vita... ..	275

List of Tables

3.1	Characterization data for four hairy nanoparticle samples with different thermoresponsive properties and the corresponding free polymers.....	135
3.2	Calculated fractions of bridging polymer chains at certain temperatures for hybrid hydrogels of ABA-N and four hairy NP samples with a NP-to-ABA mass ratio of 30 : 100.....	150

List of Figures

1.1	(A) Illustration of aqueous solution of PNIPAM that shows LCST behavior and (B) molecular structures and the cloud point of PDEGEMA, PDEGMMA and PTEGMMA.....	4
1.2	Photographs and TEM images obtained at 37 °C and 2 °C illustrating the temperature-dependent (de)gelling behavior of the disulfide-functionalized copolymer worms. .	14
1.3	Schematic representation of a close-packed crystal of spherical micelles (left) and of a nanocomposite crystal that is formed when smaller particles are inserted into the octahedral interstitial cavities (right).	16
1.4	Schematic representation of ordered microstructure of hybrid hydrogels of Pluronic and magnetic NPs: (A) before applying the magnetic field (MF), indomethacin (IMC) drug molecules are encapsulated in the hydrophobic core of micelles and the magnetic NPs are also located in the core of micelles; (B) when the MF is on, the magnetic NPs orient and approach each other, squeezing the micelles and leading to enhancement of IMC release.	17
2.1	(A) TGA of (i) the initiator NPs and (ii) P(DEGMMA- <i>co</i> -DEGEMA- <i>co</i> -NBD) brush-grafted silica NPs (NP-D). (B) Average apparent hydrodynamic diameter D_h (along with error bar) of NP-D in an aqueous dispersion with a concentration of 1.0 mg/g as a function of temperature obtained from a dynamic light scattering study.	51
2.2	(A) TGA of (i) the initiator NPs and (ii) P(TEGMMA- <i>co</i> -NBDMA) brush-grafted silica NPs (NP-T). (B) Average apparent hydrodynamic diameter D_h (along with error bar) of NP-T in water with a concentration of 1.0 mg/g as a function of temperature obtained from a dynamic light scattering study.	53

2.3	Scattered light intensity at scattering angle of 90° (A) and average apparent hydrodynamic size D_h (B), obtained from CONTIN analysis, as a function of temperature in a dynamic light scattering study of a 0.2 mg/g aqueous solution of ABA-D.	55
2.4	Fluorescence spectra of aqueous solutions of ABA-D with a concentration of 0.216 mg/g (A), NP-D with a concentration of 0.012 mg/g (B), NP-T with a concentration of 0.012 mg/g (C), a mixture of ABA-D with a concentration of 0.216 mg/g and NP-D with a concentration of 0.012 mg/g (D), and a mixture of ABA-D with a concentration of 0.217 mg/g and NP-T with a concentration of 0.012 mg/g (E) at (i) $\sim 0^\circ\text{C}$ and (ii) 27°C	57
2.5	Optical picture of aqueous solutions of (A) NP-D with a concentration of 0.28 wt %, (B) NP-T with a concentration of 1.80 wt %, (C) a mixture of ABA-D with a concentration of 4.54 wt % and NP-T with a concentration of 2.95 wt %, (D) a mixture of ABA-D with a concentration of 4.55 wt% and NP-D with a concentration of 2.96 wt %, and (E) ABA-D with a concentration of 4.54 wt % taken in dark at room temperature under the irradiation of a UV light with a wavelength of 365 nm (from a TLC detector).	59
2.6	Plots of dynamic storage modulus G' and loss modulus G'' of aqueous mixtures of ABA-D with a concentration of 10 wt %, defined as $[(\text{polymer mass})/(\text{polymer mass} + \text{water mass})] \times 100\%$, and hairy NPs with various NP-to-polymer mass ratios versus temperature. The data were collected from temperature ramp experiments performed by using a frequency of 1 Hz, a strain amplitude of 1 %, and a heating rate of $3^\circ\text{C}/\text{min}$. (A), (C), (E), (G), (I), and (K) are the heating ramps of aqueous mixtures of	

ABA-D and NP-D with NP-to-polymer mass ratios of 5:100, 10:100, 20:100, 30:100, 40:100, 50:100, respectively. (B), (D), (F), (H), (J), and (L) are the heating ramps of aqueous mixtures of ABA-D and NP-T with NP-to-polymer mass ratios of 5:100, 10:100, 20:100, 30:100, 40:100, 50:100, respectively.	61
2.7 Effect of NP-to-polymer mass ratio on $T_{\text{sol-gel}}$ (A) and G'_{max} (B) of hybrid micellar hydrogels of hairy NPs and ABA-D with a polymer concentration of 10 wt %, defined as $[(\text{polymer mass})/(\text{polymer mass} + \text{water mass})] \times 100 \%$. The values of $T_{\text{sol-gel}}$ and G'_{max} are the averages of three rheological measurements, and the error bars are included.	65
2.8 Plot of G' at 1 Hz ($G'_{1\text{Hz}}$) from frequency sweeps at 40 °C of hybrid micellar hydrogels of thermosensitive hairy NPs and ABA-D with a polymer concentration of 10 wt %, defined as $[(\text{polymer mass})/(\text{polymer mass} + \text{water mass})] \times 100 \%$ versus NP-to-polymer mass ratio. The value of $G'_{1\text{Hz}}$ for each ratio is the average of three measurements, and the error bar is included.	66
2.9 Effect of NP-to-ABA-D mass ratio on $T_{\text{sol-gel}}$ (A) and G'_{max} (B) of hybrid micellar hydrogels of NPs and ABA-D with a polymer concentration of 10 wt %, defined as $[(\text{polymer mass})/(\text{polymer mass} + \text{water mass} + \text{hairy NP mass})] \times 100 \%$. The values of $T_{\text{sol-gel}}$ and G'_{max} are the averages of three rheological measurements, and the error bars are included.	68
2.10 Plot of G' at 1 Hz ($G'_{1\text{Hz}}$) from frequency sweeps at 40 °C of hybrid hydrogels of thermosensitive hairy NPs and ABA-D with a polymer concentration of 10 wt %, defined as $[(\text{polymer mass})/(\text{polymer mass} + \text{water mass} + \text{NP mass})] \times 100\%$, versus NP-to-ABA-D mass ratio. The value of $G'_{1\text{Hz}}$ for each mass ratio is the average of	

	three measurements, and the error bar is included in the plot. The frequency sweeps can be found in Appendix A.	69
A1	¹ H NMR spectrum of the free copolymer P(DEGMMA- <i>co</i> -DEGEMA- <i>co</i> -NBDMA) formed from the free initiator ethyl 2-bromoisobutyrate in the synthesis of P(DEGMMA- <i>co</i> -DEGEMA- <i>co</i> -NBDMA) brush-grafted silica nanoparticles (NP-D). CDCl ₃ was used as solvent.	83
A2	Size exclusion chromatography (SEC) trace of the dried free copolymer P(DEGMMA- <i>co</i> -DEGEMA- <i>co</i> -NBDMA) formed from the free initiator ethyl 2-bromoisobutyrate in the synthesis of P(DEGMMA- <i>co</i> -DEGEMA- <i>co</i> -NBDMA) brush-grafted silica nanoparticles (NP-D).	84
A3	SEC trace of the dried free polymer P(TEGMMA- <i>co</i> -NBDMA) formed from the free initiator ethyl 2-bromoisobutyrate in the synthesis of P(TEGMMA- <i>co</i> -NBDMA) brush-grafted silica nanoparticles (NP-T).	85
A4	SEC trace of ABA triblock copolymer P(DEGMMA- <i>co</i> -DEGEMA- <i>co</i> -RhBMA)- <i>b</i> -PEO- <i>b</i> -P(DEGMMA- <i>co</i> -DEGEMA- <i>co</i> -RhBMA) (ABA-D). The SEC analysis was conducted using a SEC system with DMF containing 0.05 M LiBr as eluent.	86
A5	¹ H NMR spectrum of the ABA triblock copolymer P(DEGMMA- <i>co</i> -DEGEMA- <i>co</i> -RhBMA)- <i>b</i> -PEO- <i>b</i> -P(DEGMMA- <i>co</i> -DEGEMA- <i>co</i> -RhBMA) (ABA-D) in CDCl ₃	87
A6	Plots of dynamic storage modulus G' and loss modulus G'' of aqueous mixtures of ABA-D with a concentration of 10 wt %, defined as [(polymer mass)/(polymer mass + water mass)] × 100%, and hairy NPs with various NP-to-polymer mass ratios versus temperature for both NP-D and NP-T. The data were collected from temperature	

	ramp experiments performed by using a frequency of 1 Hz, a strain amplitude of 1 %, and a heating rate of 3 °C/min.	88
A7	Frequency dependences of dynamic storage modulus G' (black square) and loss modulus G'' (red circle) at 40 °C of the hybrid micellar hydrogels of the ABA triblock copolymer ABA-D and thermosensitive hairy NPs with various NP-to-polymer mass ratios and a polymer concentration of 10 wt % defined as $[(\text{polymer mass})/(\text{polymer mass} + \text{water mass})] \times 100\%$. A strain amplitude of 1.0% was used in the frequency sweep experiments.	95
A8	Plots of dynamic storage modulus G' and loss modulus G'' of aqueous mixtures of ABA-D with a concentration of 10 wt %, defined as $[(\text{polymer mass})/(\text{polymer mass} + \text{water mass} + \text{hairy NP mass})] \times 100\%$, and hairy NPs with various NP-to-polymer mass ratios versus temperature for both NP-D and NP-T. The data were collected from temperature ramp experiments performed by using a frequency of 1 Hz, a strain amplitude of 1 %, and a heating rate of 3 °C/min.	105
A9	Frequency dependences of dynamic storage modulus G' (black square) and loss modulus G'' (red circle) at 40 °C of the hybrid micellar hydrogels of the ABA triblock copolymer ABA-D and thermosensitive hairy NPs with various NP-to-polymer mass ratios and a polymer concentration of 10 wt % defined as $[(\text{polymer mass})/(\text{polymer mass} + \text{water mass} + \text{hairy NP mass})] \times 100\%$. A strain amplitude of 1.0% was used in the frequency sweep experiments.	112
A10	Fluorescence spectra of aqueous solutions of ABA-D with a concentration of 0.216 mg/g (A), NP-T with a concentration of 0.012 mg/g (B), the mixture of ABA-D with	

a concentration of 0.217 mg/g and NP-T with a concentration of 0.012 mg/g at ~ 0 °C (C), 27 °C (D), and 50 °C (E).	118
3.1 Plots of dynamic storage modulus G' and loss modulus G'' of aqueous mixtures of ABA-N with a concentration of 10 wt % and NP-29 with various NP-to-polymer mass ratios versus temperature. The rheological data were collected from heating ramp experiments performed by using a frequency of 1 Hz, a strain amplitude of 1 %, and a heating rate of 3 °C/min.	137
3.2 Plots of dynamic storage modulus G' versus temperature for aqueous mixtures of ABA-N and NP-29 with different mass ratios. The data were replotted from Figure 3.1.	139
3.3 Representative plots of dynamic storage modulus G' versus temperature for aqueous mixtures of ABA-N and (A) NP-34, and (B) NP-44, and (C) NP-51 with various NP-to-ABA-N mass ratios. The data were replotted from one of the three heating ramps for each mass ratio that can be found in Appendix B.	142
3.4 Plots of dynamic storage modulus G' of aqueous mixtures of ABA-N and four thermosensitive hairy NPs with different LCSTs at a NP-to-polymer mass ratio of 30 : 100 as a function of temperature. The rheological data were from Figures 3.2 and 3.3. For the sake of clarity, the G' vs T curve for ABA-N and NP-51 was vertically shifted by -200 Pa.	143
3.5 Effect of NP-to-polymer mass ratio on G'_{\max} of hybrid micellar hydrogels of thermoresponsive hairy NPs and ABA-N with a polymer concentration of 10 wt %. The values of G'_{\max} are the averages of three rheological measurements. NP-29 (red solid square); NP-35 (green solid circle); NP-44 (blue upward pointing solid triangle);	

NP-51 (magenta downward pointing solid triangle); NP-D (black empty diamond); NP-T (black left-pointing empty triangle). The data for NP-D and NP-T are from Ref. 36 and used here for comparison.	145
3.6 Plot of the intensity ratio of the emission peaks at 521 nm and 575 nm (I_{521}/I_{575}) versus temperature for an aqueous mixture of (A) ABA-N (concentration: 0.208 mg/g) and NP-29 (conc.: 0.010 mg/g), (B) ABA-N (conc.: 0.208 mg/g) and NP-34 (conc.: 0.011 mg/g), (C) ABA-N (conc.: 0.206 mg/g) and NP-44 (conc.: 0.010 mg/g), and (D) ABA-N (conc.: 0.205 mg/g) and NP-51 (conc.: 0.013 mg/g).	153
B1 (A) Size exclusion chromatography (SEC) trace of thermosensitive ABA triblock copolymer P(DEGMMA- <i>co</i> -DEGEMA- <i>co</i> -RhBMA)- <i>b</i> -PEO- <i>b</i> -P(DEGMMA- <i>co</i> -DEGEMA- <i>co</i> -RhBMA) (ABA-N). DMF-LiBr was the carrier solvent in SEC analysis. (B) ^1H NMR spectrum of ABA-N. CDCl_3 was used as solvent in ^1H NMR spectroscopy analysis.	160
B2 Average apparent hydrodynamic size D_h (A), obtained from CONTIN analysis, and scattered light intensity at scattering angle of 90° (B) as a function of temperature in a dynamic light scattering study of a 0.2 mg/g aqueous solution of P(DEGMMA- <i>co</i> -DEGEMA- <i>co</i> -RhBMA)- <i>b</i> -PEO- <i>b</i> -P(DEGMMA- <i>co</i> -DEGEMA- <i>co</i> -RhBMA) (ABA-N).	161
B3 (A) Size exclusion chromatography and (B) ^1H NMR spectroscopy analysis of the free copolymer formed from the free initiator in the synthesis of P(DEGMMA- <i>co</i> -TEGMMA- <i>co</i> -NBDMA) brush-grafted silica nanoparticles with a LCST transition of 29°C (NP-29). (C) Thermogravimetric analysis (TGA) of (i) the ATRP initiator-	

	functionalized silica nanoparticles and (ii) P(DEGMMA- <i>co</i> -TEGMMA- <i>co</i> -NBDMA) brush-grafted silica nanoparticles (NP-29).	162
B4	Average apparent hydrodynamic size D_h (A), obtained from CONTIN analysis, and scattered light intensity at scattering angle of 90° (B) as a function of temperature in a dynamic light scattering study of a 1.0 mg/g aqueous dispersion of P(DEGMMA- <i>co</i> -TEGMMA- <i>co</i> -NBDMA) brush-grafted silica nanoparticles (NP-29).	163
B5	(A) Size exclusion chromatography (SEC) and (B) ^1H NMR spectroscopy analysis of free copolymer formed from the free initiator in the synthesis of P(DEGMMA- <i>co</i> -TEGMMA- <i>co</i> -NBDMA) brush-grafted silica nanoparticles with a LCST transition of 34 °C (NP-34). (C) Thermogravimetric analysis (TGA) of (i) the ATRP initiator-functionalized silica nanoparticles and (ii) P(DEGMMA- <i>co</i> -TEGMMA- <i>co</i> -NBDMA) brush-grafted silica nanoparticles (NP-34).	164
B6	Average apparent hydrodynamic size D_h (A), obtained from CONTIN analysis, and scattered light intensity at scattering angle of 90° (B) as a function of temperature in a dynamic light scattering study of a 1.0 mg/g aqueous dispersion of P(DEGMMA- <i>co</i> -TEGMMA- <i>co</i> -NBDMA) brush-grafted silica nanoparticles (NP-34).	165
B7	(A) Size exclusion chromatography (SEC) analysis of free copolymer P(TEGMMA- <i>co</i> -NBDMA) formed from the free initiator in the synthesis of P(TEGMMA- <i>co</i> -NBDMA) brush-grafted silica nanoparticles with a LCST transition of 44 °C (NP-44). DMF-LiBr was the carrier solvent. (B) TGA of (i) the ATRP initiator-functionalized silica nanoparticles and (ii) P(TEGMMA- <i>co</i> -NBDMA) brush-grafted silica nanoparticles (NP-44).	166

B8	Average apparent hydrodynamic size D_h (A), obtained from CONTIN analysis, and scattered light intensity at scattering angle of 90° (B) as a function of temperature in a dynamic light scattering study of a 1.0 mg/g aqueous dispersion of P(TEGMMA- <i>co</i> -NBDMA) brush-grafted silica nanoparticles (NP-44).	167
B9	SEC analysis (A) and ^1H NMR spectroscopy analysis (B) of the free copolymer formed from the free initiator in the synthesis of P(TEGMMA- <i>co</i> -TrEGMMA- <i>co</i> -NBDMA) brush-grafted silica nanoparticles with a LCST transition of 51°C (NP-51). (C) TGA of (i) the ATRP initiator-functionalized silica nanoparticles and (ii) P(TEGMMA- <i>co</i> -TrEGMMA- <i>co</i> -NBDMA) brush-grafted silica nanoparticles (NP-51).	168
B10	Average apparent hydrodynamic size D_h (A), obtained from CONTIN analysis, and scattered light intensity at scattering angle of 90° (B) as a function of temperature in a dynamic light scattering study of a 1.0 mg/g aqueous dispersion of P(TEGMMA- <i>co</i> -TrEGMMA- <i>co</i> -NBDMA) brush-grafted silica nanoparticles (NP-51).	169
B11	Plots of dynamic storage modulus G' and loss modulus G'' of an aqueous solution of ABA-N with a concentration of 10 wt%. The data were collected from temperature ramp experiments performed by using a frequency of 1 Hz, a strain amplitude of 1 %, and a heating rate of $3^\circ\text{C}/\text{min}$	170
B12	Plots of dynamic storage modulus G' and loss modulus G'' of aqueous mixtures of ABA-N with a concentration of 10 wt% and NP-29 with various NP-to-polymer mass ratios versus temperature. The rheological data were collected from heating ramp experiments performed by using a frequency of 1 Hz, a strain amplitude of 1 %, and a heating rate of $3^\circ\text{C}/\text{min}$	171

B13	Plots of dynamic storage modulus G' and loss modulus G'' of aqueous mixtures of ABA-N with a concentration of 10 wt% and NP-34 with various NP-to-polymer mass ratios versus temperature. The rheological data were collected from heating ramp experiments performed by using a frequency of 1 Hz, a strain amplitude of 1 %, and a heating rate of 3 °C/min. For each NP-to-ABA-N mass ratio, three rheological measurements were taken.	174
B14	Plots of dynamic storage modulus G' and loss modulus G'' of aqueous mixtures of ABA-N with a concentration of 10 wt% and NP-44 with various NP-to-polymer mass ratios versus temperature. The rheological data were collected from heating ramp experiments performed by using a frequency of 1 Hz, a strain amplitude of 1 %, and a heating rate of 3 °C/min. For each NP-to-ABA-N mass ratio, three rheological measurements were taken.	178
B15	Plots of dynamic storage modulus G' and loss modulus G'' of aqueous mixtures of ABA-N with a concentration of 10 wt% and NP-51 with various NP-to-polymer mass ratios versus temperature. The rheological data were collected from heating ramp experiments performed by using a frequency of 1 Hz, a strain amplitude of 1 %, and a heating rate of 3 °C/min. For each NP-to-ABA-N mass ratio, three rheological measurements were taken.	182
B16	Fluorescence emission spectra at room temperature (~ 20 °C) of an aqueous solution of (A) ABA-N with a concentration of 0.208 mg/g, (B) NP-29 with a concentration of 0.010 mg/g, (C) NP-34 with a concentration of 0.012 mg/g, (D) NP-44 with a concentration of 0.011 mg/g, (E) NP-51 with a concentration of 0.012 mg/g.	186

B17	(A) Fluorescence emission spectra of an aqueous solution of ABA-N with a concentration of 0.208 mg/g and NP-29 with a concentration of 0.010 mg/g at various temperatures. (B) Plot of fluorescence emission intensity at 521 nm versus temperature.	187
B18	(A) Fluorescence spectra of an aqueous solution of ABA-N with a concentration of 0.208 mg/g and NP-34 with a concentration of 0.011 mg/g at various temperatures. (B) Plot of fluorescence emission intensity at 521 nm (I_{521}) versus temperature.	188
B19	(A) Fluorescence emission spectra of an aqueous solution of ABA-N with a concentration of 0.206 mg/g and NP-44 with a concentration of 0.010 mg/g at various temperatures. (B) Plot of fluorescence emission intensity at 521 nm (I_{521}) versus temperature.	189
B20	(A) Fluorescence emission spectra of an aqueous solution of ABA-N with a concentration of 0.205 mg/g and NP-51 with a concentration of 0.013 mg/g at various temperatures. (B) Plot of fluorescence emission intensity at 521 nm (I_{521}) versus temperature.	190
4.1	Size exclusion chromatography traces of PDEGEMA, PDEGEMA- <i>b</i> -PDMAEMA, and PDEGEMA- <i>b</i> -PDMAEMA- <i>b</i> -P(DEGMMA- <i>co</i> -RhBMA).	208
4.2	^1H NMR spectrum of PDEGEMA- <i>b</i> -PDMAEMA macro-CTA in CDCl_3 (A), PDEGEMA- <i>b</i> -PDMAEMA- <i>b</i> -P(DEGMMA- <i>co</i> -RhBMA) in CDCl_3 (B) and PDEGEMA- <i>b</i> -P(TMAEMA- <i>I</i>)- <i>b</i> -P(DEGMMA- <i>co</i> -RhBMA) in DMSO-d_6 (C). ...	209
4.3	Plot of scattering intensity at scattering angle of 90° (A) and average apparent hydrodynamic diameter D_h (B), obtained from CONTIN, versus temperature from a	

dynamic light scattering study of a 2.0 mg/g solution of PDEGEMA- <i>b</i> -P(TMAEMA-I)- <i>b</i> -P(DEGMMA- <i>co</i> -RhBMA) in pure water.	211
4.4 (A) Size exclusion chromatography of the free copolymer formed from the free initiator in the synthesis of P(DEGMMA- <i>co</i> -TEGMMA- <i>co</i> -NBDMA) brush-grafted silica nanoparticles (NP-29.5). (B) Thermogravimetric analysis (TGA) of (i) the ATRP initiator-functionalized silica nanoparticles and (ii) P(DEGMMA- <i>co</i> -TEGMMA- <i>co</i> -NBDMA) brush-grafted silica nanoparticles (NP-29.5). (B) ¹ H NMR spectroscopy analysis of the free copolymer formed from the free initiator in the synthesis of NP-29.5.	213
4.5 Plot of scattering intensity at scattering angle of 90° (A) and average apparent hydrodynamic size D_h (B), obtained from CONTIN analysis, as a function of temperature from a dynamic light scattering study of a 1.0 mg/g aqueous dispersion of P(DEGMMA- <i>co</i> -TEGMMA- <i>co</i> -NBDMA) brush-grafted silica nanoparticles (NP-29.5).....	215
4.6 Representative plots of dynamic storage modulus G' and loss modulus G'' of aqueous mixtures of PDEGEMA- <i>b</i> -P(TMAEMA-I)- <i>b</i> -P(DEGMMA- <i>co</i> -RhBMA) with a concentration of 6 wt% and NP-29.5 with various polymer-to-NP mass ratio versus temperature. The rheological data were collected from oscillatory shear experiments conducted in heating ramps using a frequency of 1 Hz, a strain amplitude of 1 %, and a heating rate of 3 °C/min.	216
4.7 Plots of dynamic storage modulus G' versus temperature for aqueous mixtures of ABC-Q and NP-29.5 (A) and NP-51 (B) at various NP-to-polymer mass ratios (replotted from Figures 4.6 and 4.8); (C) plots of average G'_{max} versus NP-to-	

	polymer mass ratio for NP-29.5 and NP-51; (D) plots of average $G'_{1\text{Hz}}$ versus NP-to-polymer mass ratio for NP-29.5 and NP-51.	219
4.8	Representative plots of dynamic storage modulus G' and loss modulus G'' of aqueous mixtures of PDEGEMA- <i>b</i> -P(TMAEMA- <i>I</i>)- <i>b</i> -P(DEGMMA- <i>co</i> -RhBMA) with a concentration of 6 wt% and NP-51 with various polymer-to-NP mass ratio versus temperature. The rheological data were collected from oscillatory shear experiments conducted in heating ramps using a frequency of 1 Hz, a strain amplitude of 1 %, and a heating rate of 3 °C/min.	221
4.9	Plots of calculated fractions of bridging chains versus NP-to-polymer mass ratio for hybrid hydrogels of (A) 6 wt% ABC-Q solution with various amounts of NP-29.5 and (B) 6 wt% aqueous solution of ABC-Q with various NP-51-to-ABC-Q mass ratios at 50 and 65 °C. Average G' values from three heating ramps at 50 and 65 °C were used in the calculations.	225
4.10	Fluorescence spectra of aqueous solutions of (A) ABC-Q with a concentration of 0.431 mg/g and NP-29.5 with a concentration of 0.013 mg/g and of (B) ABC-Q with a concentration of 0.376 mg/g and NP-51 with a concentration of 0.012 mg/g at 15 (black curves) and 40 °C (red curves).	226
C1	Plots of dynamic storage modulus G' and loss modulus G'' of an aqueous solution of PDEGEMA- <i>b</i> -P(TMAEMA- <i>I</i>)- <i>b</i> -P(DEGMMA- <i>co</i> -RhBMA) with a concentration of 6 wt%. The rheological data were collected from heating ramp experiments performed by using a frequency of 1 Hz, a strain amplitude of 1 %, and a heating rate of 3 °C/min.	233

C2	Plots of dynamic storage modulus G' and loss modulus G'' of aqueous mixtures of ABC-Q with a concentration of 6 wt% and NP-29.5 with various polymer-to-NP mass ratios versus temperature. The rheological data were collected from oscillatory shear experiments conducted in heating ramps using a frequency of 1 Hz, a strain amplitude of 1 %, and a heating rate of 3 °C/min.	234
C3	Plots of dynamic storage modulus G' and loss modulus G'' of aqueous mixtures of ABC-Q with a concentration of 6 wt% and NP-51 with various polymer-to-NP mass ratio versus temperature. The rheological data were collected from heating ramp experiments performed by using a frequency of 1 Hz, a strain amplitude of 1 %, and a heating rate of 3 °C/min.	237
C4	Frequency dependences of dynamic storage modulus G' (black square) and loss modulus G'' (red circle) at 40 °C of hybrid 3-D network micellar hydrogels of ABC-Q and NP-29.5 NPs with various NP-to-polymer mass ratios and a polymer concentration of 6 wt % defined as $[(\text{polymer mass})/(\text{polymer mass} + \text{water mass})] \times 100\%$. A strain amplitude of 1.0% was used in the frequency sweep experiments...	240
C5	Frequency dependences of dynamic storage modulus G' (black square) and loss modulus G'' (red circle) at 40 °C of hybrid 3-D network micellar hydrogels of ABC-Q and NP-51 NPs with various NP-to-polymer mass ratios and a polymer concentration of 6 wt % defined as $[(\text{polymer mass})/(\text{polymer mass} + \text{water mass})] \times 100\%$. A strain amplitude of 1.0% was used in the frequency sweep experiments...	244
C6	Fluorescence spectra of an aqueous solution at 15 (black curve) and 40 °C (red curve) of ABC-Q with a concentration of 0.40 mg/g loaded with 2.44×10^{-4} mg/g NBD-Cl. NBD-Cl was loaded into the PDEGEMA micelle core at 15 °C.	248

C7	Fluorescence emission spectra of an aqueous solution of (A) ABC-Q with a concentration of 0.414 mg/g, (B) NP-29.5 with a concentration of 0.013 mg/g, (C) NP-51 with a concentration of 0.011 mg/g at both 15 °C and 40 °C.	249
5.1	TEM pictures of (A) ATRP initiator-functionalized MSNs and (B) PDEGMMA-grafted MSNs (PDEGMMA-MSNs).	259
5.2	SEC trace of the free polymer PDEGMMA formed from the free initiator in the synthesis of PDEGMMA-grafted MSNs by surface-initiated atom transfer radical polymerization.	261
5.3	¹ H NMR spectra of (A) chlorodimethylsilane-terminated ATRP initiator (MA-CDMS) and (B) PDEGMMA grafted MSNs (in CDCl ₃).	262
5.4	TGA data of ATRP initiator-functionalized MSNs and PDEGMMA-grafted mesoporous silica NPs.	263
5.5	Plot of the average apparent hydrodynamic size D_h , obtained from CONTIN analysis, as a function of temperature from a dynamic light scattering study of a 1.0 mg/g aqueous dispersion of PDEGMMA brush-grafted mesoporous silica nanoparticles (PDEGMMA-MSNs).	265

List of Schemes

1.1	Physical Packing-based Micellar Hydrogels Formed from Thermosensitive AB Diblock or ABA Triblock Copolymers.....	6
1.2	Physically Crosslinked Network Hydrogels Formed from Thermosensitive ABA Triblock Copolymers.....	9
1.3	Illustration of Hybrid Micelles of Citrate Stabilized Magnetic NPs with a Quaternized Pq2VP- <i>b</i> -PEO- <i>b</i> -P(GME- <i>co</i> -EGE) Triblock Copolymer, and Subsequent Reversible Gelation via Open Association of Hybrid Micelles at Temperatures above the Cloud Point of P(GME- <i>co</i> -EGE) Block.....	19
1.4	Synthesis of Thermoresponsive Hairy Nanoparticles by SI-ATRP.....	21
2.1	Control of Spatial Location of NPs, Either Inside or Outside the Core of Micelles, in Hybrid Micellar Hydrogels of Thermosensitive ABA Triblock Copolymer and Hairy NPs.....	36
2.2	Synthesis of Thermosensitive ABA Triblock Copolymer P(DEGMMA- <i>co</i> -DEGEMA- <i>co</i> -RhBMA)- <i>b</i> -PEO- <i>b</i> -P(DEGMMA- <i>co</i> -DEGEMA- <i>co</i> -RhBMA) (ABA-D) by ATRP.....	38
2.3	Synthesis of Thermosensitive P(DEGMMA- <i>co</i> -DEGEMA- <i>co</i> -NBDMA) Brush-Grafted (NP-D) and P(TEGMMA- <i>co</i> -NBDMA) Brush-Grafted Silica NPs (NP-T) by Surface-Initiated ATRP from 17 nm Silica NPs.....	39
2.4	Collapsed Polymer Brushes of NP-T Adsorb Polymer Chains to Form New Bridges.....	72
A1	Synthesis of NBDMA.....	79
A2	Synthesis of RhBMA.....	81

3.1	Molecular structures of monomers used in this work and scheme for the synthesis of hairy nanoparticles by surface-initiated atom transfer radical polymerization (SI-ATRP).....	126
3.2	Schematic illustration of formation of 3-D network by ABA-N in the presence of hairy NPs and reorganization of network structure upon heating above the LCST transition temperature of hairy NPs.....	147
4.1	Schematic Illustration of the Formation of a 3-D Network Hydrogel by ABC Triblock Copolymer Composed of a Lower LCST A Block, a Permanently Hydrophilic B Block, and a Higher LCST C Block in the Presence of Hairy NPs with a LCST Similar to that of the Thermosensitive C Block of the ABC Triblock Copolymer.....	196
4.2	Synthesis of Doubly Thermosensitive ABC Linear Triblock Copolymer PDEGEMA- <i>b</i> -P(TMAEMA-I)- <i>b</i> -P(DEGMMA- <i>co</i> -RhBMA) by Reversible Addition-Fragmentation Chain Transfer (RAFT) Polymerization and Subsequent Quaternization, and Molecular Structure of RhBMA.....	198
4.3	Synthesis of Thermoresponsive Hairy Nanoparticles by Surface-Initiated Atom Transfer Radical Polymerization (SI-ATRP) from Initiator Functionalized, 20 nm Silica Nanoparticles (NP) and Molecular Structure of NBDMA.....	199
5.1	Molecular Structure of the ATRP Initiator, 2-(9-(((2-Bromo-2-Methylpropanoyl)Oxy)Methyl)-12,14-Dioxo-11,12,14,15-Tetrahydro-9 <i>H</i> -9,10-[3,4]Epipyrroloanthracen-13(10 <i>H</i>)-yl)Ethyl Pent-4-Enoate (MA-)=.....	255

List of Abbreviations

3-D: 3-Dimensional

ABA-D, ABA-N: P(DEGMMA-*co*-DEGEMA-*co*-RhBMA)-*b*-PEO-*b*-P(DEGMMA-*co*-DEGEMA-*co*-RhBMA)

ABC-Q: PDEGEMA-*b*-P(TMAEMA-I)-*b*-(PDEGMMA-*co*-RhBMA)

AIBN: 2,2'-Azobis(2-methylpropionitrile)

ATRP: Atom transfer radical polymerization

BET: Brunauer-Emmett-Teller method

C/Co NPs: Carbon-coated cobalt nanoparticles

CGC: Critical gelation concentration

CMT: Critical micellization temperature

¹³C NMR: Carbon-13 nuclear magnetic resonance spectroscopy

CP: Cloud point

CPDB: 2-(2-Cyanopropyl)dithiobenzoate

CTA: Chain transfer agent

CTAB: Cetyltrimethylammonium bromide

DART: Direct analysis in real time

DEGEMA: Di(ethylene glycol) ethyl ether methacrylate

DEGMMA: Di(ethylene glycol) methyl ether methacrylate

D_h : Hydrodynamic size

DLS: Dynamic light scattering

DMAEMA: *N,N*-Dimethylaminoethyl methacrylate

DMF: *N,N*-Dimethylformamide

DMSO: Dimethyl sulfoxide

DP: Degree of polymerization

EBiB: Ethyl 2-bromoisobutyrate

EGDMA: Ethylene glycol dimethacrylate

FRET: Fluorescence resonance energy transfer

$G'_{1\text{Hz}}$: Value of dynamic storage modulus G' at 1 Hz from frequency sweep

G'_{calc} : Calculated maximum storage modulus at specific temperature

G'_{expt} : The value of dynamic storage modulus at specific temperature from heating ramp

G'_{max} : Maximum value of dynamic storage modulus G' from temperature ramp

GPC: Gel permeation chromatography

HEMA: 2-Hydroxyethyl methacrylate

HMTETA: 1,1,4,7,10,10-Hexamethyltriethylenetetramine

^1H NMR: Proton nuclear magnetic resonance spectroscopy

HPLC: High performance liquid chromatography

$I_{521/575}$: The intensity ratio of the peaks at 521 and 575 nm from the fluorescence emission spectra

IMC: Indomethacin

LCST: Lower critical solution temperature

LCST_{ABA} : Lower critical solution temperature of ABA triblock copolymer

LCST_{end} : End temperature of the LCST transition

LCST_{H} : Higher LCST from the C block of doubly thermosensitive ABC triblock copolymer

LCST_{L} : Lower LCST from the A block of doubly thermosensitive ABC triblock copolymer

LCST_{mid} : middle point of the LCST transition

LCST_{NP}: Lower critical solution temperature of hairy nanoparticles

LCST_{onset}: Onset temperature of the LCST transition

MA-=: An ATRP initiator, anchored by a maleimide-anthracene cycloadduct, 2-(9-(((2-bromo-2-methylpropanoyl)oxy)methyl)-12,14-dioxo-11,12,14,15-tetrahydro-9*H*-9,10-[3,4]epipyrroloanthracen-13(10*H*)-yl)ethyl pent-4-enoate

MA-CDMS: A chlorodimethylsilane-terminated ATRP initiator anchored by a maleimide-anthracene cycloadduct

MF: Magnetic field

MIBK: Methyl isobutyl ketone

MIBK-ST: A dispersion of silica NPs with a size of 10-15 nm in methyl isobutyl ketone (30-31 wt % SiO₂)

M_n : Number average molecular weight

MS: Mass spectrometry

MSNs: Mesoporous silica nanoparticles

MWCO: Molecular weight cut-off

NBD-Cl: 4-Chloro-7-nitro-2,1,3-benzoxadiazole

NBDMA: 4-(2-Methacryloyloxyethylamino)-7-nitro-2,1,3-benzoxadiazole

NBD-OH: 4-(2-Hydroxyethylamino)-7-nitro-2,1,3-benzoxadiazole

NMRP: Nitroxide-mediated radical polymerization

NP: Nanoparticle

NP-29, NP-29.5, NP-34, NP-44, NP-51: Thermoresponsive polymers brush-grafted nanoparticles with a middle point of LCST transition of 29, 29.5, 34, 44 and 51 °C, respectively

NP-D: P(DEGMMA-*co*-DEGEMA-*co*-NBDMA) brush-grafted nanoparticles

NP-T: P(TEGMMA-*co*-NBDMA) brush-grafted nanoparticles

PCLA: Poly(ϵ -caprolactone-*co*-lactide)

P(DEGMMA-*co*-MAA): Poly(methoxydi(ethylene glycol) methacrylate-*co*-methacrylic acid)

PDEGMMA-MSNs: PDEGMMA-grafted mesoporous silica nanoparticles

PDI: Polydispersity index

PDMA: Poly(*N,N*-dimethylacrylamide)

PE: Polyethylene

PEO: Poly(ethylene oxide)

PEO-*b*-PPO-*b*-PEO, Pluronics: poly(ethylene oxide)-*b*-poly(propylene oxide)-*b*-poly(ethylene oxide)

PEP: Poly(ethylene-*alt*-propylene)

PGMA-*b*-PHPMA: Poly(glycerol monomethacrylate)-*b*-poly(2-hydroxypropyl methacrylate)

PHPMA_{lac}: Poly(*N*-(2-hydroxypropyl) methacrylamide lactate)

PLGA: Poly(*L*-lactic acid-*co*-glycolide)

PMDETA: *N,N,N',N',N''*-Pentamethyldiethylenetriamine

PMPC: Poly(2-methacryloyoxyethyl phosphorylcholine)

PNIPAM: Poly(*N*-isopropylacrylamide)

Pq2VP-*b*-PEO-*b*-P(GME-*co*-EGE): Partly quaternized poly(2-vinylpyridine)-*b*-PEO-*b*-poly(glycidyl methyl ether-*co*-ethyl glycidyl ether)

P(TEGEA-*co*-NBA): Poly(ethoxytri(ethylene glycol) acrylate-*co*-*o*-nitrobenzyl acrylate)

PTFE: Polytetrafluoroethylene

P(TMAEMA-I): Poly(2-(methacryloyloxy)ethyltrimethylammonium iodide)

RAFT: Reversible addition-fragmentation chain transfer

RhBMA: Rhodamine B-containing methacrylate

SEC: Size exclusion chromatography

SI-ATRP: Surface-initiated atom transfer radical polymerization

TBOS: Tetrabutoxysilane

TEGMMA: Methoxytri(ethylene glycol) methacrylate

TEM: Transmission electron microscopy

TEOS: Tetraethyl orthosilicate

TGA: Thermogravimetric analysis

THF: Tetrahydrofuran

TMOS: Tetramethoxysilane

TOF: Time-of-flight

TPOS: Tetrapropoxysilane

TrEGMMA: Methoxytetra(ethylene glycol) methacrylate

$T_{\text{sol-gel}}$: Sol-gel transition temperature

UCST: Upper critical solution temperature

UV: Ultraviolet

Chapter 1. Introduction

1.1. Introduction

Thermosensitive hydrophilic block copolymers have received great attention in the past years due to their thermally induced micellization in dilute aqueous solutions and sol-gel transitions of moderately concentrated aqueous solutions. They have many potential applications, such as controlled and sustained release of substances, tissue engineering, chemical sensing, smart surfaces, viscosity modification of aqueous systems, etc. Meanwhile inorganic and metal nanoparticles (NPs) with a size of tens of nanometers exhibit intriguing optical, magnetic, or mechanical properties that are usually not possessed by organic polymers. Thus, rationally incorporating NPs into polymer hydrogels can produce functional composite hydrogels materials with synergistic combinations between these two components. In the following sections, thermosensitive polymers and thermosensitive block copolymer micellar hydrogels will be introduced first, followed by the introduction of hybrid hydrogels of thermosensitive block copolymers and nanoparticles as well as polymer brush-grafted nanoparticles (hairy NPs).

1.1.1. Thermosensitive Polymers

Thermosensitive water-soluble polymers are the polymers that undergo a transition from soluble to insoluble in water when the temperature is changed. One of the unique properties of thermosensitive polymers is the presence of a critical solution temperature. Typically there are two types of thermosensitive polymers: one having a lower critical solution temperature (LCST), below which the aqueous polymer solution has one phase and above which the polymer solution is phase-separated, and the other having an upper critical solution temperature (UCST), above which the polymers are soluble in water and below which the solution is phase-separated.¹ It is worth noting that intramolecular collapse occurs before intermolecular aggregation through LCST and the cloud

point is the temperature at which the collapse of individual polymer chains increases the scattering of light in water.² Phase separation between the collapsed polymer molecules and the expelled water follows the cloud point.³ Compared to UCST polymers, polymers that display LCST transitions in water are more widely studied. For example, many polymers that contain amide groups show LCST behaviors, such as poly(*N*-isopropylacrylamide) (PNIPAM), which is the most widely used thermosensitive polymer that has a cloud point at around 32 °C (Figure 1.1A).^{3,4} More recent studies have shown that the introduction of a short oligo(ethylene glycol) chain to the polymer backbone as pendant group makes the polymers water-soluble and thermosensitive and the LCST can be tuned by changing the side chain length and end group.^{5,6} For example, the cloud points of poly(di(ethylene glycol) ethyl ether methacrylate) (PDEGEMA), poly(di(ethylene glycol) methyl ether methacrylate) (PDEGMMA), and poly(tri(ethylene glycol) methyl ether methacrylate) (PTEGMMA) are 4 °C, 26 °C and 52 °C, respectively (Figure 1.1B).^{6,7} In addition, the cloud points can be easily tuned by copolymerizing two or more monomers to make random copolymers using various feed molar ratios of monomers.⁸

Intermolecular interactions of thermosensitive water-soluble polymers in water are noteworthy, for these forces are responsible for micellar aggregation, physical crosslinking, or hydrogel shrinkage.⁹ Generally, there are two types of intermolecular forces in aqueous thermosensitive polymer solutions: hydrogen bonding and hydrophobic interactions. Hydrogen bonding between different pendant groups and water is sensitive to temperature, and the hydrophobic interactions of a collapsed thermosensitive block of a block copolymer result in the formation of micelles above a critical micelle temperature (CMT). At high concentrations, these thermosensitive block copolymers can undergo sol-gel transitions and form hydrogels when the temperature is changed, which will be discussed in detail in the following section.

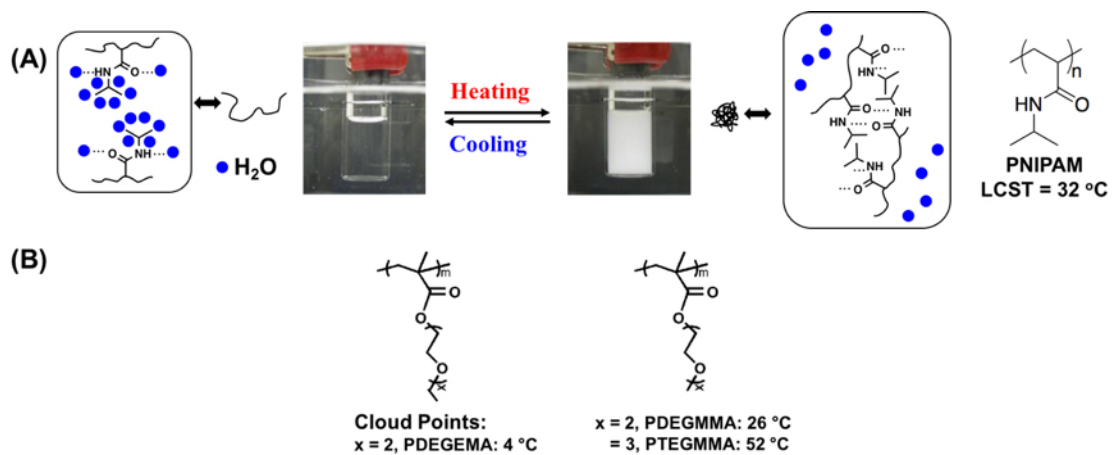


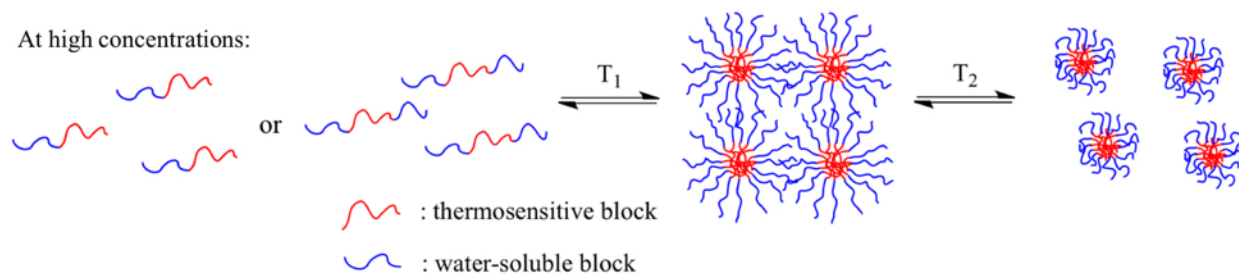
Figure 1.1. (A) Illustration of aqueous solution of PNIPAM that shows LCST behavior and (B) molecular structures and the cloud points of PDEGEMA, PDEGMMA and PTEGMMA.

1.1.2. Thermosensitive Block Copolymer Hydrogels

Thermosensitive block copolymers that contain a thermosensitive block and a more water-soluble block have been studied extensively because they have many potential applications such as triggered control release of substances.¹⁰⁻¹² Generally, there are three types of block copolymer hydrogels. First one is formed by jamming or packing of discrete micelles, often spherical, into an ordered structure upon changes of temperature. The second type of thermosensitive block copolymer hydrogel is the physical crosslinked hydrogels, or 3-dimensional (3-D) network hydrogels. Typically, the outer blocks of thermosensitive ABA or ABC triblock copolymers are thermosensitive and associate into the core of micelles upon temperature changes and the central block forms bridges among neighboring micellar cores. The last type is block copolymer worm-like micellar gels. These block copolymer systems can undergo sol-gel transitions between the spherical block copolymer micelles or short worm-like micelles and entangled long worm-like micelles when the temperature changes.

1.1.2.1. Gels Based on Jamming/Packing of Discrete Micelles of Thermosensitive Block Copolymers in Water

At sufficiently high concentrations, discrete spherical micelles of thermosensitive hydrophilic block copolymers are packed into an ordered structure in water, forming physically jammed or packing micellar hydrogels. The spherical micelles can be formed from either thermosensitive AB diblock or ABA triblock copolymers (Scheme 1.1). AB diblock copolymers consist of a thermosensitive block and a more water-soluble block with an appropriate block length ratio undergo a transition from hydrated to a dehydrated state when the temperature is above the LCST of the thermosensitive block and thus self-assemble into spherical micelles with the



Scheme 1.1. Physical Packing-based Micellar Hydrogels Formed from Thermosensitive AB Diblock or ABA Triblock Copolymers

thermosensitive block associating into the core and the water soluble block forming the corona. For example, water-soluble poly(ethylene oxide) (PEO)-based AB block copolymers have been widely studied. Hennink et al. synthesized block copolymers composed of a PEO block and a thermosensitive PNIPAM block that contained lactate side chains and found an increase of the LCST of the thermosensitive block with the hydrolysis of the lactate side groups.¹³ Based on the PEO-containing AB diblock copolymers, our group developed a series of multi-responsive diblock copolymers, such as thermo- and light-responsive, or thermo- and pH-responsive, by incorporating a small amount of light- or pH-responsive polymers into the thermosensitive block.^{14,15} Besides the PEO-containing block copolymers, other thermosensitive water-soluble AB diblock copolymers that can form spherical micellar gels have also been reported. Aoshima et al. synthesized double thermosensitive diblock copolymers with different LCSTs and found unique physical gelation which exhibited four different stages, including clear liquid, transparent gel, hot clear liquid and opaque mixture by phase separation with increasing temperature.¹⁶

For the ABA triblock copolymers composed of a thermosensitive central block and water soluble outer blocks, such as PEO-*b*-poly(propylene oxide)-*b*-PEO (PEO-*b*-PPO-*b*-PEO, Pluronics), the dehydrated central block self-associates into a core at temperatures above the LCST of the thermosensitive block and the outer blocks forming the corona; at sufficiently high concentrations, the aqueous solutions of these polymers can undergo thermally induced sol-gel transitions, forming micellar hydrogels.^{10,17}

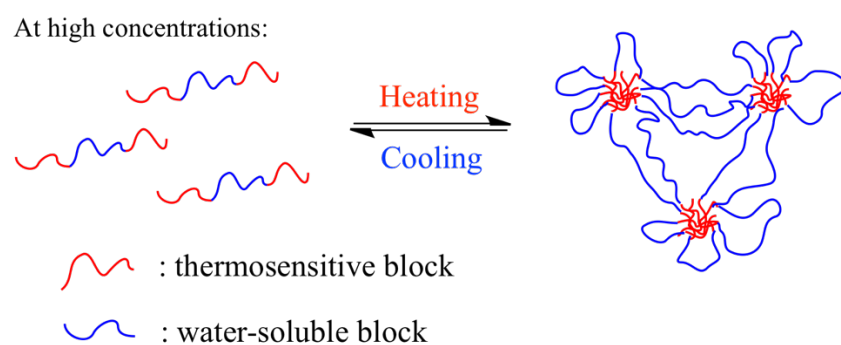
An interesting behavior of moderately concentrated aqueous solutions of thermosensitive block copolymer spherical micelles is that they can undergo sol-gel-sol transitions upon heating. The sol-gel phase diagrams of these block copolymers in water is usually a C-shaped curve. For the PEO-containing block copolymers, the lower temperature sol-gel boundary is driven by the

micellization and the ordering of micelles with increasing temperature and the upper gel-sol boundary results from the shrinking of PEO corona at higher temperatures (Scheme 1.1). Doubly thermosensitive diblock copolymers composed of two thermosensitive polymers with different LCSTs exhibit similar C-shaped sol-gel diagrams in water. It has been reported that the two boundaries of the sol-gel phase diagram can be tuned via changing the LCST of each thermosensitive block by incorporating a small portion of pH-responsive polymers into the thermosensitive block.¹⁸⁻²⁰ The LCST of each thermosensitive block can then be tuned by changing the solution pH value.

However, to form micellar hydrogels by jamming or packing of discrete block copolymer micelles into an ordered structure, this gelation mechanism usually requires a minimum polymer concentration of around 20 wt%.²¹ In contrast, the critical gelation concentrations for the formation of physical crosslinked, 3-dimensional network hydrogels of thermosensitive block copolymers are usually < 10 wt % and it can be as low as 5 wt % to form a free-standing gel.²²

1.1.2.2. Physically Crosslinked Network Hydrogels of Thermosensitive Block Copolymers

For thermosensitive hydrophilic ABA triblock copolymers, if the central block is permanently water soluble while the outer blocks are thermoresponsive, the outer blocks will self-associate in a dilute aqueous solution into the core and the central block form loops in the corona layer (i.e., flower micelles) when the temperature is increased to above the LCST of the outer blocks. If the concentration is above the critical gelation concentration, a physically crosslinked, 3-D micellar network hydrogel is formed, in which the central block forming bridges among neighboring micellar cores (Scheme 1.2). Compared with chemically crosslinked hydrogels, the thermosensitive physically crosslinked gels are advantageous for certain biomedical applications



Scheme 1.2. Physically Crosslinked Network Hydrogels Formed from Thermosensitive ABA Triblock Copolymers

due to their reversible sol-gel transitions. Also, thermosensitive ABA triblock copolymers can form hydrogels at concentrations much lower than AB diblock copolymers as discussed in the previous section. Thus physically crosslinked block copolymer hydrogels received tremendous interest in the past years and they have great potentials in a variety of applications including drug delivery and tissue engineering.^{11,12,23,24} There have been many reports on such hydrogels formed by thermosensitive ABA triblock copolymers. For example, Armes et al. synthesized biocompatible PNIPAM-*b*-poly(2-methacryloyloxyethyl phosphorylcholine)-*b*-PNIPAM (PNIPAM-*b*-PMPC-*b*-PNIPAM) and this ABA triblock copolymer with a concentration of 6.5 wt% was capable of forming a free-standing physical gel upon increasing temperatures.²⁵ Other water-soluble polymers were also used as the central block, such as poly(*N,N*-dimethylacrylamide) (PDMA), and similar thermosensitive ABA triblock copolymer PNIPAM-*b*-PDMA-*b*-PNIPAM was also synthesized.²⁶

Among all ABA triblock copolymers for the formation of network-based hydrogels, PEO is a commonly used central block because the narrow dispersed PEO polymers with different molecular weights are commercially available and the chain ends can be easily functionalized. Joergensen et al. studied the phase behavior of PPO-*b*-PEO-*b*-PPO in aqueous solutions.²⁷ Bae, Lee and coworkers developed a series of injectable ABA triblock copolymer hydrogels, including poly(*L*-lactic acid-*co*-glycolide)-*b*-PEO-*b*-poly(*L*-lactic acid-*co*-glycolide) (PLGA-*b*-PEO-*b*-PLGA), poly(ϵ -caprolactone-*co*-lactide)-*b*-PEO-*b*-poly(ϵ -caprolactone-*co*-lactide) (PCLA-*b*-PEO-*b*-PCLA).^{11,28,29} Similar to doubly responsive AB diblock copolymers, various well-defined doubly responsive ABA triblock copolymers were thoroughly investigated, such as thermo- and pH- responsive triblock copolymer poly(methoxydi(ethylene glycol) methacrylate-*co*-methacrylic acid)-*b*-PEO-*b*-poly(methoxydi(ethylene glycol) methacrylate-*co*-methacrylic acid)

(P(DEGMMA-*co*-MAA)-*b*-PEO-*b*-P(DEGMMA-*co*-MAA)) and thermo- and light-responsive triblock copolymer poly(ethoxytri(ethylene glycol) acrylate-*co*-*o*-nitrobenzyl acrylate)-*b*-PEO-*b*-poly(ethoxytri(ethylene glycol) acrylate-*co*-*o*-nitrobenzyl acrylate) (P(TEGEA-*co*-NBA)-*b*-PEO-*b*-P(TEGEA-*co*-NBA)).^{22,30-32} These narrow-dispersed doubly responsive ABA triblock copolymers were synthesized via “living”/controlled radical polymerization. For example, the ATRP initiator can be easily functionalized onto the chain ends of PEO so that the A blocks can be grown on both sides simultaneously via ATRP.

The rheological properties of aqueous physical crosslinked gels of thermosensitive ABA triblock copolymers have been studied. For example, Hennink et al. prepared poly(*N*-(2-hydroxypropyl) methacrylamide lactate)-*b*-PEO-*b*-poly(*N*-(2-hydroxypropyl) methacrylamide lactate) (PHPMAM_{lac}-*b*-PEO-*b*-PHPMAM_{lac}) triblock copolymer samples at different high concentrations and found that the dynamic storage modulus G' became higher with increasing concentration and the strengths of the gels were negatively correlated to the molecular weight of the thermosensitive outer blocks.³³ The plateau modulus of an “ideal” physically crosslinked hydrogel formed by a thermosensitive ABA triblock copolymer can be described by a theoretical equation, $G' = \nu k_B T$, where ν is the number of elastically active bridging chains per unit volume, k_B is Boltzmann constant, and T is the absolute temperature. If every central blocks were elastically effective, then $\nu = cN_A/M$, where c is the concentration of polymer solution, N_A is the Avogadro's number and M is the molecular weight of the triblock copolymer.³⁴ It has been previously reported that the sol-to-gel transition of an ABA triblock copolymer aqueous solution is broader than the AB diblock copolymer with similar compositions due to the different gelation mechanisms between the physical crosslinked gels and jamming of spherical micellar gels.³⁰ Also for the PEO-based ABA triblock copolymer hydrogels, there is a decrease of G' at elevated temperatures

because the solubility of PEO in water becomes poor at high temperatures such that the PEO bridges in the gel undergo shrinkage.³⁰

For thermosensitive hydrophilic ABA triblock copolymers in water, the temperature-induced micellization and gelation occur simultaneously, which leads to a formation of loops during the gelation process for a large portion of polymer molecules. This has prompted the investigation of thermosensitive ABC triblock copolymer gelators, where the micellization and gelation can be separated. Armes et al. synthesized the doubly thermoresponsive PPO-*b*-PMPC-*b*-PNIPAM ABC triblock copolymers with different LCSTs for the outer blocks and a water-soluble block as the central block.³⁵ However, the gelation efficiency was even worse than that of ABA triblock copolymers because of the occurrence of intramicellar collapse of the outer block prior to the intermicellar hydrophobic interactions. Later Zhou et al. prepared two-compartment hydrogels of thermoresponsive poly(ethylene-*alt*-propylene)-*b*-PEO-*b*-PNIPAM (PEP-*b*-PEO-*b*-PNIPAM) via a two-step process.^{36,37} The triblock copolymer completely self-assembled into spherical micelles with the water-insoluble block forming the core at lower temperatures, and then the solution turned into a two-compartment micellar hydrogel upon increasing the temperature to above the LCST of PNIPAM. Thus the two-compartment gelation process resulted in a higher gelation efficiency, with a free-standing gel formed from a 5 wt% concentration, and the CGC is around only 2 wt%. These thermosensitive ABC triblock copolymers provide new methods to design and develop smart hydrogels with enhanced properties.

1.1.2.3. Worm-Like Block Copolymer Micellar Hydrogels

For AB diblock copolymers, wormlike micellar gels can be formed at a specific ratio of degrees of polymerization (DP) of the water-soluble block and water-insoluble block. Armes et al. reported

a thermosensitive diblock copolymer poly(glycerol monomethacrylate)-*b*-poly(2-hydroxypropyl methacrylate) (PGMA-*b*-PHPMA) that can form a free-standing physical hydrogel at 21 °C by interworm entanglements and the gel dissolves on cooling to 4 °C due to the unusual worm-to-sphere transition.³⁸ The thermosensitive behavior of the PGMA-*b*-PHPMA diblock copolymer is due to the weakly hydrophilic nature of the PHPMA blocks, which have intrachain and interchain hydrogen bonding.³⁹ However, the wormlike morphology is very difficult to target than spherical and vesicular phases because their phase region is relatively narrow and the worm gels were insufficiently robust.^{40,41} Later they designed the worm micellar gels that contained disulfide bonds within some of the PGMA chains which improved the gel property and adhered more strongly to the mesh sheet (Figure 1.2).^{41,42} These worm gels offer an interesting opportunity for biomedical applications such as drug delivery via mucosal membranes.

1.1.3. Hybrid Hydrogels of Thermosensitive Block Copolymers and Nanoparticles

Inorganic or metallic nanoparticles (NPs) with a size of a few to tens of nanometers, such as gold, magnetic, silica NPs, exhibit intriguing optical, magnetic, mechanical, or electronic properties and thus are widely studied in the past years and they have potential applications including catalysis and biomedicine.⁴³⁻⁴⁶ Incorporating these NPs into the hydrogels imparts the hybrid hydrogel materials new properties that are usually not possessed by the polymers.⁴⁷⁻⁵⁰ For example, Stark et al. functionalized carbon-coated cobalt nanoparticles (C/Co NPs) with 4-vinyl-biphenyl and then copolymerized them with 2-hydroxyethyl methacrylate (HEMA) crosslinked by ethylene glycol dimethacrylate (EGDMA). Under an electromagnetic field, the magnetic hydrogels with 60 wt% metallic cobalt could be stretched to 123 % of their initial length without negatively affecting the stability and shape memory.⁵¹ These hybrid magnetic hydrogels may

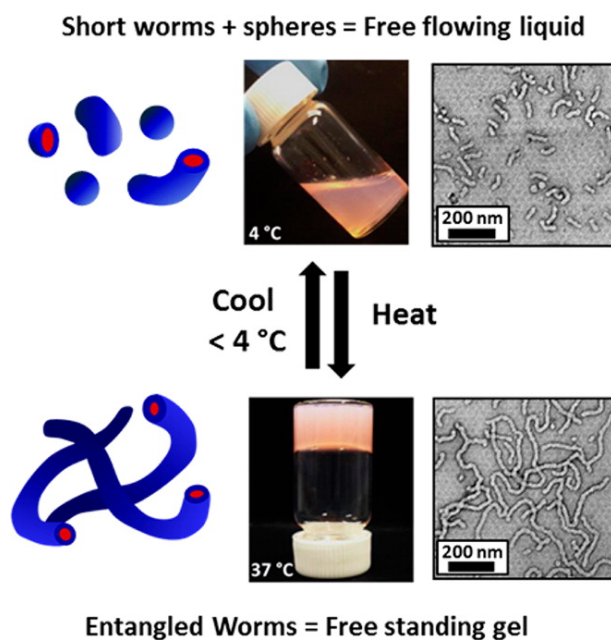


Figure 1.2. Photographs and TEM images obtained at 37 °C and 2 °C illustrating the temperature-dependent (de)gelling behavior of the disulfide-functionalized copolymer worms. (Reprinted from Ref. 41, with permission from American Chemical Society).

facilitate the use of soft actuators in medical implants or micro-pumps. Schmidt et al. synthesized nanocomposite hydrogels by photo-crosslinking PEO-*b*-PPO-*b*-PEO triblock copolymer diacrylates in the presence of silicate nanoparticles, Laponite. The resulting hybrid materials allow extensive stretching up to 1300 % and improved toughness, because the covalent crosslinking of polymer chains leads to the formation of an elastic network, whereas physical crosslinking between nanoparticles and polymer chains induces viscoelastic properties.⁵² Ding and coworkers made hybrid hydrogels composed of PNIPAM and gold nanoparticles by copolymerization of vinyl group-functional Au nanoparticles with *N*-isopropylacrylamide. They found that the electrical conductivity of the nanocomposite changed by two orders of magnitude upon temperature changes.⁵³

For the hybrid micellar hydrogels of thermosensitive block copolymers and NPs, there were some intriguing reports related to the locations of NPs in thermosensitive block copolymer micellar gels. For example, Walker et al. added pre-made hydrophilic silica NPs into the aqueous solution of PEO-*b*-PPO-*b*-PEO (Pluronic) and found that the block copolymer formed cubic crystal template upon increasing temperature and the hydrophilic NPs were located in the interstitial space among micelles (Figure 1.3).⁵⁴⁻⁵⁶ Muhammed et al. functionalized superparamagnetic iron oxide NPs with Pluronic F127 copolymers and mixed the resultant magnetic NPs in the aqueous solution of Pluronic F127. Upon heating, the Pluronic associated into micelles via hydrophobic interaction of the PPO blocks, and the magnetic NPs were located in the core of micelles (Figure 1.4).⁵⁷ They loaded a hydrophobic drug into the hybrid hydrogels and showed that the controlled release of the drug can be modulated with a magnetic field. In the above examples, the NPs were located either inside or outside the core of micelles in block copolymer hydrogels, depending on whether the NPs were either hydrophobic or hydrophilic. Besides the hydrophobic interactions

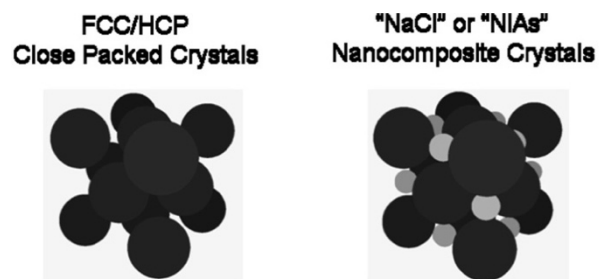


Figure 1.3. Schematic representation of a close-packed crystal of spherical micelles (left) and of a nanocomposite crystal that is formed when smaller particles are inserted into the octahedral interstitial cavities (right). (Reproduced from Ref. 55, with permission from American Chemical Society).

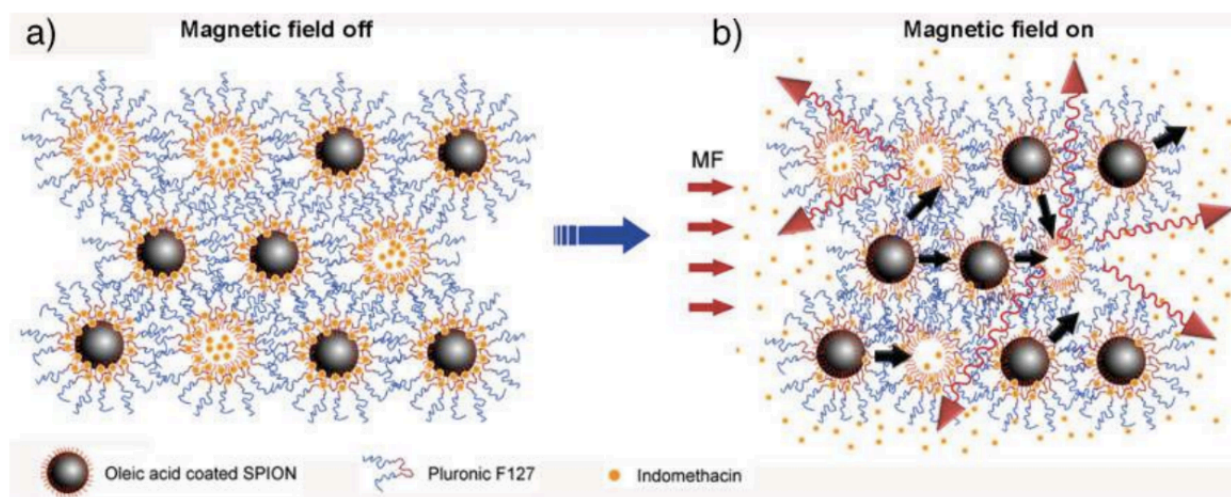


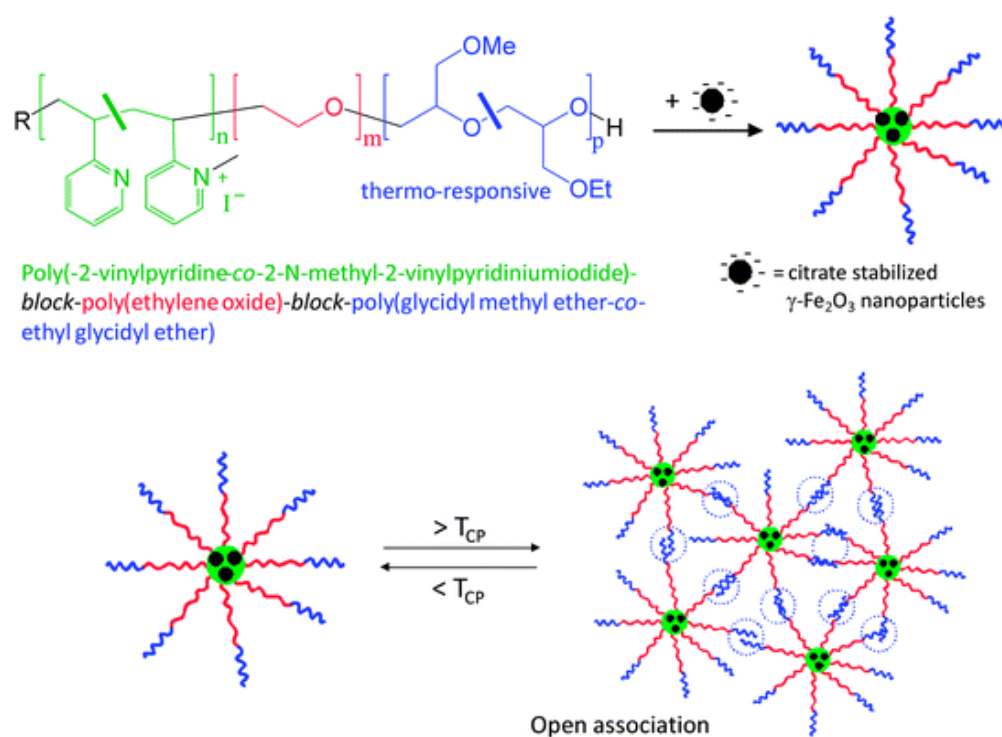
Figure 1.4. Schematic representation of ordered microstructure of hybrid hydrogels of Pluronic and magnetic NPs: (A) before applying the magnetic field (MF), indomethacin (IMC) drug molecules are encapsulated in the hydrophobic core of micelles and the magnetic NPs are also located in the core of micelles; (B) when the MF is on, the magnetic NPs orient and approach each other, squeezing the micelles and leading to enhancement of IMC release. (Reproduced from Ref. 57, with permission from John Wiley and Sons).

between the collapsed core of micelles and hydrophobic NPs, the NPs can also be located in the core of micelles via electrostatic interactions. Schmalz et al. synthesized an ABC triblock copolymer poly(2-vinylpyridine)-*b*-PEO-*b*-poly(glycidyl methyl ether-*co*-ethyl glycidyl ether) (Pq2VP-*b*-PEO-*b*-P(GME-*co*-EGE)). They mixed the ABC triblock copolymer with superparamagnetic maghemite nanoparticles stabilized with sodium citrate in water, thus the negatively charged magnetic NPs were located in the positively charged Pq2VP core of the micelles.⁵⁸ These hybrid hydrogels exhibited reversible gelation upon magnetic inductive heating using an AC magnetic field (Scheme 1.3).

However, it remains unknown how the locations of NPs affect the rheological behavior of the hybrid hydrogels. It is worthwhile to investigate the rheological behavior of hybrid hydrogels because their mechanical properties are crucial to many biomedical fields, such as cell growth and differentiation.⁵⁹ Therefore, a fundamental study of the effects of NP locations on hybrid hydrogel properties will be useful for the future design and development of new hydrogel materials.

1.1.4. Polymer Brush-Grafted Nanoparticles

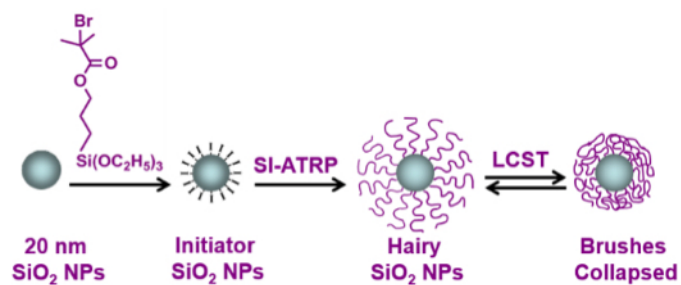
Polymer brush-grafted particles are composed of an inorganic or metallic core and a layer of polymer chains densely tethered by one end to the surface of the core NP. These hybrid nanoparticles have received growing interests because they can exhibit combined advantages of both the nanoparticles, such as optical, magnetic or mechanical properties, and polymers, such as stimuli-responsive properties. Generally, these hairy particles can be made by growing polymer brushes from initiator-functionalized particles via surface-initiated polymerization or by grafting end-functionalized polymers onto the particle surface.⁶⁰⁻⁶² Among these techniques, the surface-initiated “living”/controlled polymerization methods are advantageous because the grafting



Scheme 1.3. Illustration of Hybrid Micelles of Citrate Stabilized Magnetic NPs with a Quaternized Pq2VP-*b*-PEO-*b*-P(GME-*co*-EGE) Triblock Copolymer, and Subsequent Reversible Gelation via Open Association of Hybrid Micelles at Temperatures above the Cloud Point of P(GME-*co*-EGE) block. (Reprinted from Ref. 58, with permission from Royal Society of Chemistry)

densities of the hairy particles made by “grafting-from” are usually higher than those made by “grafting-to” and the “living”/controlled polymerization techniques can provide control on the molecular weight and molecular weight distribution of the grafted polymers.⁶³ Many surface-initiated “living”/controlled polymerization techniques have been developed, including ATRP, reversible radical addition-fragmentation chain transfer (RAFT) polymerization, nitroxide-mediated radical polymerization (NMRP), and living anionic polymerization.^{62,64-66} By using SI-ATRP or SI-NMRP, our group has developed a series of hairy particles and studied their stimuli-responsive, stimuli-triggered phase transfer, phase separation, as well as some unique reversible sol-gel transition behaviors.^{7,67-71}

Among these studies, hairy particles that can undergo structural or conformation changes in response to external triggers are an intriguing class of responsive hybrid materials.^{60, 72} These environmentally responsive properties are usually due to the stimuli-responsive polymer brushes grafted on the particles. For example, thermosensitive PDEGMMA and PTEGMMA brush-grafted silica particles were synthesized via SI-ATRP and their thermoresponsive properties were investigated by Li and coworkers (Scheme 1.4).⁷ They observed a decrease in hydrodynamic size of the hairy particles upon increasing the temperature above their LCST and the thermally-induced LCST transitions of polymer brushes on silica particles began at a lower temperature and the transition range was broader than those of free polymers in water. Other stimuli-responsive hairy particles, such as light-responsive and pH-responsive hairy particles, have also been reported. Yang et al. synthesized photoresponsive poly(methacrylated spiropyran) grafted silica particles via SI-ATRP and found that the polymer brushes underwent a reversible transition from a hydrophobic state to a hydrophilic state upon UV irradiation.⁷³ Duan et al. prepared mixed PEO/pH responsive poly(2-(diethylamino)ethyl methacrylate) brush-grafted gold nanoparticles via a sequential



Scheme 1.4. Synthesis of Thermoresponsive Hairy Nanoparticles by SI-ATRP

“grafting to” and SI-RAFT method; these hairy nanoparticles could assemble into two-dimensional arrays at oil-water interfaces controlled by pH changes.⁷⁴

Nanoparticles with a size range from a few to tens nanometers have received growing interest due to their exceptional promising applications in medicine, biomedical imaging, and energy harvesting and storage field.⁷⁵⁻⁷⁷ For the hybrid hydrogels of thermosensitive block copolymers and NPs, the hydrodynamic size of the block copolymer micelles is usually around 50 nm to a few hundred nm based on the molecular weight and structure of the block copolymer micelles. Thus the size of particles should be reasonably small for use in the study of hybrid hydrogels. However, because of their small sizes, surface forces dominate and nanoparticles tend to aggregate. Currently two approaches have been extensively employed in practice; one is electrostatic stabilization which utilizes the charges on the surface of nanoparticles in solution for stabilization and the other is steric stabilization which uses physically or chemically attached polymers.^{78,79} Thus the polymer brushes that are grafted onto nanoparticles not only stabilize the nanoparticles but could also endow the nanoparticles with new functions and properties.

1.2. Dissertation Overview

This dissertation research is devoted to the synthesis and rheology study of hybrid micellar hydrogels of thermosensitive triblock copolymers and thermoresponsive polymer brush-grafted NPs. In particular, we developed a method to tune and control the locations of hairy NPs in the micellar network hydrogels via tuning the LCST of NPs relative to that of thermosensitive triblock copolymers and investigated the rheological behaviors of the hybrid hydrogels.

Chapter 2 presents a systematic study on the effect of the locations of thermoresponsive hairy NPs in the thermosensitive ABA triblock copolymer micellar network hydrogels on gel properties.

The hairy NPs were synthesized from an ATRP initiator-functionalized silica NPs with a size of around 20 nm by SI-ATRP and the thermosensitive ABA triblock copolymer was synthesized by ATRP using a difunctional macroinitiator Br-PEO-Br. During the polymerization, a very small amount of fluorescence resonance energy transfer (FRET) donor monomer rhodamine B-functionalized methacrylate was incorporated in the outer blocks of the ABA copolymer and a very small fraction of FRET acceptor monomer nitrobenzofurazan-functionalized methacrylate was incorporated in the polymer brushes that were grown on the surface of NPs. The LCST of the thermoresponsive hairy NPs ($LCST_{NP}$) and the thermosensitive ABA triblock copolymer ($LCST_{ABA}$) can be tuned by using distinct thermoresponsive polymers or by copolymerizing two different monomers at a specific ratio. The NPs will be located in the core of block copolymer micelles if the $LCST_{NP}$ is similar to the $LCST_{ABA}$ upon heating from below to above their LCSTs, while the NPs will be located outside the micelles if the $LCST_{NP}$ is much higher to the $LCST_{ABA}$. The different locations of hairy NPs were confirmed by FRET in dilute solutions and the effects of locations of hairy NPs and NP-to-polymer mass ratio on properties of hybrid hydrogels with a polymer concentration at 10 wt% and various amounts of hairy NPs were investigated by rheological measurements. When the hairy NPs were located inside the core of micelles, both the sol-gel transition temperature ($T_{sol-gel}$) and the dynamic storage modulus G' did not change much with the increase of the NP-to-polymer mass ratio. In contrast, the $T_{sol-gel}$ of the hybrid hydrogels with NPs in the interstitial space increased slightly while the G' decreased significantly with increasing the NP-to-polymer mass ratio. In addition, a noticeable increased in G' was observed at the $LCST_{NP}$ for the hybrid hydrogels with NPs in the interstitial space. A further study of this phenomenon in detail will be presented in the next chapter.

Chapter 3 describes a study of the rheological effect of LCST_{NP} on hybrid micellar network hydrogels with the hairy NPs located in the interstitial space of micelles. Four batches of hairy NPs with different LCSTs and a thermosensitive ABA triblock copolymer that has a similar composition and LCST to the one used in Chapter 2 were synthesized; all of the LCST_{NP} were higher than the LCST_{ABA} so that the hairy NPs were all located initially in the interstitial space of micelles. The rheological measurements were conducted for all hybrid micellar network hydrogels composed of the ABA triblock copolymer and hairy NPs with different LCSTs with a polymer concentration of 10 wt% and various NP-to-polymer mass ratios. A sharp increase of G' was observed in the heating ramp at a temperature around the LCST_{NP} for all the hybrid hydrogel samples. An explanation for this phenomenon was proposed and confirmed by FRET experiments.

Chapter 4 presents a method to improve the gelation efficiency of doubly thermosensitive hydrophilic ABC triblock copolymers with outer blocks being thermosensitive and having different LCSTs by adding thermoresponsive hairy NPs with a LCST similar to that of the higher LCST C block of the ABC copolymer. The triblock copolymer, synthesized by sequential RAFT polymerizations, was composed of a thermosensitive A block that shows a lower LCST (LCST_{L}), a permanently water-soluble, charged B block, and a thermosensitive C block that has a higher LCST (LCST_{H}). Two batches of thermoresponsive hairy NPs were synthesized using the same method described in the previous chapters with one batch (NP-29.5) having a similar LCST to LCST_{H} and the other one (NP-51) having a much higher LCST. By incorporating NP-29.5 into the aqueous solutions of the ABC triblock copolymer with a polymer concentration 6 wt%, we observed a significant increase of G' from the heating ramps. This is because the hairy NPs acted as “seeds” to adsorb the collapsed higher LCST block of the ABC copolymer upon increasing temperature above LCST_{H} , promoting the formation of bridging chains among micellar cores and

NPs and thus enhancing the gelation efficiency. In contrast, no such benefit was observed when NP-51 was loaded into aqueous solutions of the ABC copolymer.

Chapter 5 describes a route for the synthesis of thermoresponsive polymer brushes grafted mesoporous silica nanoparticles (MSNs) with a size of 30-40 nm by SI-ATRP. Studies by nuclear magnetic resonance spectroscopy (NMR), thermogravimetric analysis (TGA), dynamic light scattering (DLS), and transmission electron microscopy (TEM) indicated the grafting of polymer brushes on MSNs. The hairy MSNs are ideal candidates for preparation of hybrid hydrogels of thermosensitive block copolymers and hairy NPs because they introduce new functions to the injectable hydrogels.

A summary of this dissertation research and future work are provided in Chapter 6.

1.3 References

1. Seuring, J.; Agarwal, S. *Macromol. Rapid Comm.* **2012**, *33*, 1898-1920.
2. Aseyev, V.; Tenhu, H.; Winnik, F. M. *Adv. Polym. Sci.* **2010**, *242*, 29-89.
3. Schild, H. G. *Prog. Polym. Sci.* **1992**, *17*, 163-249.
4. Dautzenberg, H.; Gao, Y.; Hahn, M. *Langmuir* **2000**, *16*, 9070-9081.
5. Han, S.; Hagiwara, M.; Ishizone, T. *Macromolecules* **2003**, *36*, 8312-8319.
6. Ishizone, T.; Seki, A.; Hagiwara, M.; Han, S.; Yokoyama, H.; Oyane, A.; Deffieux, A.; Carlotti, S. *Macromolecules* **2008**, *41*, 2963-2967.
7. Li, D.; Jones, G. L.; Dunlap, J. R.; Hua, F.; Zhao, B. *Langmuir* **2006**, *22*, 3344-3351.
8. Lutz, J.-F.; Hoth, A. *Macromolecules* **2006**, *39*, 893-896.
9. Gil, E. S.; Hudson, S. M. *Prog. Polym. Sci.* **2004**, *29*, 1173-1222.
10. Hamley, I. W., *Block Copolymers in Solution: Fundamentals and Applications*. John Wiley & Sons: Chichester, UK, 2005.
11. He, C.; Kim, S. W.; Lee, D. S. *J. Control Release.* **2008**, *127*, 189-207.
12. Yu, L.; Ding, J. *Chem. Soc. Rev.* **2008**, *37*, 1473-1481.
13. Neradovic, D.; van Steenberg, M. J.; Vansteelant, L.; Meijer, Y. J.; van Nostrum, C. F.; Hennink, W. E. *Macromolecules* **2003**, *36*, 7491-7498.
14. Jiang, X.; Jin, S.; Zhong, Q.; Dadmun, M. D.; Zhao, B. *Macromolecules* **2009**, *42*, 8468-8476.
15. Jiang, X.; Zhao, B. *Macromolecules* **2008**, *41*, 9366-9375.
16. Sugihara, S.; Kanaoka, S.; Aoshima, S. *Macromolecules* **2005**, *38*, 1919-1927.
17. Hvidt, S.; Joergensen, E. B.; Brown, W.; Schillen, K. *J. Phys. Chem.* **1994**, *98*, 12320-12328.

18. Jin, N.; Woodcock, J. W.; Xue, C.; O'Lenick, T. G.; Jiang, X.; Jin, S.; Dadmun, M. D.; Zhao, B. *Macromolecules* **2011**, *44*, 3556-3566.
19. Jin, N.; Zhang, H.; Jin, S.; Dadmun, M. D.; Zhao, B. *The Journal of Physical Chemistry B* **2012**, *116*, 3125-3137.
20. Jin, N.; Zhang, H.; Jin, S.; Dadmun, M. D.; Zhao, B. *Macromolecules* **2012**, *45*, 4790-4800.
21. Jeong, B.; Bae, Y. H.; Lee, D. S.; Kim, S. W. *Nature* **1997**, *388*, 860-862.
22. Woodcock, J. W.; Wright, R. A. E.; Jiang, X.; O'Lenick, T. G.; Zhao, B. *Soft Matter* **2010**, *6*, 3325-3336.
23. Joo, M. K.; Park, M. H.; Choi, B. G.; Jeong, B. *J. Mater. Chem.* **2009**, *19*, 5891-5905.
24. Ahn, S.-k.; Kasi, R. M.; Kim, S.-C.; Sharma, N.; Zhou, Y. *Soft Matter* **2008**, *4*, 1151-1157.
25. Li, C.; Tang, Y.; Armes, S. P.; Morris, C. J.; Rose, S. F.; Lloyd, A. W.; Lewis, A. L. *Biomacromolecules* **2005**, *6*, 994-999.
26. Kirkland, S. E.; Hensarling, R. M.; McConaughy, S. D.; Guo, Y.; Jarrett, W. L.; McCormick, C. L. *Biomacromolecules* **2008**, *9*, 481-486.
27. Mortensen, K.; Brown, W.; Joergensen, E. *Macromolecules* **1994**, *27*, 5654-5666.
28. Jeong, B.; Kim, S. W.; Bae, Y. H. *Adv. Drug Deliver. Rev* **2002**, *54*, 37-51.
29. Shim, W. S.; Yoo, J. S.; Bae, Y. H.; Lee, D. S. *Biomacromolecules* **2005**, *6*, 2930-2934.
30. O'Lenick, T. G.; Jiang, X.; Zhao, B. *Langmuir* **2010**, *26*, 8787-8796.
31. Woodcock, J. W.; Jiang, X.; Wright, R. A. E.; Zhao, B. *Macromolecules* **2011**, *44*, 5764-5775.
32. Henn, D. M.; Wright, R. A. E.; Woodcock, J. W.; Hu, B.; Zhao, B. *Langmuir* **2014**, *30*, 2541-2550.

33. Vermonden, T.; Besseling, N. A. M.; van Steenberghe, M. J.; Hennink, W. E. *Langmuir* **2006**, *22*, 10180-10184.
34. Noro, A.; Matsushita, Y.; Lodge, T. P. *Macromolecules* **2009**, *42*, 5802-5810.
35. Li, C.; Buurma, N. J.; Haq, I.; Turner, C.; Armes, S. P.; Castelletto, V.; Hamley, I. W.; Lewis, A. L. *Langmuir* **2005**, *21*, 11026-11033.
36. Zhou, C.; Hillmyer, M. A.; Lodge, T. P. *J. Am. Chem. Soc.* **2012**, *134*, 10365-10368.
37. Zhou, C.; Toombes, G. E. S.; Wasbrough, M. J.; Hillmyer, M. A.; Lodge, T. P. *Macromolecules* **2015**, *48*, 5934-5943.
38. Verber, R.; Blanazs, A.; Armes, S. P. *Soft Matter* **2012**, *8*, 9915-9922.
39. Madsen, J.; Armes, S. P.; Lewis, A. L. *Macromolecules* **2006**, *39*, 7455-7457.
40. Blanazs, A.; Madsen, J.; Battaglia, G.; Ryan, A. J.; Armes, S. P. *J. Am. Chem. Soc.* **2011**, *133*, 16581-16587.
41. Simon, K. A.; Warren, N. J.; Mosadegh, B.; Mohammady, M. R.; Whitesides, G. M.; Armes, S. P. *Biomacromolecules* **2015**, *16*, 3952-3958.
42. Warren, N. J.; Rosselgong, J.; Madsen, J.; Armes, S. P. *Biomacromolecules* **2015**, *16*, 2514-2521.
43. Roucoux, A.; Schulz, J.; Patin, H. *Chem. Rev.* **2002**, *102*, 3757-3778.
44. Daniel, M.-C.; Astruc, D. *Chem. Rev.* **2004**, *104*, 293-346.
45. Lu, A.-H.; Salabas, E. L.; Schüth, F. *Angewandte Chemie International Edition* **2007**, *46*, 1222-1244.
46. Lucky, S. S.; Soo, K. C.; Zhang, Y. *Chem. Rev.* **2015**, *115*, 1990-2042.
47. Balazs, A. C.; Emrick, T.; Russell, T. P. *Science* **2006**, *314*, 1107-1110.
48. Schexnailder, P.; Schmidt, G. *Colloid Polym. Sci.* **2009**, *287*, 1-11.

49. Messing, R.; Schmidt, A. M. *Polymer Chemistry* **2011**, *2*, 18-32.
50. Haraguchi, K. *Curr. Opin. Solid State Mater. Sci.* **2007**, *11*, 47-54.
51. Fuhrer, R.; Athanassiou, E. K.; Luechinger, N. A.; Stark, W. J. *Small* **2009**, *5*, 383-388.
52. Wu, C.-J.; Gaharwar, A. K.; Chan, B. K.; Schmidt, G. *Macromolecules* **2011**, *44*, 8215-8224.
53. Zhao, X.; Ding, X.; Deng, Z.; Zheng, Z.; Peng, Y.; Long, X. *Macromol. Rapid. Comm.* **2005**, *26*, 1784-1787.
54. Pozzo, D. C.; Walker, L. M. *Macromol. Symp.* **2005**, *227*, 203-210.
55. Pozzo, D. C.; Walker, L. M. *Macromolecules* **2007**, *40*, 5801-5811.
56. Pozzo, D. C.; Walker, L. M. *Eur. Phys. J. E* **2008**, *26*, 183-189.
57. Qin, J.; Asempah, I.; Laurent, S.; Fornara, A.; Muller, R. N.; Muhammed, M. *Adv. Mater.* **2009**, *21*, 1354-1357.
58. Reinicke, S.; Dohler, S.; Tea, S.; Krekhova, M.; Messing, R.; Schmidt, A. M.; Schmalz, H. *Soft Matter* **2010**, *6*, 2760-2773.
59. Seliktar, D. *Science* **2012**, *336*, 1124-1128.
60. Li, D.; Sheng, X.; Zhao, B. *J. Am. Chem. Soc.* **2005**, *127*, 6248-6256.
61. Kawahara, T.; Takeuchi, Y.; Wei, G.; Shirai, K.; Yamauchi, T.; Tsubokawa, N. *Polym. J* **2009**, *41*, 744-751.
62. Li, C.; Benicewicz, B. C. *Macromolecules* **2005**, *38*, 5929-5936.
63. Barbey, R.; Lavanant, L.; Paripovic, D.; Schüwer, N.; Sugnaux, C.; Tugulu, S.; Klok, H.-A. *Chem. Rev.* **2009**, *109*, 5437-5527.
64. Pyun, J.; Kowalewski, T.; Matyjaszewski, K. *Macromol. Rapid. Comm.* **2003**, *24*, 1043-1059.
65. Zhou, Q.; Wang, S.; Fan, X.; Advincula, R.; Mays, J. *Langmuir* **2002**, *18*, 3324-3331.

66. Bartholome, C.; Beyou, E.; Bourgeat-Lami, E.; Chaumont, P.; Zydowicz, N. *Macromolecules* **2003**, *36*, 7946-7952.
67. Horton, J. M.; Bao, C.; Bai, Z.; Lodge, T. P.; Zhao, B. *Langmuir* **2011**, *27*, 13324-13334.
68. Horton, J. M.; Bai, Z.; Jiang, X.; Li, D.; Lodge, T. P.; Zhao, B. *Langmuir* **2011**, *27*, 2019-2027.
69. Jiang, X.; Zhao, B.; Zhong, G.; Jin, N.; Horton, J. M.; Zhu, L.; Hafner, R. S.; Lodge, T. P. *Macromolecules* **2010**, *43*, 8209-8217.
70. Bao, C.; Tang, S.; Horton, J. M.; Jiang, X.; Tang, P.; Qiu, F.; Zhu, L.; Zhao, B. *Macromolecules* **2012**, *45*, 8027-8036.
71. Wright, R. A. E.; Hu, B.; Henn, D. M.; Zhao, B. *Soft Matter* **2015**, *11*, 6808-6820.
72. Zhao, B.; Zhu, L. *Macromolecules* **2009**, *42*, 9369-9383.
73. Wu, Y.; Zhang, C.; Qu, X.; Liu, Z.; Yang, Z. *Langmuir* **2010**, *26*, 9442-9448.
74. Cheng, L.; Liu, A.; Peng, S.; Duan, H. *ACS Nano* **2010**, *4*, 6098-6104.
75. Davis, M. E.; Chen, Z.; Shin, D. M. *Nat Rev Drug Discov* **2008**, *7*, 771-782.
76. Phillips, E.; Penate-Medina, O.; Zanzonico, P. B.; Carvajal, R. D.; Mohan, P.; Ye, Y.; Humm, J.; Gönen, M.; Kalaigian, H.; Schöder, H.; Strauss, H. W.; Larson, S. M.; Wiesner, U.; Bradbury, M. S. *Sci. Transl. Med.* **2014**, *6*, 260ra149-260ra149.
77. Srivastava, S.; Schaefer, J. L.; Yang, Z.; Tu, Z.; Archer, L. A. *Adv. Mater.* **2014**, *26*, 201-234.
78. Fritz, G.; Schädler, V.; Willenbacher, N.; Wagner, N. J. *Langmuir* **2002**, *18*, 6381-6390.
79. Zhulina, E. B.; Borisov, O. V.; Priamitsyn, V. A. *J. Colloid Interf. Sci* **1990**, *137*, 495-511.

**Chapter 2. Hybrid Micellar Hydrogels of a Thermosensitive ABA Triblock
Copolymer and Hairy Nanoparticles: Effect of Spatial Location of Hairy
Nanoparticles on Gel Properties**

Abstract

This chapter presents a method for control of spatial location of nanoparticles (NPs) in hybrid micellar hydrogels of a thermosensitive ABA triblock copolymer and polymer brush-grafted NPs (hairy NPs), either inside or outside the core of micelles, and the study of the effect of different locations of NPs on gel properties. Two batches of thermosensitive polymer brush-grafted, 17 nm silica NPs with different lower critical solution temperatures (LCSTs) and a thermosensitive ABA triblock copolymer composed of a poly(ethylene oxide) central block and thermosensitive outer blocks (ABA-D) were synthesized. The different locations of NPs were achieved by controlling the LCST of hairy NPs ($LCST_{NP}$) relative to that of the thermosensitive outer blocks of ABA-D ($LCST_{ABA}$). When the $LCST_{NP}$ and $LCST_{ABA}$ were similar, the NPs resided in the core of micelles upon heating from below the $LCST_{NP}$ and $LCST_{ABA}$. When the $LCST_{NP}$ was significantly higher, the NPs were located outside the core of micelles as confirmed by fluorescent resonance energy transfer. The effects of different locations of hairy NPs and NP-to-polymer mass ratio on properties of hybrid micellar hydrogels formed from aqueous solutions of ABA-D with a concentration of 10 wt % and various amounts of hairy NPs were studied by rheological measurements. The sol-gel transition temperature ($T_{sol-gel}$) and dynamic storage modulus G' of the gels with NPs inside the core of micelles did not change much with increasing the NP-to-polymer mass ratio. In contrast, the $T_{sol-gel}$ of gels with NPs in the interstitial space among micelles increased slightly and the G' decreased significantly with the increase of the NP-to-polymer ratio. The hairy NPs in the interstitial space appeared to affect the formation of polymer networks and increase the fraction of polymer loops, resulting in a lower density of bridging chains and thus a lower G' . In addition, for gels with NPs in the interstitial space, a noticeable increase in G' was observed in the heating

ramps above 40 °C, which was likely caused by the collapsed hairy NPs adsorbing polymer chains in the dangling and loop forms, increasing the density of bridging chains.

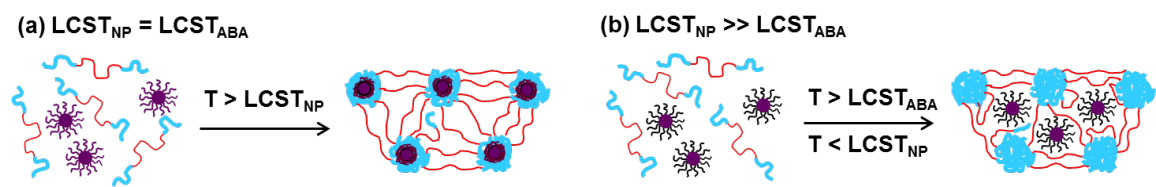
2.1. Introduction

Aqueous micellar gels of stimuli-responsive hydrophilic block copolymers have received considerable attention in the past years due to their in situ sol-gel transitions induced by external stimuli such as temperature, pH, light, etc. and their potential in a wide variety of applications including controlled and sustained release of substances.¹⁻⁵ Generally, there are two types of block copolymer micellar hydrogels.¹ One is the 3-dimensional (3-D) network hydrogels. For example, at a sufficiently high concentration, ABA triblock copolymers composed of a permanently hydrophilic central block and thermosensitive outer blocks can self-assemble into a 3-D network in water with the central block forming bridges among micelles at elevated temperatures.⁶⁻⁹ The second type of block copolymer hydrogels is formed by jamming or packing of discrete micelles into an ordered structure upon application of external stimuli. Examples of this type include the hydrogels of thermosensitive hydrophilic diblock copolymers.^{1, 10-11}

Inorganic and metal nanoparticles (NPs) with a size in the range of a few to tens of nanometers exhibit intriguing optical, electronic, magnetic, or mechanical properties that are usually not possessed by polymers.¹²⁻¹⁴ Rationally incorporating NPs into polymer hydrogels can produce functional nanocomposite hydrogel materials with synergistic combinations of two components.¹⁵⁻²⁹ Hybrid micellar hydrogels composed of thermosensitive hydrophilic block copolymers and various NPs have been reported in the literature.²²⁻²⁹ For example, Pozzo and Walker made hybrid aqueous micellar gels by adding hydrophilic silica NPs into aqueous solutions of poly(ethylene oxide)-*b*-poly(propylene oxide)-*b*-poly(ethylene oxide) (PEO-*b*-PPO-*b*-PEO, Pluronics) block copolymers.²²⁻²⁴ The hydrophilic silica NPs, which were smaller than the micelles, partitioned themselves into the interstitial cavities between the block copolymer micelles. The hybrid hydrogels were cocrystals of micelles and silica NPs, analogous to metallic alloys. Ferrogels,

which contained magnetic NPs, can respond to an external magnetic field.²⁵⁻²⁹ Qin et al. report a ferrogel by using Pluronic F127 to transfer hydrophobic 10.6 nm magnetic NPs into an aqueous solution and dispersing them in a 17.5 w/v % aqueous solution of F127 at low temperatures.²⁶ Gelation of the mixture occurred upon warming with NPs encapsulated in the micellar core. They reported that the release profile of a hydrophobic drug from the hybrid hydrogel can be modulated by using a static magnetic field. Krekhova et al. prepared hydroferrogels via gelation of aqueous maghemite ferrofluids using Pluronic P123 and showed that magnetic NPs can be effectively templated by the ordered P123 mesophases in a concentration range of 33–38 wt% for P123 and up to 14 wt% for NPs.²⁷ Philip et al. studied hybrid hydrogels composed of Pluronic F108 and iron oxide NPs and found that the addition of 1-5 wt % of Fe₃O₄ NPs into 15 wt % aqueous solutions of Pluronic F108 resulted in a decrease in the onset gelation temperature and dramatic alteration of the viscoelastic moduli.²⁸ Reinicke et al. reported magnetically responsive hydrogels based on hybrid micelles of ABC triblock copolymers and maghemite NPs.²⁹ The formation of hybrid micelles was driven by the electrostatic interaction between the charged NPs and the oppositely charged block of the triblock copolymer. The aqueous solutions of hybrid micelles exhibited reversible gelation upon magnetic inductive heating using an AC magnetic field.

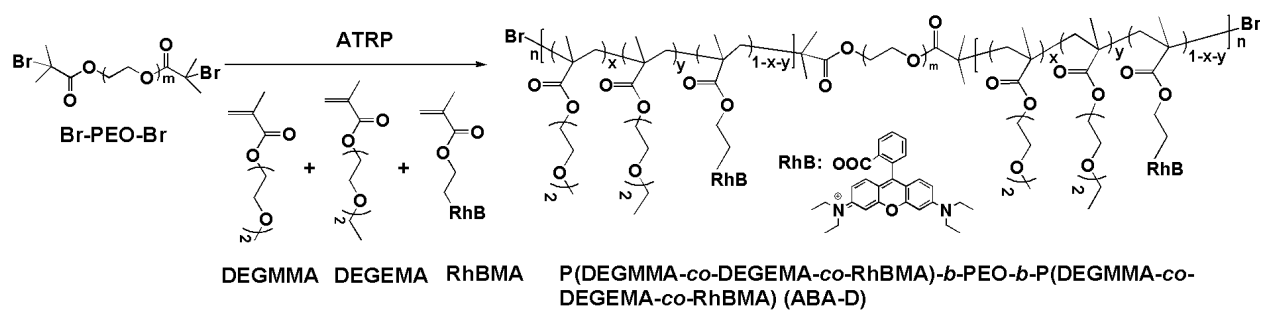
In the above studies, the NPs were either hydrophobic or hydrophilic and thus were positioned either inside or outside the core of micelles in block copolymer hydrogels.²²⁻²⁹ We are particularly interested in how different locations of NPs affect the gel properties. In the present work, we prepared hybrid micellar hydrogels of a thermosensitive ABA triblock copolymer and polymer brush-grafted silica NPs (hairy NPs) with NPs located either inside or outside the core of micelles (Scheme 2.1), and studied the effect of different locations of NPs on gel properties by rheological measurements. The different locations of NPs are achieved by controlling the lower critical



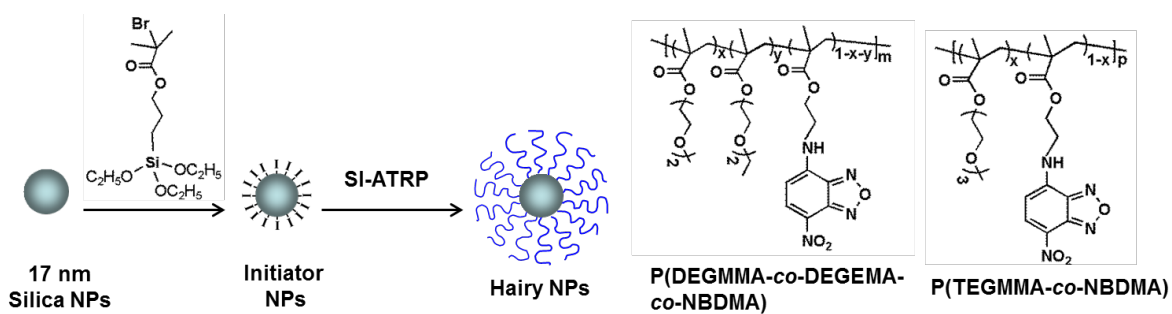
Scheme 2.1. Control of Spatial Location of NPs, Either Inside or Outside the Core of Micelles, in Hybrid Micellar Hydrogels of Thermosensitive ABA Triblock Copolymer and Hairy NPs

solution temperature (LCST) of hairy NPs ($LCST_{NP}$) relative to that of thermosensitive outer blocks of the ABA copolymer ($LCST_{ABA}$). When the $LCST_{NP}$ and $LCST_{ABA}$ are similar, the NPs are expected to reside in the core of micelles upon heating from below the $LCST_{NP}$ and $LCST_{ABA}$. If the $LCST_{NP}$ is significantly higher, the NPs will be outside the micelles.

The thermosensitive ABA triblock copolymer, P(DEGMMA-*co*-DEGEMA-*co*-RhBMA)-*b*-PEO-*b*-P(DEGMMA-*co*-DEGEMA-*co*-RhBMA) (designated as ABA-D, Scheme 2.2), was synthesized by atom transfer radical polymerization (ATRP) from a difunctional PEO macroinitiator with a molecular weight of 20 kDa. Two batches of thermosensitive hairy NPs, P(DEGMMA-*co*-DEGEMA-*co*-NBDMA) brush-grafted NPs (designated as NP-D) and P(TEGMMA-*co*-NBDMA) brush-grafted NPs (designated as NP-T) with different LCSTs, were prepared from the same batch of ATRP-initiator-functionalized, 17 nm silica NPs by surface-initiated ATRP (Scheme 2.3). The LCST of NP-D was designed to be similar to that of the thermosensitive outer blocks of ABA-D, while the LCST of NP-T was significantly higher. Note that the cloud points (CPs) of PDEGMMA, PDEGEMA, and PTEGMMA in water are 26, 4, and 52 °C, respectively.³⁰⁻³³ Fluorescence resonance energy transfer (FRET) was used to determine the location of NPs in the micellar solutions of ABA-D. FRET occurs only when the FRET donor and acceptor are within 1 to 10 nm.³⁴⁻³⁵ We incorporated NBDMA, a FRET donor,³⁵ into the polymer brushes and RhBMA, a FRET acceptor,³⁵ into the thermosensitive outer blocks of ABA-D via copolymerizations (Schemes 2 and 3). The NBD group in NBDMA emits at ~ 520 nm when excited at 480 nm, while Rhodamine B in RhBMA exhibits a broad absorbance band in the range of 500-600 nm and fluorescence emission at ~ 580 nm. If the NPs reside in the core of ABA-D micelles, the donor-acceptor pair would be within 10 nm and FRET is expected to occur. If the NPs are located outside the micelles, the distance between the FRET pair would be greater than



Scheme 2.2. Synthesis of Thermosensitive ABA Triblock Copolymer P(DEGMMA-*co*-DEGEMA-*co*-RhBMA)-*b*-PEO-*b*-P(DEGMMA-*co*-DEGEMA-*co*-RhBMA) (ABA-D) by ATRP



Scheme 2.3. Synthesis of Thermosensitive P(DEGMMA-*co*-DEGEMA-*co*-NBDMA) Brush-Grafted (NP-D) and P(TEGMMA-*co*-NBDMA) Brush-Grafted Silica NPs (NP-T) by Surface-Initiated ATRP from 17 nm Silica NPs

10 nm, result in either no or weak FRET. Two sets of hybrid micellar hydrogels of ABA-D and hairy NPs were prepared, and the effects of different locations of hairy NPs and NP-to-polymer mass ratio on properties of hybrid micellar hydrogels formed from aqueous solutions of ABA-D with a 10 wt % concentration and hairy NPs were studied by rheological measurements.

2.2. Experimental Section

2.2.1. Materials

Triethoxysilane (95%, Acros) was used as received. MIBK-ST (Nissan Chemical) is a dispersion of silica NPs with a size of 10-15 nm (according to the manufacturer) in methyl isobutyl ketone (30-31 wt % SiO₂). A platinum–divinyltetramethyldisiloxane complex in xylene (2.1–2.4% Pt concentration in xylene) was purchased from Gelest, Inc. CuBr (98%, Aldrich) was stirred in glacial acetic acid overnight, filtered, and washed with absolute ethanol and diethyl ether. The purified CuBr was dried under vacuum. *N,N,N',N',N''*-Pentamethyldiethylenetriamine (PMDETA, 99%, Aldrich) and ethyl 2-bromoisobutyrate (EBiB, 98%, Aldrich) were dried with CaH₂ and distilled under reduced pressure. 1,1,4,7,10,10-Hexamethyltriethylenetetramine (HMTETA, 97%, Aldrich) was used as received. Di(ethylene glycol) methyl ether methacrylate (DEGMMA, 97%, TCI) was stirred with CaH₂, distilled under vacuum, and stored in a refrigerator prior to use. Di(ethylene glycol) ethyl ether methacrylate (DEGEMA) was synthesized via the reaction of di(ethylene glycol) monoethyl ether (>99.0%, TCI) and methacryloyl chloride (95%, Acros) in dry methylene chloride in the presence of triethylamine (99%, Acros).³⁶ Methoxytri(ethylene glycol) methacrylate (TEGMMA) and allyl 2-bromo-2-methylpropionate were made according to the procedures reported previously.^{31, 37} The difunctional PEO macroinitiator, Br–PEO–Br, was prepared by reacting PEO (HO–PEO–OH, molecular weight = 20 kDa, Aldrich) with 2-

bromoisobutyryl bromide.³⁶ 4-Chloro-7-nitro-2,1,3-benzoxadiazole (NBD-Cl, 98 %, Acros), rhodamine B (Acros), ethanolamine (99 %, Fisher Scientific), and oxalyl chloride (98 %, Fisher Scientific) were used as received. 4-(2-Methacryloyloxyethylamino)-7-nitro-2,1,3-benzoxadiazole (NBDMA) was synthesized according to a literature procedure.³⁸ The synthesis of NBDMA and RhBMA is detailed in the Supporting Information. All other chemical reagents were purchased from either Aldrich or Fisher/Acros and used without further purification.

2.2.2. General Characterization

¹H and ¹³C NMR spectra were recorded on a Varian Mercury 300 NMR spectrometer and the residual solvent proton signal was used as the internal standard. Size exclusion chromatography (SEC) of the free polymers formed in the synthesis of hairy NPs was carried out at ambient temperature using PL-GPC 20 (an integrated SEC system from Polymer Laboratories, Inc.) with a refractive index detector, one PLgel 5 μ m guard column (50 \times 7.5 mm), and two PLgel 5 μ m mixed-C columns (each 300 \times 7.5 mm, linear range of molecular weight from 200 to 2,000,000 Da). THF was used as the solvent and the flow rate was 1.0 mL/min. Narrow-disperse polystyrene standards were used to calibrate the system. The data were processed using CirrusTM GPC/SEC software (Polymer Laboratories, Inc.). The molecular weight and molecular weight distribution of ABA-D were analyzed using a SEC system composed of a Waters 510 pump, a Knauer Smartline 2300 RI detector, and three PSS GRAM linear columns (each 8 \times 300 mm, 3000 Å, 1000 Å, 100 Å in series from Polymer Standards Service-USA, Inc.). HPLC grade *N,N*-dimethylformamide (DMF) with 0.05 M LiBr was used as the mobile phase with a flow rate of 1.0 mL/min. The system was calibrated by using polystyrene standards, and the data were processed using CirrusTM GPC/SEC software. Mass spectroscopy was performed using a JEOL Model JMS-T100LC (AccuTOF) orthogonal time-of-flight (TOF) mass spectrometer with an IonSense DART source.

Thermogravimetric analysis (TGA) was performed in air at a heating rate of 20 °C/min from room temperature to 800 °C using TA Q-series Q50. The NPs were dried at 45 °C in vacuum for > 5 h prior to analysis.

2.2.3. Preparation of ATRP Initiator-Functionalized Silica NPs (Initiator NPs)

Allyl 2-bromo-2-methylpropionate (2.084 g, 10.1 mmol), triethoxysilane (3 mL), and the platinum-divinyltetramethyldisiloxane complex in xylenes (2.1-2.4 % platinum concentration, 60 µL) were added into a 50 mL two-necked flask. The mixture was stirred at 45 °C under N₂ and ¹H NMR spectroscopy was used to monitor the reaction. Once the reaction was complete, excess triethoxysilane was removed under vacuum at 30 °C. The yield of the product 3-(triethoxysilyl)propyl 2-bromo-2-methylpropanoate was 3.695 g (98.9%).

MIBK-ST (6.885 g, corresponding to 2.066 g of bare silica NPs) was added into a 250 mL round bottom flask along with ethanol (39.41 g), ammonia (615.5 mg, 25 wt % in water), and 3-(triethoxysilyl)propyl 2-bromo-2-methylpropanoate (3.183 g). The flask was placed in an oil bath with a preset temperature of 40 °C, and the temperature was gradually heated to 55 °C over a period of 5 h. After being stirred at 55 °C overnight, the temperature was raised to 60 °C and the mixture was kept stirring for additional 7.5 h. The total reaction time was 30 h. DMF (15 mL) was then added into the reaction mixture and the lower boiling point volatiles were removed by a rotovap. The initiator NPs were precipitated twice in a mixture of hexanes (200 mL) and acetone (70 mL). The NPs were then dispersed in DMF and separated by ultracentrifugation (Beckman Optima L-90K Ultracentrifuge with type 60 Ti rotor, 35,000 rpm, 30 min). This dispersion-centrifugation cycle was repeated one more time. The initiator NPs were then dispersed in DMF, forming a stable dispersion. The concentration of initiator NPs in the dispersion was determined by gravimetric analysis. A portion of the NP dispersion (0.549 g) was taken out and dried in a

small vial under high vacuum overnight. The mass of the initiator NPs was 34.3 mg; thus, the concentration of the initiator NPs in the dispersion was 6.25 wt%.

2.2.4. Synthesis of Thermosensitive P(DEGMMA-*co*-DEGEMA-*co*-NBDMA) Brush-Grafted Silica NPs (NP-D)

CuBr (17.9 mg, 125 μ mol), CuBr₂ (7.8 mg, 34.9 μ mol), and a dispersion of the initiator NPs in DMF with a concentration of 6.25 wt% (4.188 g, corresponding to 262 mg initiator NPs) were weighed into a two-necked flask, followed by the addition of DMF (19.91 g). The mixture was sonicated at room temperature to achieve a homogeneous dispersion. DEGMMA (2.349 g, 12.5 mmol), DEGEMA (1.683 g, 8.32 mmol), NBDMA (10.2 mg, 34.9 μ mol), and free initiator EBiB (29.0 mg, 149 μ mol) were added into the flask. After the mixture was degassed by three freeze-pump-thaw cycles, PMDETA (34.4 mg, 198 μ mol) was added via a microsyringe at the point when the frozen mixture was thawing. The flask was then placed in a 45 °C oil bath. ¹H NMR spectroscopy was employed to monitor the polymerization. After the reaction proceeded for 23 h and 40 min, the flask was removed from the oil bath and opened to air; the mixture was diluted with THF (20 mL). The polymerization mixture was precipitated in a mixture of diethyl ether and hexane (2 : 1, v/v), and the precipitate, including hairy NPs and the free polymer, was then redispersed/re-dissolved in THF (30 mL). The hairy NPs were isolated by ultracentrifugation (Beckman Optima L-90K Ultracentrifuge with type 60 Ti rotor, 35,000 rpm, 30 min). The hairy NPs were then dispersed in THF (25 mL), and separated by centrifugation again. This dispersion-ultracentrifugation process was conducted for a total of five times. A portion of the supernatant liquid from the first cycle was passed through a column of silica gel (bottom)/activated basic aluminum oxide (top) (2 : 1, v/v). The free polymer was precipitated in a mixture of hexanes and diethyl ether (3 : 1, v/v), dissolved in CH₂Cl₂, and then precipitated again. This process was

repeated for additional two times. The free polymer was then dried under high vacuum for 6 h, and analyzed by SEC. The number average molecular weight ($M_{n,SEC}$) and polydispersity index (PDI) of the free polymer were 10.2 kDa and 1.19, respectively. The monomer conversion was 49.8 %, calculated from the 1H NMR spectrum of the sample taken from the reaction mixture when the polymerization was stopped using the integrals of the peaks at 3.77-3.95 ppm ($-COOCH_2CH_2$ from PDEGMMA and PDEGEMA) and 3.98-4.10 ppm ($-COOCH_2CH_2$ from DEGMMA and DEGEMA). The DP of the copolymer was 55. The numbers of DEGMMA and DEGEMA monomer units in the copolymer were 33 and 22, respectively, determined from the 1H NMR spectrum of the free copolymer using the integrals of the peaks at 1.14-1.29 ppm ($CH_3CH_2OCH_2-$ of DEGEMA monomer units and 3.29-3.42 ppm ($CH_3OCH_2CH_2O-$ of DEGMMA monomer units) and the total DP of the copolymer.

The aqueous dispersion of NP-D was prepared by dialysis. NP-D, isolated by ultracentrifugation, was dispersed in DMF (10 g) using an ultrasonic bath. Ethanol (2 mL) and water (2 mL) were then added sequentially in a dropwise fashion under the stirring conditions. The mixture was dialyzed against water in an ice/water bath by using a regenerated cellulose tubular membrane with nominal MWCO 3500. The ice/water bath-cooled water was changed at least ten times in 5 days. The concentration of NP-D in the final aqueous dispersion is 2.84 mg/g, determined by gravimetric analysis as for the dispersion of initiator NPs.

2.2.5. Synthesis of P(TEGMMA-*co*-NBDMA) Brush-Grafted Silica NPs (NP-T)

CuBr (22.0 mg, 153 μ mol), a dispersion of the initiator NPs in DMF with a NP concentration of 6.25 wt% (3.962 g, corresponding to 248 mg of the initiator NPs), and DMF (19.67 g) were added into a 50 mL two-necked flask. The mixture was sonicated in an ultrasonic bath at room temperature until a homogeneous dispersion was obtained. TEGMMA (4.837 g, 20.82 mmol),

NBDMA (10.4 mg, 35.6 μmol), and free initiator EBiB (31.2 mg, 160 μmol) were added into the flask. After the mixture was degassed by three freeze-pump-thaw cycles, PMDETA (33.0 mg, 190 μmol) was added via a microsyringe at the thawing point of the frozen mixture. The flask was then placed in a 50 °C oil bath, and the polymerization was monitored by ^1H NMR spectroscopy. After the reaction proceeded for 47 h and 40 min, the flask was removed from the oil bath and opened to air, and the mixture was diluted with THF (20 mL). The reaction mixture was precipitated in a solvent mixture of diethyl ether and hexane (2 : 1, v/v). The precipitate was then redispersed in 30 mL THF and centrifugated using an ultracentrifuge (Beckman Optima L-90K Ultracentrifuge with type 60 Ti rotor, 35,000 rpm, 30 min). This dispersion/centrifugation cycle was conducted for a total of 5 times. A portion of the supernatant liquid from the first cycle was passed through a column of silica gel (bottom)/activated basic aluminum oxide (top) (2 : 1, v/v). The free polymer was precipitated in a mixture of hexane and diethyl ether (3 : 1, v/v), re-dissolved in CH_2Cl_2 , and precipitated again for additional two times. After being dried under high vacuum for 6 h, the free polymer was analyzed by SEC. The $M_{n,\text{SEC}}$ and PDI were 9.4 kDa and 1.19, respectively. The final monomer conversion was 45.3 %, calculated from the ^1H NMR spectrum using the integrals of the peaks at 3.74-3.93 ppm ($-\text{COOCH}_2\text{CH}_2\text{O}-$ from PTEGMMA) and 3.95-4.13 ppm ($-\text{COOCH}_2\text{CH}_2\text{O}-$ from TEGMMA monomer).

The aqueous dispersion of NP-T was also prepared by dialysis. The procedure was the same as that for the preparation of the aqueous dispersion of NP-D except that the dialysis was conducted at room temperature. The final concentration of NP-D in the dispersion was 18.0 mg/mL, determined by gravimetric analysis.

2.2.6. Synthesis of P(DEGMMA-*co*-DEGEMA-*co*-RhBMA)-*b*-PEO-*b*-P(DEGMMA-*co*-DEGEMA-*co*-RhBMA) (ABA-D)

CuBr (12.7 mg, 88.5 μmol) and the difunctional PEO macroinitiator Br-PEO-Br (1.520 g, 0.0749 mmol) were weighed into a 50 mL two-necked flask, followed by the addition of DEGMMA (3.613 g, 19.2 mmol), DEGEMA (5.845 g, 28.9 mmol), RhBMA (16.5 mg, 29.7 μmol), and anisole (13.07 g). The mixture was stirred under N_2 . HMTETA (17.8 mg, 77.3 μmol) was then injected into the flask via a microsyringe. After the mixture was degassed by three freeze-pump-thaw cycles, the flask was placed into a 60 $^{\circ}\text{C}$ oil bath. The polymerization was monitored by ^1H NMR spectroscopy. After 8 h, the flask was removed from the oil bath and opened to air. The mixture was diluted with THF, and the copper catalyst was removed by passing the solution through a neutral aluminum oxide/silica gel column. The polymer was purified by precipitation in a mixture of hexanes and diethyl ether (3 : 1, v/v) five times and then dried under high vacuum at 35 $^{\circ}\text{C}$ for 5 h. SEC analysis results (polystyrene standards): $M_{n,\text{SEC}} = 46.9$ kDa, PDI = 1.15.

2.2.7. Dynamic Light Scattering (DLS) Studies of Thermoresponsive Properties of Hairy NPs and ABA-D

DLS studies of aqueous solutions of NP-D (1.0 mg/g), NP-T (1.0 mg/g), and ABA-D (0.2 mg/g) were conducted using a Brookhaven Instruments BI-200SM goniometer equipped with a PCI BI-9000AT digital correlator, a temperature controller, and a solid-state laser (model 25-LHP-928-249, $\lambda = 633$ nm) at a scattering angle of 90 $^{\circ}$. The solutions were filtered into borosilicate glass tubes with an inner diameter of 7.5 mm using Millipore hydrophilic PTFE filters (0.2 μm pore size), and the tubes were sealed with PE stoppers. The glass tube was placed in the cell holder of the light scattering instrument and the temperature was gradually changed. At each selected

temperature, the solution was equilibrated for 20 min prior to data recording. The time intensity–intensity correlation functions were analyzed with a Laplace inversion program (CONTIN). For each temperature, multiple measurements (8 to 10 measurements) were taken and the average hydrodynamic sizes were calculated along with the standard deviations.

2.2.8. Fluorescence Resonance Energy Transfer (FRET) Study of Aqueous Mixtures of Thermosensitive Hairy NPs and ABA-D

Prior to fluorescence spectrometry study, a 0.216 mg/g aqueous solution of ABA-D, a 0.012 mg/g aqueous dispersion of NP-D, a 0.012 mg/g aqueous dispersion of NP-T, an aqueous mixture of ABA-D with a concentration of 0.216 mg/g and NP-D with a concentration of 0.012 mg/g, and an aqueous mixture of ABA-D with a concentration of 0.217 mg/g and NP-T with a concentration of 0.012 mg/g were prepared. All the solutions were ultrasonicated in an ultrasonic ice/water bath for 15 min and then stirred vigorously in an ice/water bath for 3 h. The icy water-cooled samples were used immediately for fluorescence spectrometry measurements (done in ~ 2 min, ~ 0 °C). The samples were then allowed to warm to room temperature and kept stirring overnight. The mixtures were further heated to 27 °C in an oil bath and stirred for additional 2 h. The samples were used immediately for fluorescence spectroscopy measurements. All fluorescence emission spectra were recorded on a Perkin Elmer LS 55 luminescence spectrometer. The slit widths were set at 10 nm for both excitation and emission with a scan speed of 100 nm/min. The excitation wavelength was 480 nm, and fluorescence spectra were collected from 500 to 700 nm.

2.2.9. Rheology Studies of Hybrid Micellar Hydrogels of ABA-D and Thermosensitive Hairy NPs

The preparation of aqueous mixtures of ABA-D and NP-D is described below. The other hybrid samples with different NP-to-polymer mass ratios were prepared using similar procedures.

ABA-D was thoroughly dried in a vial under high vacuum and weighed (301.3 mg), followed by the addition of water (2.712 g). The mixture was stored in a refrigerator (4 °C) overnight and then ultrasonicated in an ultrasonic ice/water bath for 30 min to ensure that the polymer was fully dissolved and the solution was homogeneous. The sample was subjected to rheological measurements. To prepare the aqueous mixture of ABA-D and NP-D with a polymer concentration of 10 wt%, defined as $[\text{polymer mass}/(\text{polymer mass} + \text{water})] \times 100\%$, and a NP-to-polymer weight ratio of 2.5 : 100, an aqueous solution of NP-D with a concentration of 2.84 mg/g (stored in a refrigerator, 2.303 g, corresponding to 6.54 mg of NP-D) was added into the aqueous solution of ABA-D with a concentration of 10 wt % (2.604 g). To maintain the polymer concentration at 10 wt %, a gentle stream of air was used to evaporate water until the weight of the sample reached 2.610 g. The sample was sealed with a Teflon tape and then sonicated in an ultrasonic ice/water bath for 30 min prior to the rheological measurement. After that, a calculated amount of hairy NPs was added into the solution to increase the NP-to-polymer mass ratio to 5 : 100, and again a gentle stream of air was used to evaporate water to maintain the polymer concentration at 10 wt % as defined previously. Two sets of hybrid samples (ABA-D + NP-D and ABA-D + NP-T) were prepared using this method, with the NP-to-polymer weight ratios of 2.5 : 100, 5 : 100, 10 : 100, 15 : 100, 20 : 100, 30 : 100, 40 : 100, and 50 : 100.

Rheological experiments were conducted using a rheometer from TA Instruments (Model TA AR 2000ex). A cone–plate geometry with a cone diameter of 20 mm and an angle of 2° (truncation 52 µm) was used. The temperature was controlled by the bottom Peltier plate. In each measurement, 90 µL of the sample was loaded onto the plate by a micropipet. The solvent trap was filled with water, and a solvent trap cover was used to minimize water evaporation. Dynamic viscoelastic properties (dynamic storage modulus G' and loss modulus G'') of a sample were measured by

oscillatory shear experiments performed at a fixed frequency of 1 Hz in a heating ramp at a heating rate of 3 °C/min. The frequency dependences of G' and G'' of the samples at 40 °C were obtained by frequency sweep tests from 0.1 to 100 Hz. A strain amplitude of $\gamma = 1.0\%$ was used in all dynamic viscoelastic measurements. For each rheology study, three measurements were taken and the average value was used.

2.3. Results and Discussion

2.3.1. Synthesis and Thermosensitive Property of P(DEGMMA-*co*-DEGEMA-*co*-NBDMA) Brush-Grafted 17 nm Silica NPs (NP-D)

The bare silica NPs from MIBK-ST, with an average size of 17 nm determined from transmission electron microscopy micrographs, were surface functionalized with a triethoxysilane-terminated ATRP initiator, 3-(triethoxysilyl)propyl 2-bromo-2-methylpropanoate. The original dispersion of silica NPs in MIBK was first diluted with ethanol, to which ammonia and the triethoxysilane-terminated ATRP initiator were added. Ammonia catalyzed the hydrolysis of 3-(triethoxysilyl)propyl 2-bromo-2-methylpropanoate and the immobilization on the surface of silica NPs.³⁹ The mass ratio of the silane initiator to silica NPs used here was 1.54 : 1.00, and the immobilization reaction was carried out at 40 – 60 °C for a total of 30 h. The initiator NPs were purified by precipitation and ultracentrifugation and then dispersed in DMF to produce a dispersion with a particle concentration of 6.25 wt%.

P(DEGMMA-*co*-DEGEMA-*co*-NBDMA) brushes were then grown from the initiator NPs by surface-initiated ATRP of DEGMMA, DEGEMA, and NBDMA with a molar ratio of 0.60 : 0.40 : 0.0017 at 45 °C using CuBr/CuBr₂/PMDETA as catalyst in the presence of free initiator EBiB. After a desired monomer conversion was reached, the polymerization was stopped and the

obtained hairy NPs were purified by repetitive dispersion in THF and ultracentrifugation. The aqueous dispersion of NP-D was prepared by dialysis. SEC analysis showed that the $M_{n,SEC}$ and PDI of the free copolymer formed from EBiB were 10.2 kDa and 1.19, respectively, indicating that the polymerization was controlled. Figure 2.1A shows the TGA curves of the initiator NPs and NP-D. Clearly, the brushes were successfully grown from the NPs as indicated by a weight retention of 30.76 % at 800 °C in contrast to 83.64 % for the initiator NPs. The degree of polymerization (DP) of the copolymer was calculated from the final conversion of the monomers determined from the 1H NMR spectrum and the molar ratio of the monomers to the sum of the free initiator and the surface initiator (see Appendix A). The amount of the surface initiator that successfully initiated the polymerization was estimated from the TGA data and the monomer conversion. Using the TGA data, the total amount of the grafted polymer can be calculated from the amount of the initiator NPs used in the reaction, while the total amount of the polymer can be calculated from the monomer conversion and the total of the monomers used in the reaction. Thus, the relative amount of the surface initiator can be calculated. The DP of the copolymer was found to be 55. The numbers of DEGMMA and DEGEMA monomer units were 33 and 22, respectively, which were determined from the 1H NMR spectrum of the free copolymer. Using the average size of silica NPs (17 nm), TGA data (Figure 2.1A), and the DP of the copolymer, and assuming that the density of silica NPs was 2.07 g/cm³, the grafting density of P(DEGMMA-*co*-DEGEMA-*co*-NBDMA) brushes was found to be 0.65 chains/nm².

Dynamic light scattering (DLS) was employed to study the thermosensitive property of NP-D in water. Figure 1B shows the average apparent hydrodynamic size (D_h) of NP-D in water at a concentration of 1.0 mg/g as a function of temperature. As expected, the D_h gradually decreased with increasing the temperature, from ~ 53 nm in the temperature range of 8 to 14 °C to 47 nm at

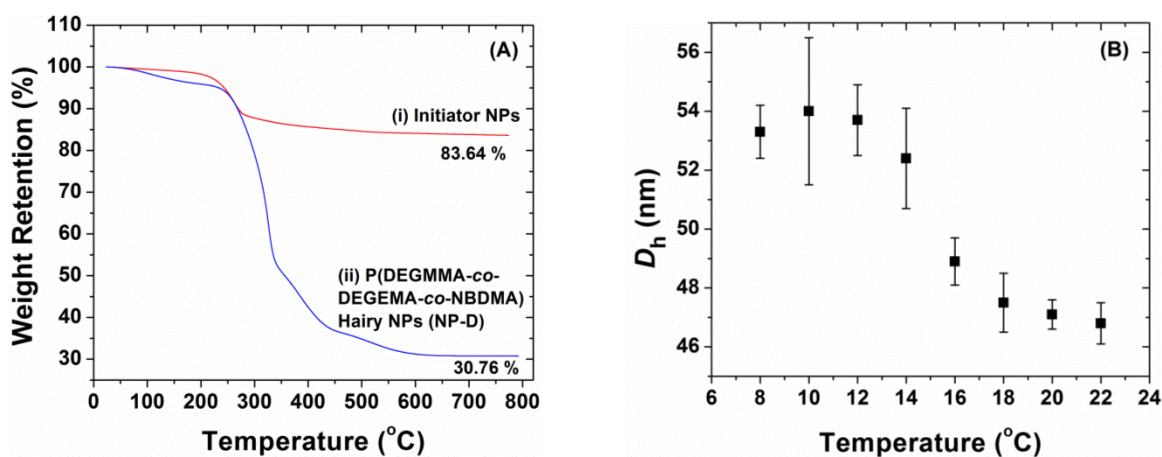


Figure 2.1. (A) TGA of (i) the initiator NPs and (ii) P(DEGMMA-*co*-DEGEMA-*co*-NBD) brush-grafted silica NPs (NP-D). (B) Average apparent hydrodynamic diameter D_h (along with error bar) of NP-D in an aqueous dispersion with a concentration of 1.0 mg/g as a function of temperature obtained from a dynamic light scattering study.

22 °C. The onset temperature of the LCST transition was 14 °C, and the LCST transition continued over a temperature range of ~ 6 °C.

2.3.2. Synthesis and Thermo-responsive Properties of P(TEGMMA-*co*-NBDMA) Brush-Grafted Silica NPs (NP-T)

The same batch of initiator NPs was used to prepare NP-T via a procedure similar to that for NP-D. The molar ratio of TEGMMA to NBDMA in the feed was 1 : 0.0017. After the monomer conversion reached 45.3 %, the polymerization was stopped, and the hairy NPs were separated by centrifugation. From SEC analysis, the $M_{n,SEC}$ and PDI of the free polymer were 9.4 kDa and 1.19, respectively. Figure 2.2A shows the TGA curve of NP-T; the weight retention at 800 °C was 31.26 %, similar to that of NP-D. Based on the monomer conversion and the molar ratio of the monomers to the sum of EBiB and the surface initiator, the DP of the polymer was found to be 48. A calculation showed that the grafting density for NP-T was 0.62 chains/nm², also similar to that of NP-D. Figure 2.2B shows the plot of the D_h of NP-T in water at a 1.0 mg/g concentration versus temperature. At 38 and 41 °C, the values of D_h were ~ 47 nm. Upon heating, the D_h began to decrease and the transition continued over a temperature range of ~ 10 °C, consistent with our previous observation of PTEGMMA brushes grafted on 133 nm particles.³¹ However, the D_h values of NP-T were smaller than NP-D, which is likely due to the smaller DP of P(TEGMMA-*co*-NBDMA) brushes and a slightly lower grafting density.

2.3.3. Synthesis and Thermo-Induced Micellization of P(DEGMMA-*co*-DEGEMA-*co*-RhBMA)-*b*-PEO-*b*-P(DEGMMA-*co*-DEGEMA-*co*-RhBMA) (ABA-D)

ABA-D was synthesized by ATRP from a difunctional PEO macroinitiator with a molecular weight of 20 kDa. The two main monomers used here, DEGMMA and DEGEMA, were the same as those in the synthesis of NP-D. However, a different DEGMMA-to-DEGEMA molar ratio (2 :

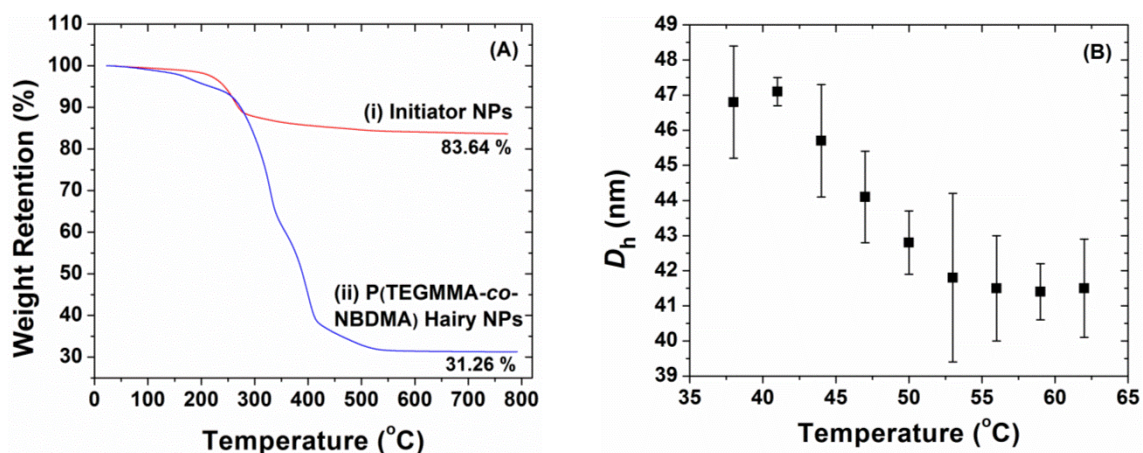


Figure 2.2. (A) TGA of (i) the initiator NPs and (ii) P(TEGMMA-co-NBDMA) brush-grafted silica NPs (NP-T). (B) Average apparent hydrodynamic diameter D_h (along with error bar) of NP-T in water with a concentration of 1.0 mg/g as a function of temperature obtained from a dynamic light scattering study.

3) was employed, instead of 3 : 2 in the synthesis of NP-D. This is because we previously observed that the LCST of polymer brushes is lower by a few degrees than that of the corresponding free polymer in water.³¹ On the other hand, when a thermosensitive polymer is attached to a more hydrophilic polymer, the LCST transition often occurs at a slightly higher temperature. If a linear relationship between CP and composition is held for thermosensitive copolymers of two monomers, the CPs of the copolymers with DEGMMA-to-DEGEMA molar ratios of 2 : 3 and 3 : 2 would be 12.8 and 17.2 °C, respectively. The difference of 4.4 °C is likely to vanish for the LCST transitions of the brushes and the thermosensitive outer blocks of ABA-D.

The polymerization was carried out in anisole at 60 °C using CuBr/HMTETA as catalyst with the DEGMMA-to-DEGEMA-to-RhBMA molar ratios of 0.40 : 0.60 : 0.00062. The polymerization was stopped after 480 min, and the reaction mixture was precipitated three times in a mixture of hexanes and ethyl ether (3 : 1, v/v). SEC showed a unimodal peak with the $M_{n,SEC}$ of 46.9 kDa and the PDI of 1.15 relative to polystyrene standards. On the basis of the DP of the PEO macroinitiator (DP = 455), the numbers of DEGMMA and DEGEMA monomer units were calculated from the ¹H NMR spectrum using the integrals of the peaks at 1.14-1.24 ppm (-OCH₂CH₃ group from PDEGEMA), 3.27-3.41 ppm (-OCH₃ group from PDEGMMA), and 3.43-3.79 ppm (-OCH₂CH₂- of PEO, CH₃OCH₂CH₂OCH₂CH₂O- of PDEGMMA, and CH₃CH₂OCH₂CH₂OCH₂CH₂O- of PDEGEMA). The numbers of DEGMMA and DEGEMA monomer units was 98 and 120, respectively. The molar ratio of DEGMMA to DEGEMA monomer units was 45 : 55, similar to that of the two monomers in the feed (40 : 60).

The thermally induced micellization of ABA-D in water at a concentration of 0.2 mg/g was studied by DLS. Figure 2.3 shows the plots of scattering intensity and D_h versus temperature. Clearly, at 14 °C and below, the scattering intensity of the polymer solution was low and the D_h

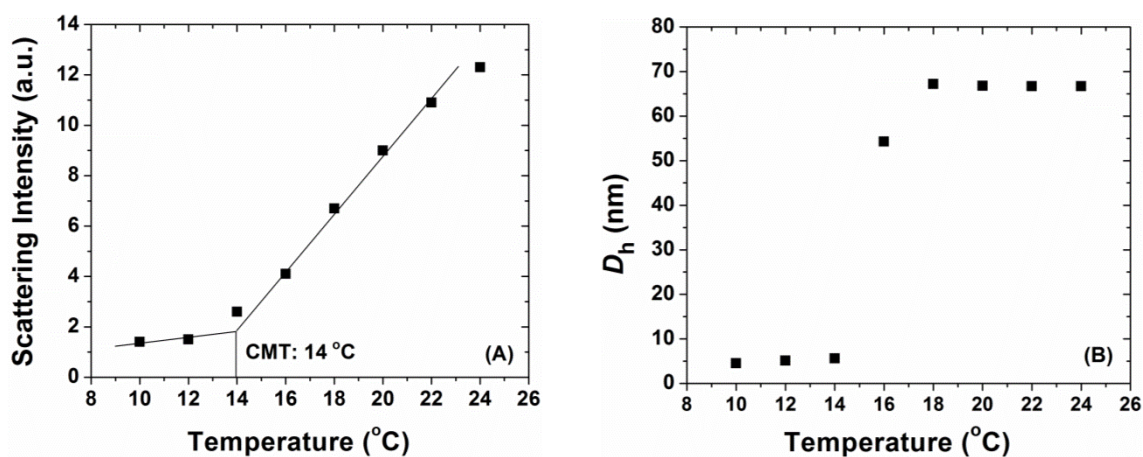


Figure 2.3. Scattered light intensity at scattering angle of 90° (A) and average apparent hydrodynamic size D_h (B), obtained from CONTIN analysis, as a function of temperature in a dynamic light scattering study of a 0.2 mg/g aqueous solution of ABA-D.

was small (< 6 nm). Upon heating above $14\text{ }^{\circ}\text{C}$, both increased. Micelles with a single distribution and a D_h value of 67 nm were observed in the temperature range of 18 to $24\text{ }^{\circ}\text{C}$. The critical micellization temperature (CMT) of ABA-D was $14\text{ }^{\circ}\text{C}$ (Figure 3A),⁹ which is essentially the same as the onset temperature of the LCST transition of NP-D.

2.3.4. FRET Study of Spatial Location of Thermosensitive Hairy NPs in Aqueous Mixtures of ABA-D and Hairy NPs

FRET was employed to determine the spatial locations of thermosensitive hairy NPs in aqueous solutions of ABA-D and hairy NPs at $\sim 0\text{ }^{\circ}\text{C}$, which is below the CMT of ABA-D, LCSTs of NP-D and NP-T, and $27\text{ }^{\circ}\text{C}$, which is above the CMT of ABA-D and the LCST of NP-D but below the LCST of NP-T. An aqueous mixture of ABA-D with a concentration of 0.216 mg/g and NP-D with a concentration of 0.012 mg/g , and an aqueous mixture of ABA-D with a concentration of 0.217 mg/g and NP-T with a concentration of 0.012 mg/g were prepared for FRET studies. For comparison, a 0.216 mg/g aqueous solution of ABA-D, a 0.012 mg/g aqueous dispersion of NP-D, and a 0.012 mg/g aqueous dispersion of NP-T were also made.

Figure 2.4 shows the fluorescence emission spectra with an excitation wavelength of 480 nm recorded at ~ 0 and $27\text{ }^{\circ}\text{C}$. The two aqueous dispersions of hairy NPs exhibited a single peak with the maximum at $\sim 521\text{ nm}$, while for ABA-D, the maximum was found at 575 nm . Little changes were observed for these fluorescence spectra between ~ 0 and $27\text{ }^{\circ}\text{C}$. Different features were observed in the fluorescence emission spectra of the two aqueous mixtures. At $\sim 0\text{ }^{\circ}\text{C}$, two peaks were observed at 520 and 575 nm for both aqueous mixtures, which are attributed to the emissions of NBDMA and RhBMA. The intensities of two peaks for the aqueous mixture of ABA-D and NP-T were essentially the same as those of the aqueous solution of ABA-D and the aqueous dispersion of NP-T, respectively, and little changes were found after the temperature was raised to

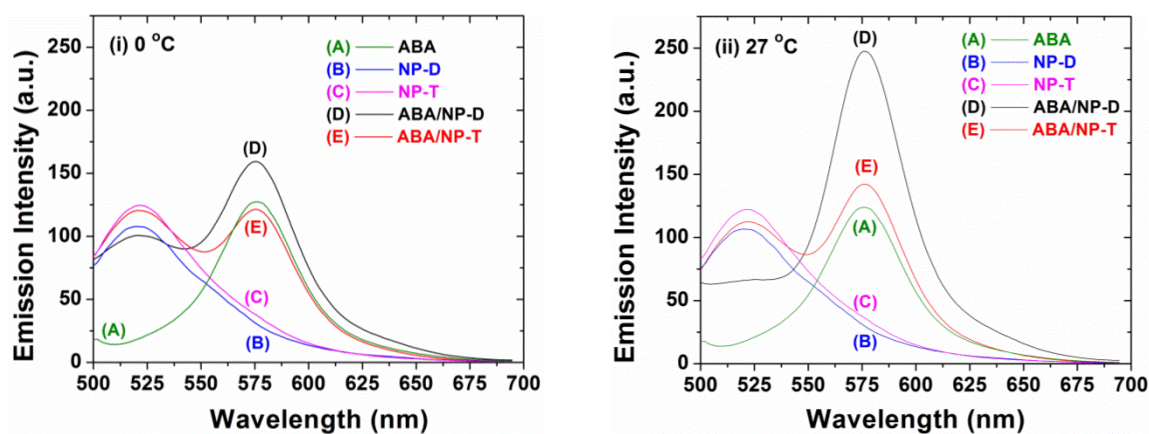


Figure 2.4. Fluorescence spectra of aqueous solutions of ABA-D with a concentration of 0.216 mg/g (A), NP-D with a concentration of 0.012 mg/g (B), NP-T with a concentration of 0.012 mg/g (C), a mixture of ABA-D with a concentration of 0.216 mg/g and NP-D with a concentration of 0.012 mg/g (D), and a mixture of ABA-D with a concentration of 0.217 mg/g and NP-T with a concentration of 0.012 mg/g (E) at (i) ~ 0 °C and (ii) 27 °C.

27 °C, indicating that there was no FRET between two fluorescent dyes and NP-T was located outside the core of micelles. For the aqueous mixture of ABA-D and NP-D at ~ 0 °C, the intensity of the peak at 520 nm was similar to that of the aqueous dispersion of NP-D, and the peak at 575 nm was slightly higher than that of the ABA-D solution, suggesting either no or very weak FRET. Upon increasing the temperature to 27 °C, no obvious peak was observed at ~ 520 nm and the intensity decreased significantly (from 101 a.u. to 66 a.u.). Meanwhile, the intensity of the peak located at 575 nm increased significantly from 159 a.u. to 247 a.u., indicating that FRET occurred and NP-D resided in the core of ABA-D micelles at 27 °C.

The difference between aqueous mixtures of ABA-D/NP-D and ABA-D/NP-T can also be seen from the optical picture of the samples in dark at room temperature under the irradiation of a 365 nm UV light (Figure 2.5). While the aqueous dispersions of NP-D and NP-T were green, the ABA-D solution was orange. The aqueous mixture of ABA-D and NP-T was yellow, a color from mixing green and orange. Differently, the color of the aqueous mixture of ABA-D and NP-D was similar to that of the ABA-D solution with a light pink tinge. Note that the concentrations of ABA-D and thermosensitive hairy NPs were different from those in the FRET study. Thus, both Figures 2.4 and 2.5 indicated that at room temperature or 27 °C NP-D resided in the core of the ABA-D micelles in water, while NP-T was located outside the micelles. It should be noted here that recently Durand-Gasselin et al studied the thermo-induced micellization of Pluronic P123 in water in the presence of gold NPs grafted with random copolymers of ethylene oxide and propylene oxide.⁴⁰ When the temperature was raised above the CMT of P123 and the aggregation temperature of hairy gold NPs, the NPs were located in the core of Pluronic micelles.

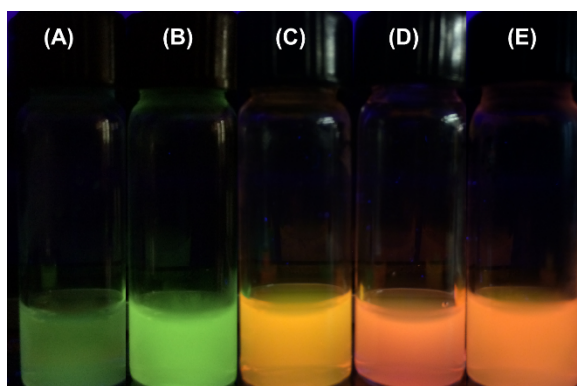
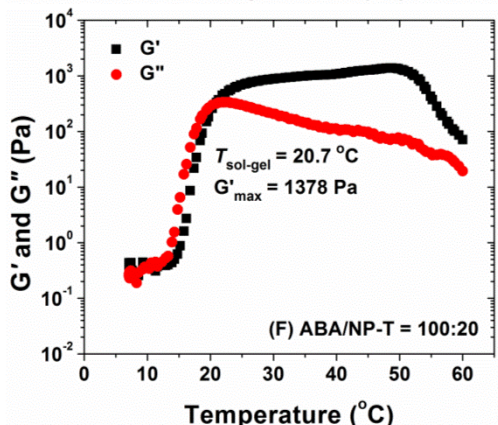
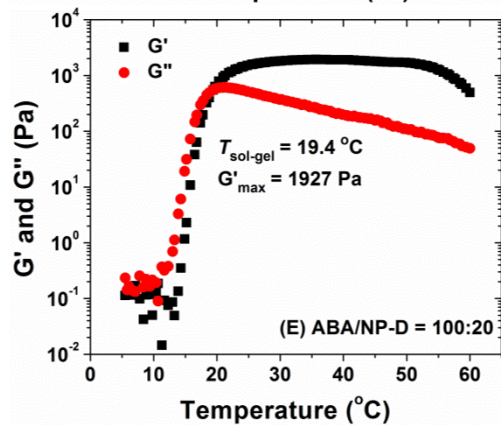
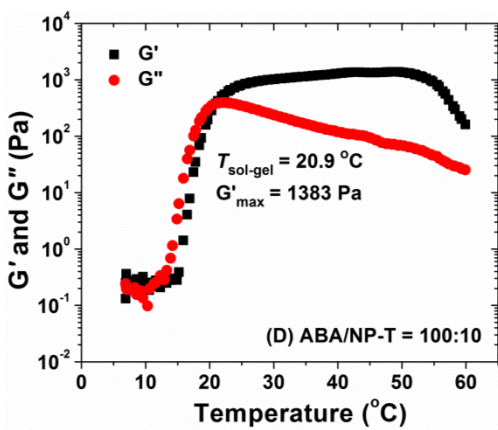
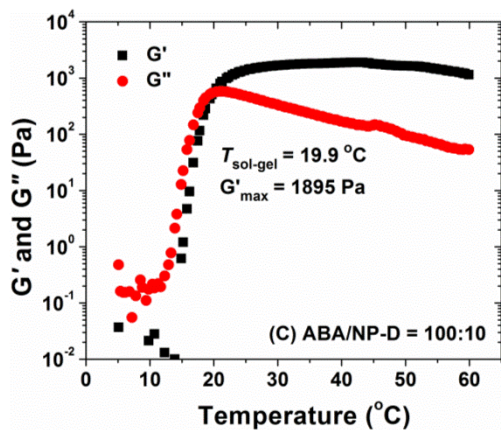
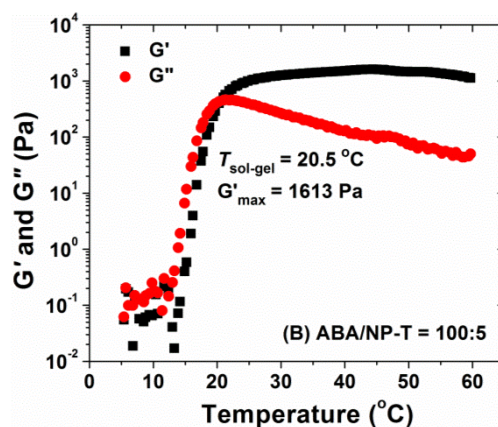
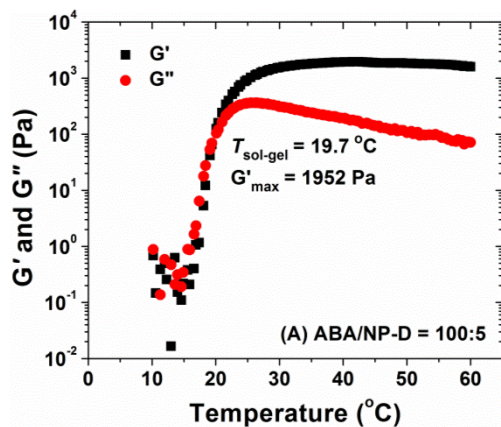


Figure 2.5. Optical picture of aqueous solutions of (A) NP-D with a concentration of 0.28 wt %, (B) NP-T with a concentration of 1.80 wt %, (C) a mixture of ABA-D with a concentration of 4.54 wt % and NP-T with a concentration of 2.95 wt %, (D) a mixture of ABA-D with a concentration of 4.55 wt% and NP-D with a concentration of 2.96 wt %, and (E) ABA-D with a concentration of 4.54 wt % taken in dark at room temperature under the irradiation of a UV light with a wavelength of 365 nm (from a TLC detector).

2.3.5. Rheological Studies of Hybrid Micellar Hydrogels of ABA-D and Thermosensitive Hairy NPs – Effects of Spatial Location of Hairy NPs and NP-to-Polymer Mass Ratio on Gel Properties

A 10 wt % aqueous solution of ABA-D was observed to undergo a sol-gel transition upon heating from ~ 0 °C (in an ice/water bath) to room temperature. To examine the effect of spatial location of NPs on properties of hybrid micellar hydrogels, we carried out rheological studies of sol-gel transitions of aqueous solutions of ABA-D with a concentration of 10 wt % and NP-to-polymer mass ratios of 0 : 100, 2.5 : 100, 5 : 100, 10 : 100, 15 : 100, 20 : 100; 30 : 100, 40 : 100, and 50 : 100 for both NP-D and NP-T. Note that here we defined the polymer concentration (10 wt%) as $[(\text{polymer mass})/(\text{polymer mass} + \text{water mass})] \times 100\%$, and the hairy NPs were not included in the calculation. For each sample, three measurements were conducted. Representative rheology curves are shown in Figure 2.6 (other rheology curves can be found in the Supporting Information), which were collected from temperature ramp experiments performed by using a fixed frequency of 1 Hz, a strain amplitude of 1 %, and a heating rate of 3 °C/min. Take the aqueous solution with the ABA-D-to-NP-D mass ratio of 100 to 5 as example (Figure 2.6A), below 16 °C, the values of dynamic storage modulus G' and loss modulus G'' are small, indicating that the sample was in the liquid state. Upon heating from 16 °C, both G' and G'' increased dramatically, and at ~ 20 °C G' became larger than G'' . If the crossover of two curves, i.e., $G' = G''$, is taken as the sol-gel transition temperature ($T_{\text{sol-gel}}$),^{9,41} then for this particular sample, the $T_{\text{sol-gel}}$ is 19.7 °C. Further raising temperature, G' levelled off and G'' gradually decreased, which is a typical behavior of an elastic physical hydrogel. For all samples, we also performed frequency sweeps at 40 °C using a strain amplitude of 1 %; both G' and G'' exhibited a weak dependence on frequency, a signature of typical physical hydrogels (the frequency sweeps can be found in Appendix A). Note

Figure 2.6. Plots of dynamic storage modulus G' and loss modulus G'' of aqueous mixtures of ABA-D with a concentration of 10 wt %, defined as $[(\text{polymer mass})/(\text{polymer mass} + \text{water mass})] \times 100\%$, and hairy NPs with various NP-to-polymer mass ratios versus temperature. The data were collected from temperature ramp experiments performed by using a frequency of 1 Hz, a strain amplitude of 1 %, and a heating rate of 3 °C/min. (A), (C), (E), (G), (I), and (K) are the heating ramps of aqueous mixtures of ABA-D and NP-D with NP-to-polymer mass ratios of 5:100, 10:100, 20:100, 30:100, 40:100, 50:100, respectively. (B), (D), (F), (H), (J), and (L) are the heating ramps of aqueous mixtures of ABA-D and NP-T with NP-to-polymer mass ratios of 5:100, 10:100, 20:100, 30:100, 40:100, 50:100, respectively.



(Figure 2.6 continued)

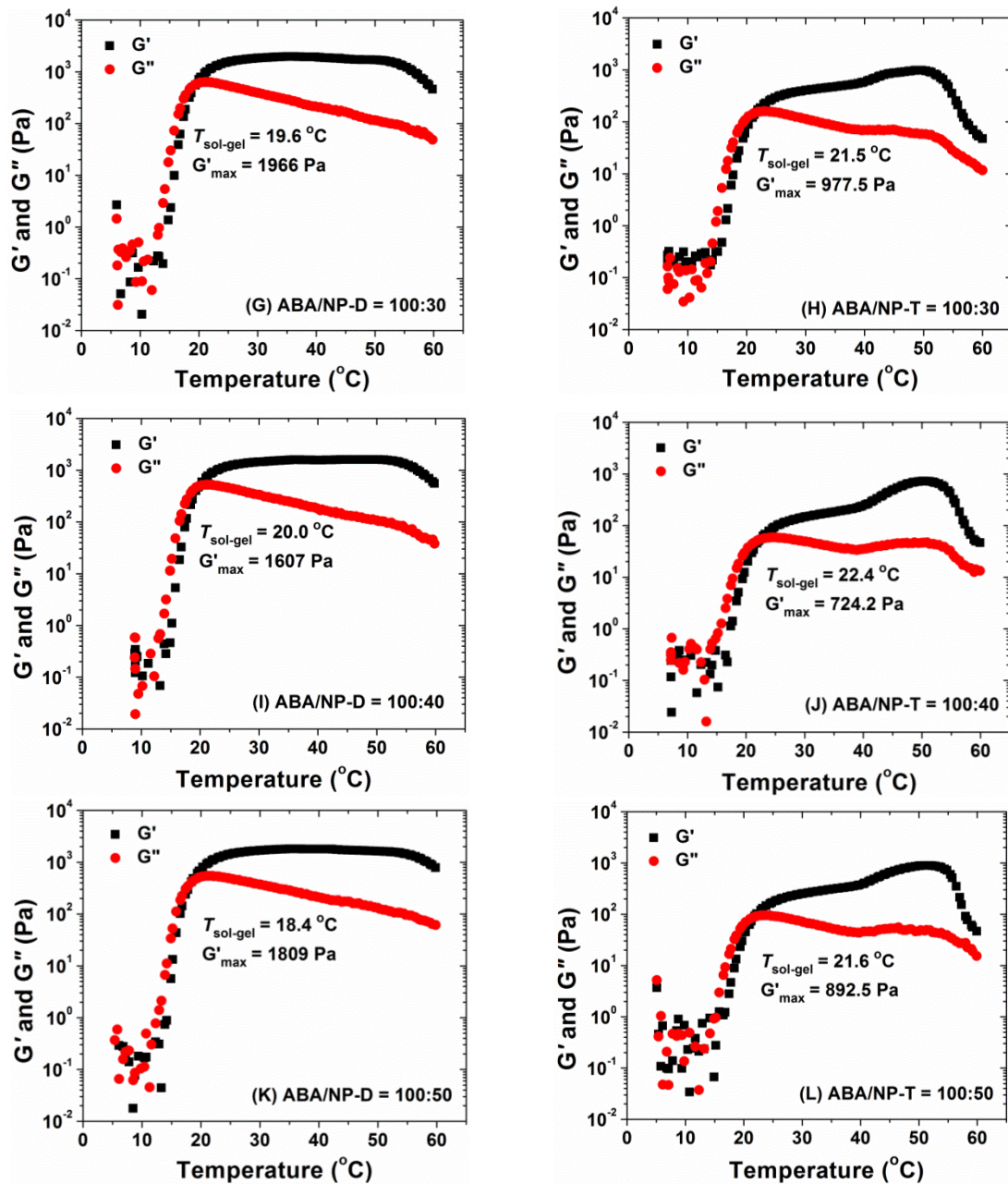


(Figure 2.6 continued)

that for micellar hydrogels of this type of thermosensitive ABA triblock copolymers, our previous dynamic strain sweep experiments showed that the gels typically exhibited a linear response up to ~15%.⁹

Figure 2.7 shows the plots of $T_{\text{sol-gel}}$ and maximum G' (G'_{max}) from heating ramps, which are the averages of three measurements, versus NP-to-polymer mass ratio along with error bars for both NP-D and NP-T. Figure 2.8 shows the G' at 1 Hz ($G'_{1\text{Hz}}$) from frequency sweeps at 40 °C of hybrid hydrogels as a function of NP-to-polymer mass ratio. Combining Figures 6 - 8, several trends can be identified with the increase of the NP-to-polymer mass ratio from 0:100 to 50:100. (i) While the $T_{\text{sol-gel}}$ for aqueous mixtures of ABA-D and NP-D exhibited no or very small changes, the $T_{\text{sol-gel}}$ for hybrid gels of ABA-D and NP-T increased slightly, from 20.1 °C to ~ 22 °C at mass ratios of 40 and 50%. (ii) For micellar hydrogels of ABA-D and NP-D, with the increase of NP-to-polymer ratio, G'_{max} decreased only slightly from 1970 Pa at a mass ratio of 0:100 to 1757 Pa at a mass ratio of 50:100. In contrast, the G'_{max} dropped significantly with the increase of the mass ratio for hybrid gels of ABA-D and NP-T, from 1987 Pa at a ratio of 2.5:100 to 903 Pa at a ratio of 50:100. Similar trends were observed for $G'_{1\text{Hz}}$ from frequency sweeps at 40 °C for the two sets of hybrid micellar gels, though there are some irregularities (Figure 2.8). (iii) Starting from the ratio of 10:100, the rheological curves of aqueous mixtures of ABA-D and NP-T exhibited a significant drop in G' above 50 °C, indicating that the gels became weaker, consistent with the observed trend for G'_{max} shown in Figure 2.7B. While the decrease in G' above 50 °C was also seen for aqueous mixtures of ABA-D and NP-D with mass ratios of 100:20 and above, the changes were much smaller. It should be noted here that we previously observed that the micellar hydrogels of ABA triblock copolymers composed of a PEO block and two thermosensitive outer blocks exhibited a decrease in G' at sufficiently high temperatures,⁸ which was explained using the fact

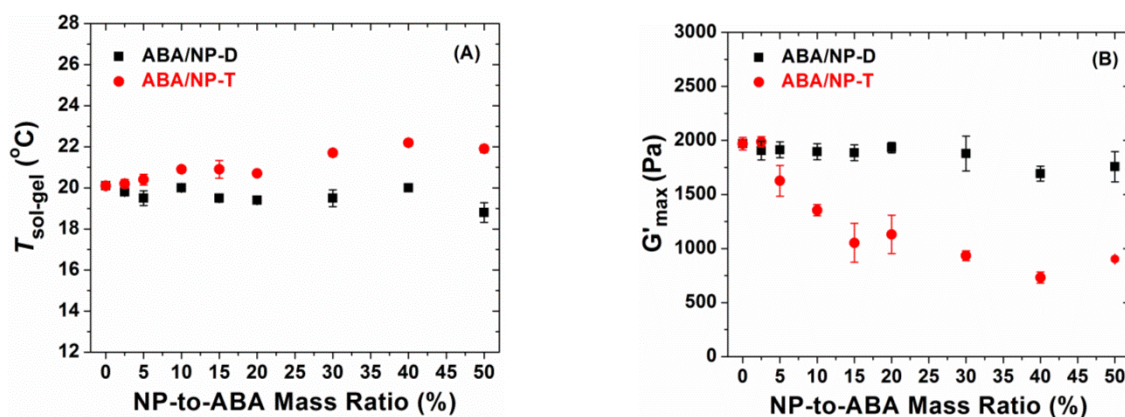


Figure 2.7. Effect of NP-to-polymer mass ratio on $T_{\text{sol-gel}}$ (A) and G'_{max} (B) of hybrid micellar hydrogels of hairy NPs and ABA-D with a polymer concentration of 10 wt %, defined as $[(\text{polymer mass})/(\text{polymer mass} + \text{water mass})] \times 100 \%$. The values of $T_{\text{sol-gel}}$ and G'_{max} are the averages of three rheological measurements, and the error bars are included.

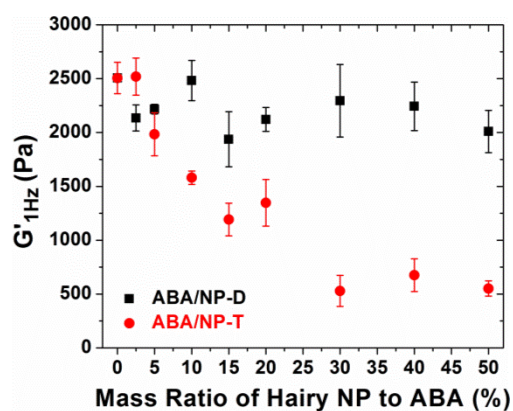


Figure 2.8. Plot of G' at 1 Hz ($G'_{1\text{Hz}}$) from frequency sweeps at 40 °C of hybrid micellar hydrogels of thermosensitive hairy NPs and ABA-D with a polymer concentration of 10 wt %, defined as $[(\text{polymer mass})/(\text{polymer mass} + \text{water mass})] \times 100 \%$ versus NP-to-polymer mass ratio. The value of $G'_{1\text{Hz}}$ for each ratio is the average of three measurements, and the error bar is included.

that the solubility of PEO in water becomes poorer with the increase of temperature. The bridging PEO chains undergo shrinking at elevated temperatures, making the formation of polymer loops become entropically comparable with or even more favorable than the formation of bridging chains among micellar cores. Consequently, the fraction of bridging PEO chains, and thus the G' , decreases upon further heating. (iv) Most interestingly, for the hybrid hydrogel of ABA-D and NP-T with a mass ratio of 100:20, the G' exhibited an increase above 40 °C (Figure 2.6F). This increase became more pronounced for the hybrid gels with mass ratios of 100:30 (Figure 2.6H), 100:40 (Figure 2.6J), and 100:50 (Figure 2.6L). The temperature at which G' began to increase was coincident with the onset temperature of the LCST transition of NP-T in water (Figure 2.2B).

In the above rheology study, the polymer concentrations were defined as $[(\text{polymer mass})/(\text{polymer mass} + \text{water mass})] \times 100\%$. If the amount of hairy NPs is taken into consideration, then the actual polymer concentration, which is $[(\text{polymer mass})/(\text{polymer mass} + \text{water mass} + \text{hairy NP mass})] \times 100\%$, decreased slightly with increasing the NP-to-polymer mass ratio. For example, for the ratio of 50:100, the actual polymer concentration is 9.5%. To eliminate the effect of the polymer concentration changes, we also conducted rheological studies on a series of samples with the actual polymer concentrations of 10 wt % in a similar fashion. Again, for each mass ratio, three measurements were taken and the average values of $T_{\text{sol-gel}}$, G'_{max} , and $G'_{1\text{Hz}}$ were used in the plots of $T_{\text{sol-gel}}$, G'_{max} , and $G'_{1\text{Hz}}$ vs. NP-to-polymer ratio (Figures 2.9 and 2.10). The rheological data can be found in Appendix A.

All the key features found in Figures 2.6-2.8 were observed for the two new sets of hybrid micellar hydrogels (Figures 2.9 and 2.10 and Appendix A): the trends of $T_{\text{sol-gel}}$, G'_{max} , and $G'_{1\text{Hz}}$ as a function of NP-to-polymer mass ratio as well as the noticeable increase of G' above 40 °C for hybrid micellar gels of ABA-D and NP-T. These confirmed that the observed phenomena were the

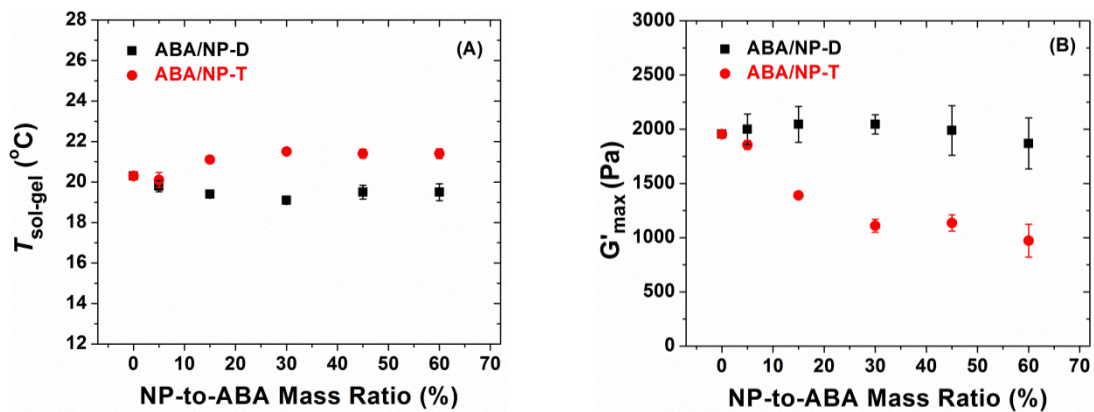


Figure 2.9. Effect of NP-to-ABA-D mass ratio on $T_{\text{sol-gel}}$ (A) and G'_{max} (B) of hybrid micellar hydrogels of NPs and ABA-D with a polymer concentration of 10 wt %, defined as $[(\text{polymer mass})/(\text{polymer mass} + \text{water mass} + \text{hairy NP mass})] \times 100 \%$. The values of $T_{\text{sol-gel}}$ and G'_{max} are the averages of three rheological measurements, and the error bars are included.

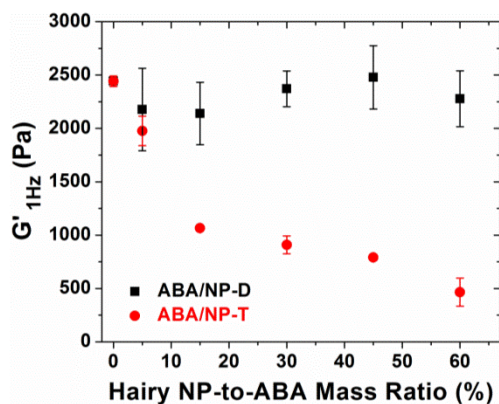


Figure 2.10. Plot of G' at 1 Hz ($G'_{1\text{Hz}}$) from frequency sweeps at 40 °C of hybrid hydrogels of thermosensitive hairy NPs and ABA-D with a polymer concentration of 10 wt %, defined as $[(\text{polymer mass})/(\text{polymer mass} + \text{water mass} + \text{NP mass})] \times 100\%$, versus NP-to-ABA-D mass ratio. The value of $G'_{1\text{Hz}}$ for each mass ratio is the average of three measurements, and the error bar is included in the plot. The frequency sweeps can be found in Appendix A.

results of the different spatial location of hairy NPs.

The G' of a transient physically associated/crosslinked gel is known to be a measure of the number density of elastically active polymer chains (or effective gel network strands): $G' \propto \nu k_B T$, where ν is the number density of elastically active polymer chains (number of elastically active bridging chains per unit volume), k_B is Boltzmann constant, and T is the absolute temperature.^{9, 42-}

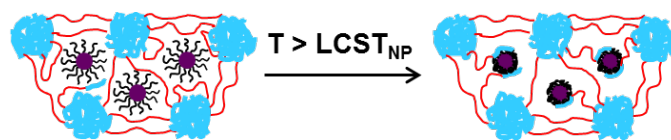
⁴³ It appears that when NP-D resided in the core of ABA-D micelles, the way of the formation of the 3-dimensional network by ABA-D was not affected, i.e., the relative fractions of bridging chains, loops, and dangling chains are not affected. Note that the loops and dangling polymer chains do not sustain the mechanical stress applied to the network and thus do not contribute the modulus of micellar hydrogels. As a result, the G' of the hybrid micellar hydrogels of ABA-D and NP-D remained about the same. For hybrid micellar hydrogels of ABA-D and NP-T, the hairy NPs were located in the interstitial space among the micelles. At sufficiently high concentrations, it can be imagined that the presence of NP-T could increase the stretching of the bridging polymer chains (Scheme 2.1); the formation of loops might become entropically favorable compared with the bridging chains among micelles, resulting in a lower density of elastically active polymer chains and hence lower G' . This can also be seen from the more significant decrease of G' at ~ 50 °C for the hybrid micellar hydrogels of ABA-D and NP-T compared with the hybrid hydrogels containing the same amounts of NP-D. Because the fraction of bridging chains in the hybrid micellar hydrogels of ABA-D and NP-T was significantly lower than that in the hybrid gels of ABA-D and NP-D, with the increase of temperature and the shrinking of the bridging PEO chains, G' decreased more significantly. In addition, the slightly higher sol-gel transition temperatures of hybrid micellar gels of ABA-D and NP-T compared with those containing NP-D at the same level of NP

loadings also suggested that the former gels were weaker and slightly higher temperatures were needed to achieve sufficient mechanical strengths to become gels.

An interesting observation for the hybrid hydrogels of ABA-D and NP-T is the noticeable increase of G' starting from 40 °C, which reflects the increase in the number of bridging polymer chains in the hydrogels. We believe that this is caused by the collapse of P(TEGMMA-*co*-NBDMA) brushes, which likely adsorb the dangling polymer chains in the interstitial space and also possibly the polymer chains in the loop form, resulting in an increase in the bridging polymer chain density (Scheme 2.4). This is supported by the observation of the increased FRET from the aqueous mixture of ABA-D with a concentration of 0.217 mg/g and NP-T with a concentration of 0.012 mg/g, the same sample shown in Figure 2.4, after equilibration at 50 °C for 24 h (Figure A10 in Appendix A). The emission intensity at ~ 520 nm decreased appreciably and the intensity at 575 nm increased noticeably, indicating that there was increasing interaction between the FRET pair, which likely came from the adsorption of ABA-D polymer chains onto the collapsed NP-T. A further study is needed to elucidate this observation.

2.4. Conclusions

We presented a method for the control of spatial location of NPs, either inside or outside the core of micelles, in hybrid micellar hydrogels of a thermosensitive ABA triblock copolymer and hairy NPs and studied the effect of different locations of NPs on gel properties. Two batches of thermosensitive hairy NPs with different LCSTs (NP-D and NP-T) and one thermosensitive ABA triblock copolymer (ABA-D) were synthesized. The control of spatial location of NPs was achieved by controlling the LCST of hairy NPs relative to that of thermosensitive outer blocks of ABA-D. When $LCST_{NP}$ and $LCST_{ABA}$ were similar to each other, co-micellization occurred and



Scheme 2.4. Collapsed Polymer Brushes of NP-T Adsorb Polymer Chains to Form New Bridges

the NPs were located in the core of micelles. When the $LCST_{NP}$ was significantly higher, the NPs were located outside the core of micelles. Rheological measurements were conducted to investigate the effect of different locations of hairy NPs on gel properties. The $T_{sol-gel}$ and G'_{max} of hybrid micellar gels of ABA-D and NP-D did not change significantly with the increase of NP-to-polymer mass ratio. In contrast, the $T_{sol-gel}$ of aqueous mixtures of ABA-D and NP-T increased slightly and G' decreased significantly with the increase of NP-to-polymer mass ratio. The presence of hairy NPs in the interstitial space appeared to affect the self-assembly of ABA-D and promoted the formation of polymer loops, resulting in a lower density of bridging chains and lower G' values. For hybrid hydrogels of ABA-D and NP-T, above 40 °C, an increase in G' was observed, which was likely caused by the collapsed brushes absorbing polymer chains in the dangling and loop forms, increasing the density of bridging chains. The findings reported here could be used for the design of injectable hybrid micellar hydrogels of thermosensitive ABA triblock copolymers and NPs for possible biomedical applications.

2.5. References

1. Hamley, I., *Block Copolymers in Solution: Fundamentals and Applications*. John Wiley & Sons: Chichester, 2005.
2. Jeong, B.; Kim, S. W.; Bae, Y. H. *Adv. Drug Deliver. Rev* **2002**, *54*, 37-51.
3. Gil, E. S.; Hudson, S. M. *Prog. Polym. Sci.* **2004**, *29*, 1173-1222.
4. He, C.; Kim, S. W.; Lee, D. S. *J. Control Release.* **2008**, *127*, 189-207.
5. Yu, L.; Ding, J. *Chem. Soc. Rev.* **2008**, *37*, 1473-1481.
6. Li, C.; Tang, Y.; Armes, S. P.; Morris, C. J.; Rose, S. F.; Lloyd, A. W.; Lewis, A. L. *Biomacromolecules* **2005**, *6*, 994-999.
7. Kirkland, S. E.; Hensarling, R. M.; McConaughy, S. D.; Guo, Y.; Jarrett, W. L.; McCormick, C. L. *Biomacromolecules* **2008**, *9*, 481-486.
8. O'Lenick, T. G.; Jiang, X. G.; Zhao, B. *Langmuir* **2010**, *26*, 8787-8796.
9. O'Lenick, T. G.; Jin, N.; Woodcock, J. W.; Zhao, B. *J. Phys. Chem. B* **2011**, *115*, 2870-2881.
10. Sugihara, S.; Kanaoka, S.; Aoshima, S. *Macromolecules* **2005**, *38*, 1919-1927.
11. Jin, N.; Woodcock, J. W.; Xue, C.; O'Lenick, T. G.; Jiang, X.; Jin, S.; Dadmun, M. D.; Zhao, B. *Macromolecules* **2011**, *44*, 3556-3566.
12. Roucoux, A.; Schulz, J.; Patin, H. *Chem. Rev.* **2002**, *102*, 3757-3778.
13. Daniel, M.-C.; Astruc, D. *Chem. Rev.* **2004**, *104*, 293-346.
14. Lu, A.-H.; Salabas, E. L.; Schüth, F. *Angewandte Chemie International Edition* **2007**, *46*, 1222-1244.
15. Haraguchi, K.; Takehisa, T. *Adv. Mater.* **2002**, *14*, 1120-1124.
16. Messing, R.; Schmidt, A. M. *Polym. Chem.* **2011**, *2*, 18-32.
17. Okay, O.; Oppermann, W. *Macromolecules* **2007**, *40*, 3378-3387.

18. Schexnaider, P.; Schmidt, G. *Colloid Polym. Sci.* **2009**, *287*, 1-11.
19. Wu, C.-J.; Gaharwar, A. K.; Chan, B. K.; Schmidt, G. *Macromolecules* **2011**, *44*, 8215-8224.
20. Fuhrer, R.; Athanassiou, E. K.; Luechinger, N. A.; Stark, W. J. *Small* **2009**, *5*, 383-388.
21. Sun, K.; Kumar, R.; Falvey, D. E.; Raghavan, S. R. *J. Am. Chem. Soc.* **2009**, *131*, 7135-7141.
22. Pozzo, D. C.; Walker, L. M. *Macromol. Symp.* **2005**, *227*, 203-210.
23. Pozzo, D. C.; Walker, L. M. *Macromolecules* **2007**, *40*, 5801-5811.
24. Pozzo, D. C.; Walker, L. M. *Colloids Surf., A* **2007**, *294*, 117-129.
25. Castelletto, V.; Ansari, I. A.; Hamley, I. W. *Macromolecules* **2003**, *36*, 1694-1700.
26. Qin, J.; Asempah, I.; Laurent, S.; Fornara, A.; Muller, R. N.; Muhammed, M. *Adv. Mater.* **2009**, *21*, 1354-1357.
27. Krekhova, M.; Lang, T.; Richter, R.; Schmalz, H. *Langmuir* **2010**, *26*, 19181-19190.
28. Nambam, J. S.; Philip, J. *Langmuir* **2012**, *28*, 12044-12053.
29. Reinicke, S.; Dohler, S.; Tea, S.; Krekhova, M.; Messing, R.; Schmidt, A. M.; Schmalz, H. *Soft Matter* **2010**, *6*, 2760-2773.
30. Han, S.; Hagiwara, M.; Ishizone, T. *Macromolecules* **2003**, *36*, 8312-8319.
31. Li, D.; Jones, G. L.; Dunlap, J. R.; Hua, F.; Zhao, B. *Langmuir* **2006**, *22*, 3344-3351.
32. Lutz, J.-F.; Hoth, A. *Macromolecules* **2006**, *39*, 893-896.
33. Ishizone, T.; Seki, A.; Hagiwara, M.; Han, S.; Yokoyama, H.; Oyane, A.; Deffieux, A.; Carlotti, S. *Macromolecules* **2008**, *41*, 2963-2967.
34. dos Remedios, C. G.; Moens, P. D. J. *J. Struct. Biol.* **1995**, *115*, 175-185.
35. Yin, J.; Hu, H.; Wu, Y.; Liu, S. *Polymer Chemistry* **2011**, *2*, 363-371.
36. Henn, D. M.; Wright, R. A. E.; Woodcock, J. W.; Hu, B.; Zhao, B. *Langmuir* **2014**, *30*, 2541-2550.

37. Horton, J. M.; Bai, Z.; Jiang, X.; Li, D.; Lodge, T. P.; Zhao, B. *Langmuir* **2011**, *27*, 2019-2027.
38. Onoda, M.; Uchiyama, S.; Santa, T.; Imai, K. *Anal. Chem.* **2002**, *74*, 4089-4096.
39. Bao, C.; Tang, S.; Horton, J. M.; Jiang, X.; Tang, P.; Qiu, F.; Zhu, L.; Zhao, B. *Macromolecules* **2012**, *45*, 8027-8036.
40. Durand-Gasselin, C.; Sanson, N.; Lequeux, N. *Langmuir* **2011**, *27*, 12329-12335.
41. Noro, A.; Matsushita, Y.; Lodge, T. P. *Macromolecules* **2009**, *42*, 5802-5810.
42. Yoshida, T.; Kanaoka, S.; Watanabe, H.; Aoshima, S. *J. Polym. Sci. A Polym. Chem.* **2005**, *43*, 2712-2722.
43. He, Y.; Boswell, P. G.; Bühlmann, P.; Lodge, T. P. *J. Phys. Chem. B* **2007**, *111*, 4645-4652.
44. The work presented in this Chapter has been published in *Langmuir* as an article (*Langmuir* **2014**, *30*, 11212-11224).

Appendix A

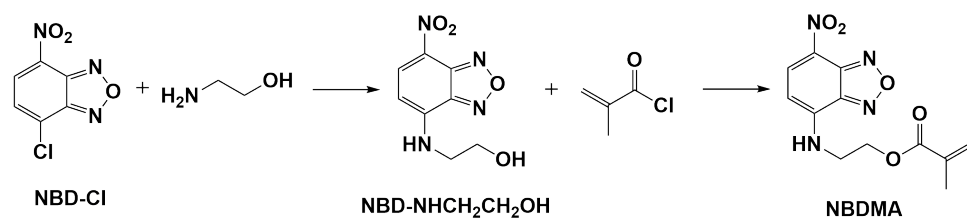
for

**Chapter 2. Hybrid Micellar Hydrogels of a Thermosensitive ABA Triblock
Copolymer and Hairy Nanoparticles: Effect of Spatial Location of Hairy
Nanoparticles on Gel Properties**

A.1. Synthesis of 4-(2-Methacryloyloxyethylamino)-7-nitro-2,1,3-benzoxadiazole (NBDMA)

4-Chloro-7-nitro-2,1,3-benzoxadiazole (NBD-Cl, 0.456 g, 2.29 mmol) was dissolved in acetonitrile (40 mL) in a 250 mL three-necked flask, followed by the addition of a solution of ethanolamine (0.194 g, 3.17 mmol) in acetonitrile (20 mL). After the mixture was stirred at room temperature overnight, the solvent was removed under a reduced pressure. The crude product was purified by silica gel column chromatography using a solvent mixture of dichloromethane and methanol (19 : 1, v/v) as eluent to afford 4-(2-hydroxyethylamino)-7-nitro-2,1,3-benzoxadiazole (NBD-OH, 0.241 g, yield 47 %) as an orange crystal. ^1H NMR δ (ppm, DMSO- d_6): 3.55 (br, 2H, $\text{NHCH}_2\text{CH}_2\text{OH}$), 3.69 (t, 2H, $\text{NHCH}_2\text{CH}_2\text{OH}$), 4.95 (b, 1H, $\text{NHCH}_2\text{CH}_2\text{OH}$), 6.46 (d, 1H, aromatic), 8.49 (d, 1H, aromatic), 9.43 (b, 1H, $\text{NHCH}_2\text{CH}_2\text{OH}$). ^{13}C NMR δ (ppm, DMSO- d_6): 46.13 ($\text{NHCH}_2\text{CH}_2\text{OH}$), 58.89 ($\text{NHCH}_2\text{CH}_2\text{OH}$), 99.38 (aromatic), 120.54 (aromatic), 137.91 (aromatic), 144.07 (aromatic), 144.41 (aromatic), 145.63 (aromatic). MS (DART-TOF): $[\text{M} + \text{H}]^+$ ion observed at m/z 225.0666.

NBD-OH (0.203 g, 0.90 mmol) was dissolved in acetonitrile (40 mL) in a 100 mL three-necked flask; methacryloyl chloride (0.418 g, 4.0 mmol) was added into the mixture in a dropwise fashion under nitrogen. The reaction mixture was refluxed at 85 °C in an oil bath for 4 h. The solvent was removed under vacuum, and the residue was dissolved in methylene chloride and washed with water three times. The organic layer was collected and dried with anhydrous sodium sulfate overnight. After the filtration of sodium sulfate and the removal of volatiles by a rotovap, the residue was purified by silica gel column chromatography with hexane and ethyl acetate (1 : 1, v/v) as the eluent to afford NBDMA as orange powder (0.151 g, yield 57 %). ^1H NMR δ (ppm, DMSO- d_6): 1.83 (s, 3H, CH_3), 3.82 (b, 2H, NHCH_2CH_2), 4.37 (t, 2H, NHCH_2CH_2), 5.66 and 6.01 (m, 2H, $\text{C}=\text{CH}_2$), 6.53 (d, 1H, aromatic), 8.52 (d, 1H, aromatic), 9.52 (b, 1H, NHCH_2). ^{13}C NMR



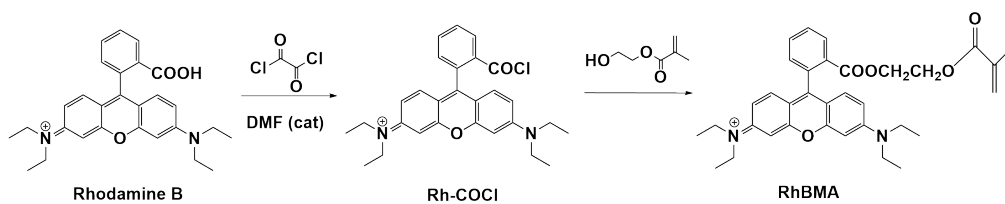
Scheme A1. Synthesis of NBDMA

δ (ppm, DMSO-d): 17.95 (CH_3), 42.18 (NHCH_2CH_2), 62.20 (NHCH_2CH_2), 99.43 (aromatic), 121.21 (aromatic), 126.25 ($\text{C}=\text{CH}_2$), 135.56 ($\text{C}=\text{CH}_2$), 137.76 (aromatic), 144.01 (aromatic), 144.40 (aromatic), 145.16 (aromatic), 166.49 ($\text{NHCH}_2\text{CH}_2\text{OC}=\text{O}$). MS (DART-TOF): $[\text{M} + \text{H}]^+$ ion observed at m/z 293.0876.

A.2. Synthesis of RhBMA.

Rhodamine B (0.477 g, 0.996 mmol) was dissolved in methylene chloride (4 mL) in a 100 mL flask in an ice/water bath, followed by the addition of oxalyl chloride (0.220 g, 1.73 mmol) and DMF (10 μL). After the reaction mixture was stirred at room temperature overnight, the volatiles were evaporated under vacuum, and the residue (Rhodamine-COCl) was dissolved in methylene chloride (3 mL).

In another 100 mL three-necked flask, 2-hydroxyethyl methacrylate (0.199 g, 1.53 mmol) was dissolved in methylene chloride (3 mL), followed by the addition of triethylamine (0.102 g, 1.01 mmol). The mixture was stirred in an ice/water bath for 30 min and then Rhodamine-COCl dissolved in methylene chloride was added in a dropwise fashion into the flask. The reaction mixture was stirred overnight and then evaporated to dryness under reduced pressure. The residue was dissolved in methylene chloride and washed with water three times. The organic layer was collected and dried with anhydrous sodium sulfate overnight. After the filtration of sodium sulfate and the removal of solvents by a rotovap, the crude product was purified by silica gel column chromatography using ethyl acetate and methanol (2 : 1, v/v) as the eluent to afford pure RhBMA (0.552 g, yield: 51.7 %). ^1H NMR (δ , ppm, CD_3Cl): 1.31 (t, 12H, $4\text{CH}_2\text{CH}_3$), 1.86 (s, 3H, CH_3), 3.61 (q, 8H, $4\text{CH}_2\text{CH}_3$), 4.17 (t, 2H, $\text{COOCH}_2\text{CH}_2$), 4.27 (t, 2H, $\text{COOCH}_2\text{CH}_2$), 5.53 (d, 1H, $\text{C}=\text{CH}_2$), 6.00 (d, 1H, $\text{C}=\text{CH}_2$), 6.78, 6.91, 7.04, 7.30, 7.76 and 8.27 (m, 10H, aromatic). ^{13}C NMR



Scheme A2. Synthesis of RhBMA

(δ , ppm, CDCl_3): 12.87 (CH_2CH_3), 18.46 (CH_3), 46.38 (CH_2CH_3), 62.25 ($\text{COOCH}_2\text{CH}_2$), 63.38 ($\text{COOCH}_2\text{CH}_2$), 96.57 (aromatic), 113.73 (aromatic), 114.57 (aromatic), 126.40 ($\text{CH}_2=\text{C}$), 129.54 (aromatic), 130.57 (aromatic), 130.65 (aromatic), 131.45 (aromatic), 131.64 (aromatic), 133.61 (aromatic), 133.96 (aromatic), 135.87 (aromatic), 155.77 (aromatic), 157.90 (aromatic), 158.77 (aromatic), 164.87 (aromatic), 167.07 (COOCH_2). MS (DART-TOF): $[\text{M}]^+$ ion observed at m/z 555.2860.

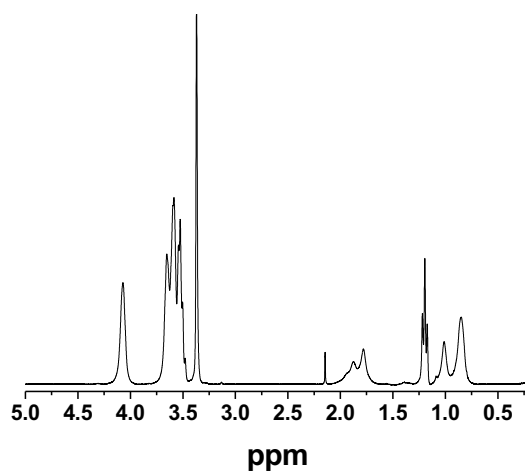


Figure A1. ^1H NMR spectrum of the free copolymer P(DEGMMA-*co*-DEGEMA-*co*-NBDMA) formed from the free initiator ethyl 2-bromoisobutyrate in the synthesis of P(DEGMMA-*co*-DEGEMA-*co*-NBDMA) brush-grafted silica nanoparticles (NP-D). CDCl_3 was used as solvent.

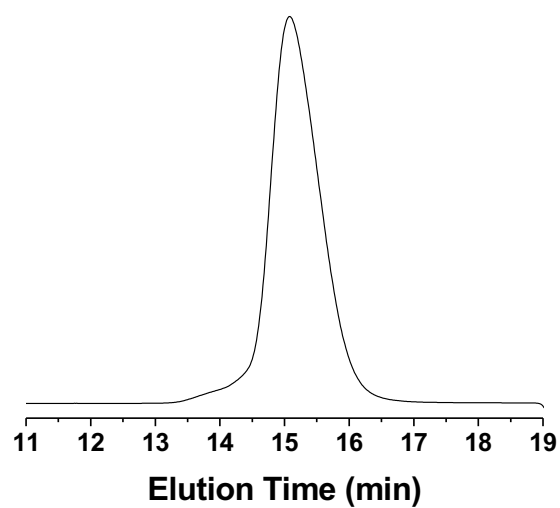


Figure A2. Size exclusion chromatography (SEC) trace of the dried free copolymer P(DEGMMA-*co*-DEGEMA-*co*-NBDMA) formed from the free initiator ethyl 2-bromoisobutyrate in the synthesis of P(DEGMMA-*co*-DEGEMA-*co*-NBDMA) brush-grafted silica nanoparticles (NP-D).

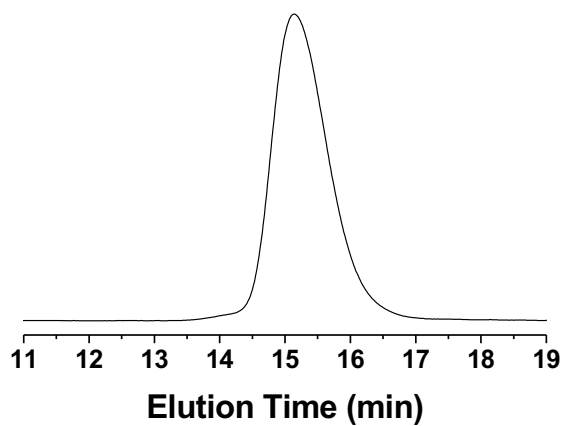


Figure A3. SEC trace of the dried free polymer P(TEGMMA-*co*-NBDMA) formed from the free initiator ethyl 2-bromoisobutyrate in the synthesis of P(TEGMMA-*co*-NBDMA) brush-grafted silica nanoparticles (NP-T).

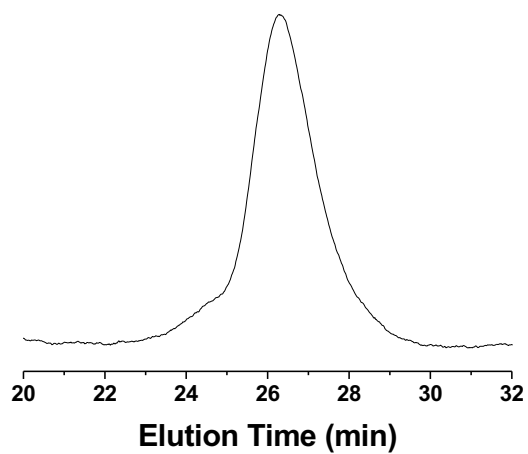


Figure A4. SEC trace of ABA triblock copolymer P(DEGMMA-*co*-DEGEMA-*co*-RhBMA)-*b*-PEO-*b*-P(DEGMMA-*co*-DEGEMA-*co*-RhBMA) (ABA-D). The SEC analysis was conducted using a SEC system with DMF containing 0.05 M LiBr as eluent.

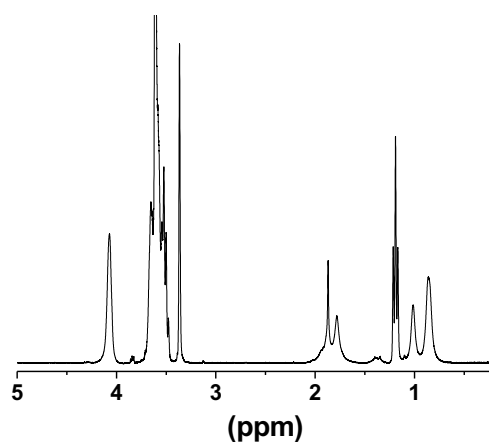
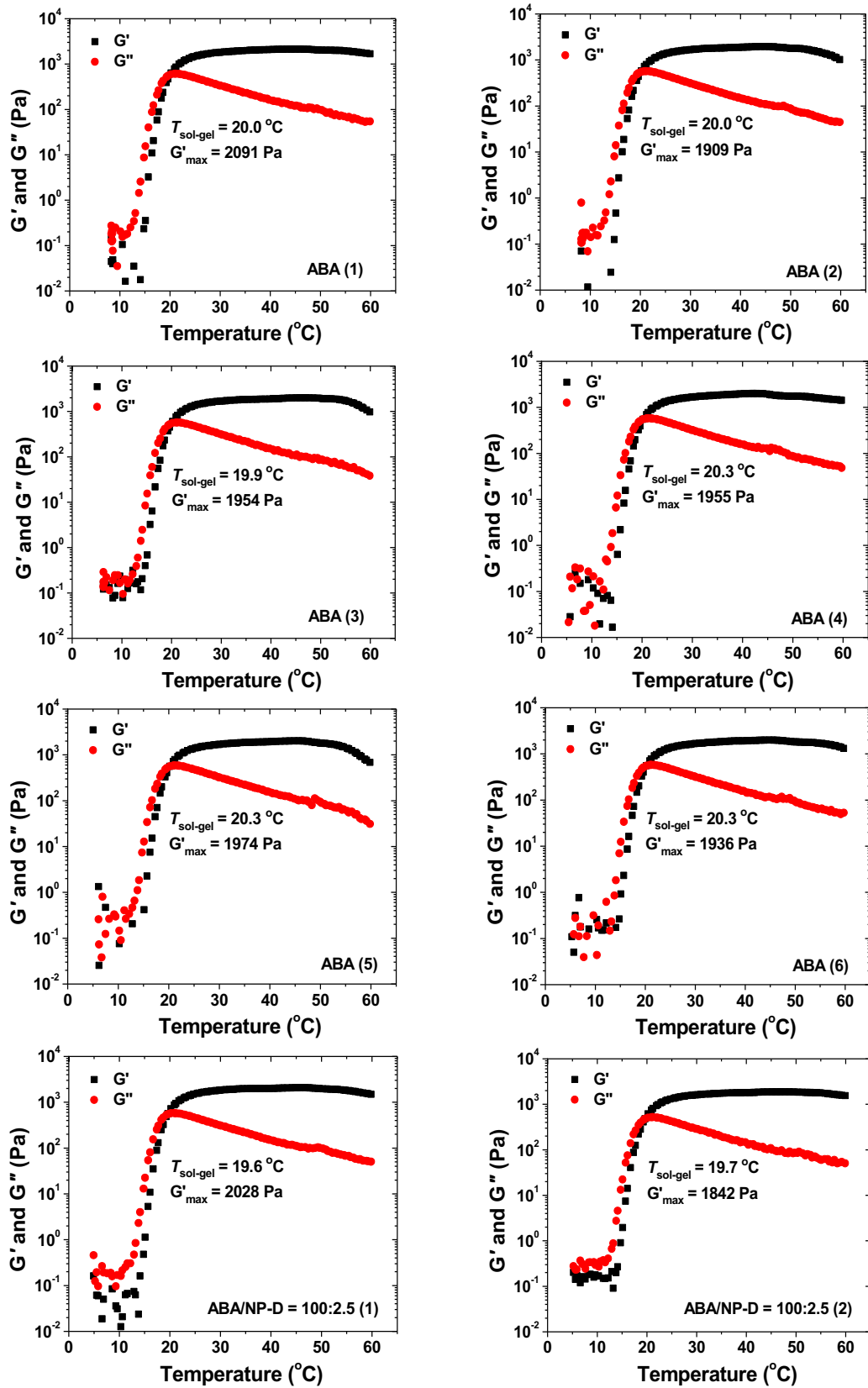
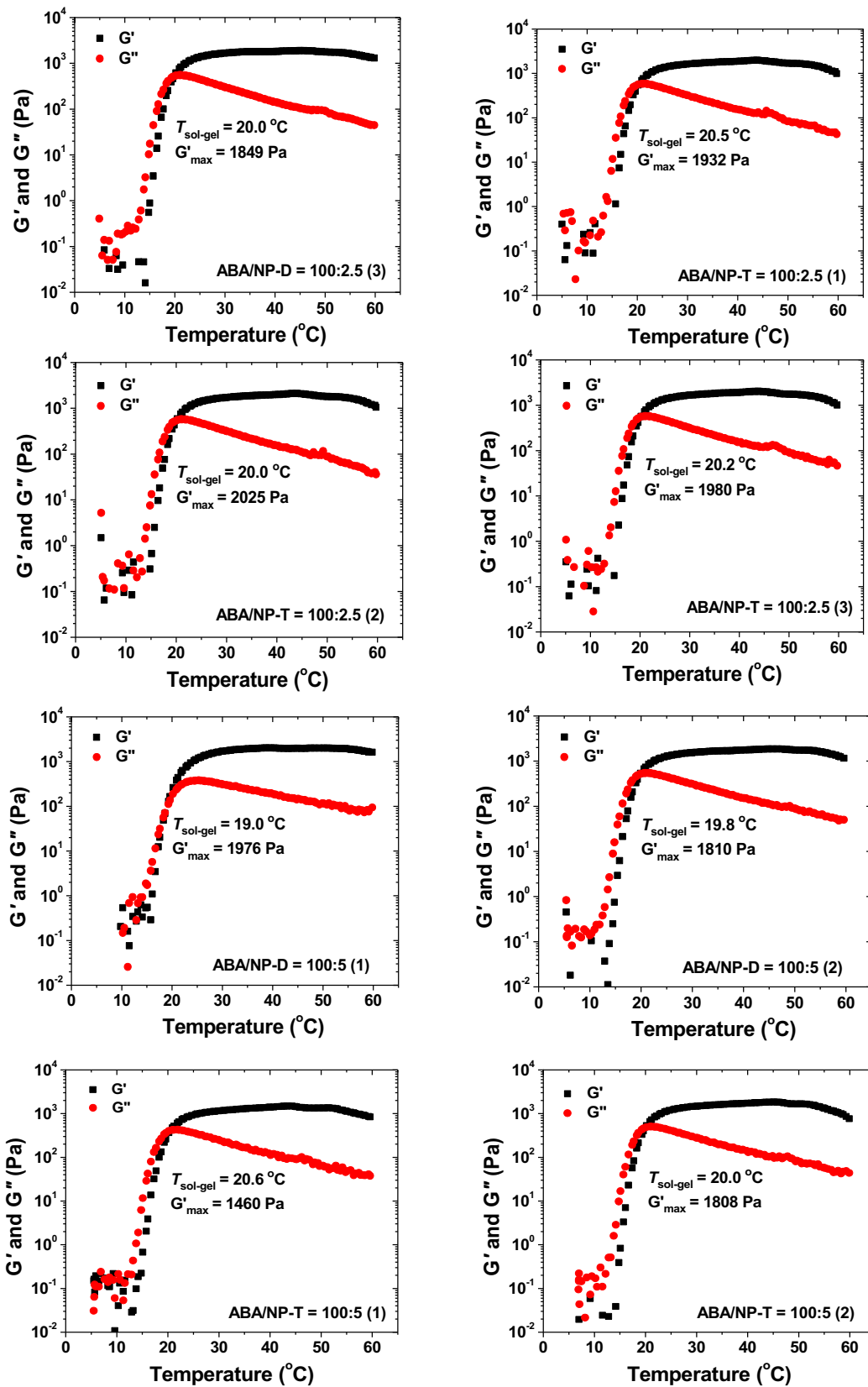


Figure A5. ^1H NMR spectrum of the ABA triblock copolymer P(DEGMMA-co-DEGEMA-co-RhBMA)-*b*-PEO-*b*-P(DEGMMA-co-DEGEMA-co-RhBMA) (ABA-D) in CDCl_3 .

Figure A6. Plots of dynamic storage modulus G' and loss modulus G'' of aqueous mixtures of ABA-D with a concentration of 10 wt %, defined as $[(\text{polymer mass})/(\text{polymer mass} + \text{water mass})] \times 100\%$, and hairy NPs with various NP-to-polymer mass ratios versus temperature for both NP-D and NP-T. The data were collected from temperature ramp experiments performed by using a frequency of 1 Hz, a strain amplitude of 1 %, and a heating rate of 3 °C/min.



(Figure A6. continued)



(Figure A6. continued)

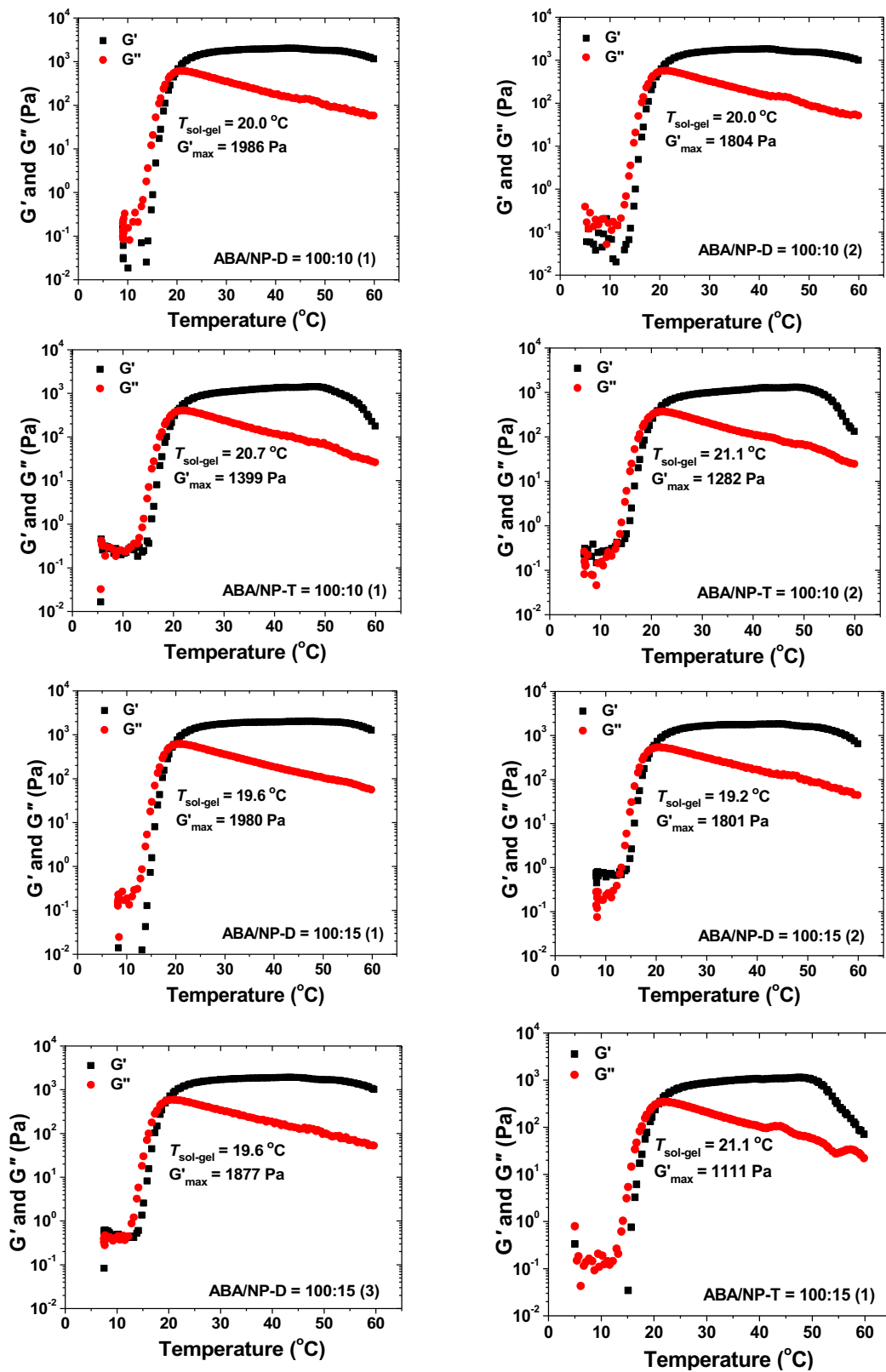


(Figure A6. continued)

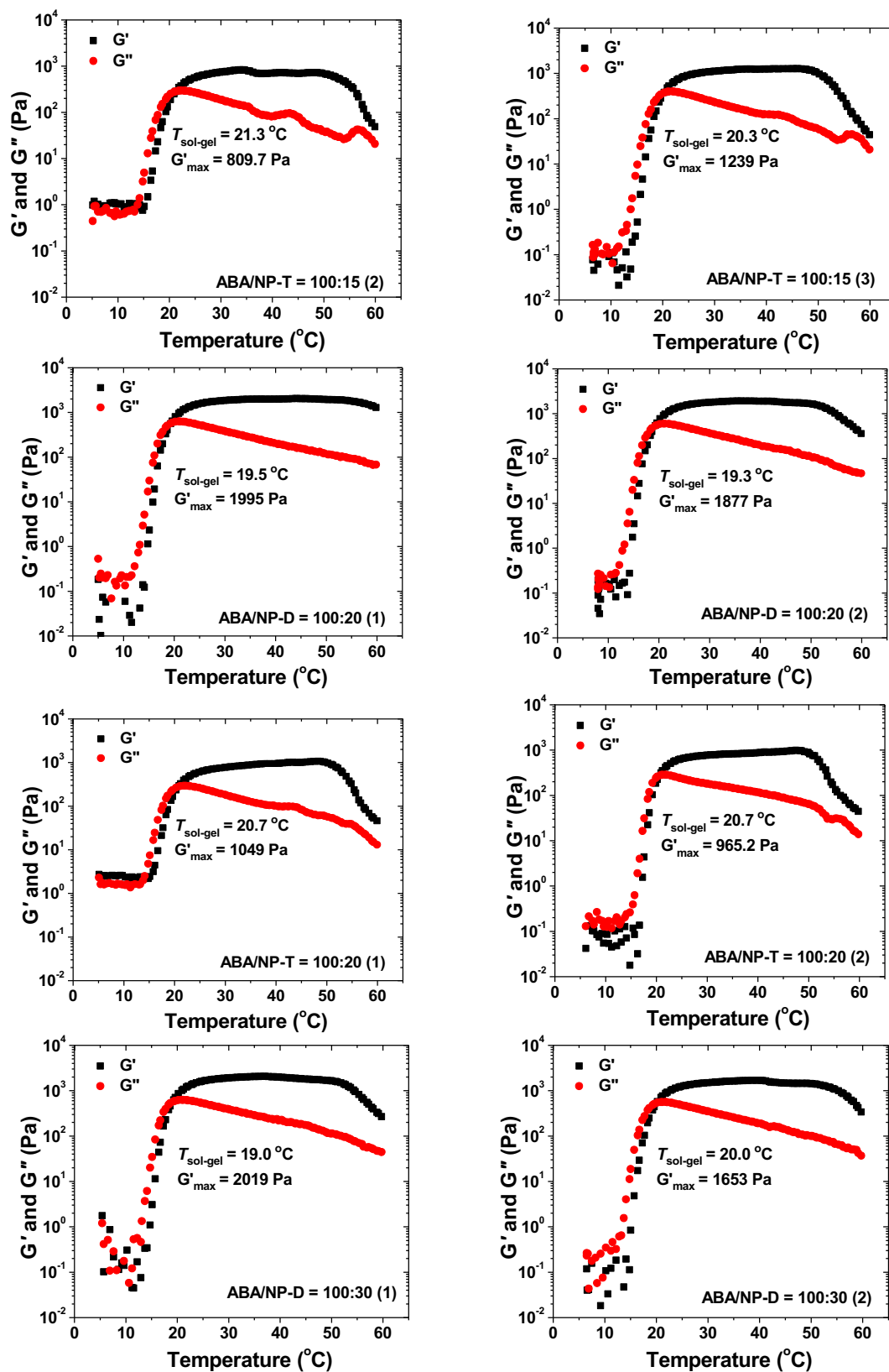


(Figure A6. continued)

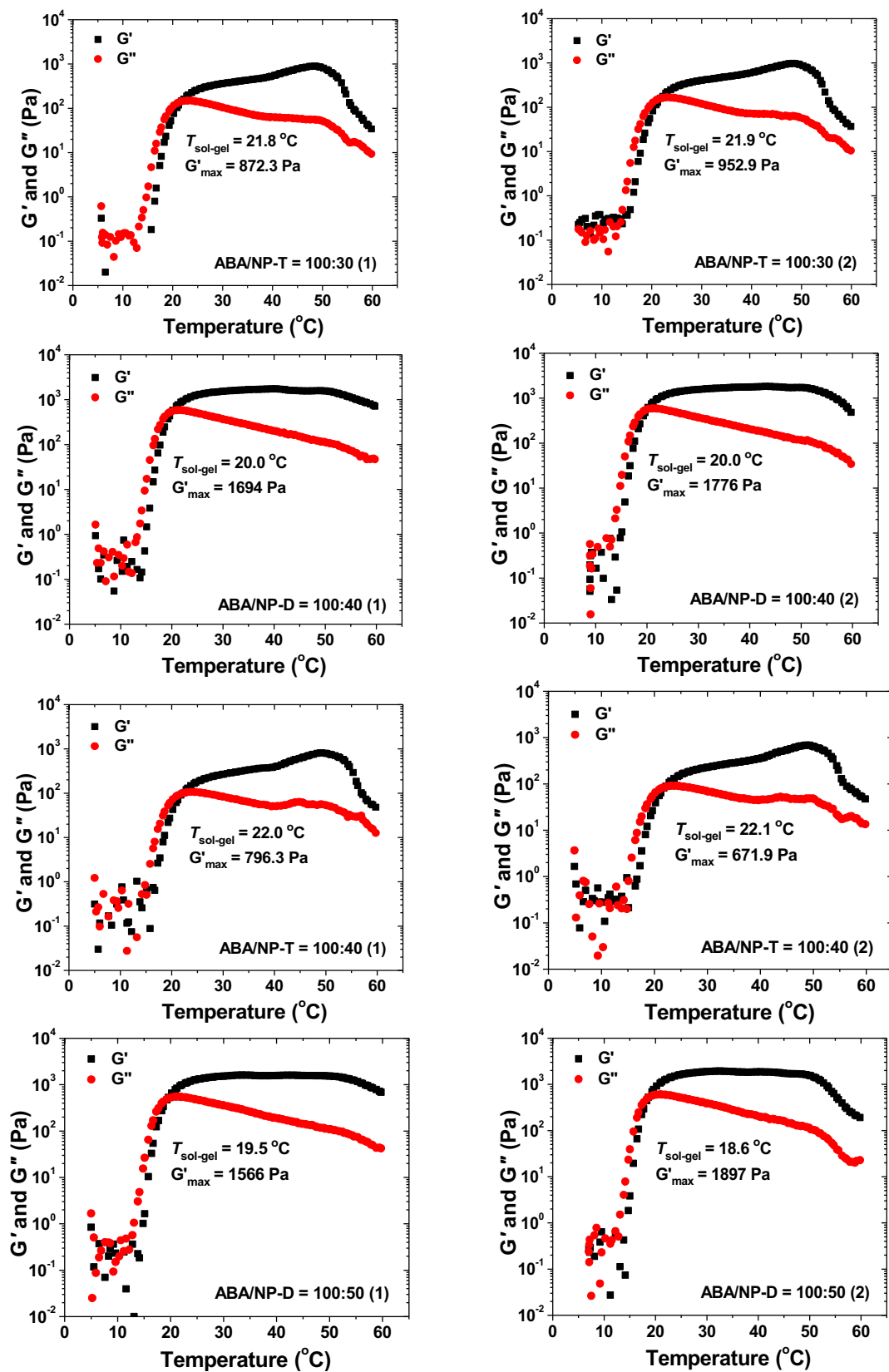


(Figure A6. continued)

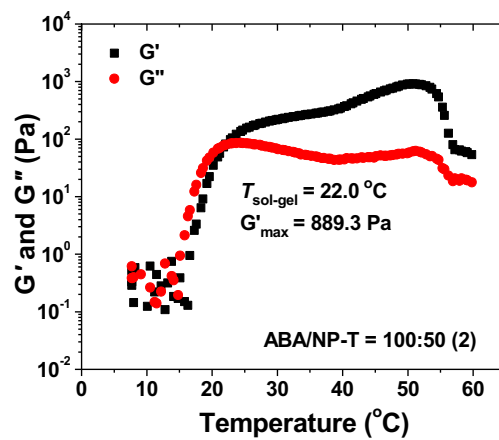
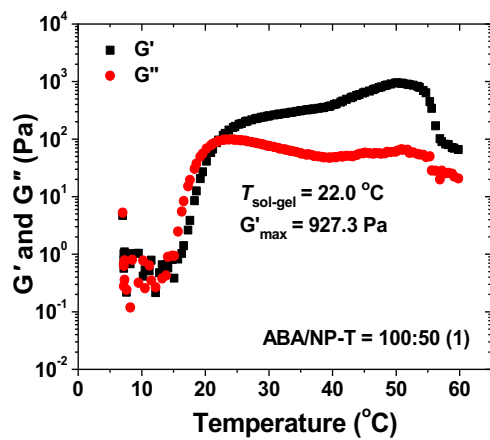


(Figure A6. Continued)

Figure A7. Frequency dependences of dynamic storage modulus G' (black square) and loss modulus G'' (red circle) at 40 °C of the hybrid micellar hydrogels of the ABA triblock copolymer ABA-D and thermosensitive hairy NPs with various NP-to-polymer mass ratios and a polymer concentration of 10 wt % defined as $[(\text{polymer mass})/(\text{polymer mass} + \text{water mass})] \times 100\%$. A strain amplitude of 1.0% was used in the frequency sweep experiments.

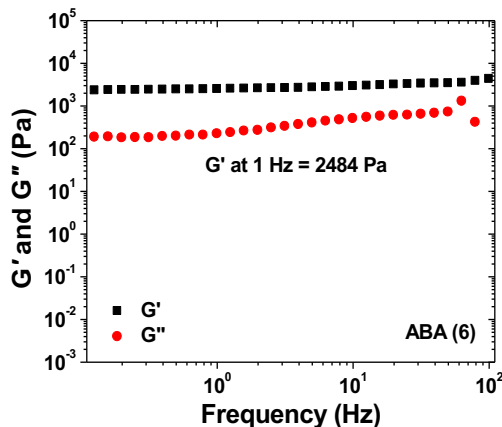
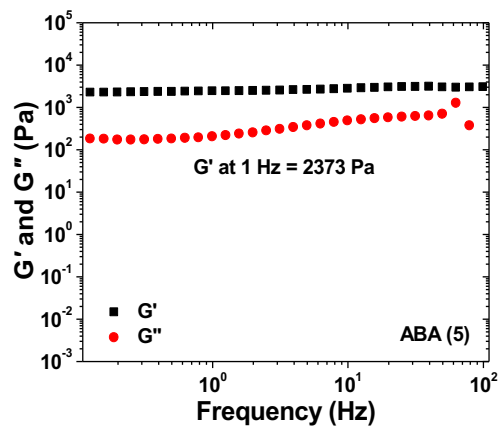
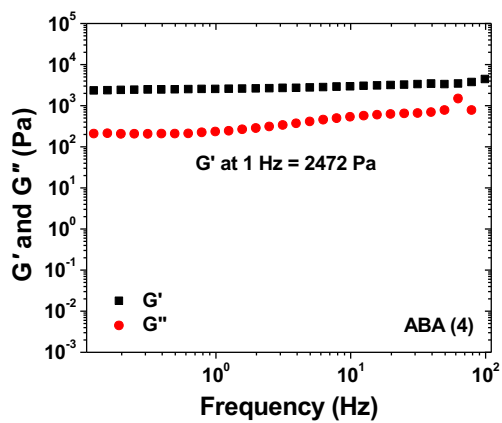
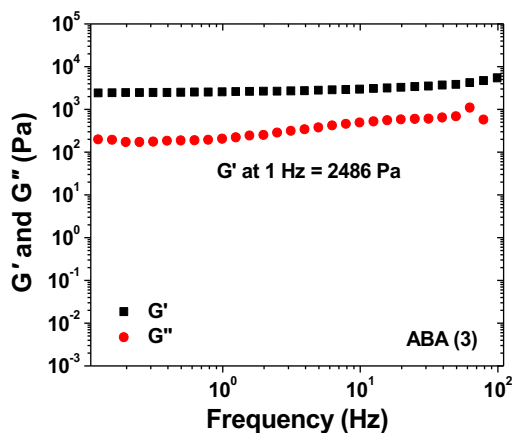
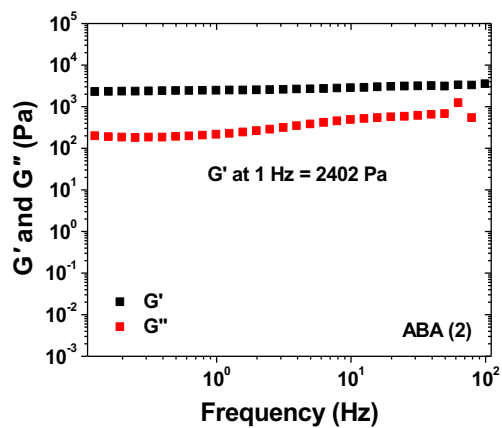
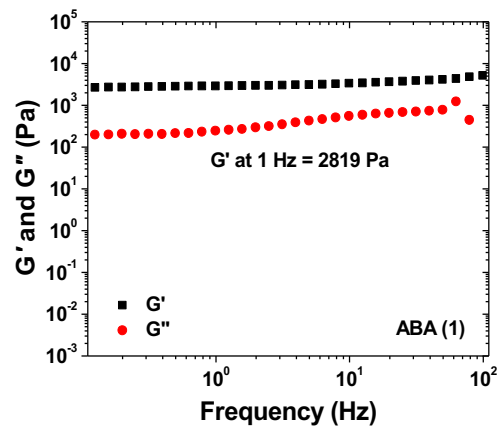


(Figure A7 continued)

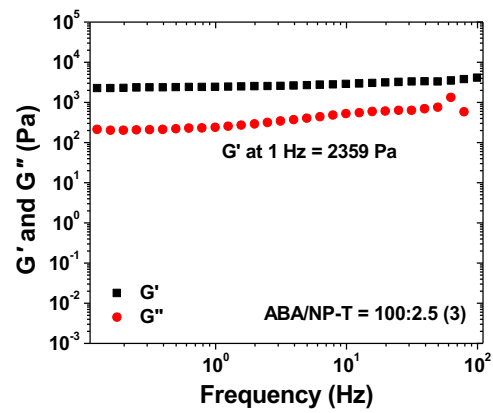
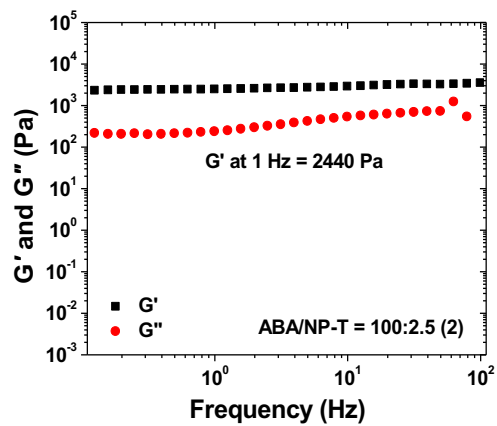
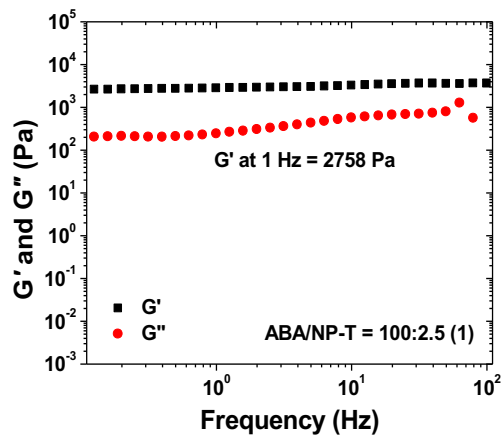
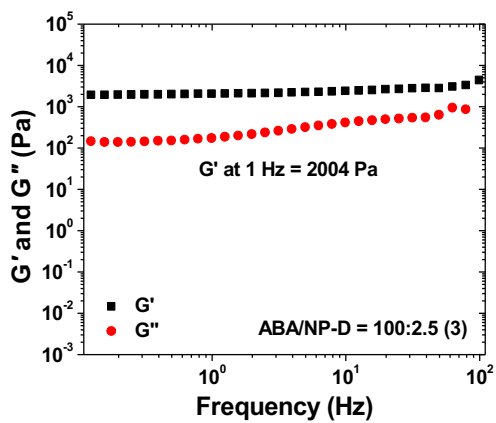
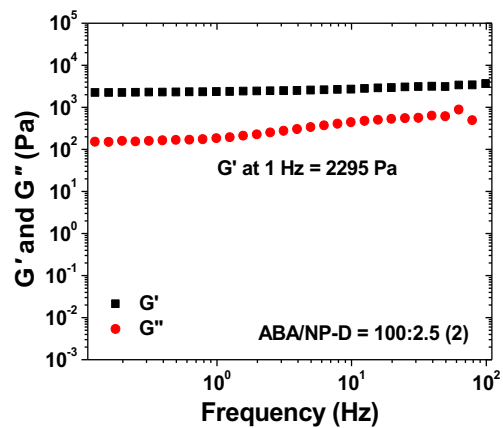
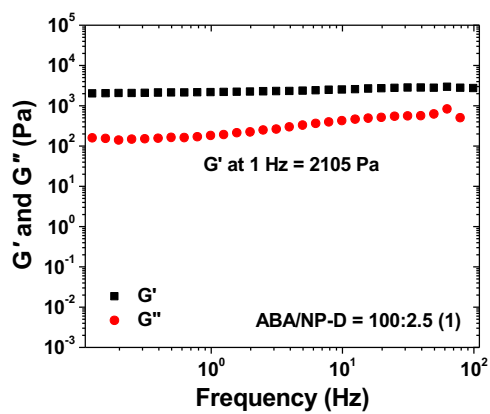


(Figure A7 continued)

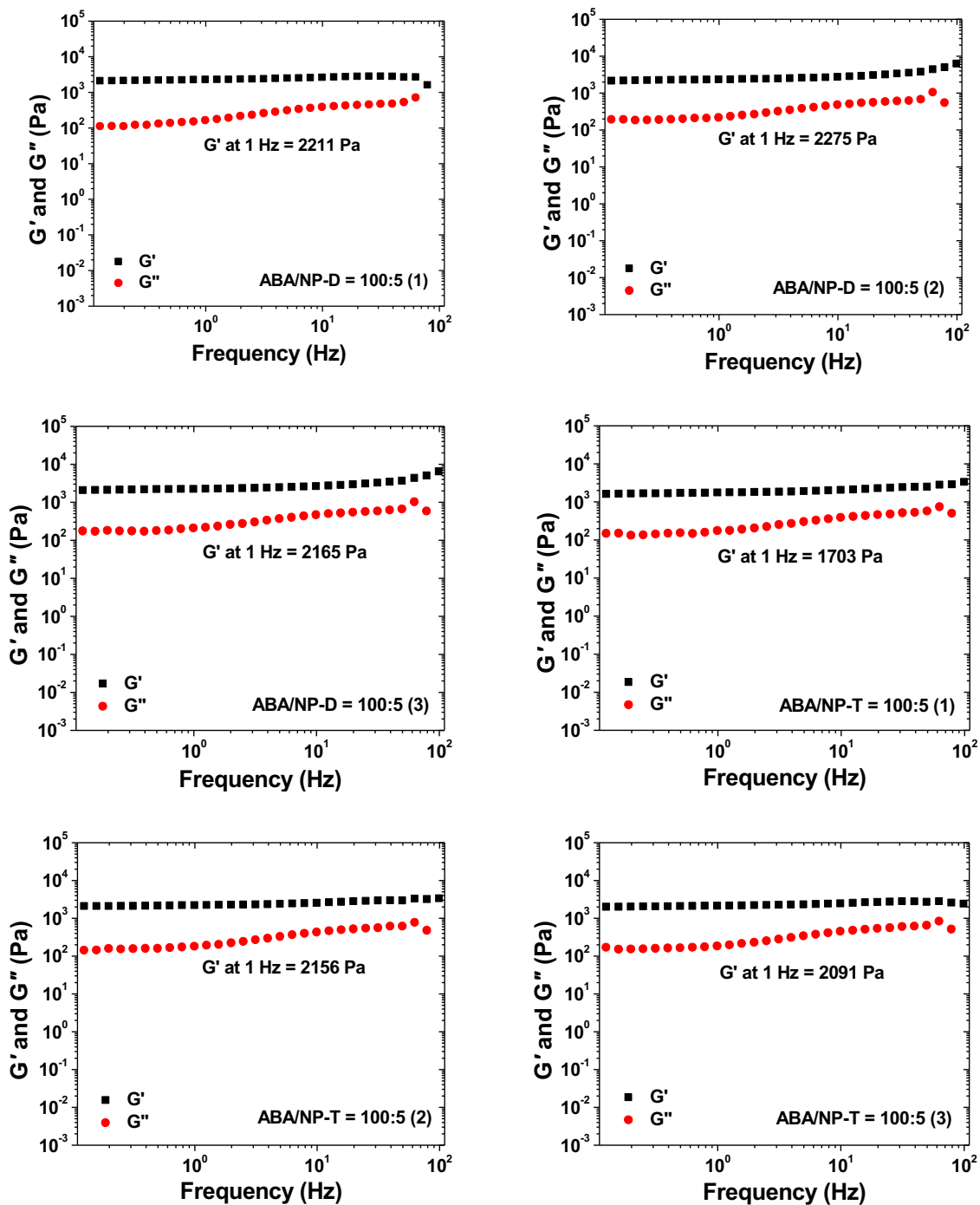


(Figure A7 continued)

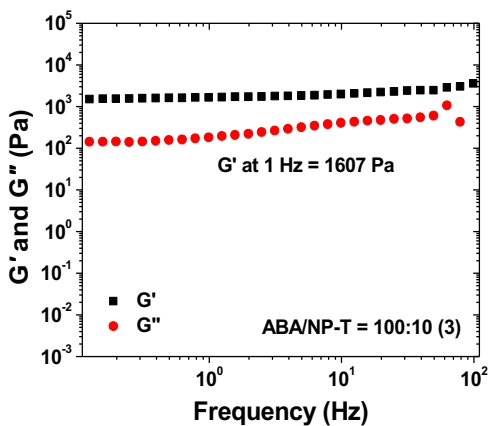
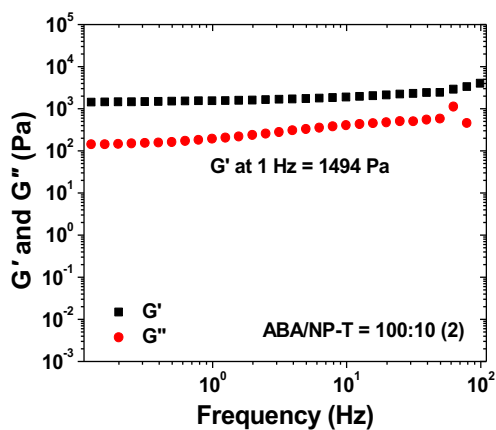
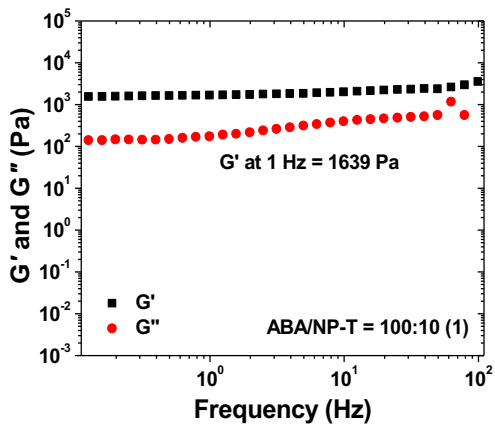
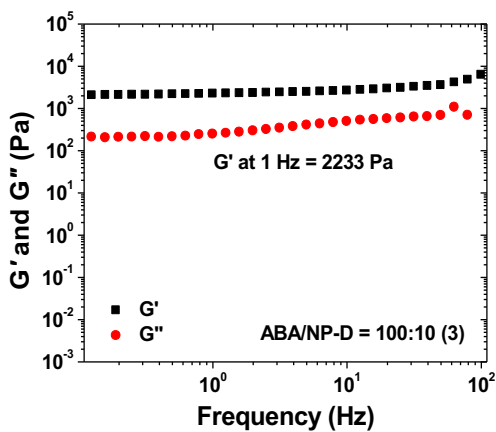
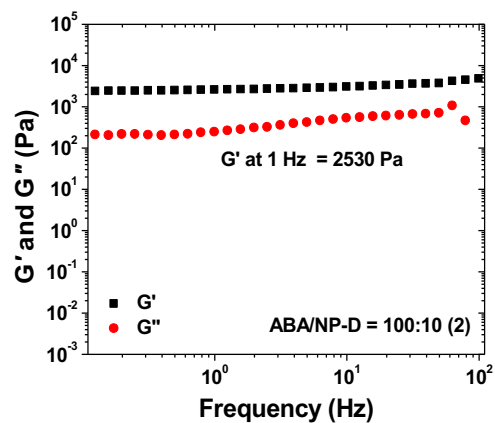
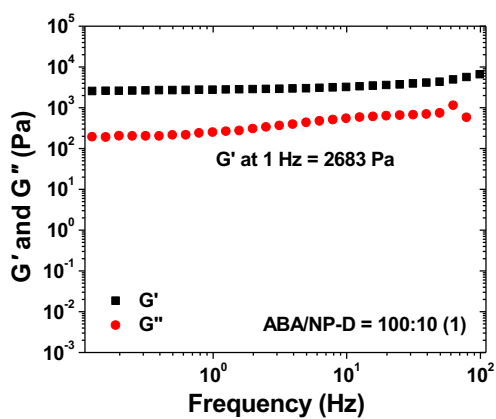


(Figure A7 continued)

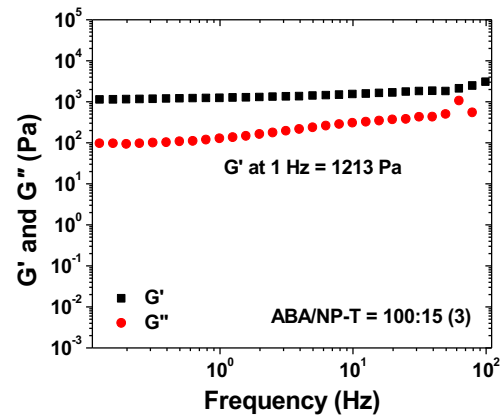
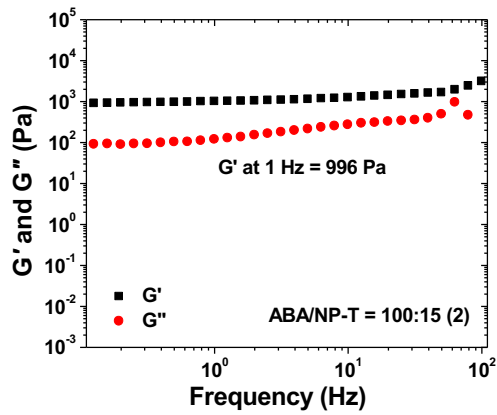
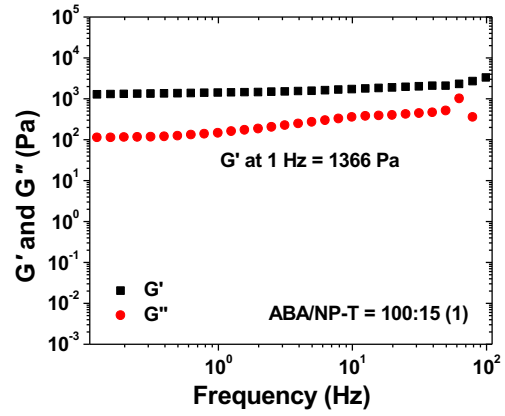
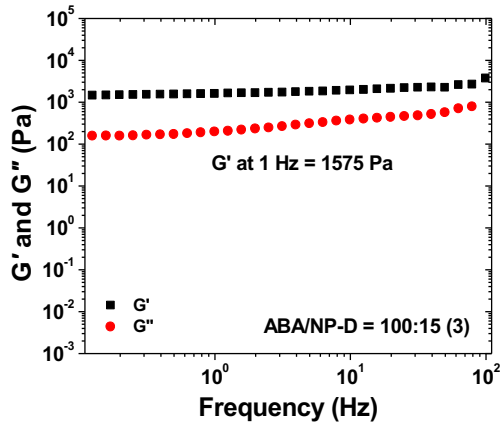
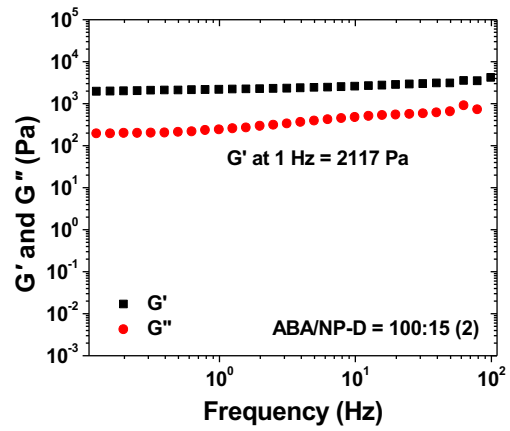
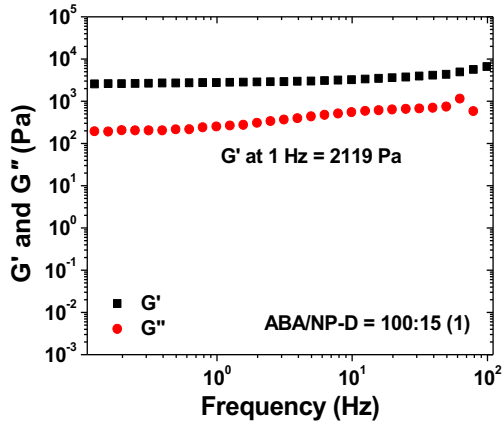


(Figure A7 continued)

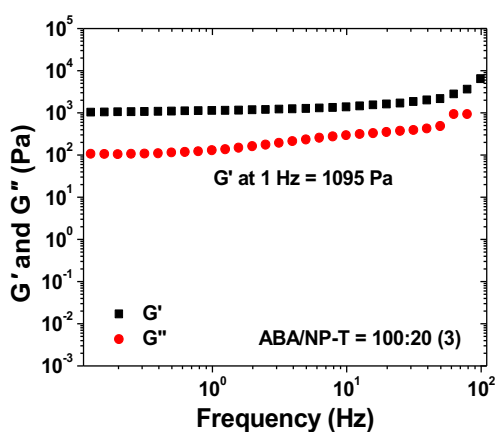
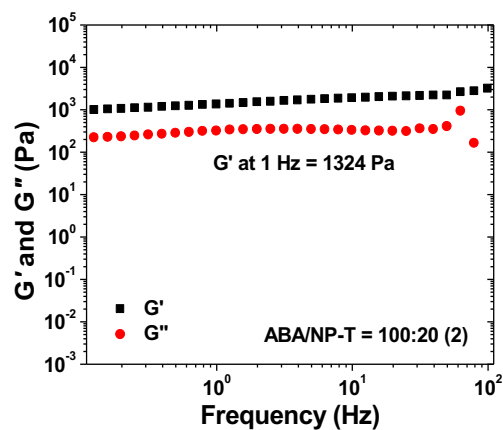
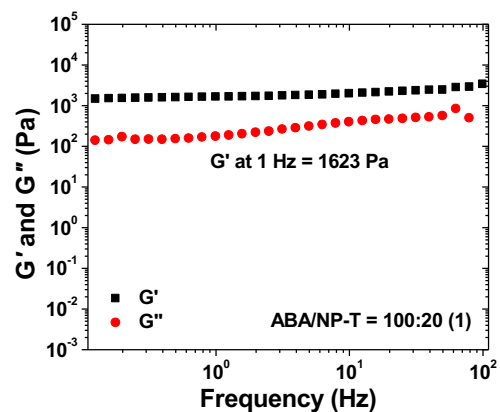
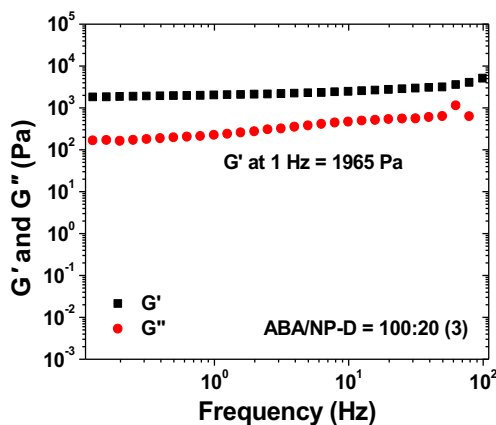
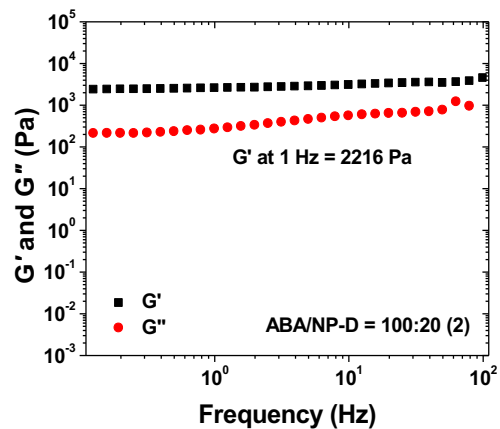
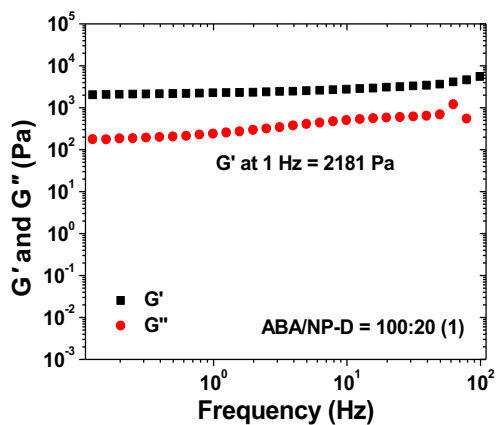


(Figure A7 continued)

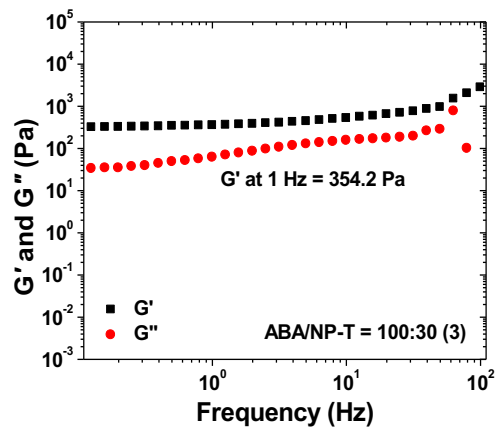
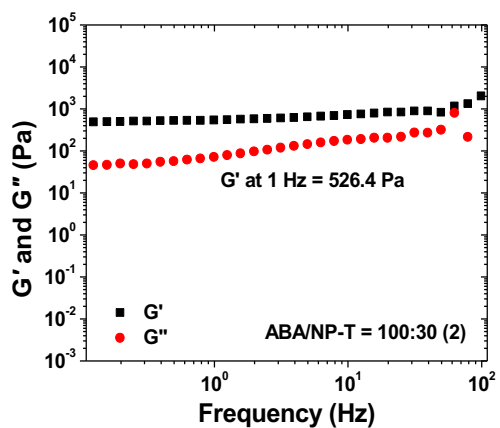
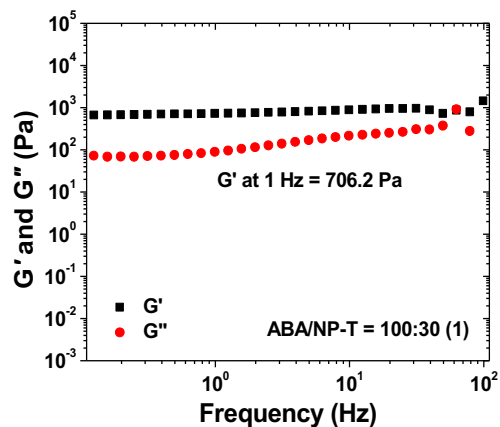
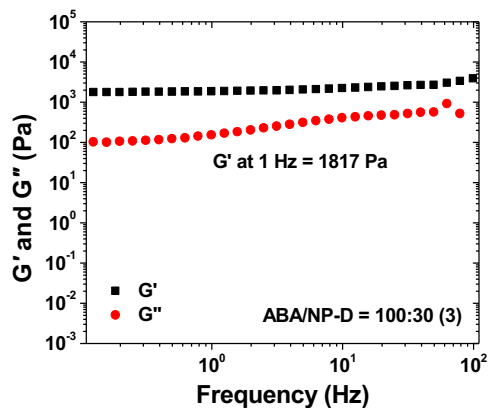
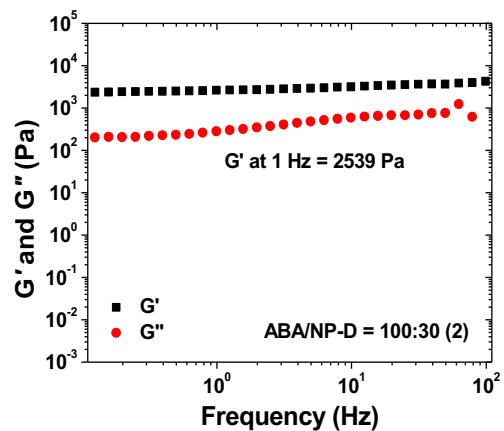
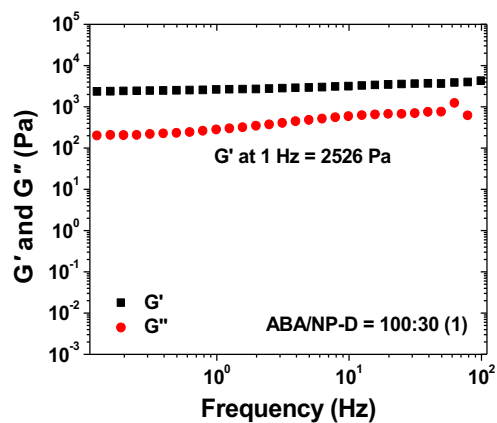


(Figure A7 continued)

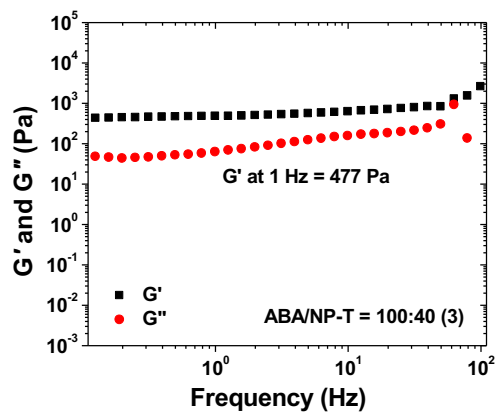
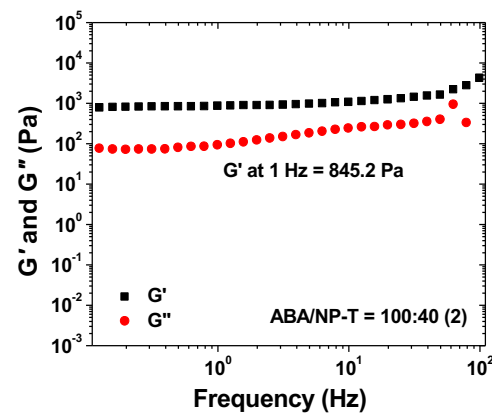
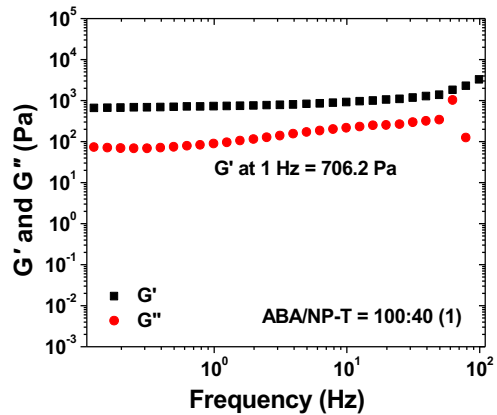
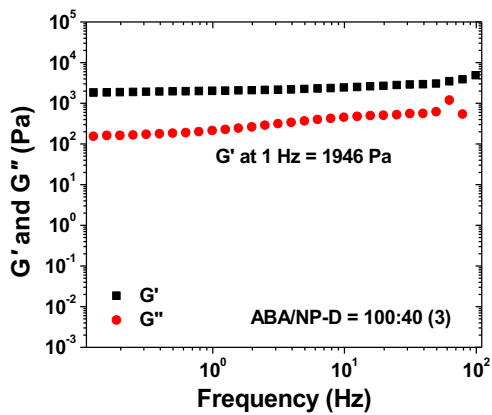
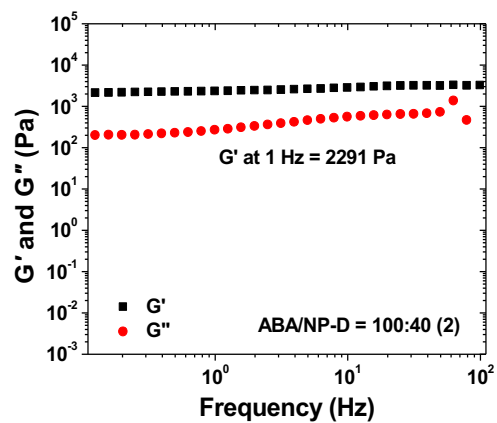
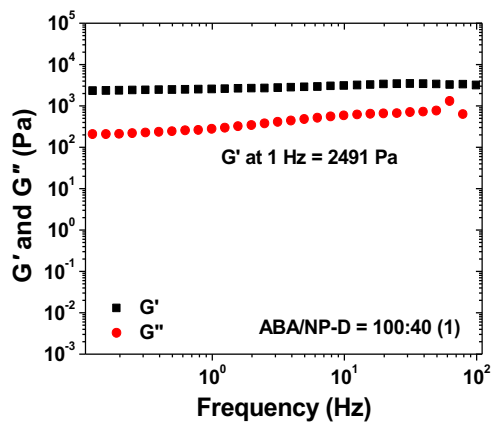


(Figure A7 continued)

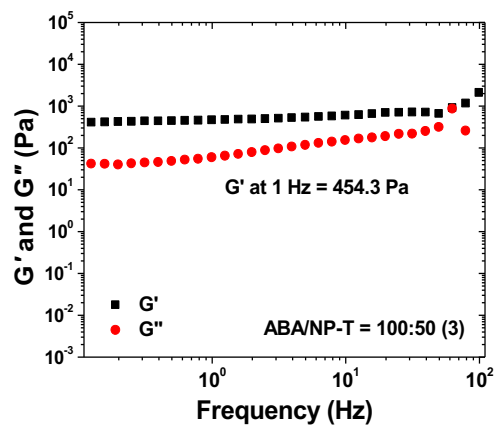
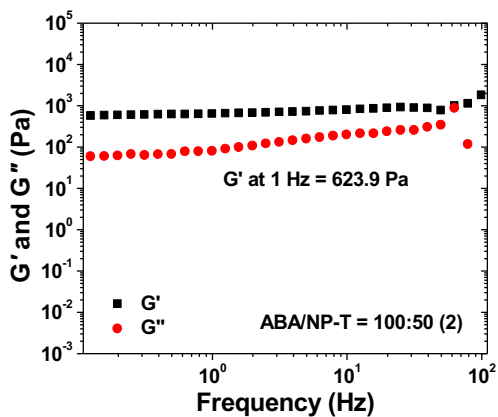
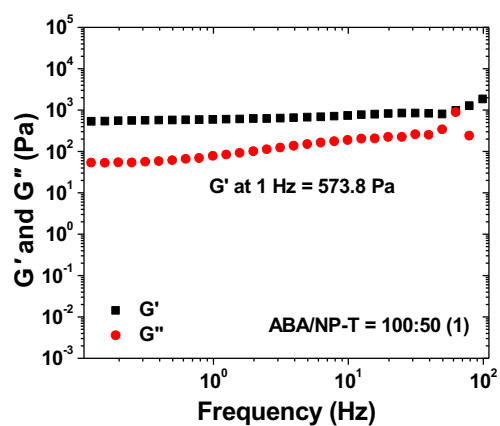
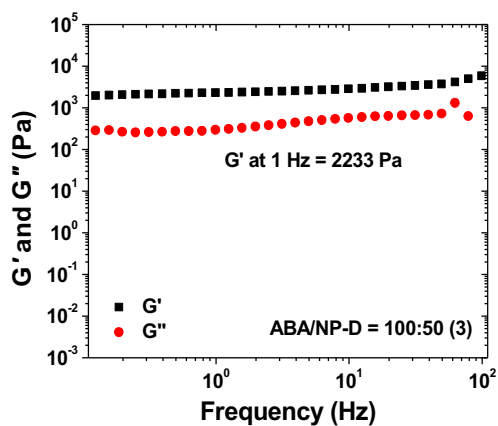
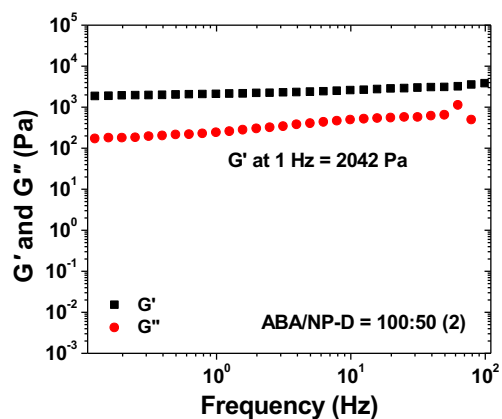
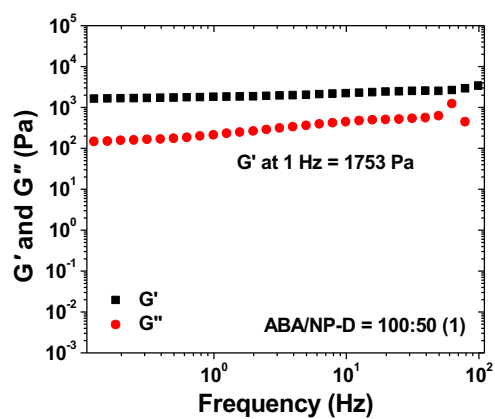


(Figure A7 continued)

Figure A8. Plots of dynamic storage modulus G' and loss modulus G'' of aqueous mixtures of ABA-D with a concentration of 10 wt %, defined as $[(\text{polymer mass})/(\text{polymer mass} + \text{water mass} + \text{hairy NP mass})] \times 100\%$, and hairy NPs with various NP-to-polymer mass ratios versus temperature for both NP-D and NP-T. The data were collected from temperature ramp experiments performed by using a frequency of 1 Hz, a strain amplitude of 1 %, and a heating rate of 3 °C/min.

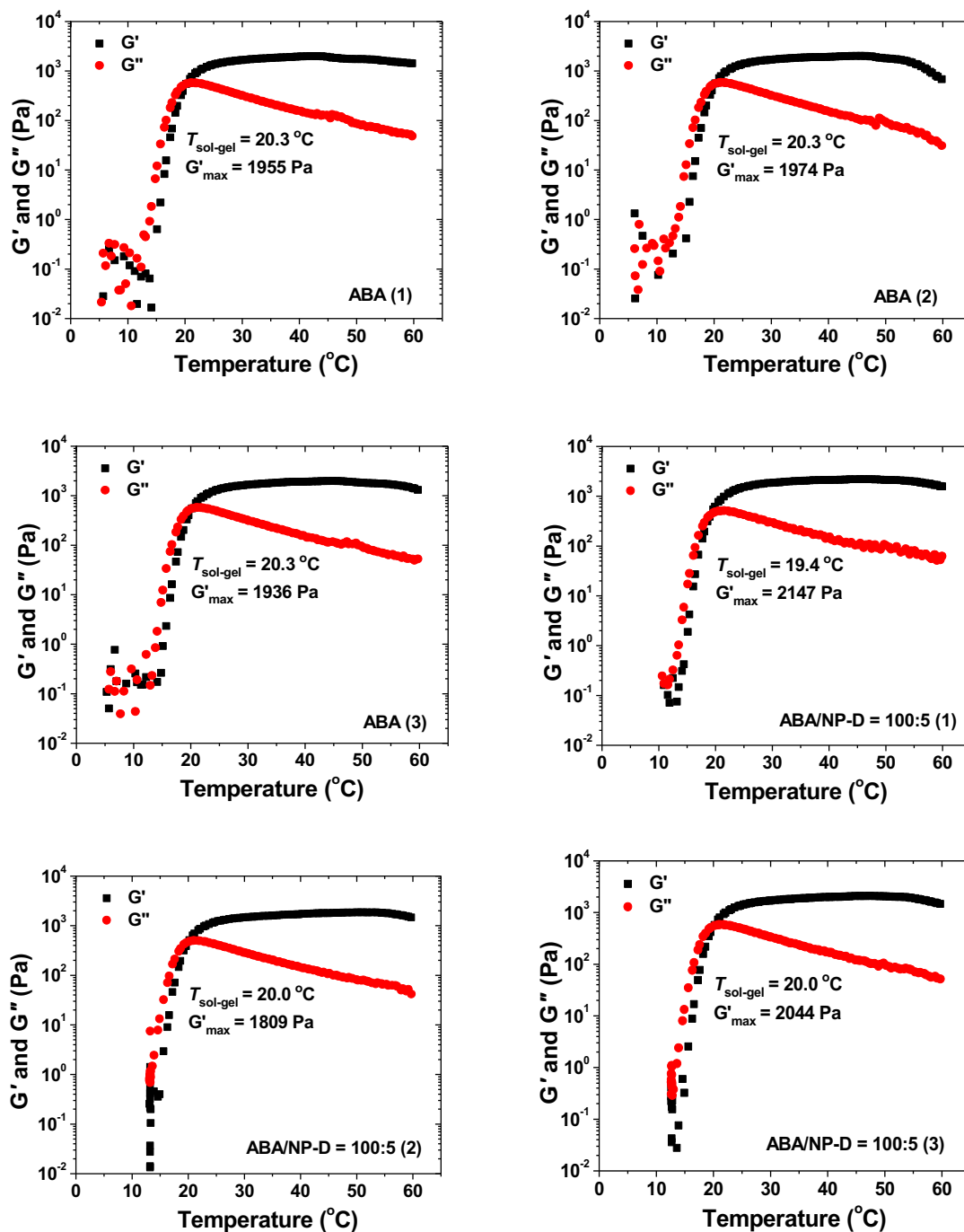


(Figure A8 continued)

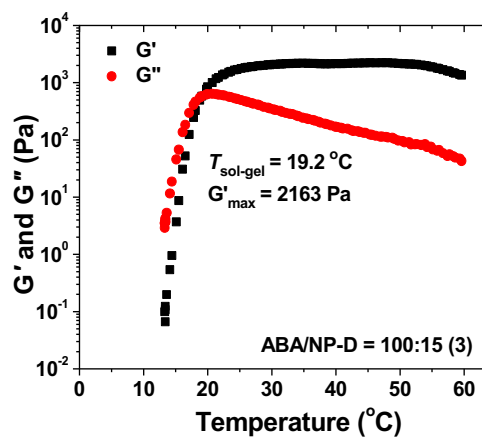
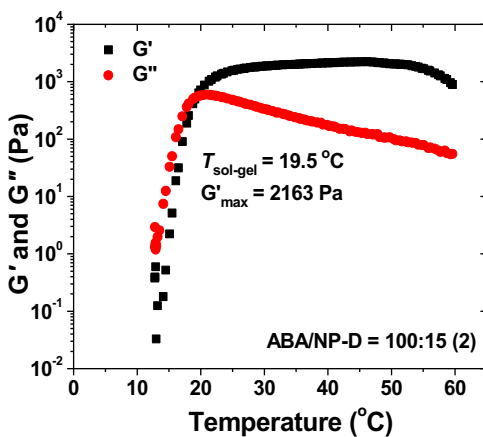
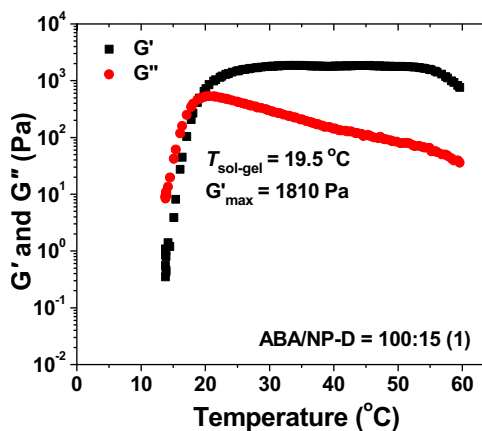
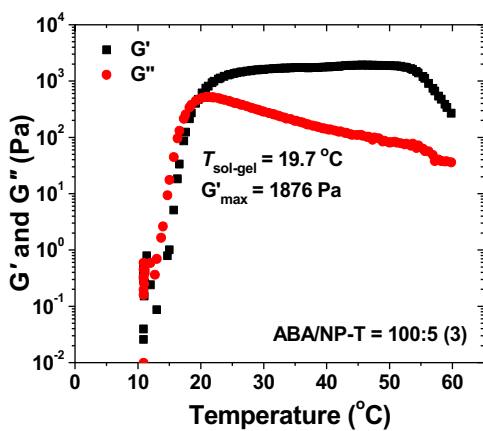
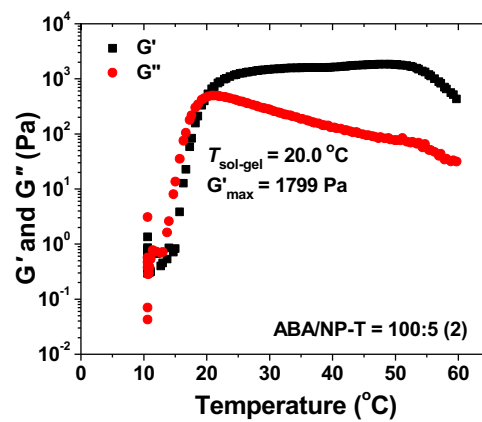
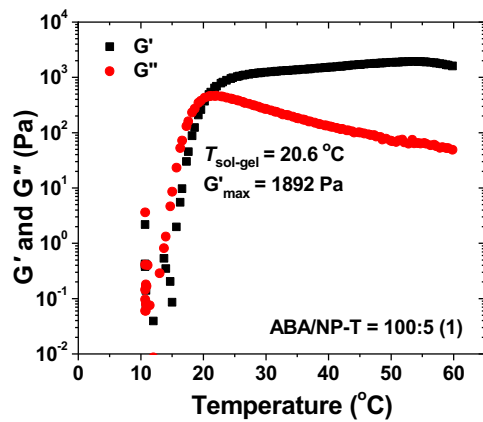


(Figure A8 continued)

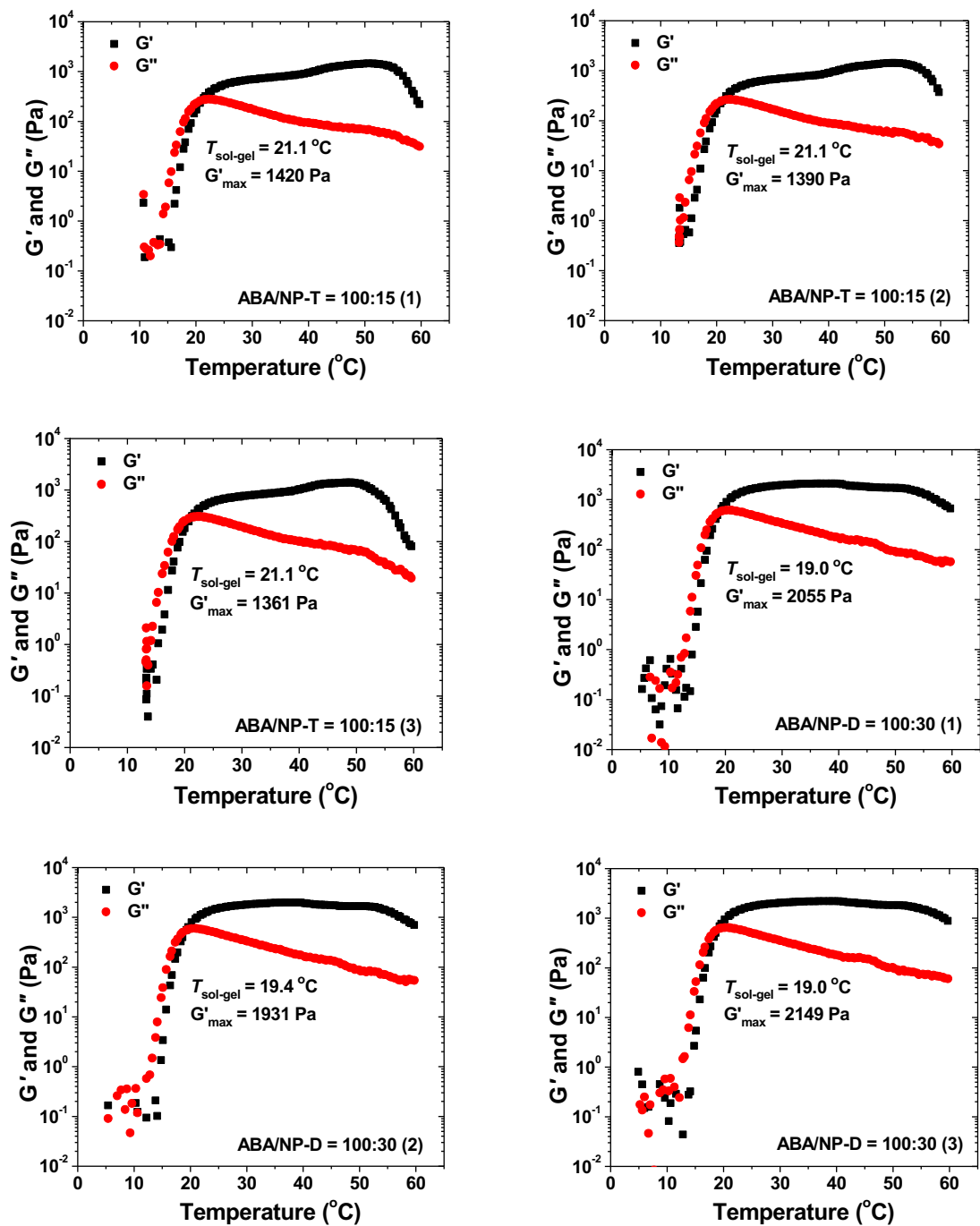


(Figure A8 continued)

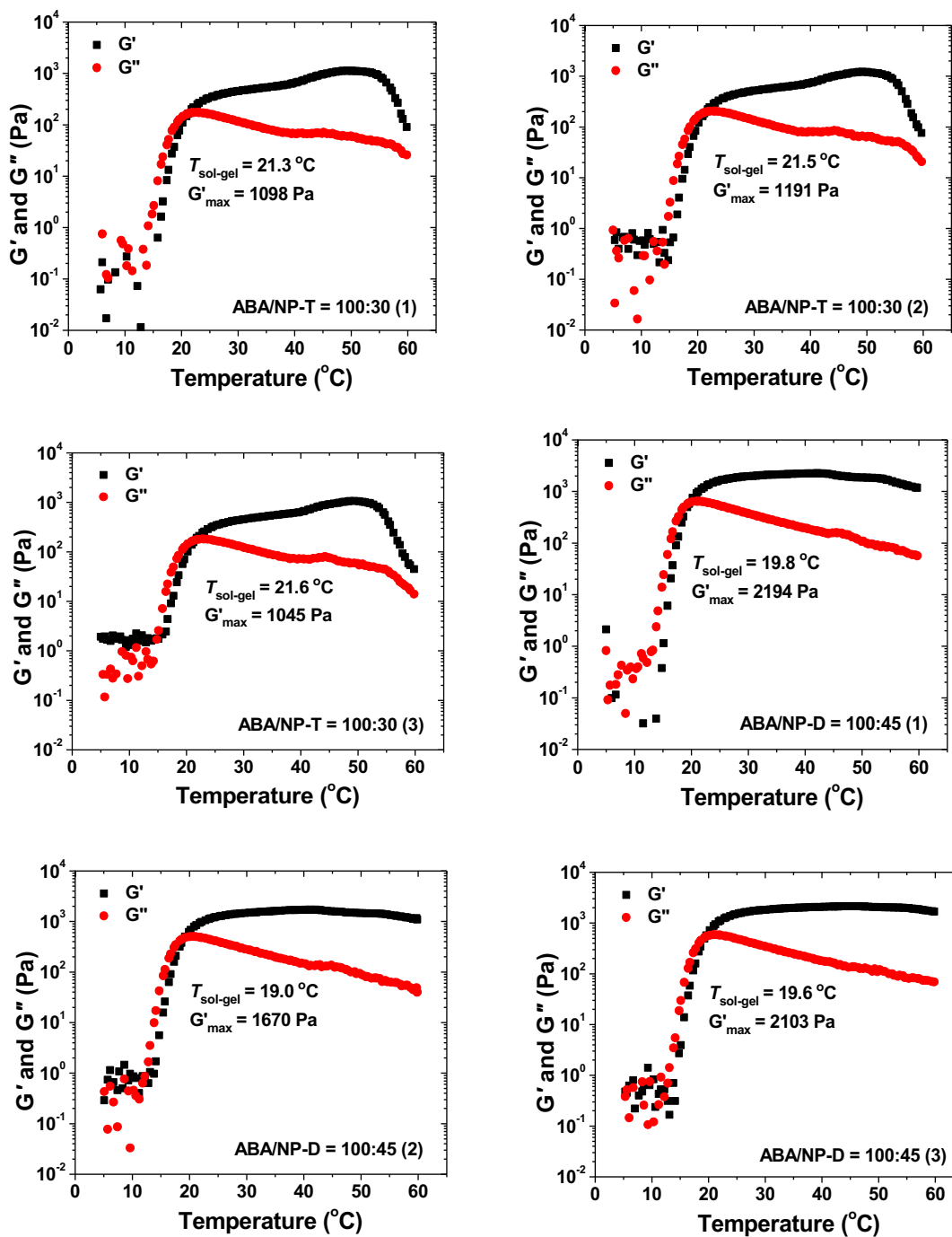


(Figure A8 continued)

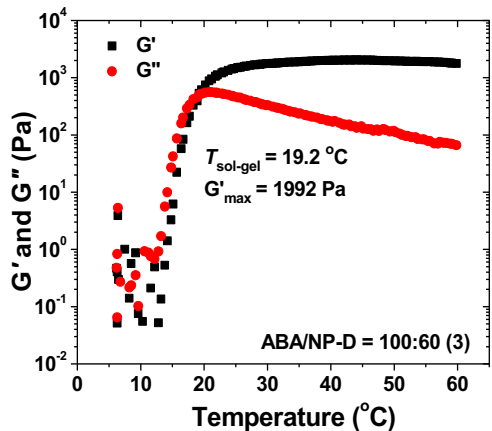
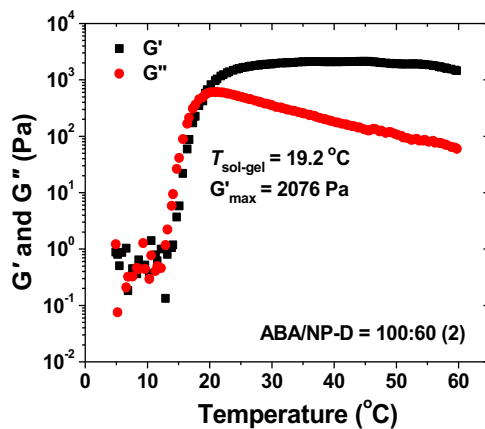
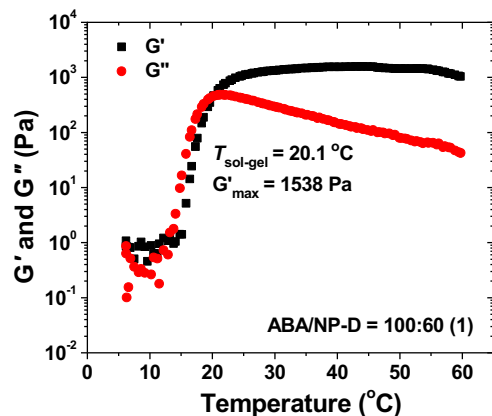
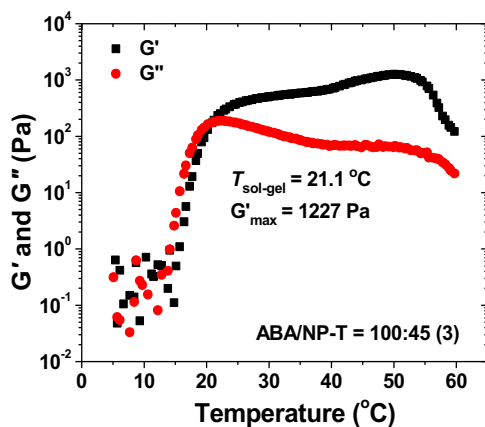
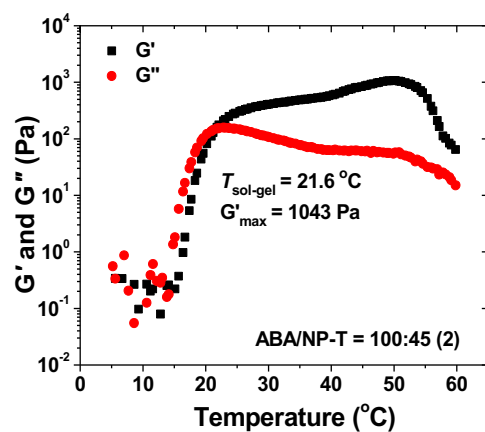
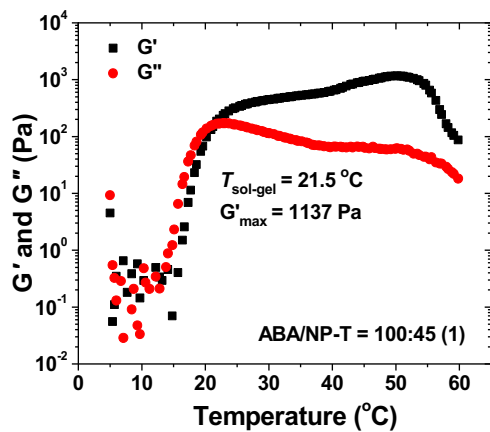


(Figure A8 continued)

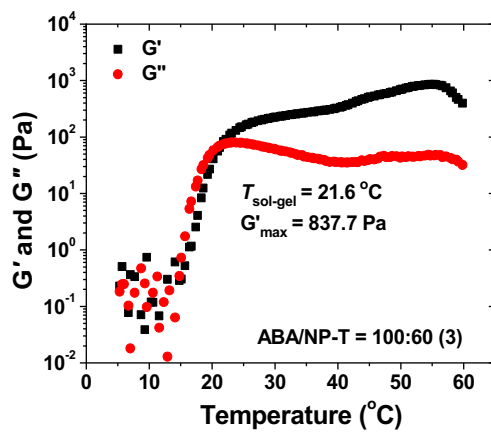
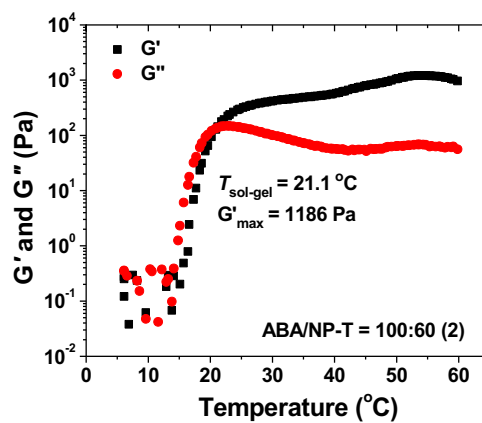
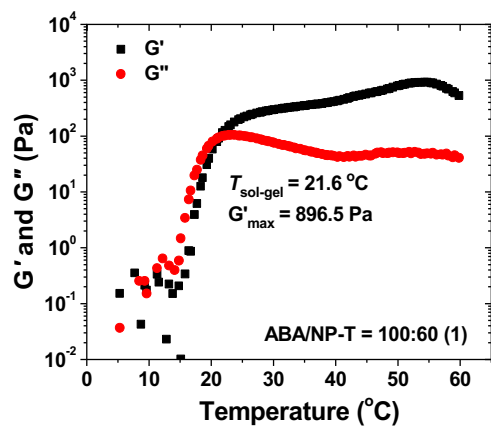


(Figure A8 continued)

Figure A9. Frequency dependences of dynamic storage modulus G' (black square) and loss modulus G'' (red circle) at 40 °C of the hybrid micellar hydrogels of the ABA triblock copolymer ABA-D and thermosensitive hairy NPs with various NP-to-polymer mass ratios and a polymer concentration of 10 wt % defined as $[(\text{polymer mass})/(\text{polymer mass} + \text{water mass} + \text{hairy NP mass})] \times 100\%$. A strain amplitude of 1.0% was used in the frequency sweep experiments.

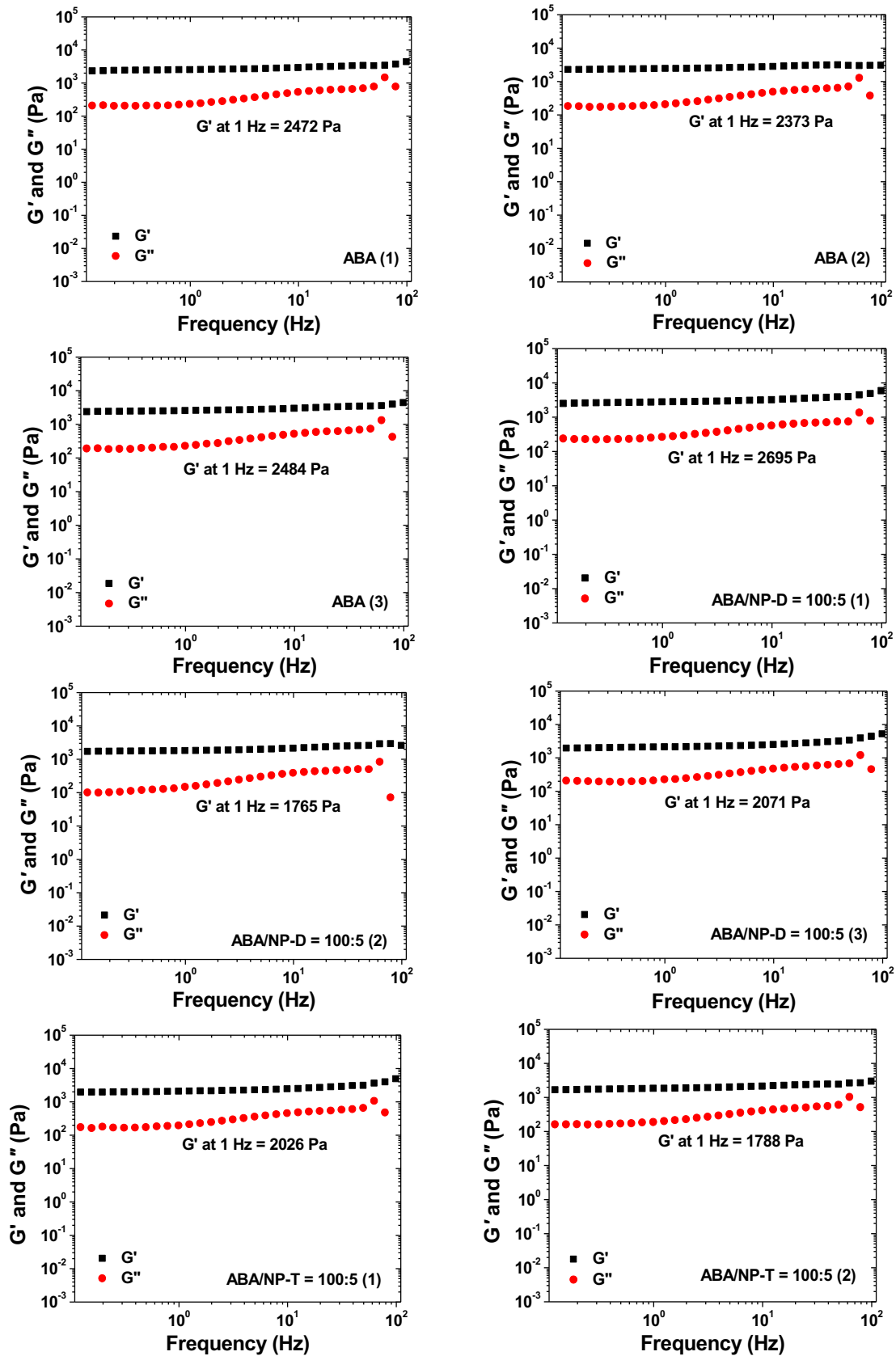


(Figure A9 continued)

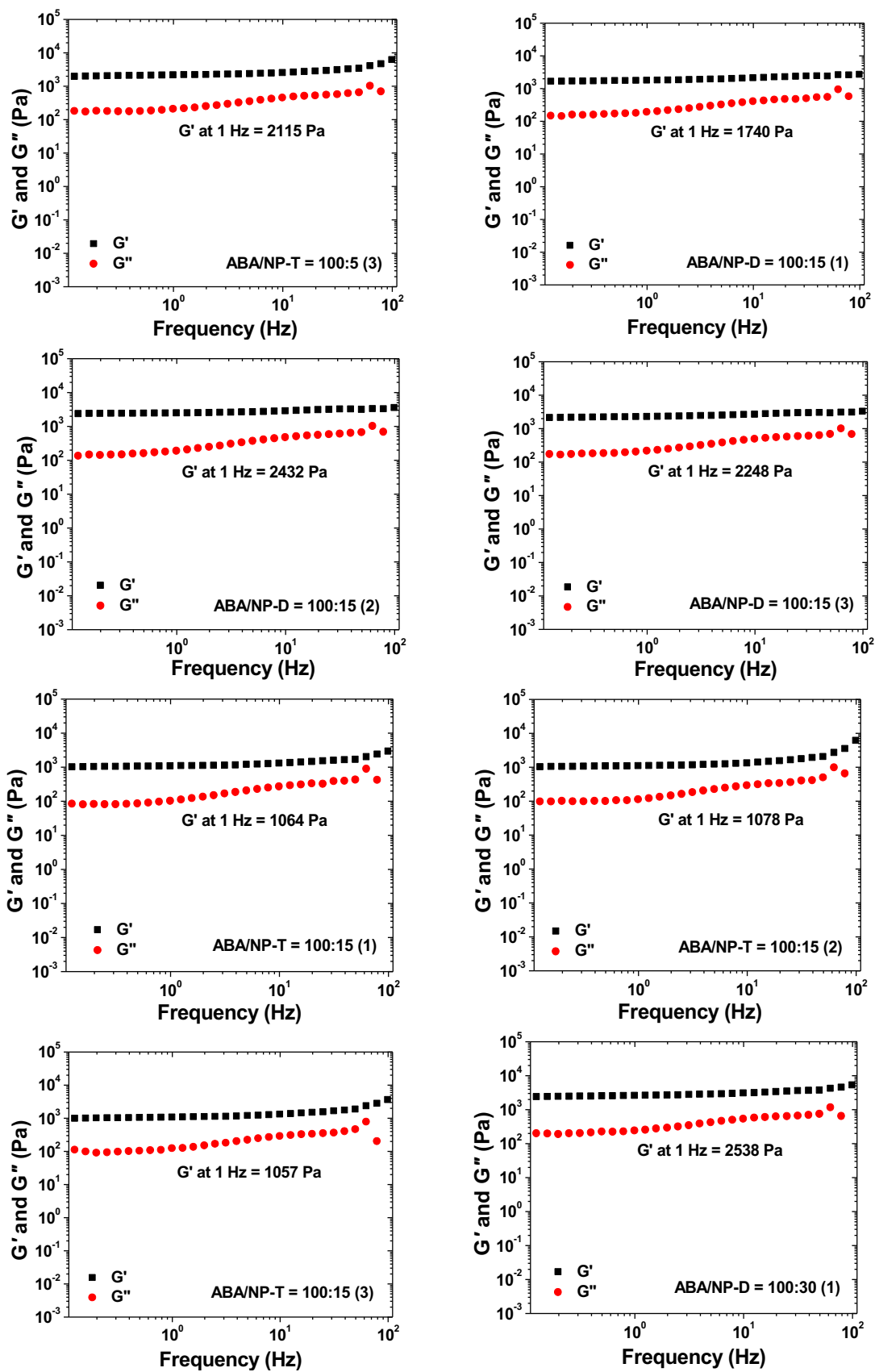


(Figure A9 continued)

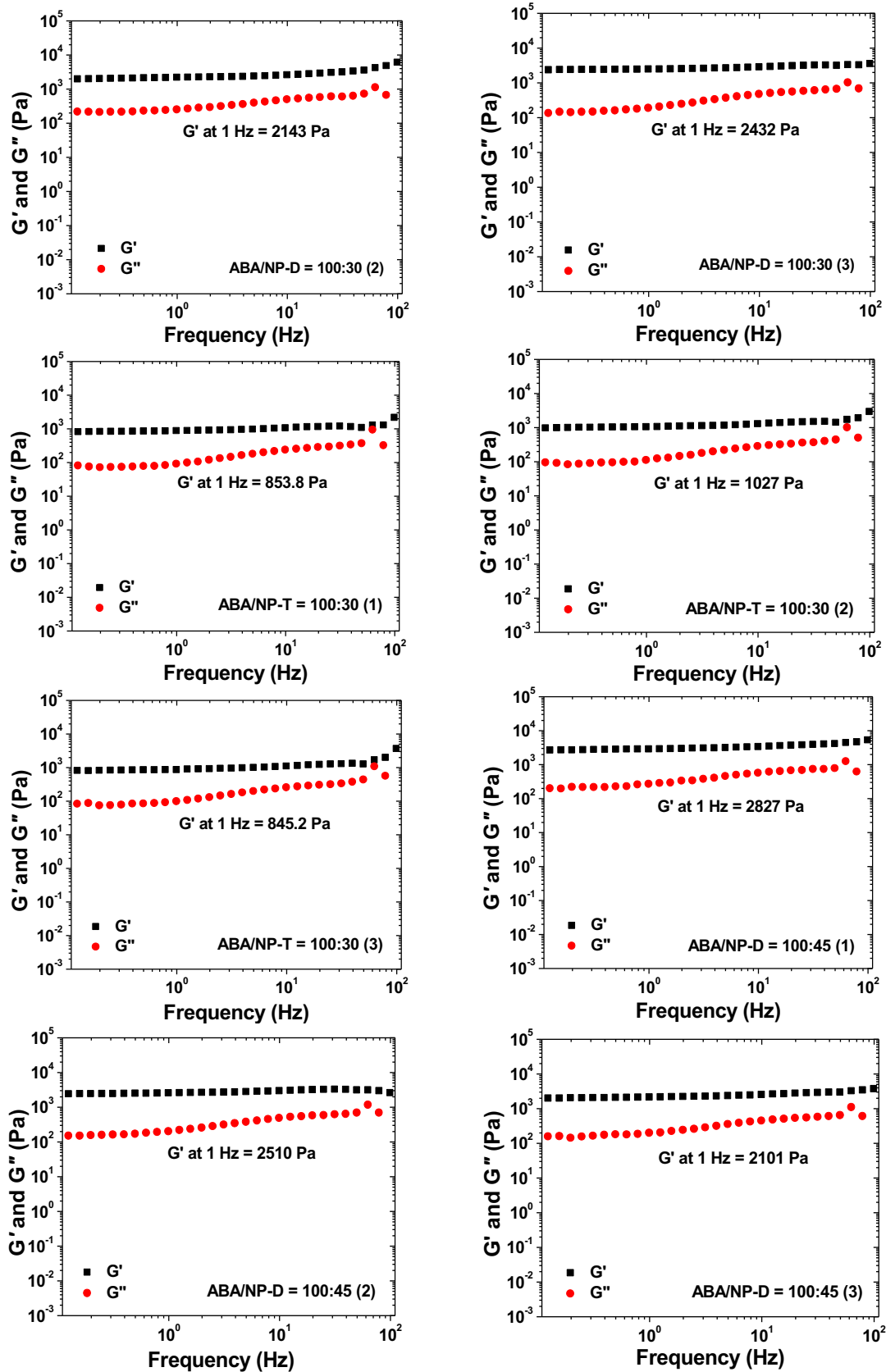


(Figure A9 continued)

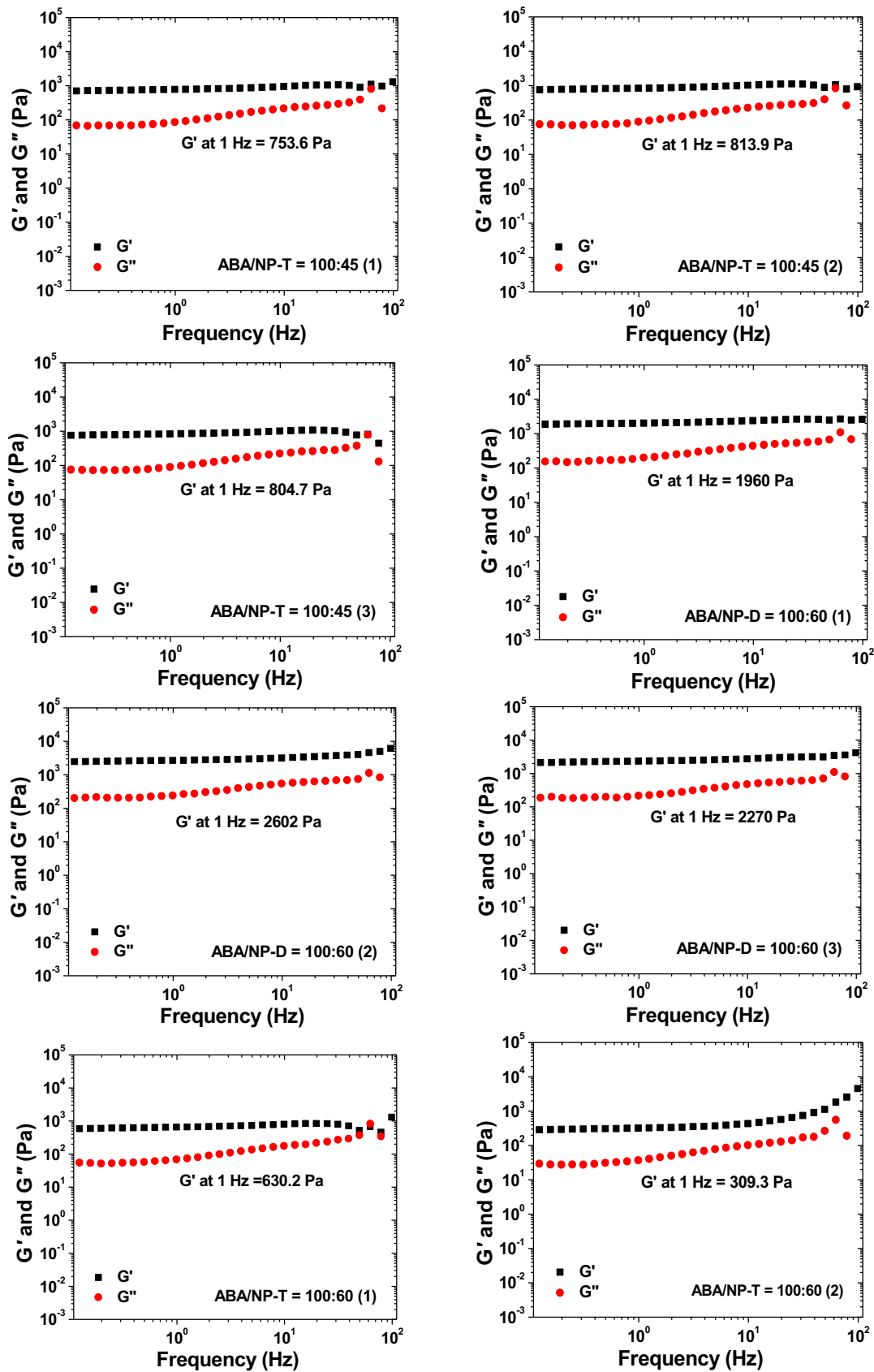


(Figure A9 continued)

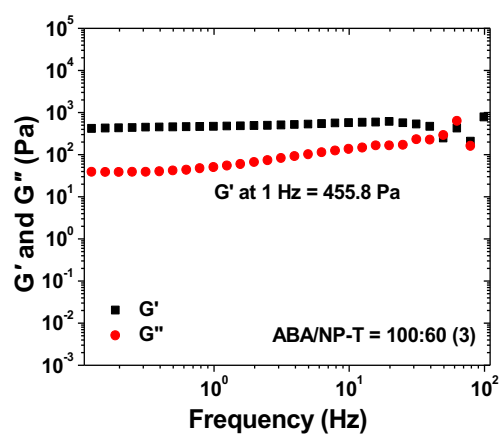


(Figure A9 continued)

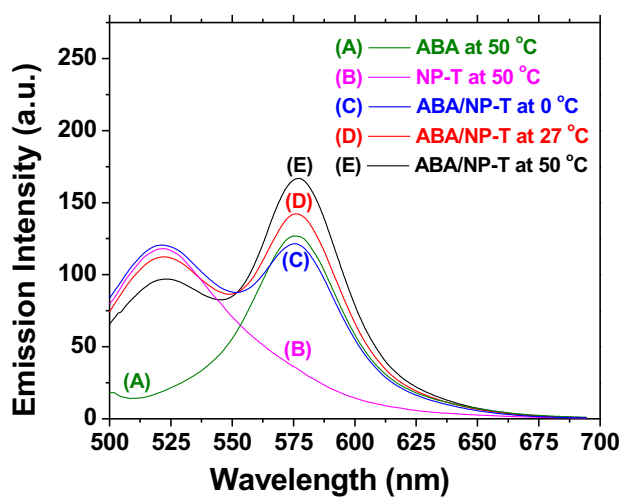


Figure A10. Fluorescence spectra of aqueous solutions of ABA-D with a concentration of 0.216 mg/g (A), NP-T with a concentration of 0.012 mg/g (B), the mixture of ABA-D with a concentration of 0.217 mg/g and NP-T with a concentration of 0.012 mg/g at ~ 0 °C (C), 27 °C (D), and 50 °C (E).

A3. Calculation of Grafting Density of P(DEGMMA-*co*-DEGEMA-*co*-NBDMA) Brushes Grafted on 17 nm Silica Nanoparticles (NP-D).

The grafting density was calculated by using the size of silica NPs, DP of the polymer, and TGA data corrected for the difference in the weight retentions at 100 °C between hairy NPs and initiator NPs. The DP of the polymer was calculated by using the monomer conversion and the molar ratio of monomer to the sum of free initiator and surface initiator.

Below is the description for the calculation of the DP of the polymer P(DEGMMA-*co*-DEGEMA-*co*-NBDMA) and the grafting density of NP-D. The TGA curve of P(DEGMMA-*co*-DEGEMA-*co*-NBDMA) brush-grafted NPs was shifted vertically so that the weight retentions of initiator NPs and NP-D at 100 °C were identical. The corrected weight retention of NP-D at 800 °C was 31.73 %. The ratio of the silica residue to the volatile portion at 800 °C was 100 : 19.56 for initiator NPs and 100 : 215.16 for hairy NPs. Since the mass of the initiator NPs used in the polymerization is 262 mg, the total mass of the grafted polymer is $[(215.16-19.56)/(100 + 19.56)] \times 262 \text{ mg} = 429 \text{ mg}$. Because the mass of total monomers was 4.042 g and the monomer conversion was 49.80 %, the total mass of the polymer, including the free polymer and the grafted polymer, was 2.013 g. Thus, the mass of the free polymer was 1.584 g. The free initiator used in the polymerization was 29.0 mg (149 μmol), which means that the surface initiator was 40.35 μmol . Therefore, the sum of the free initiator and the surface initiator was 189.35 μmol . Since the total moles of monomers was 20.855 mmol, the monomer-to-initiator ratio was calculated to be 110 : 1 and the DP was 55. From the ^1H NMR spectrum, the calculated numbers of PDEGMMA and PDEGEMA monomer units were 33 and 22, respectively.

For the calculation of grafting density, assuming the silica NPs are spherical and the density is 2.07 g/cm³, the mass of a single silica NP with a diameter of 17 nm is $5.32 \times 10^{-18} \text{ g}$. Therefore,

the amount of the grafted P(DEGMMA-*co*-DEGEMA-*co*-NBDMA) on one silica NP is 1.04×10^{-17} g. The molecular weight of P(DEGMMA-*co*-DEGEMA-*co*-NBDMA) calculated from DP is 10648 g/mol. Thus, the number of the grafted P(DEGMMA-*co*-DEGEMA-*co*-NBDMA) chains on one silica NP is $(1.04 \times 10^{-17} \text{ g}/10648 \text{ g/mol}) \times 6.022 \times 10^{23} = 588$ chains. The surface area of one bare silica NP is $\pi D^2 = 908 \text{ nm}^2$. Therefore, the grafting density of P(DEGMMA-*co*-DEGEMA-*co*-NBDMA) brushes on silica NPs is 0.65 chains/nm².

Using the same method, the DP of P(TEGMMA-*co*-NBDMA) and the grafting densities of P(TEGMMA-*co*-NBDMA) brushes in NP-T were calculated. The DP of the polymer was 48 and the grafting density was 0.62 chains/nm².

**Chapter 3. Hybrid Micellar Network Hydrogels of Thermosensitive ABA
Triblock Copolymer and Polymer Brush-Grafted Nanoparticles: Effect of
LCST Transition of Polymer Brushes on Gel Property**

Abstract

This chapter presents a study of the effect of LCST transition of polymer brushes on properties of hybrid micellar network hydrogels of a thermosensitive ABA triblock copolymer and polymer brush-grafted nanoparticles (hairy NPs) with NPs initially residing outside the core of micelles. Four batches of thermosensitive polymer brush-grafted, 20 nm silica NPs with different lower critical solution temperatures (LCSTs) and a thermosensitive ABA triblock copolymer composed of a poly(ethylene oxide) central block and thermosensitive outer blocks (ABA-N) were prepared. The LCSTs of hairy NPs were significantly higher than the critical micellization temperature of ABA-N, resulting in the NPs being initially located outside the core of micelles. The effects of LCST transition of hairy NPs and NP-to-polymer mass ratio on properties of hybrid micellar hydrogels of ABA-N with a concentration of 10 wt% and hairy NPs were investigated by rheological measurements. For all hybrid hydrogels studied in this work, the dynamic storage modulus G' exhibited a sharp increase on top of a plateau that was forming in the heating ramp at a temperature corresponding to the LCST transition of hairy NPs. This phenomenon was caused by the collapse of the brushes on NPs triggering the absorption of thermosensitive outer blocks of ABA-N molecules in the dangling and loop forms and the reorganization of the 3-D gel network structure, which increased the density of bridging chains and thus the G' . This explanation was supported by the results from fluorescence resonance energy transfer studies. The maximum values of G' (G'_{\max}) of the gels containing higher LCST hairy NPs were noticeably lower compared with the gels with lower LCST hairy NPs and the gel with no NPs. The G'_{\max} of all hybrid hydrogels decreased gradually with the increase of the NP-to-polymer ratio.

3.1. Introduction

Thermosensitive block copolymer micellar hydrogels have great potential in a variety of applications, including controlled or triggered release of drugs and tissue engineering.¹⁻⁶ Unlike chemically crosslinked hydrogels, these polymer gels can undergo in situ thermally-induced, reversible sol-gel transitions, making it possible to use syringe and needle to administer the gel systems; the aqueous polymer solution can be loaded into a syringe as a liquid, which turns into a gel after the injection due to the temperature changes. The intriguing sol-gel transition and the accompanied property change have motivated a tremendous amount of research activities, both basic and application-oriented.¹⁻¹⁵ For example, Jeong et al. developed injectable drug delivery systems using poly(ethylene oxide) (PEO)-based reversible block copolymer hydrogels.¹⁵

Incorporating inorganic or metallic nanoparticles (NPs) into stimuli-responsive hydrophilic block copolymer hydrogels can greatly increase the gels' functions, because NPs exhibit unique mechanical, optical, magnetic, or electronic properties that are usually not associated with responsive organic polymers.¹⁶⁻¹⁸ A synergistic combination of two vastly different components could yield properties that might not be possible with either only block copolymers or NPs.¹⁹⁻³⁵ There have been many reports in the literature on hybrid micellar hydrogels of stimuli-responsive block copolymers and NPs. Earlier examples include those reported by Pozzo and Walker;²⁷⁻²⁹ in their work, hydrophilic silica NPs were added into the aqueous solution of PEO-*b*-poly(propylene oxide)-*b*-PEO triblock copolymers (PEO-*b*-PPO-*b*-PEO, i.e., Pluronics) and were partitioned into the interstitial space, forming cocrystals with micelles. Qin et al. reported ferrogels by using PEO-*b*-PPO-*b*-PEO to encapsulate magnetic NPs and dispersing them into moderately concentrated aqueous solutions of a pluronic at low temperatures.³³ Upon heating, the mixtures underwent gelation with NPs residing in the core of micelles. The hybrid hydrogels were used as matrices for

sustained release of a hydrophobic drug, and they showed that the release profile can be modulated with a static magnetic field. Reinicke et al. showed that aqueous solutions of hybrid micelles of ABC triblock copolymers and maghemite NPs, formed via the electrostatic interaction between the charged NPs and the oppositely charged block of the triblock copolymer, exhibited reversible gelation upon magnetic inductive heating using an AC magnetic field.³⁵

We have been particularly interested in hybrid micellar hydrogels of thermosensitive ABA triblock copolymers and polymer brush-grafted NPs (hairy NPs). In Chapter 2, we studied the effect of NP's locations, either inside or outside the core of micelles, on properties of hydrogels of a thermosensitive ABA triblock copolymer (ABA-D) and hairy NPs.³⁶ A method was devised to control the location of NPs in the gels. When the LCST of hairy NPs ($LCST_{NP}$) was about the same as that of the thermosensitive outer blocks ($LCST_{ABA}$), the NPs (named as NP-D) resided in the core of micelles upon heating from below the $LCST_{NP}$. When the $LCST_{NP}$ was much higher than the $LCST_{ABA}$, the NPs were excluded from the core of micelles. The NPs with a higher LCST were poly(methoxytri(ethylene glycol) methacrylate) (PTEGMMA)-grafted silica NPs (NP-T). We found that the dynamic storage modulus G' of the hydrogels containing NP-D exhibited little change with increasing the NP-to-polymer mass ratio (up to 50 : 100). In contrast, the G' of the gels with NP-T in the interstitial space dropped significantly with the increase of NP-to-polymer ratio. In addition, for the gels containing NP-T, we observed a noticeable increase in G' in the heating ramps around the LCST transition of hairy NPs. This observation motivated the present work; we further studied the effect of incorporating various thermosensitive hairy NPs with LCSTs greater than the $LCST_{ABA}$ on properties of resultant hybrid hydrogels.

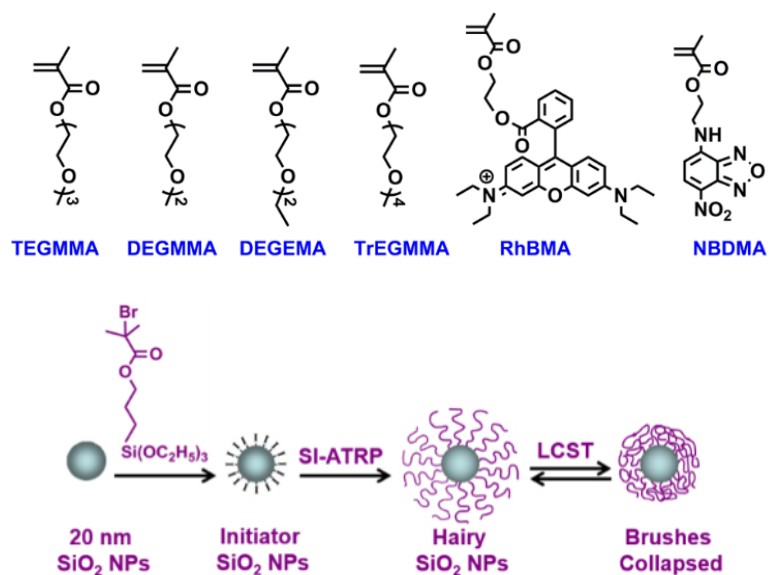
A thermosensitive ABA triblock copolymer (ABA-N) was prepared by atom transfer radical polymerization (ATRP) of a mixture of methoxydi(ethylene glycol) methacrylate (DEGMMA),

ethoxydi(ethylene glycol) methacrylate (DEGEMA), and RhBMA (Scheme 3.1) from a difunctional PEO macroinitiator with a molecular weight of 20 kDa.³⁶ The critical micellization temperature (CMT) of ABA-N in water was 13 °C, measured by dynamic light scattering (DLS). Four hairy NP samples with LCSTs of 29, 34, 44, and 51 °C were made by surface-initiated ATRP from initiator-functionalized, 20 nm silica NPs using either pure monomers or mixtures of DEGMMA, TEGMMA, and methoxytetra(ethylene glycol) methacrylate (TrEGMMA). The cloud points of homopolymers of DEGEMA, DEGMMA, TEGMMA, and TrEGMMA in water are 4, 26, 52 and 68 °C, respectively.³⁷⁻⁴² A very small amount of NBDMA was incorporated into the brushes; NBDMA and RhBMA form a pair for fluorescence resonance energy transfer (FRET).^{43,44} The effects of LCSTs of hairy NPs on gel properties were studied by rheometry. We found that all hybrid hydrogels exhibited a sharp increase in G' at temperatures corresponding to the LCST transitions of hairy NPs. However, the effects of NPs with lower and higher LCSTs are different.

3.2. Experimental Section

3.2.1. Materials

Triethoxysilane (95%) was purchased from Acros and used as received. MIBK-ST, a dispersion of silica NPs in methyl isobutyl ketone (30-31 wt % SiO₂) with an average size of 10-15 nm (according to the manufacturer), was obtained from Nissan Chemical. The platinum–divinyltetramethyldisiloxane complex in xylene with a Pt concentration of 2.1–2.4% was purchased from Gelest, Inc. CuBr (98%, Aldrich) was purified via a procedure described previously.¹¹ *N,N,N',N',N''*-Pentamethyldiethylenetriamine (PMDETA, 99%, Aldrich), ethyl 2-bromoisobutyrate (EBiB, 98%, Aldrich), and di(ethylene glycol) methyl ether methacrylate (DEGMMA, 97%, TCI) were each stirred with CaH₂ and distilled under reduced pressure.



Scheme 3.1. Molecular structures of monomers used in this work and scheme for the synthesis of hairy nanoparticles by surface-initiated atom transfer radical polymerization (SI-ATRP)

Di(ethylene glycol) ethyl ether methacrylate (DEGEMA), tri(ethylene glycol) methyl ether methacrylate (TEGMMA), and tetra(ethylene glycol) methyl ether methacrylate (TrEGMMA) were made via the reactions of methacryloyl chloride (95%, Acros) with di(ethylene glycol) monoethyl ether (> 99.0%, TCI), tri(ethylene glycol) monomethyl ether, and tetra(ethylene glycol) monomethyl ether, respectively, in dry CH_2Cl_2 in the presence of triethylamine (99%, Acros).³⁷⁻³⁹ Their molecular structures were confirmed by ^1H NMR spectroscopy. The synthesis of allyl 2-bromo-2-methylpropionate, 4-(2-methacryloyloxyethylamino)-7-nitro-2,1,3-benzoxadiazole (NBDMA), and the Rhodamine B-containing methacrylate (RhBMA) was reported in the literature.^{36,45} The PEO macroinitiator, Br-PEO-Br , was prepared by reacting PEO (HO-PEO-OH , 20 kDa, Aldrich) with 2-bromoisobutyryl bromide.³⁶ All other chemical reagents were purchased from either Aldrich or Fisher/Acros and used without further purification.

3.2.2. General Characterization

NMR spectra were recorded on a Varian Mercury 300 NMR spectrometer and the residual solvent proton signal was used as the internal standard. Size exclusion chromatography (SEC) of the free polymers formed in the synthesis of hairy NPs (NP-29, -34, and -51) was carried out at room temperature using PL-GPC 20 (Polymer Laboratories, Inc.) with a refractive index detector, one PLgel 5 μm guard column (50×7.5 mm), and two PLgel 5 μm mixed-C columns (each 300×7.5 mm, linear range of molecular weight from 200 to 2,000,000 Da). THF was used as the solvent and the flow rate was 1.0 mL/min. Narrow-disperse polystyrene standards were used to calibrate the system. The data were processed using CirrusTM GPC/SEC software (Polymer Laboratories, Inc.). The molecular weights and polydispersity indexes (PDI) of ABA-N and the free polymer formed in the synthesis of NP-44 were determined using PL-GPC 50 Plus (Polymer Laboratories, Inc.) consisting of a differential refractive index detector, one PSS GRAL guard column (50×8

mm, Polymer Standards Service-USA, Inc.), and two PSS GRAL linear columns (each 300×8 mm, molecular weight range from 500 to 1,000,000). The carrier solvent is *N,N*-dimethylformamide (DMF) containing 50 mM LiBr, and the flow rate was 1.0 mL/min. The system was calibrated by polystyrene standards, and the data were processed with CirrusTM GPC/SEC software. Thermogravimetric analysis (TGA) was performed in air at a heating rate of 20 °C/min from room temperature to 800 °C using TA Q-series Q50. The NPs were dried at 45 °C in vacuum for > 5 h prior to analysis.

3.2.3. Synthesis of Thermosensitive ABA Triblock Copolymer P(DEGMMA-co-DEGEMA-co-RhBMA)-b-PEO-b-P(DEGMMA-co-DEGEMA-co-RhBMA) (ABA-N)

ABA-N was synthesized by ATRP of a mixture of DEGMMA, DEGEMA, and RhBMA with a molar ratio of 1.00 : 1.48 : 0.0014 from the PEO difunctional initiator Br-PEO-Br via a procedure similar to that for the synthesis of ABA-D described in a previous publication.³⁶ SEC analysis using PL-GPC 50 Plus with DMF-LiBr as the carrier solvent showed that the $M_{n,SEC}$ was 92.6 kDa and the PDI was 1.20, relative to polystyrene standards. From the ¹H NMR spectrum of ABA-N, the numbers of DEGMMA and DEGEMA monomer units were calculated to be 238 and 324, respectively.⁴⁶

3.2.4. Synthesis of Thermosensitive Polymer Brush-Grafted Silica Nanoparticles.

Silica NPs (MIBK-ST, Nissan Chemical) were surface-functionalized with 3-(triethoxysilyl)propyl 2-bromo-2-methylpropanoate, prepared by hydrosilation of allyl 2-bromo-2-methylpropionate with triethoxysilane as reported previously.^{36,41} The initiator-functionalized NPs were then dispersed in DMF to form an NP dispersion with a concentration of 15.5 wt%, which was determined by gravimetric analysis. Four thermoresponsive polymer brush-grafted, 20 nm silica NP samples with different thermosensitive properties were synthesized by surface-

initiated ATRP from the same batch of initiator NPs. Shown below is the procedure for the synthesis of P(DEGMMA-*co*-TEGMMA-*co*-NBDMA) brush-grafted silica NPs with an LCST transition of 29 °C (NP-29).

CuBr (19.7 mg, 137 μ mol), CuBr₂ (5.6 mg, 25.0 μ mol), the dispersion of the ATRP initiator-functionalized NPs in DMF with a concentration of 15.5 wt% (2.703 g of solution, corresponding to 419 mg of initiator NPs), and DMF (19.83 g) were added into a two-necked flask. The mixture was sonicated in an ultrasonic water bath to form a homogeneous dispersion. DEGMMA (2.839 g, 15.1 mmol), TEGMMA (1.506 g, 6.49 mmol), NBDMA (11.7 mg, 4.0×10^{-2} mmol), and ethyl 2-bromoisobutyrate (29.5 mg, 151 μ mol) were then added into the flask. After the mixture was degassed by three freeze-pump-thaw cycles, PMDETA (32.6 mg, 188 μ mol) was injected into the flask at the thawing point of the frozen mixture by using a microsyringe. The flask was then placed in an oil bath with a preset temperature of 45 °C, and the progress of the polymerization was monitored by ¹H NMR spectroscopy analysis. After 2 h and 55 min, the flask was taken out from the oil bath and opened to air, and an aliquot was withdrawn immediately for ¹H NMR spectroscopy analysis to determine the monomer conversion. The mixture was diluted with THF (20 mL), and the polymer-grafted NPs were isolated by ultracentrifugation at 35 k rpm for 40 min. The NPs were then dispersed in THF and separated again by centrifugation. This dispersion-centrifugation washing process was repeated for a total of 5 times. The supernatant liquid from the first cycle was passed through a column of silica gel (bottom)/activated basic aluminum oxide (top) (2/1, v/v) to remove the copper catalyst. The free polymer was precipitated in a mixture of hexanes and diethyl ether (3:1, v/v), re-dissolved in CH₂Cl₂ and precipitated again. The precipitation-dissolution process was repeated for additional two times. The purified free copolymer, P(DEGMMA-*co*-TEGMMA-*co*-NBDMA), was dried under high vacuum for 6 h, and then

analyzed by SEC (PL-GPC 20) relative to polystyrene standards. The values of $M_{n,SEC}$ and PDI were 10.4 k and 1.20, respectively. The monomer conversion was 36.9 %, determined by 1H NMR spectroscopy analysis. The degree of polymerization (DP) of the polymer was 42, which was calculated from the monomer conversion and the monomer-to-the sum of surface initiator and free initiator as detailed in Chapter 2. The chemical composition of P(DEGMMA-*co*-TEGMMA-*co*-NBDMA) was determined from the 1H NMR spectrum of the purified free copolymer, and the numbers of DEGMMA and TEGMMA units were 28 and 14, respectively.

The aqueous dispersion of NP-29 was prepared by dialysis, detailed below. NP-29, isolated by ultracentrifugation from the THF dispersion, was fully dispersed in DMF (10 g) using an ultrasonic water bath. Ethanol (2 mL) and water (2 mL) were then added dropwise into the hairy NP dispersion under the stirring condition. The resultant NP dispersion was dialyzed against water in an ice/water bath using a regenerated cellulose tubular dialysis membrane with a nominal MWCO of 3500. The ice/water bath-cooled water was changed frequently to ensure that DMF and ethanol were completely removed. The concentration of NP-29 in the final aqueous dispersion was 17.36 mg/g, which was determined by gravimetric analysis as for the dispersion of initiator NPs in DMF.

Other thermosensitive hairy NP samples (NP-34, NP-44, and NP-51) were prepared via similar procedures. A small amount of NBDMA was incorporated in all hairy NP samples. NP-34 was synthesized by SI-ATRP of a mixture of DEGMMA and TEGMMA with a molar ratio of 1 : 2.32. The concentration of NP-34 in the final aqueous dispersion was 14.72 mg/g. NP-44 and -51 were PTEGMMA and P(TEGMMA-*co*-TrEGMMA) brush-grafted silica NPs, respectively. NP-51 was prepared by ATRP of a mixture of TEGMMA and TrEGMMA with a molar ratio of 1 : 1. The concentrations of NP-44 and -51 in the final dispersions were 5.43 and 6.85 mg/g, respectively.

3.2.5. DLS Studies of LCST Transitions of Thermosensitive Hairy NPs and ABA-N in Water

DLS studies of thermosensitive properties of hairy NPs and thermally induced micellization of ABA-N in dilute aqueous solutions were performed on a Brookhaven Instruments BI-200SM goniometer equipped with a PCI BI-9000AT digital correlator, a temperature controller, and a solid-state laser (model 25-LHP-928-249, $\lambda = 633$ nm) at a scattering angle of 90° . The NP concentrations of aqueous dispersions of thermosensitive hairy NPs employed in the DLS studies were 1.0 mg/g, and the polymer concentration in the aqueous solution of ABA-N was 0.2 mg/g. The samples were filtered using Millipore hydrophilic PTFE filters (0.2 μm pore size), and the DLS tubes were sealed with PE stoppers. The temperature was gradually increased, and at each chosen temperature, the sample was equilibrated for 20 min before the measurements were taken.

3.2.6. Fluorescence Spectroscopy Study of Aqueous Mixtures of Thermosensitive Hairy NPs and ABA-N

For fluorescence measurements, aqueous solutions containing only thermosensitive hairy NPs, only ABA-N, and both hairy NPs and ABA-N were prepared. The following is a description of the detailed procedure for NP-29. Other samples were prepared via similar procedures. A 0.208 mg/g aqueous solution of ABA-N, a 0.010 mg/g aqueous dispersion of NP-29, and an aqueous mixture of ABA-N with a concentration of 0.208 mg/g and NP-29 with a concentration of 0.010 mg/g were prepared. All samples were sonicated in an ultrasonic ice/water bath for 15 min and stirred in an ice/water bath for 3 h. The solutions were then placed in an Isotemp and were equilibrated at the set temperature for 20 min. The samples were used for fluorescence spectroscopy measurements, which were done in ~ 2 min. The samples were then heated in the Isotemp at an interval of 5°C and equilibrated at each temperature for 20 min, followed by fluorescence measurements. All fluorescence studies were performed on a Perkin Elmer LS 55 luminescence spectrometer. The slit

widths were set at 10 nm for both excitation and emission with a scan speed of 100 nm/min. The fluorescence emission spectra were recorded from 500 to 700 nm, with the excitation wavelength set at 480 nm.

3.2.7. Rheology Studies of Aqueous Mixtures of ABA-N and Thermosensitive Hairy NPs

Described below is the preparation of aqueous mixtures of ABA-N and NP-29. Other samples with different NP-to-ABA-N mass ratios for rheological measurements were prepared via similar procedures. ABA-N was dried thoroughly in a 100 mL flask in vacuum and weighed (1.184 g). Water (10.597 g) was then added, and the mixture was stored in a refrigerator (4 °C) overnight and then sonicated in an ultrasonic ice/water bath to ensure that ABA-N was fully dissolved to form a homogeneous solution with a polymer concentration of 10 wt%. A small portion of the sample was used for rheological measurements to study the thermally induced sol-gel transition. For the aqueous mixtures of ABA-N and hairy NPs, the polymer concentration was defined as $[\text{polymer mass}/(\text{polymer mass} + \text{water mass})] \times 100\%$. To prepare the aqueous mixture of ABA-N and NP-29 with a polymer concentration of 10 wt% and a NP-to-polymer weight ratio of 30 : 100, an aqueous dispersion of NP-29 with a concentration of 17.36 mg/g (stored in a refrigerator, 3.828 g, corresponding to 66.5 mg of NP-29) was added into the aqueous solution of ABA-N with a concentration of 10 wt% (2.215 g). To maintain the polymer concentration at 10 wt%, a gentle air stream was used to evaporate water until the calculated weight of the sample was reached. A Teflon tape was used to seal the capped sample tightly and then the mixture was sonicated in an ultrasonic ice/water bath for 15 min. After the rheological measurement, a calculated amount of NP-29 was added into the sample to increase the NP-to-polymer mass ratio to 40 : 100, and again a calculated amount of water was evaporated to maintain the polymer concentration at 10 wt %.

Rheological experiments were performed on a rheometer from TA Instruments (Model TA AR 2000ex). A cone–plate geometry with a cone diameter of 20 mm and an angle of 2° (truncation 52 μm) was employed, and the temperature was controlled by the bottom Peltier plate. For each rheological measurement, 90 μL of the sample was loaded onto the plate by a micropipet. To minimize water loss at elevated temperatures, the solvent trap was filled with water and covered with the solvent trap cover. Dynamic storage modulus G' and loss modulus G'' of a sample at various temperatures were measured by oscillatory shear experiments performed at a fixed frequency of 1 Hz in a heating ramp at a heating rate of 3 $^{\circ}\text{C}/\text{min}$. The strain amplitude used in all dynamic viscoelastic measurements was $\gamma = 1.0\%$. Note that for micellar hydrogels of this type of thermosensitive ABA triblock copolymers, our previous dynamic strain sweep experiments showed that the gels typically exhibited a linear response up to $\sim 15\%$.¹¹ For each rheological study, three measurements were taken and the average value was used.

3.3. Results

3.3.1. Synthesis and Thermoresponsive Properties of ABA Triblock Copolymer P(DEGMMA-co-DEGEMA-co-RhBMA)-b-PEO-b-P(DEGEMA-co-DEGEMA-co-RhBMA) (ABA-N) and Thermosensitive Hairy NPs with Various LCST Transitions

This work was intended to study the effect of LCST transition of thermosensitive hairy NPs on properties of hybrid micellar hydrogels of a thermosensitive ABA triblock copolymer and hairy NPs with the NPs initially located in the interstitial space among micellar cores. The hairy NPs were designed to exhibit LCST transitions at temperatures significantly higher than the CMT of the thermosensitive ABA triblock copolymer. We previously reported the synthesis of a thermosensitive ABA triblock copolymer (ABA-D) exhibiting a CMT of 14 $^{\circ}\text{C}$ in water.³⁶

Following the same procedure, we made a new ABA triblock copolymer (ABA-N) by ATRP of a mixture of DEGMMA, DEGEMA, and RhBMA with a molar ratio of 1.00 : 1.48 : 0.0014 from a difunctional PEO macroinitiator with a molecular weight of 20,000 Da. A very small amount of RhBMA was incorporated into the thermosensitive outer blocks for fluorescence resonance energy transfer (FRET) study of the mixtures of ABA-N and hairy NPs. SEC analysis using DMF-LiBr as carrier solvent showed that the $M_{n,SEC}$ was 92.6 kDa and the PDI was 1.20 relative to polystyrene standards, which indicated that the polymerization was well controlled. From the ^1H NMR spectrum, the numbers of DEGMMA and DEGEMA monomer units in ABA-N were calculated to be 238 and 324; the molar ratio of two monomers in the copolymer was close to the feed ratio. The CMT of ABA-N in water at a concentration of 0.2 mg/g, measured by DLS, was 13 °C,⁴⁶ consistent with what we expected.

Four thermosensitive hairy NP samples with different thermoresponsive properties (Table 3.1) were synthesized by surface-initiated ATRP from the same batch of ATRP initiator-functionalized silica NPs. NP-29 and -34 were made by using DEGMMA and TEGMMA with different feed ratios in the polymerization mixtures. NP-44 was PTEGMMA brush-grafted silica NPs, and NP-51 was prepared by SI-ATRP of TEGMMA and TrEGMMA with a molar ratio of 1 : 1. A free initiator, ethyl 2-bromoisobutyrate, was added, and the polymerizations were monitored by ^1H NMR spectroscopy analysis. After desired monomer conversions were reached, the polymerizations were stopped and the NPs were separated by ultracentrifugation. The hairy NPs were washed by five dispersion-ultracentrifugation cycles to remove untethered polymers. The PDIs of all free polymers were < 1.25, indicating that the polymerizations were controlled. The hairy NPs were characterized by thermogravimetric analysis (TGA) and transmission electron microscopy (TEM). From the TEM micrographs of hairy NPs, the average size of silica core NPs

Table 3.1. Characterization data for four hairy nanoparticle samples with different thermoresponsive properties and the corresponding free polymers

Sample	$M_{n,SEC}$ (Da), PDI ^a	DP ^b	σ ^f (chains/nm ²)	LCST _{onset} (°C) ^g	LCST _{end} (°C) ^g	LCST _{mid} (°C) ^g
NP-29	10.4 k, 1.20	42 (28, 14) ^c	0.42	25	32	29
NP-34	9.2 k, 1.24	36 (11, 25) ^d	0.43	30	38	34
NP-44	15.1 k, 1.22	60	0.38	40	48	44
NP-51	11.6 k, 1.20	46 (22, 24) ^e	0.40	45	56	51

^a $M_{n,SEC}$ and PDI were number average molecular weight and polydispersity index of the free polymer measured by size exclusion chromatography (SEC) relative to polystyrene standards. ^b DP: degree of polymerization. ^c The DP of P(DEGMMA-*co*-TEGMMA-*co*-NBDMA) was 42, and the numbers of DEGMMA and TEGMMA monomer units were 28 and 14, respectively. ^d the DP of P(DEGMMA-*co*-TEGMMA-*co*-NBDMA) was 36, and the numbers of DEGMMA and TEGMMA units were 11 and 25, respectively. ^e The DP of P(TEGMMA-*co*-TrEGMMA-*co*-NBDMA) was 46, and the numbers of TEGMMA and TrEGMMA monomer units were 22 and 24, respectively. ^f σ : grafting density. ^g LCST_{onset}, LCST_{end}, and LCST_{mid} were onset temperature, end temperature, and middle point of the LCST transition determined by DLS study.

was found to be 20 nm. On the basis of the TGA data, DP of the polymer, average size of silica core NPs, and the assumption that the molecular weight and the PDI of the grafted polymer are the same as those of the free polymer, the grafting densities of four hairy NP samples were calculated,^{36,47} they were in the range of 0.38 – 0.43 chains/nm². The characterization data of four hairy NP samples and the corresponding free polymers are summarized in Table 3.1.

The thermoresponsive properties of four hairy NP samples in dilute aqueous solutions were studied by DLS.⁴⁶ Consistent with previous reports,^{36,39} the LCST transitions of the brushes grafted on NPs were broader than those of the corresponding free polymers in water. The onset temperature (LCST_{onset}), end temperature (LCST_{end}), and middle point (LCST_{mid}) of the LCST transition of each sample were measured and are summarized in Table 3.1. From NP-29, to -34, to -44, and -51, the LCST_{onset} increased from 25, to 30, to 40, and 45 °C, and the LCST_{mid} changed from 29, to 34, to 44, and 51 °C. Note that all these temperatures are significantly higher than the CMT (13 °C) of ABA-N. Thus, if aqueous mixtures of ABA-N and hairy NPs are gradually heated from ~ 0 °C to above the CMT, the hairy NPs would be located outside the micellar core.^{36,48} This allows us to study how the LCST transition of hairy NPs affect the properties of hybrid hydrogels of ABA-N and hairy NPs with NPs initially residing outside the core of micelles.

3.3.2. Rheological Study of Aqueous Mixtures of ABA-N and NP-29 with a Polymer Concentration of 10 wt% and Various NP-to-Polymer Mass Ratios.

We first made a 10 wt% aqueous solution of ABA-N, which as expected exhibited a sol-gel transition upon heating from ~ 0 ° in an ice/water to room temperature. Figure 3.1A shows the dynamic storage modulus G' and loss modulus G'' as a function of temperature obtained from a heating ramp experiment performed by using a constant frequency of 1 Hz, a strain amplitude of 1 %, and a heating rate of 3 °C/min. At 14 °C and below, the values of G' and G'' were small,

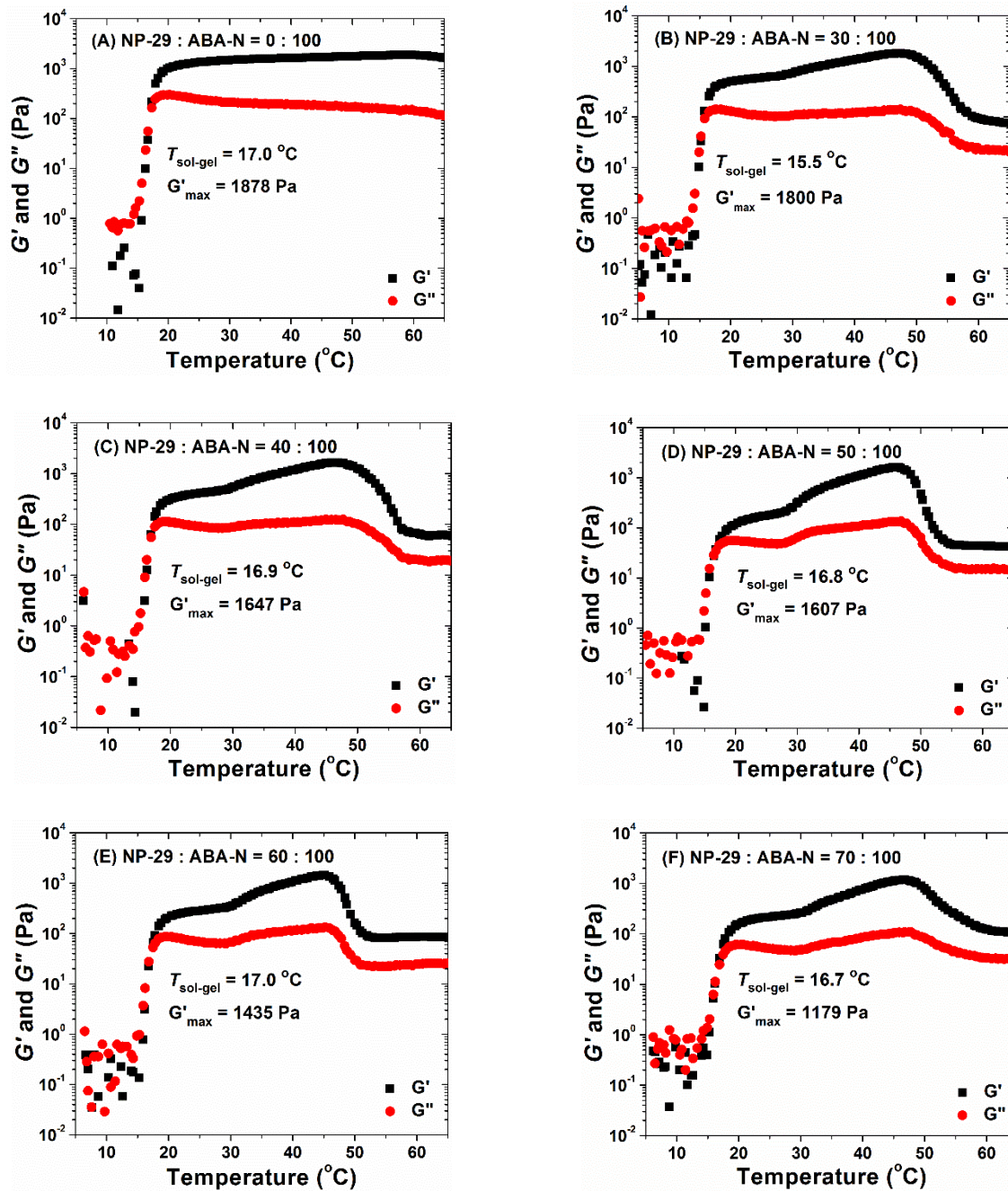


Figure 3.1. Plots of dynamic storage modulus G' and loss modulus G'' of aqueous mixtures of ABA-N with a concentration of 10 wt % and NP-29 with various NP-to-polymer mass ratios versus temperature. The rheological data were collected from heating ramp experiments performed by using a frequency of 1 Hz, a strain amplitude of 1 %, and a heating rate of 3 °C/min.

indicative of the liquid state of the sample. With temperature going up, both G' and G'' increased significantly. The crossover of the two curves, at which $G' = G''$, occurred at 17.0 °C, which is commonly taken as the sol-gel transition temperature ($T_{\text{sol-gel}}$).^{11,49} Above the $T_{\text{sol-gel}}$, G' quickly levelled off and G'' gradually decreased; this is a typical behavior of an elastic physical hydrogel.

To study the effect of incorporating NP-29 into the thermosensitive micellar hydrogel of ABA-N, the aqueous dispersion of NP-29 was added into the aforementioned 10 wt% aqueous solution of ABA-N. The concentration of ABA-N, defined as $[(\text{polymer mass})/(\text{polymer mass} + \text{water mass})] \times 100\%$, was maintained at 10 wt % by evaporating a calculated amount of water from the sample. The mass ratio of NP-29 to ABA-N was gradually increased from 30 : 100 to 40 : 100, to 50 : 100, to 60 : 100, and 70 : 100. For each mass ratio, three rheological measurements were taken using the same conditions as for the pure ABA sample. Representative rheological curves are presented in Figure 1; the other two heating ramps are included in Appendix B.

By looking through Figure 1B-F, one can find that there was little change in $T_{\text{sol-gel}}$ with the increase of NP-to-polymer mass ratio, which indicates that the presence of NP-29 did not affect the ability of ABA-N to form a 3-dimensional network in water, even when the NP-to-polymer ratio reached 70 : 100. However, several new features were observed from the rheological curves for aqueous mixtures of ABA-N and NP-29 compared with that of the 10 wt% aqueous solution of ABA-N (Figure 3.1A). To better appreciate the effect of adding NP-29 into the 10 wt% aqueous solution of ABA-N, we re-plotted G' versus temperature for all six samples on a linear scale (Figure 3.2). (i) With the increase of temperature from 17 to 29 °C, for all hybrid samples, G' increased gradually and a plateau was forming just like that for the 10 wt% solution of ABA-N. Most notably, when the temperature reached ~ 29 °C, G' exhibited a sharp increase for all aqueous mixtures of ABA-N and NP-29. This transition temperature coincided with the LCST transition of

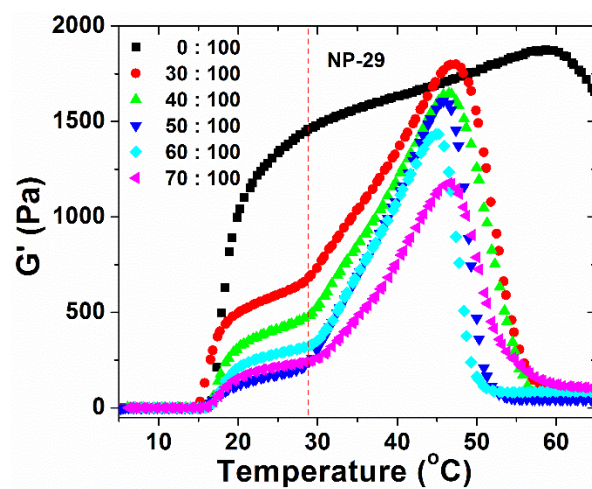


Figure 3.2. Plots of dynamic storage modulus G' versus temperature for aqueous mixtures of ABA-N and NP-29 with different mass ratios. The data were replotted from Figure 3.1.

NP-29, which was in the range of 25 – 32 °C with the middle point at 29 °C. For the mixture with the NP-to-ABA mass ratio of 30 : 100, the G' increased dramatically upon further heating and at 47.4 °C reached 1800 Pa, which is almost the same as the maximum value of G' (G'_{\max}) of the sample without NPs (1878 Pa). Note that at 47.4 °C the G' value was even greater than that of the pure ABA sample. This is totally different from the hybrid hydrogels of ABA-D and NP-D that were reported previously,³⁶ where NP-D, having a LCST essentially same as the CMT of ABA-D, resided in the core of micelles and little change in G' was observed compared with the pure ABA sample. The behavior of NP-29 was similar to our previous observation for NP-T [36], the hairy NPs with a LCST significantly higher than the CMT of ABA-D; the hybrid samples of ABA-D and NP-T exhibited a noticeable increase in G' at a temperature around the LCST of NP-T. We believe this observation is caused by the thermally induced collapse of polymer brushes on NPs.

(ii) While the G' of the sample containing no hairy NPs exhibited a slight drop at temperatures above 60 °C (Figure 2), a more dramatic decrease was observed for all mixed samples, with the lowest G' values at ~ 60 °C in the range of 40 – 125 Pa. In addition, the decrease occurred at lower temperatures, e.g., ~ 47.4 °C for the sample with a NP-to-polymer mass ratio of 30 : 100, and there was a general trend that the onset temperature shifted to the lower temperature side with the increase of the NP content. (iii) The G'_{\max} decreased gradually with the increase of the NP-to-polymer ratio, with the average G'_{\max} value of three measurements dropping from 1879 Pa for the NP-to-polymer mass ratio of 0 : 100, to 1266 Pa for the ratio of 70 : 100. Apparently, the hydrogel became weaker when more NPs were added into the system.

3.3.3. Rheological Study of Aqueous Mixtures of ABA-N and NP-34, -44, and -51 with a Polymer Concentration of 10 wt% and Various NP-to-Polymer Mass Ratios.

The gel properties of hybrid samples of ABA-N and NP-34, -44, and -51 with a polymer concentration of 10 wt% and various NP-to-polymer mass ratios were also studied by rheological measurements using the same conditions. Again, for each ratio, three rheological measurements were taken. Figure 3.3 shows the representative plots of G' versus temperature for various NP-to-polymer ratios for NP-34, -44, and -51. The original heating ramps can be found in Appendix B.

As can be seen from Figure 3, for all three thermosensitive hairy NP samples, the G' exhibited a characteristic, sharp increase on top of a plateau at a critical temperature, as for NP-29. The critical temperatures for NP-34, -44, and -51 were 32, 40, and 45 °C, respectively, which corresponded to their LCST transitions. For NP-34, the onset temperature for the sharp increase of G' is between the $LCST_{onset}$ (30 °C) and $LCST_{mid}$ (34 °C), while for NP-44 and NP-51, the critical temperatures from rheological curves appeared to be the same as the onset temperatures of their LCST transitions in water (40 and 45 °C, respectively). It should be emphasized here that the LCST transitions of thermosensitive hairy NPs were determined by DLS studies of hairy NPs in dilute aqueous solutions with a concentration of 1.0 mg/mL. Much like the cloud point of a thermosensitive polymer in water,⁵⁰ the LCST transition of thermosensitive hairy NPs in the hybrid samples could be affected by many factors such as NP concentration and the presence of ABA-N. For NP-44, the sharp increase of G' occurred at a temperature essentially the same as that we previously observed for hybrid hydrogels of ABA-D and NP-T.³⁶ Note that NP-44 and NP-T both were PTEGMMA brush-grafted NPs. The shift in the onset temperature for G' to increase sharply can be better appreciated from Figure 4, where G' was plotted against temperature for the aqueous mixtures of ABA-N and four thermosensitive hairy NPs with a mass ratio of 30 : 100.

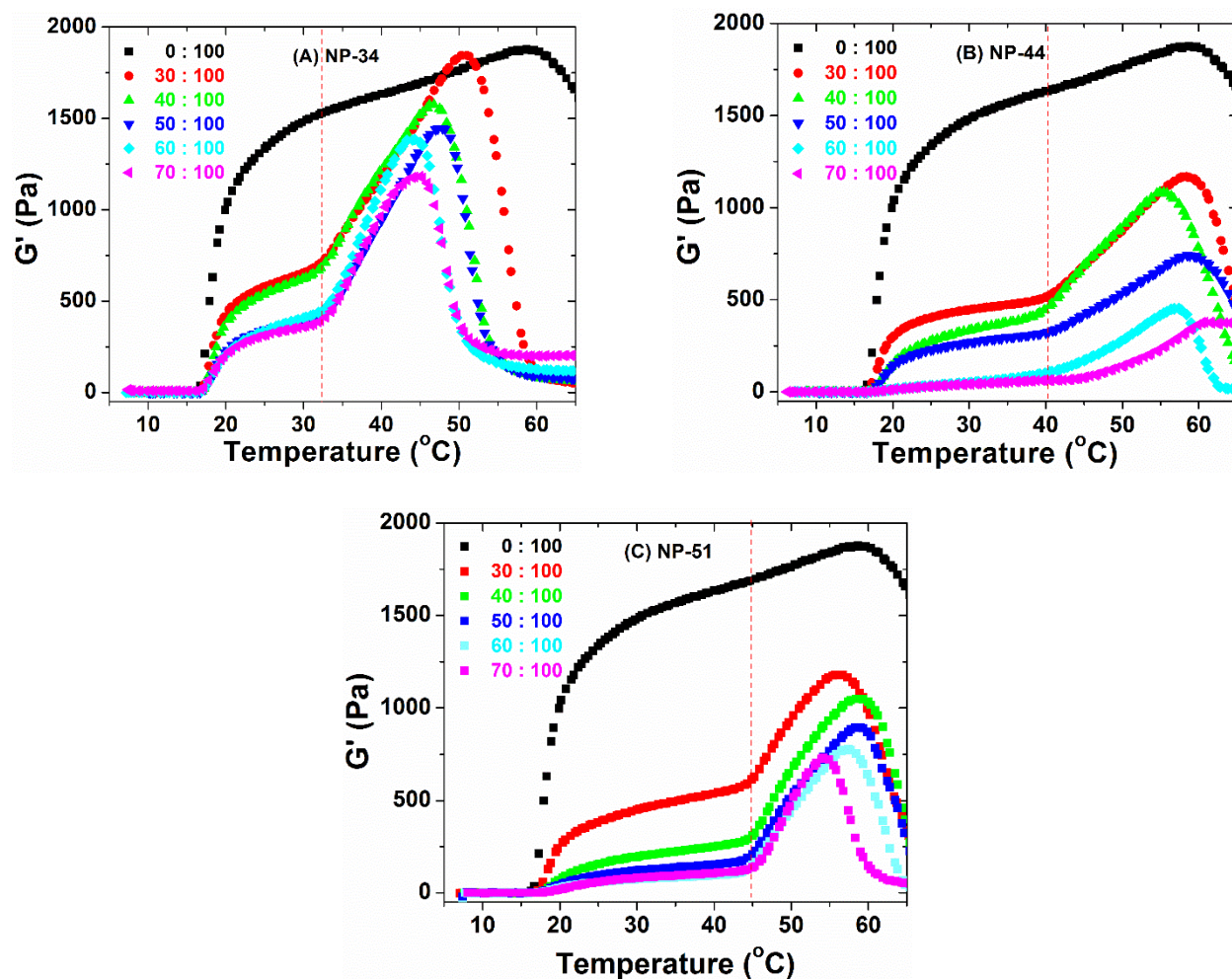


Figure 3.3. Representative plots of dynamic storage modulus G' versus temperature for aqueous mixtures of ABA-N and (A) NP-34, and (B) NP-44, and (C) NP-51 with various NP-to-ABA-N mass ratios. The data were replotted from one of the three heating ramps for each mass ratio that can be found in Appendix B.

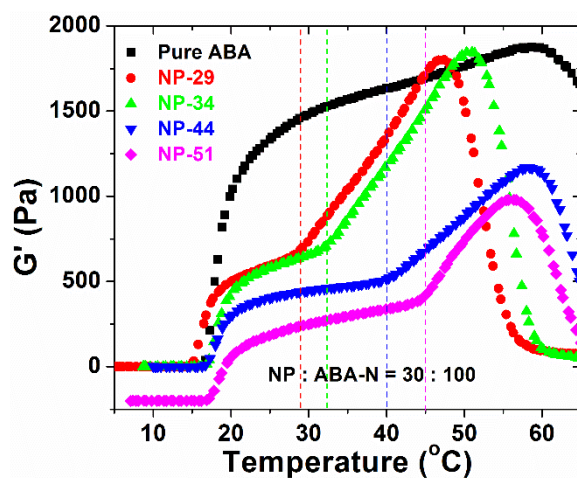


Figure 3.4. Plots of dynamic storage modulus G' of aqueous mixtures of ABA-N and four thermosensitive hairy NPs with different LCSTs at a NP-to-polymer mass ratio of 30 : 100 as a function of temperature. The rheological data were from Figures 3.2 and 3.3. For the sake of clarity, the G' vs T curve for ABA-N and NP-51 was vertically shifted by -200 Pa.

From Figures 3 and 4, one can find that the G'_{\max} of the hybrid hydrogel of NP-34 and ABA-N at a mass ratio of 30 : 100 is comparable to that of the 10 wt% solution of ABA-N, which is similar to the observation for NP-29. In contrast, for hybrid hydrogels of ABA and NP-44 and NP-51, the G'_{\max} values are significantly lower. It appears that the incorporation of NPs with a higher LCST results in weaker micellar hydrogels. Same as NP-29, G' exhibited a large drop at elevated temperatures for all three hairy NP samples, and the extent of decrease was significantly higher than that of the 10 wt% sample of ABA-N without any hairy NPs. In addition, there was a general trend that the G'_{\max} decreased with the increase of NP-to-polymer mass ratio (Figure 3).

3.3.4. Comparison of Hybrid Micellar Hydrogels of Four Hairy NP Samples.

Although the hybrid hydrogels of ABA-N with four hairy NP samples share some common features such as the sharp increase of G' at the LCST of hairy NPs and the large drop of G' at elevated temperatures, there are differences. Figure 5 shows the plots of average G'_{\max} of three rheological measurements versus the NP-to-polymer mass ratio. For comparison, we also included the data from the previous publication for hybrid hydrogels of ABA-D and NP-D (with a LCST \approx the CMT of ABA-D) and ABA-D and NP-T (with a LCST higher than the CMT of ABA-D by nearly 30 °C).³⁶ For NP-29 and -34, the decrease of G'_{\max} with the increase of NP-to-polymer ratio is small, with the largest drop observed at a ratio of 70 : 100. At mass ratios of 30 – 50 %, the G' values for both NP-29 and -34 are more in line with those of hybrid hydrogels of ABA-D and NP-D. It should be noted that for the hybrid hydrogels of ABA-D and NP-D, there was no dramatic increase in G' on the plateau of G' vs. T , similar to that of the pure ABA sample. For NP-44 and -51, the G' values were significantly lower (by > 500 Pa), even at a NP-to-polymer ratio of 30 : 100 (Figure 5), which further corroborated our previous results for hybrid micellar hydrogels of ABA-D and NP-T.³⁶

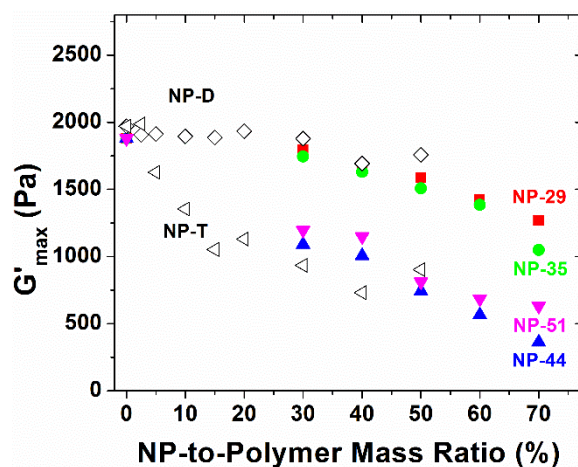
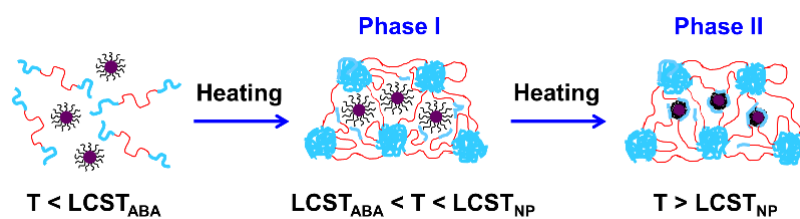


Figure 3.5. Effect of NP-to-polymer mass ratio on G'_{max} of hybrid micellar hydrogels of thermoresponsive hairy NPs and ABA-N with a polymer concentration of 10 wt %. The values of G'_{max} are the averages of three rheological measurements. NP-29 (red solid square); NP-35 (green solid circle); NP-44 (blue upward pointing solid triangle); NP-51 (magenta downward pointing solid triangle); NP-D (black empty diamond); NP-T (black left-pointing empty triangle). The data for NP-D and NP-T are from Ref. 36 and used here for comparison.

3.4. Discussion

It is clear from the results presented above that for hybrid micellar hydrogels of thermosensitive ABA triblock copolymers and hairy NPs with NPs residing initially outside the micellar core, the LCST transition of hairy NPs has a significant effect on gel property. In particular, a sharp increase of G' on top of a plateau in the heating ramp was observed at a temperature corresponding to the LCST transition of the incorporated thermosensitive hairy NPs. Interestingly, for all four thermosensitive hairy NP samples, the G' values right before the sharp increase were much smaller than that of the hydrogel formed from the 10 wt% aqueous solution of ABA-N at the same temperature. According to the trend, if there was no sharp increase in G' at the LCST of hairy NPs, the G'_{\max} would be significantly smaller than that of the hydrogel of the 10 wt% solution of pure ABA-N. The G' of a transient physically crosslinked hydrogel is known to be a measure of the number density of effective gel network strands and can be described by $G' = \nu k_B T$, where ν is the number density of elastically active/bridging polymer chains per unit volume, k_B is Boltzmann constant, and T is the absolute temperature.^{11,51,52} This observation suggests that the incorporation of thermosensitive hairy NPs with LCST transitions higher than the CMT of the ABA triblock copolymer affected the formation of the 3-D network in a negative way (Phase I in Scheme 3.2), likely by increasing the fraction of loops (both thermosensitive outer blocks of an ABA triblock copolymer molecule are located in the same micellar core) assuming the number of dangling polymer chains is only a function of temperature. The loops and dangling polymer chains do not sustain the mechanical stress applied to the network and thus do not contribute the modulus of micellar hydrogels.^{2,11} These observations are different from the hybrid micellar gels of ABA-D and NP-D, where the addition of NPs with a LCST \approx the CMT of ABA-D resulted in a negligible effect on the gel strength, presumably because of the incorporation of NPs into the network's



Scheme 3.2. Schematic illustration of formation of 3-D network by ABA-N in the presence of hairy NPs and reorganization of network structure upon heating above the LCST transition temperature of hairy NPs

nodes.³⁶ For all four hairy NP samples, there was a general trend that the G'_{\max} decreased with the increase of the NP-to-polymer mass ratio, which meant that incorporating more NPs into the system affected the formation of the network to a greater extent. It can be imagined that the presence of a sufficient amount of such thermosensitive hairy NPs in the gel could increase the stretching of the bridging PEO blocks; the formation of loops thus could become entropically more favorable compared with the bridging chains among micelles. Apparently, adding more NPs would disrupt the network formation to a greater extent. As a result, a network with a lower density of bridging chains and thus lower G' values is formed.

The sharp increase in G' is believed to be caused by the collapse of polymer brushes in hairy NPs, which triggered reorganization of the 3-D network to achieve the lowest energy (Phase II in Scheme 3.2). This reorganization likely involves the conversion of entropically unfavorable polymer loops into bridging chains as well as the adsorption of dangling thermosensitive blocks of the ABA triblock copolymer, resulting in an increase in the density of elastically active polymer chains and thus G' values. Interestingly, for NP-29 and -34, the G'_{\max} values at lower NP-to-polymer mass ratios were comparable to that of the gel with no hairy NPs, while for NP-44 and -51, the G'_{\max} values were significantly lower. We speculate that this might be a result of the lower LCST transition temperatures of NP-29 and -34, at which the reorganization of the polymer networks is energetically and kinetically easier compared with NP-44 and -51. Note that the LCST of hairy NPs was determined by the chemical structure/composition of the grafted polymer brushes on NPs; the longer the oligo(ethylene glycol) side chain, the higher the LCST. The trend that G'_{\max} decreased with the increase of NP-to-polymer mass ratio reflected the fact that the network became increasingly weaker with the number of NPs in the system increasing, despite that the LCST transition of hairy NPs triggered reorganization of polymer chains in the system.

To estimate the change in the fraction of bridging polymer chains before and after the LCST transition of hairy NPs, we took hybrid hydrogels with a NP-to-ABA-N mass ratio of 30 : 100 as an example and calculated the maximum possible moduli at the onset temperature for G' to begin to increase sharply and the temperature at which G'_{\max} occurred using $G' = \nu k_B T$. We assumed that all hybrid samples have a density of 1.0 g/mL and every polymer chain is elastically active. The calculated G' values and the fractions of bridging polymer chains are shown in Table 3.2. Clearly, for every hybrid hydrogel, there is a dramatic increase in the fraction of bridging polymer chains at the temperature of G'_{\max} compared with that at the onset temperature. For example, the fraction of bridging polymer chains for ABA-N/NP-29 was 35% at 29 °C but increased to 88% at 47 °C. Apparently, the LCST transition of hairy NPs triggered reorganization of the 3-D network structure and increased the crosslinking density as discussed earlier.

Another feature is the dramatic decrease of G' at elevated temperatures, which reflects the breakdown of the network structure. Although a slight decrease in G' was also seen for the 10 wt% solution of pure ABA-N, the decrease of G' occurred at lower temperatures and to a greater extent for hybrid micellar hydrogels. We believe that this is caused by the thermally induced shrinking of the bridging PEO blocks and the less uniform network because of the presence of thermosensitive hairy NPs. It is known that water becomes an increasingly poor solvent for PEO upon heating, and thus the bridging PEO block underwent shrinking at elevated temperatures,¹¹ making the formation of polymer loops become entropically comparable with or even more favorable than the formation of bridging chains among micellar cores. Consequently, the fraction of bridging PEO blocks, and thus the G' , decreases upon further heating. In addition, the 3-D networks of hybrid micellar hydrogels was formed via two steps (Scheme 2); the network was less uniform and had more defects, caused by the reorganization of the network and adsorption of

Table 3.2. Calculated fractions of bridging polymer chains at certain temperatures for hybrid hydrogels of ABA-N and four hairy NP samples with a NP-to-ABA mass ratio of 30 : 100

Sample	ABA-N/NP-29		ABA-N/NP-34		ABA-N/NP-44		ABA-N/NP-51	
	T_{onset}	T at G'_{max}	T_{onset}	T at G'_{max}	T_{onset}	T at G'_{max}	T_{onset}	T at G'_{max}
Temperature	29 °C	47 °C	32 °C	51 °C	40 °C	58 °C	45 °C	56 °C
G'_{calc} (Pa) ¹	1930	2045	1949	2070	2000	2115	2032	2102
G'_{expt} (Pa) ²	685	1800	699	1845	514	1168	584	1179
Fraction of Bridging Chains	35%	88%	36%	89%	26%	55%	29%	56%

¹ G'_{calc} is the calculated maximum modulus at T_{onset} or T of G'_{max} based on $G' = \nu k_B T$. ² G'_{expt} values at T_{onset} and T for G'_{max} are from Fig. 4. ³ The fraction of bridging chains at a particular temperature is calculated from the ratio of G'_{expt} to G'_{calc} .

dangling chains, compared with the gel formed by the 10 wt% aqueous solution of ABA-N. This can also be seen from the general trend for all four thermosensitive hairy NP samples that the temperature for G'_{\max} shifted to the lower temperature side, though there are some exceptions, particularly for NP-44 (Figure 3.3B). We speculate that the exceptions from the general trend might be related to the preparation of samples and the rheological measurements. At this point, we cannot provide an explanation for the observation that the breakdown of hydrogels containing NP-44 and -51 took place at higher temperatures than NP-29 and -34 (Figure 3.4). It should be noted here that the grafting densities of four hairy NP samples were very similar to each other (0.42 chains/nm² for NP-29, 0.43 chains/nm² for NP-34, 0.38 chains/nm² for NP-44, and 0.40 chains/nm² for NP-51). Thus, the effect of the grafting density difference on gel property in our study should be negligible. Nevertheless, the grafting density of hairy NPs could affect the LCST transition of polymer brushes and thus the properties of hybrid hydrogels.

To experimentally elucidate the origin of the sharp increase of G' in the heating ramps shown in Figures 3.2-3.4 and confirm our hypothesis that it is caused by the LCST transitions of hairy NPs, we conducted fluorescence resonance energy transfer (FRET) studies for four dilute aqueous mixtures of ABA-N and hairy NPs at various temperatures. Note that a fluorescent dye NBD-containing monomer, NBDMA, was incorporated into the polymer brushes of all four hairy NP samples and Rhodamine B-containing monomer RhBMA was copolymerized into the thermosensitive outer blocks of ABA-N. NBDMA and RhBMA are a FRET pair; NBDMA and Rhodamine B emit at 521 and 575 nm, respectively, upon excitation with 480 nm light.⁴⁶ We previously employed FRET to study the spatial location of thermosensitive hairy NPs in aqueous solutions of a thermosensitive ABA triblock copolymer.³⁶ Here four aqueous mixtures of ABA-N and hairy NPs with polymer concentrations of ~ 0.21 mg/g and NP concentrations of ~ 0.010 mg/g

were prepared, and the fluorescence emission spectra with an excitation wavelength of 480 nm were recorded at various temperatures. All four samples exhibited two peaks with one maximum at ~ 521 nm, which is attributed to the emission of NBDMA, and another at 575 nm, which is from RhBMA. If NBDMA and RhBMA are in close proximity (within 1-10 nm), FRET would occur,⁴³ resulting in a decrease in the fluorescence emission intensity at 521 nm and an increase in the intensity at 575 nm. To quantify the FRET data,⁴⁶ we plot the intensity ratio of the peaks at 521 and 575 nm ($I_{521/575}$) against temperature for four mixtures, as shown in Figure 6.

Clearly, with increasing temperature, a sharp decrease in $I_{521/575}$ was observed for all four aqueous mixtures, suggesting that the FRET occurred to a much greater extent. The onset temperatures for the sharp decrease of $I_{521/575}$ were 23, 30, 40, and 45 °C for the solutions containing NP-29, -34, -44, and -51, respectively. Except the first one, which was 2 °C lower than the $LCST_{onset}$ of NP-29 and 6 °C lower than the critical temperature for the sharp increase of G' , the other three onset temperatures are essentially the same as those observed in the rheology studies. Note that similar fast decreases were observed for I_{521} from the plots of I_{521} vs T .⁴⁶ Apparently, when the temperature reached the LCST of hairy NPs, the brushes collapsed and absorbed the thermosensitive outer blocks of ABA-N, resulting in a closer proximity of NBDMA and RhBMA and thus a more substantial FRET. This supports our hypothesis that the LCST transition of hairy NPs triggered absorption of thermosensitive blocks of ABA-N and reorganization of the network structure in the hybrid micellar hydrogels. Note that below the LCST of hairy NPs, the $I_{521/575}$ ratio also decreased with increasing temperature but at a slower pace than that at the LCST. This is because with the increase of temperature, water becomes an increasingly poor solvent for the PEO-type thermosensitive water-soluble polymers, which undergo shrinking, though small, even when the temperature is still below the LCST.⁵³ Thus, there is an increasing

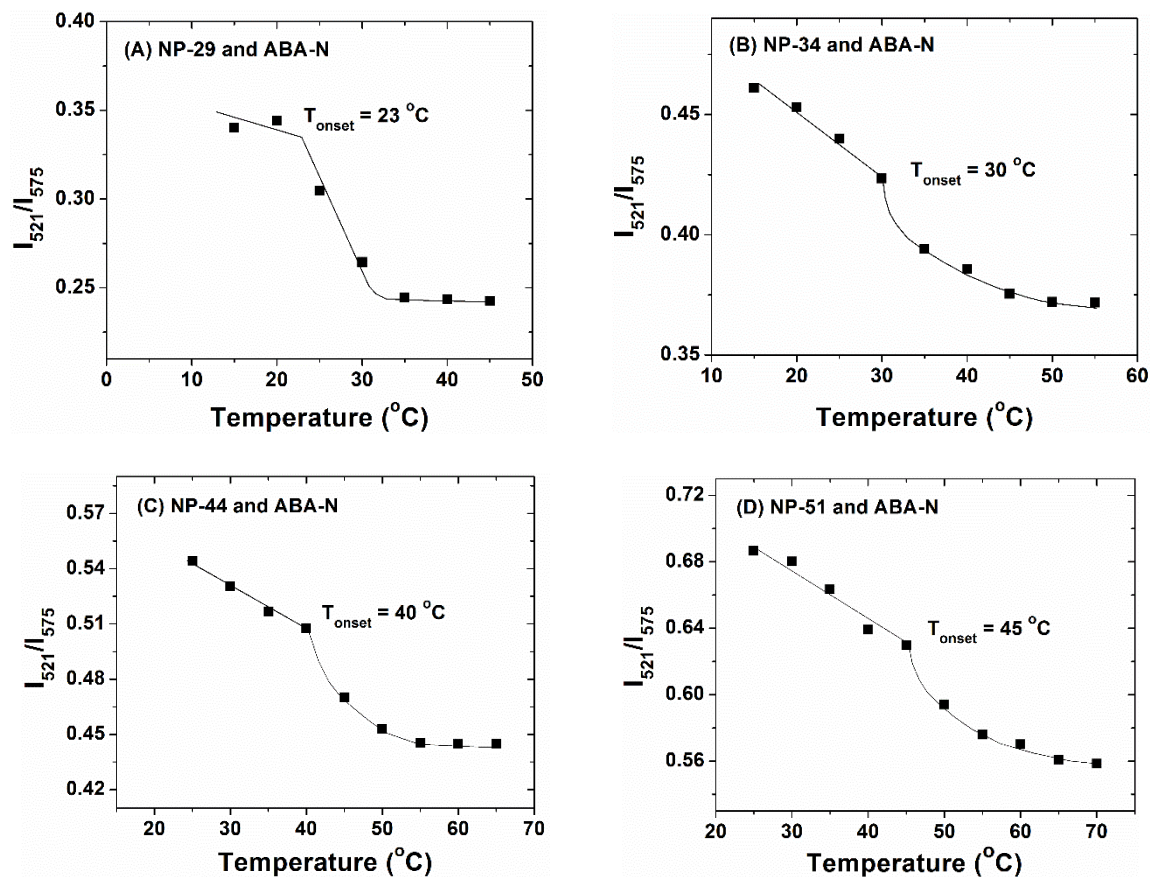


Figure 3.6. Plot of the intensity ratio of the emission peaks at 521 nm and 575 nm (I_{521}/I_{575}) versus temperature for an aqueous mixture of (A) ABA-N (concentration: 0.208 mg/g) and NP-29 (conc.: 0.010 mg/g), (B) ABA-N (conc.: 0.208 mg/g) and NP-34 (conc.: 0.011 mg/g), (C) ABA-N (conc.: 0.206 mg/g and NP-44 (conc.: 0.010 mg/g), and (D) ABA-N (conc.: 0.205 mg/g) and NP-51 (conc.: 0.013 mg/g).

interaction between the ABA-N micelles and hairy NPs, resulting in FRET to some extent and consequently a decrease in I_{521}/I_{575} .

3.5. Conclusions

A thermosensitive ABA triblock copolymer with a CMT of 13 °C and four thermoresponsive hairy NPs with LCSTs of 29, 34, 44, and 51 °C in water were prepared for study of the effect of LCST transition of hairy NPs on properties of hybrid hydrogels of the triblock copolymer and hairy NPs with NPs located initially outside the micellar core. From rheological measurements, for all hairy NPs, a sharp increase in G' occurred on top of the plateau at a temperature around the LCST transition of hairy NPs for aqueous solutions with a polymer concentration of 10 wt% and NP-to-ABA-N mass ratios from 30 : 100 to 70 : 100. This phenomenon was caused by the collapse of hairy NPs, which triggered the reorganization of the 3-D gel network nanostructure with the absorption of thermosensitive outer blocks of ABA-N molecules in the dangling, loop, or stretched bridging forms. This was supported by the results from the FRET experiments where upon heating a sharp decrease of I_{521}/I_{575} of aqueous solutions of ABA-N and hairy NPs was observed at a temperature corresponding to the LCST of hairy NPs. In addition, the G'_{\max} decreased with the increase of NP-to-ABA-N mass ratio, but the effects were different for hairy NPs with different LCSTs. The G'_{\max} values of the hydrogels containing NP-29 and -34 at lower NP-to-polymer mass ratios were comparable to that of the gel with no hairy NPs, while for NP-44 and -51, the G'_{\max} values were significantly lower. Hydrogels have been used in biomedical applications, and their stiffness has been shown to exert a significant effect on, e.g., cell growth and differentiation.⁵⁴ The hybrid hydrogels reported here might be useful in studying the effect of mechanical properties of hydrogels on cell behavior because the moduli of these gels can be easily tuned.

3.6. References

1. Hamley, I. W. *The Physics of Block Copolymers*, Oxford University Press: Oxford, 1998.
2. Hamley, I. W. *Block Copolymers in Solution: Fundamentals and Applications*; John Wiley & Sons: Chichester, 2005.
3. Hamley, I. W. *Philos. Trans. R. Soc. London, Ser. A* **2001**, *359*, 1017-1044.
4. Jeong, B.; Kim, S. W.; Bae, Y. H. *Adv. Drug Delivery Rev.* **2002**, *54*, 37–51.
5. He, C. L.; Kim, S. W.; Lee, D. S. *J. Controlled Release* **2008**, *127*, 189-207.
6. Park, M. H.; Joo, M. K.; Choi, B. G.; Jeong, B. *Acc. Chem. Res.* **2012**, *45*, 424-433.
7. Madsen, J.; Armes, S. P.; Lewis, A.L. *Macromolecules* **2006**, *39*, 7455-7457.
8. Aoshima, S.; Sugihara, S.; *J. Polym. Sci. Part A: Polym. Chem.* **2000**, *38*, 3962-3965.
9. Kirkland, S. E.; Hensarling, R. M.; McConaught, S. D.; Guo, Y.; Jarrett, W. L.; McCormick, C. L. *Biomacromolecules* **2008**, *9*, 481–486.
10. O'Lenick, T. G.; Jiang, X. G.; Zhao, B. *Langmuir* **2010**, *26*, 8787-8796.
11. O'Lenick, T. G.; Jin, N. X.; Woodcock, J. W.; Zhao, B. *J. Phys. Chem. B* **2011**, *115*, 2870–2881.
12. Woodcock, J. W.; Jiang, X. G.; Wright, R. A. E.; Zhao, B. *Macromolecules* **2011**, *44*, 5764-5775.
13. Jin, N. X.; Zhang, H.; Jin, S.; Dadmun, M. D.; Zhao, B. *Macromolecules* **2012**, *45*, 4790-4800.
14. Henn, D. M.; Wright, R. A. E.; Woodcock, J. W.; Hu, B.; Zhao, B. *Langmuir* **2014**, *30*, 2541–2550.
15. Jeong, B. M.; Bae, Y. H.; Lee, D. S.; Kim, S.W. *Nature* **1997**, *388*, 860-862.
16. Daniel, M. C.; Astruc, D. *Chem. Rev.* **2004**, *104*, 293-346.

17. Lu, A.-H.; Salabas, E. L.; Schuth, F. *Angew. Chem. Int. Ed.* **2007**, *46*, 1222-1244.
18. Lucky, S. S.; Soo, K. C.; Zhang, Y. *Chem. Rev.* **2015**, *115*, 1990-2042.
19. Balazs, A. C.; Emrick, T.; Russell, T. P. *Science* **2006**, *314*, 1107-1110.
20. Haraguchi, K.; Takehisa, T. *Adv. Mater.* **2002**, *14*, 1120-1124.
21. Oguz, O.; Wilhelm, O. *Macromolecules* **2007**, *40*, 3378-3387.
22. Haraguchi, K. *Curr. Opin. Solid State Mater. Sci.* **2007**, *11*, 47-54.
23. Schexnailder, P.; Schmidt, G. *Colloid Polym. Sci.* **2009**, *287*, 1-11.
24. Messing, R.; Schmidt, A.M. *Polym. Chem.* **2011**, *2*, 18-32.
25. Wu, C.-J.; Gaharwar, A. K.; Chan, B. K.; Schmidt, G. *Macromolecules* **2011**, *44*, 8215-8224.
26. Fuhrer, R.; Athanassiou, E. K.; Luechinger, N. A.; Stark, W. J. *Small* **2009**, *5*, 383-388.
27. Pozzo, D. C.; Walker, L. M. *Macromol. Symp.* **2005**, *227*, 203-210.
28. Pozzo, D. C.; Walker, L. M. *Macromolecules* **2007**, *40*, 5801-5811.
29. Pozzo, D. C.; Walker, L. M. *Eur. Phys. J. E.* **2008**, *26*, 183-189.
30. Ilg, P. *Soft Matter* **2013**, *9*, 3465-3468.
31. Roeder, L.; Bender, P.; Kundt, M.; Tschöpe, A.; Schmidt, A. M. *Phys. Chem. Chem. Phys.* **2015**, *17*, 1290-1298.
32. Krekhova, M.; Lang, T.; Richter, R.; Schmalz, H. *Langmuir* **2010**, *26*, 19181-19190.
33. Qin, J.; Asempah, I.; Laurent, S.; Fornara, A.; Muller, R. N.; Muhammed, M. *Adv. Mater.* **2009**, *21*, 1354-1357.
34. Nambam, J. S.; Philip, J. *Langmuir* **2012**, *28*, 12044-12053.
35. Reinicke, S.; Döhler, S.; Tea, S.; Krekhova, M.; Messing, R.; Schmidt, A. M.; Schmalz, H. *Soft Matter* **2010**, *6*, 2760-2773.
36. Hu, B.; Henn, D. M.; Wright, R. A. E.; Zhao, B. *Langmuir* **2014**, *30*, 11212-11224.

37. Han, S.; Hagiwara, M.; Ishizone, T. *Macromolecules* **2003**, *36*, 8312-8319.
38. Ishizone, T.; Seki, A.; Hagiwara, M.; Han, S.; Yokoyama, H.; Oyane, A.; Deffieux, A.; Carlotti, A. *Macromolecules* **2008**, *41*, 2963-2967.
39. Li, D. J.; Jones, G. J.; Dunlap, J. R.; Hua, F. J.; Zhao, B. *Langmuir* **2006**, *22*, 3344-3351.
40. Lutz, J.-F.; Hoth, A. *Macromolecules* **2006**, *39*, 893-896.
41. Horton, J. M.; Bai, Z.; Jiang, X.; Li, D.; Lodge, T. P.; Zhao, B. *Langmuir* **2011**, *27*, 2019-2027.
42. Horton, J. M.; Bao, C.; Bai, Z.; Lodge, T. P.; Zhao, B. *Langmuir* **2011**, *27*, 13324-13334.
43. Dosremedios, C. G.; Moens, P. D. J. *J. Struct. Biol.* **1995**, *115*, 175-185.
44. Yin, J.; Hu, H. B.; Wu, Y. H.; Liu, S. Y. *Polym. Chem.* **2011**, *2*, 363-371.
45. Onoda, M.; Uchiyama, S.; Santa, T.; Imai, K. *Anal. Chem.* **2002**, *74*, 4089-4096.
46. The data can be found in Appendix B.
47. Wright, R. A. E.; Hu, B.; Henn, D. M.; Zhao, B. *Soft Matter* **2015**, *11*, 6808-6820.
48. Durand-Gasselin, C.; Sanson, N.; Lequeux, N. *Langmuir* **2011**, *27*, 12329-12335.
49. Noro, A.; Matsushita, Y.; Lodge, T. P. *Macromolecules* **2009**, *42*, 5802-5810.
50. Gil, E. S.; Hudson, S. M.; *Prog. Polym. Sci.* **2004**, *29*, 1173-1222.
51. He, Y. Y.; Boswell, P. G.; Bühlmann, P.; Lodge, T. P. *J. Phys. Chem. B* **2007**, *111*, 4645-4652.
52. Yoshida, T.; Kanaoka, S.; Watanabe, H.; Aoshima, A. *J. Polym. Sci., Part A: Polym. Chem.* **2005**, *43*, 2712-2722.
53. Bai, Z. F.; Lodge, T. P. *J. Phys. Chem. B* **2009**, *113*, 14151-14157.
54. Seliktar, D. *Science* **2012**, *336*, 1124-118.

55. The work presented in this Chapter has been published in *Polymer* as an article (*Polymer*, **2016**, 82, 206-216).

Appendix B

for

Chapter 3. Hybrid Micellar Network Hydrogels of Thermosensitive ABA Triblock Copolymer and Polymer Brush-Grafted Nanoparticles: Effect of LCST Transition of Polymer Brushes on Gel Property

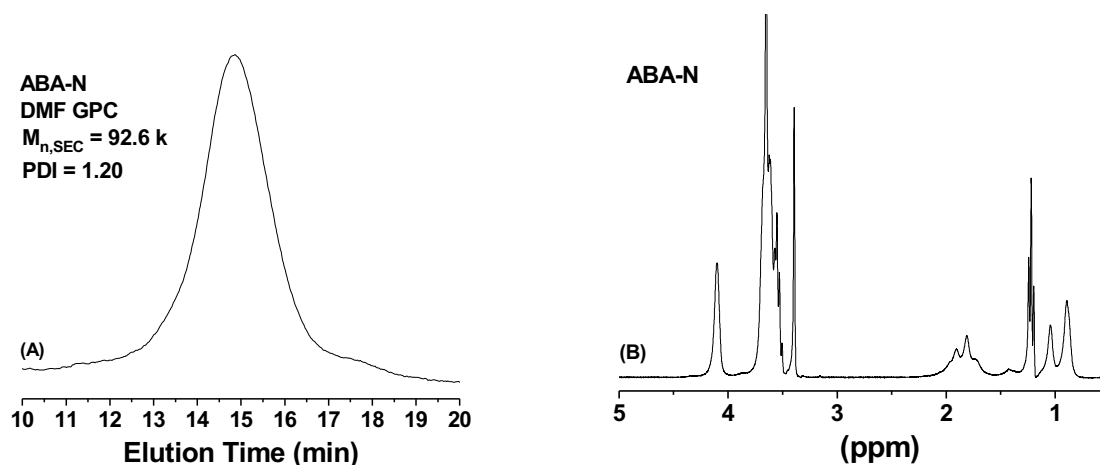


Figure B1. (A) Size exclusion chromatography (SEC) trace of thermosensitive ABA triblock copolymer $\text{P}(\text{DEGMMA-}co\text{-DEGEMA-}co\text{-RhBMA})\text{-}b\text{-PEO-}b\text{-P}(\text{DEGMMA-}co\text{-DEGEMA-}co\text{-RhBMA})$ (ABA-N). DMF-LiBr was the carrier solvent in SEC analysis. (B) ^1H NMR spectrum of ABA-N. CDCl_3 was used as solvent in ^1H NMR spectroscopy analysis.

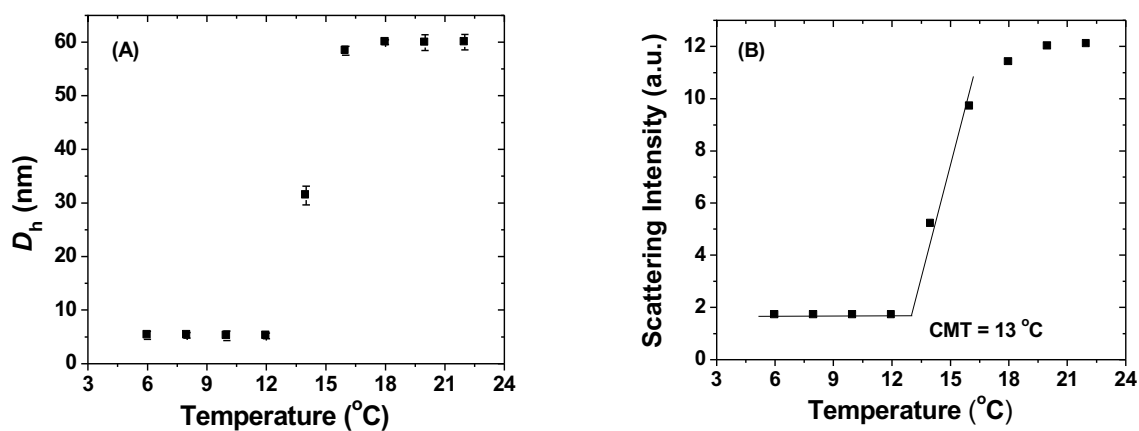
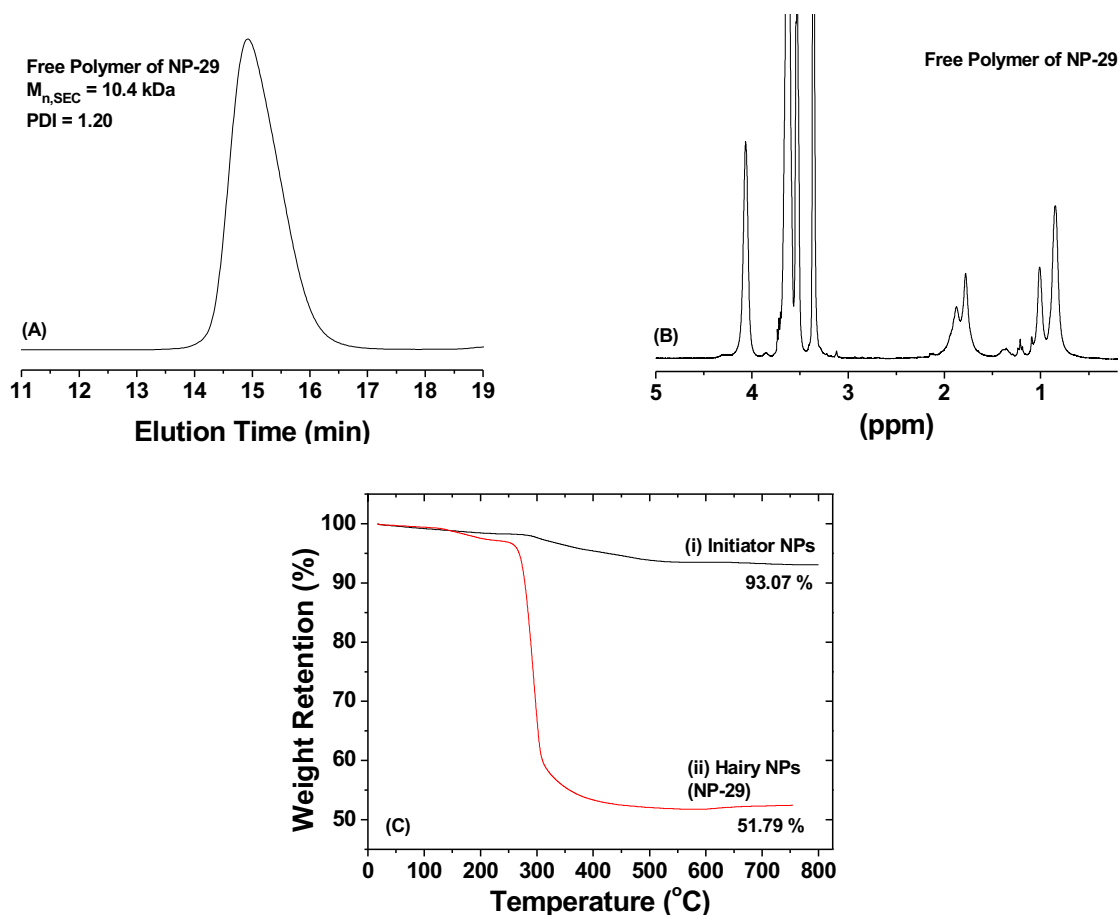


Figure B2. Average apparent hydrodynamic size D_h (A), obtained from CONTIN analysis, and scattered light intensity at scattering angle of 90° (B) as a function of temperature in a dynamic light scattering study of a 0.2 mg/g aqueous solution of P(DEGMMA-*co*-DEGEMA-*co*-RhBMA)-*b*-PEO-*b*-P(DEGMMA-*co*-DEGEMA-*co*-RhBMA) (ABA-N).



Figures B3. (A) Size exclusion chromatography and (B) ^1H NMR spectroscopy analysis of the free copolymer formed from the free initiator in the synthesis of P(DEGMMA-*co*-TEGMMA-*co*-NBDMA) brush-grafted silica nanoparticles with a LCST transition of 29 °C (NP-29). (C) Thermogravimetric analysis (TGA) of (i) the ATRP initiator-functionalized silica nanoparticles and (ii) P(DEGMMA-*co*-TEGMMA-*co*-NBDMA) brush-grafted silica nanoparticles (NP-29).

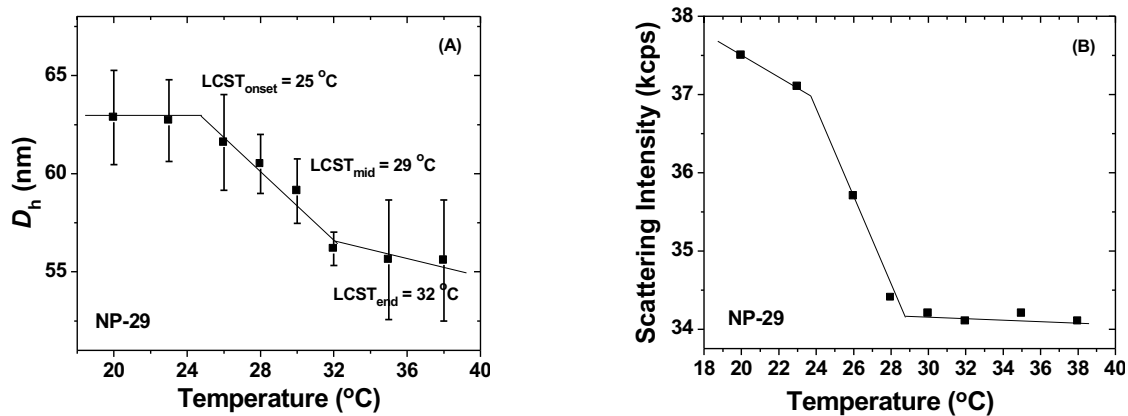
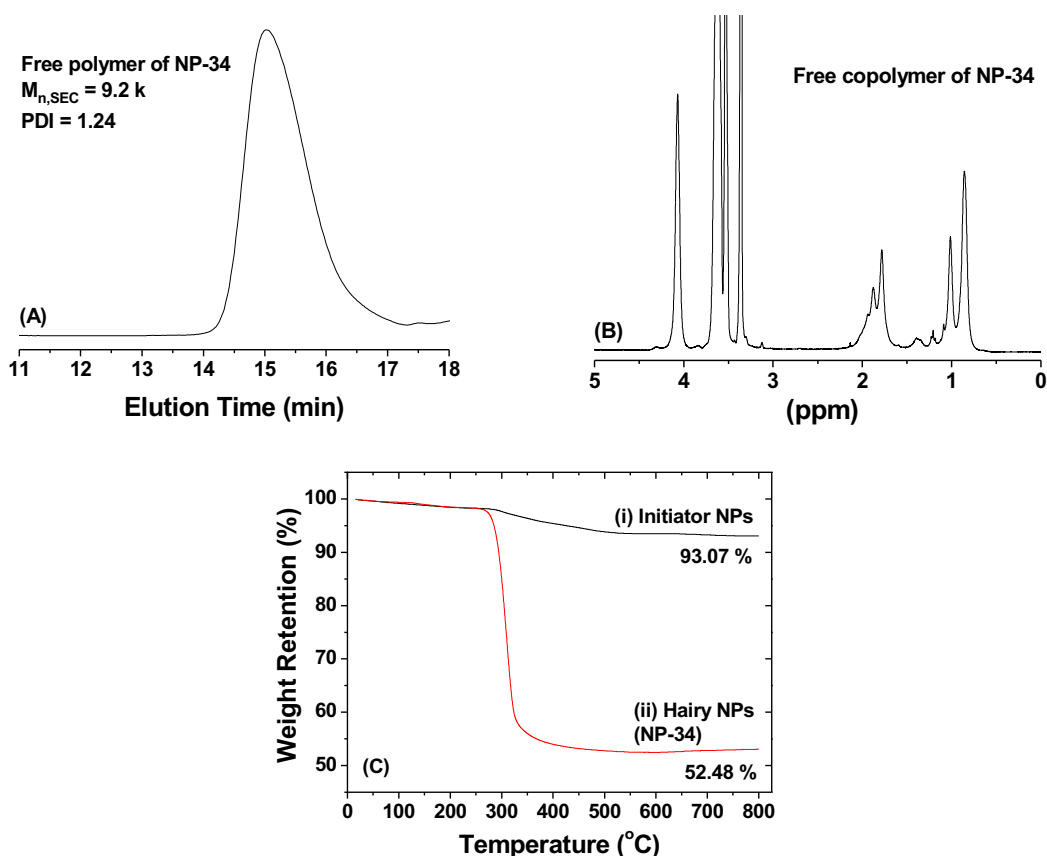


Figure B4. Average apparent hydrodynamic size D_h (A), obtained from CONTIN analysis, and scattered light intensity at scattering angle of 90° (B) as a function of temperature in a dynamic light scattering study of a 1.0 mg/g aqueous dispersion of P(DEGMMA-*co*-TEGMMA-*co*-NBDMA) brush-grafted silica nanoparticles (NP-29).



Figures B5. (A) Size exclusion chromatography (SEC) and (B) ^1H NMR spectroscopy analysis of free copolymer formed from the free initiator in the synthesis of P(DEGMMA-*co*-TEGMMA-*co*-NBDMA) brush-grafted silica nanoparticles with a LCST transition of $34\text{ }^{\circ}\text{C}$ (NP-34). (C) Thermogravimetric analysis (TGA) of (i) the ATRP initiator-functionalized silica nanoparticles and (ii) P(DEGMMA-*co*-TEGMMA-*co*-NBDMA) brush-grafted silica nanoparticles (NP-34).

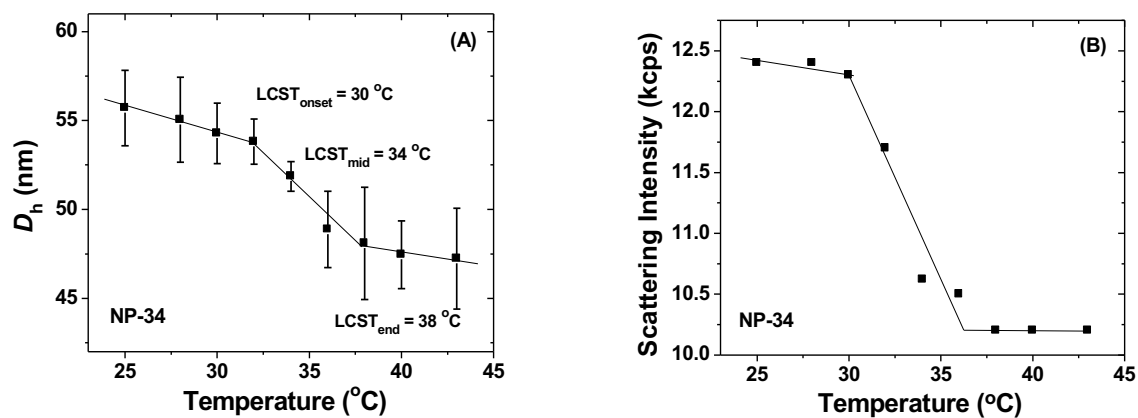
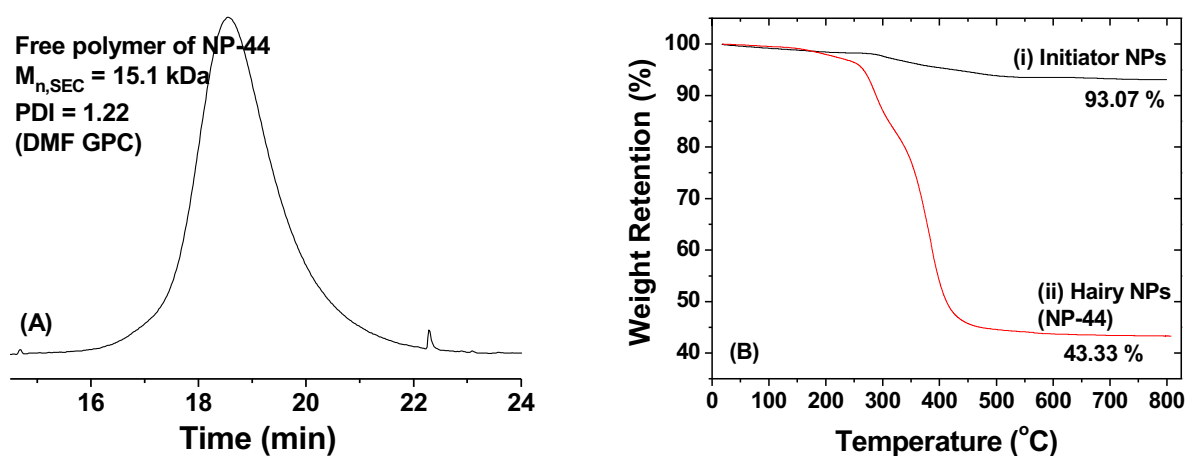


Figure B6. Average apparent hydrodynamic size D_h (A), obtained from CONTIN analysis, and scattered light intensity at scattering angle of 90° (B) as a function of temperature in a dynamic light scattering study of a 1.0 mg/g aqueous dispersion of P(DEGMMA-*co*-TEGMMA-*co*-NBDMA) brush-grafted silica nanoparticles (NP-34).



Figures B7. (A) Size exclusion chromatography (SEC) analysis of free copolymer P(TEGMMA-*co*-NBDMA) formed from the free initiator in the synthesis of P(TEGMMA-*co*-NBDMA) brush-grafted silica nanoparticles with a LCST transition of 44 $^{\circ}\text{C}$ (NP-44). DMF-LiBr was the carrier solvent. (B) TGA of (i) the ATRP initiator-functionalized silica nanoparticles and (ii) P(TEGMMA-*co*-NBDMA) brush-grafted silica nanoparticles (NP-44).

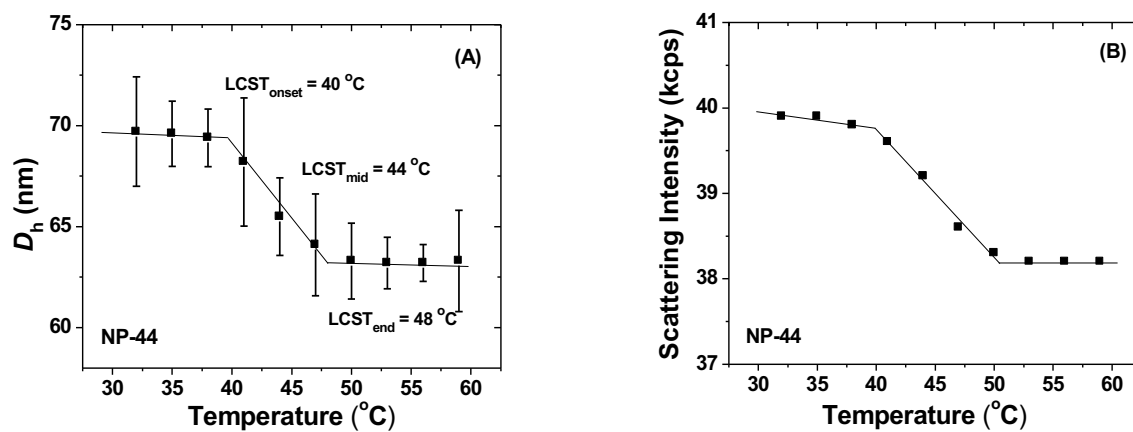
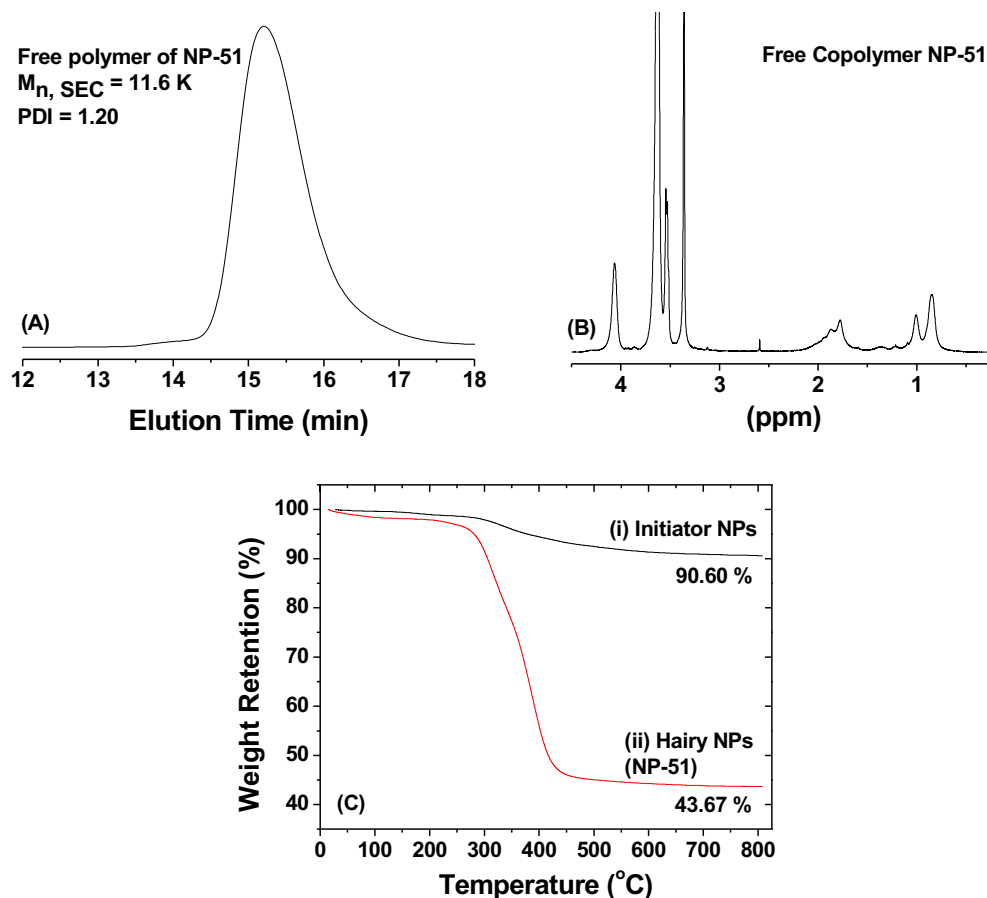


Figure B8. Average apparent hydrodynamic size D_h (A), obtained from CONTIN analysis, and scattered light intensity at scattering angle of 90° (B) as a function of temperature in a dynamic light scattering study of a 1.0 mg/g aqueous dispersion of P(TEGMMA-*co*-NBDMA) brush-grafted silica nanoparticles (NP-44).



Figures B9. SEC analysis (A) and ^1H NMR spectroscopy analysis (B) of the free copolymer formed from the free initiator in the synthesis of P(TEGMMA-*co*-TrEGMMA-*co*-NBDMA) brush-grafted silica nanoparticles with a LCST transition of 51 $^{\circ}\text{C}$ (NP-51). (C) TGA of (i) the ATRP initiator-functionalized silica nanoparticles and (ii) P(TEGMMA-*co*-TrEGMMA-*co*-NBDMA) brush-grafted silica nanoparticles (NP-51).

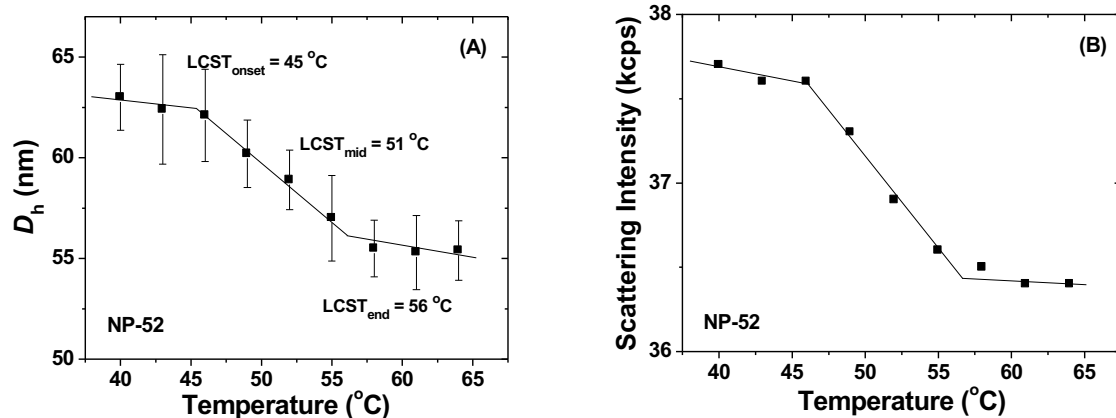


Figure B10. Average apparent hydrodynamic size D_h (A), obtained from CONTIN analysis, and scattered light intensity at scattering angle of 90° (B) as a function of temperature in a dynamic light scattering study of a 1.0 mg/g aqueous dispersion of P(TEGMMA-*co*-TrEGMMA-*co*-NBDMA) brush-grafted silica nanoparticles (NP-51).

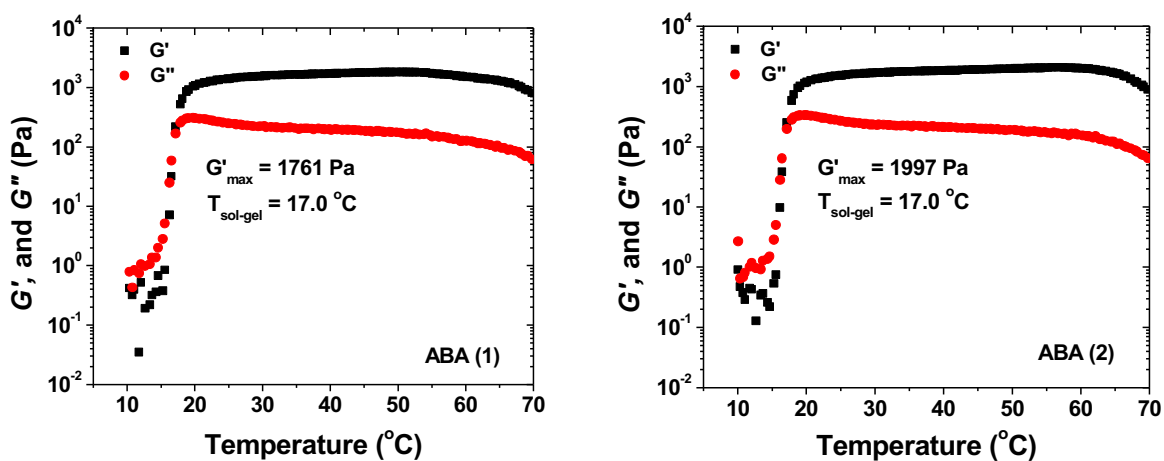
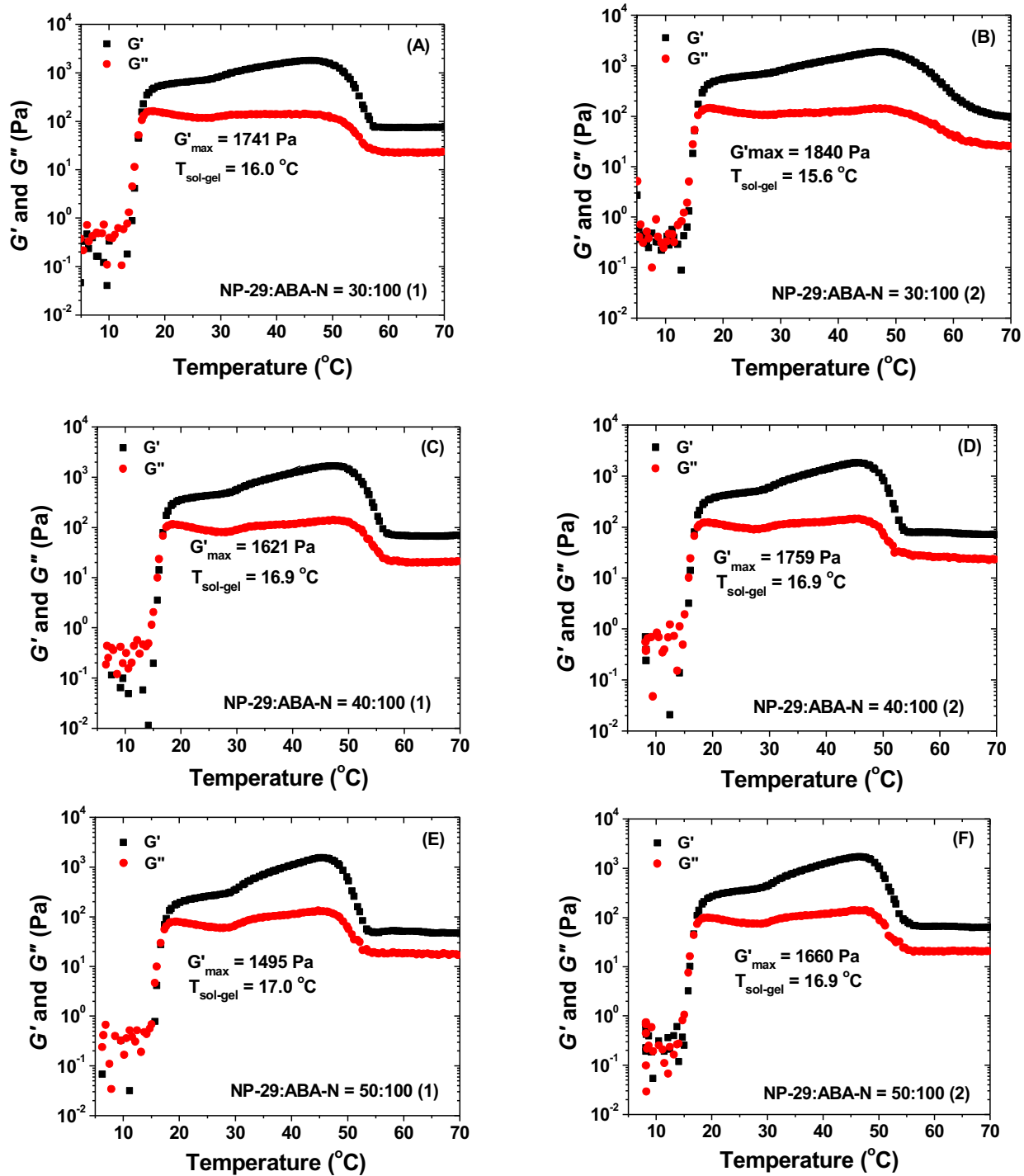
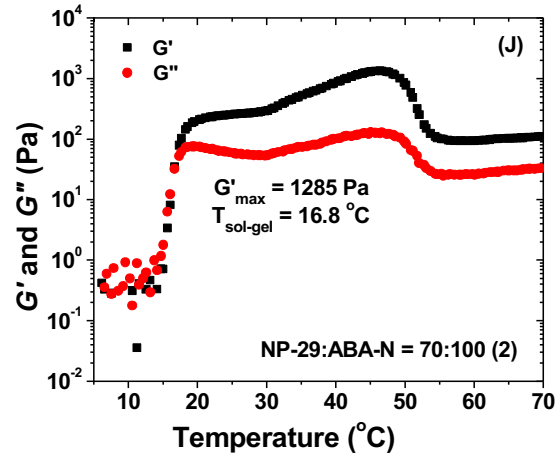
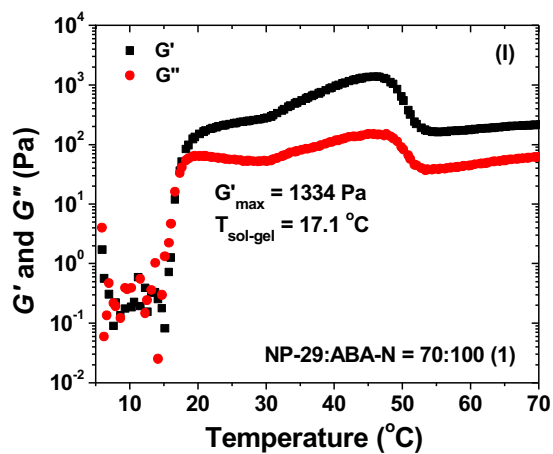
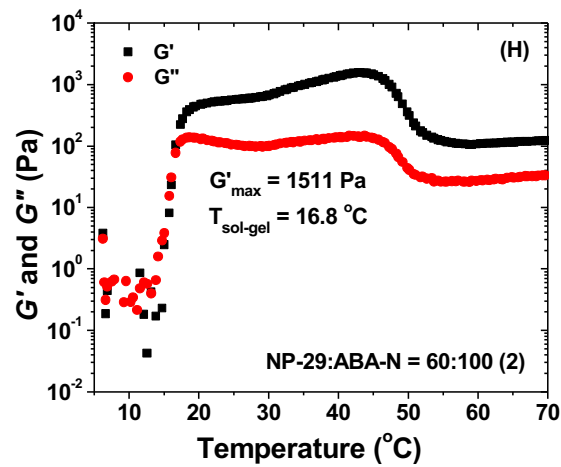
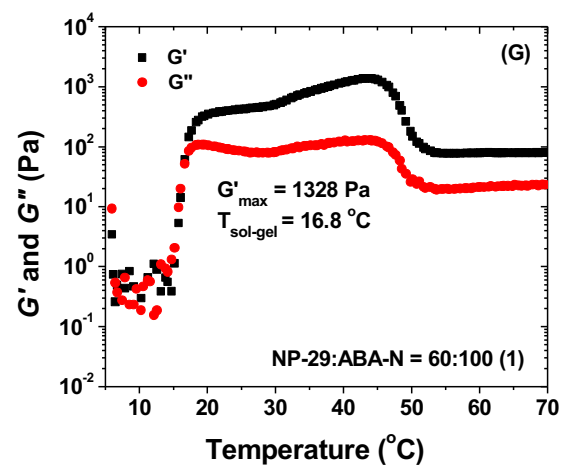


Figure B11. Plots of dynamic storage modulus G' and loss modulus G'' of an aqueous solution of ABA-N with a concentration of 10 wt%. The data were collected from temperature ramp experiments performed by using a frequency of 1 Hz, a strain amplitude of 1 %, and a heating rate of 3 °C/min.

Figure B12. Plots of dynamic storage modulus G' and loss modulus G'' of aqueous mixtures of ABA-N with a concentration of 10 wt% and NP-29 with various NP-to-polymer mass ratios versus temperature. The rheological data were collected from heating ramp experiments performed by using a frequency of 1 Hz, a strain amplitude of 1 %, and a heating rate of 3 °C/min.



(Figure B12 continued)



(Figure B12 continued)

Figure B13. Plots of dynamic storage modulus G' and loss modulus G'' of aqueous mixtures of ABA-N with a concentration of 10 wt% and NP-34 with various NP-to-polymer mass ratios versus temperature. The rheological data were collected from heating ramp experiments performed by using a frequency of 1 Hz, a strain amplitude of 1 %, and a heating rate of 3 °C/min. For each NP-to-ABA-N mass ratio, three rheological measurements were taken.

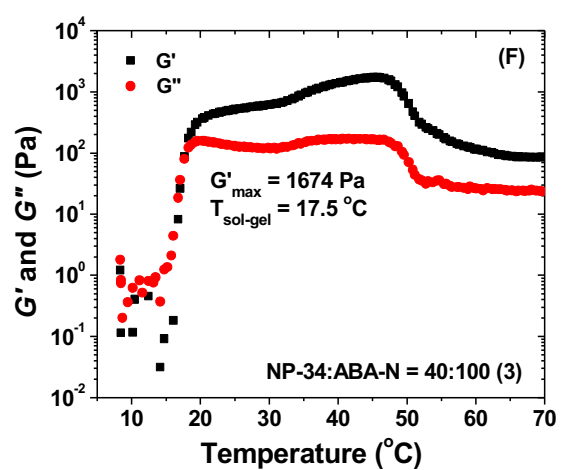
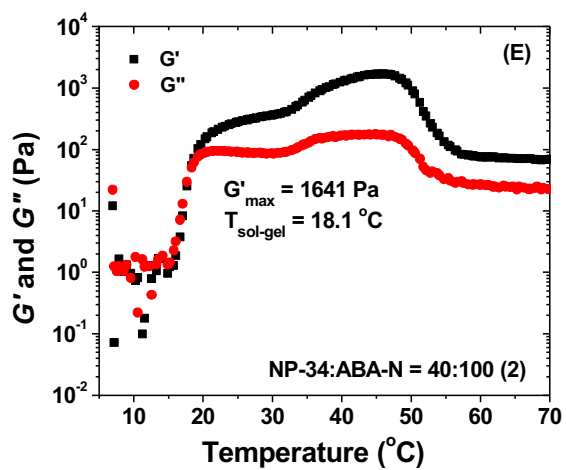
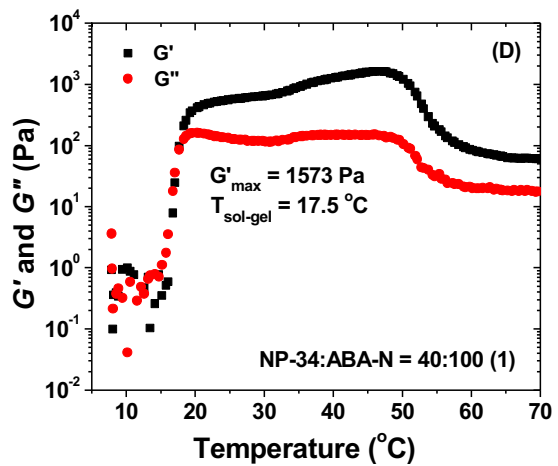
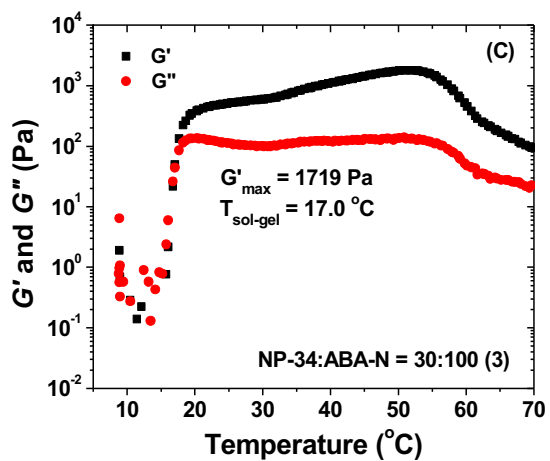
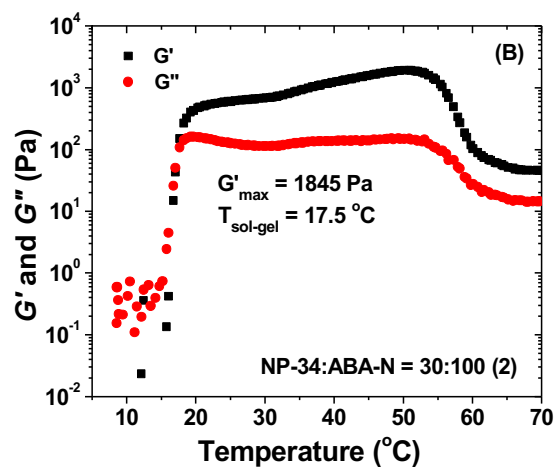
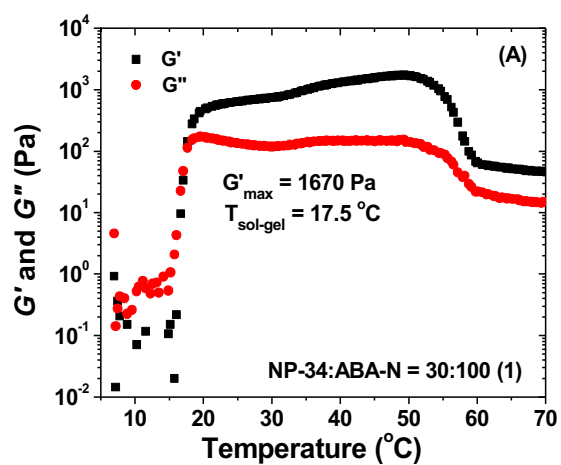


(Figure B13 continued)

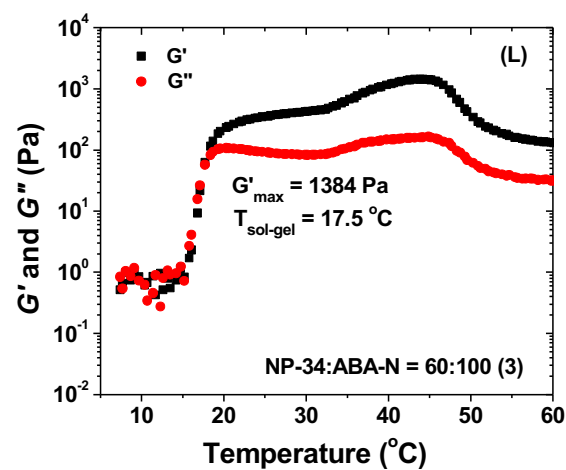
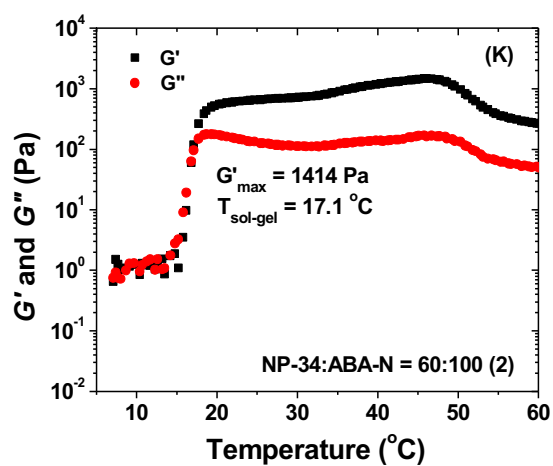
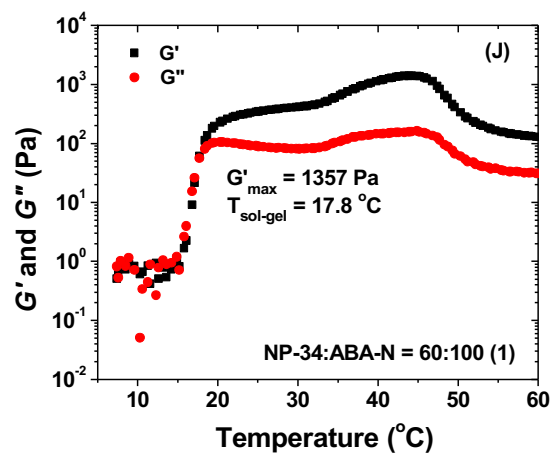
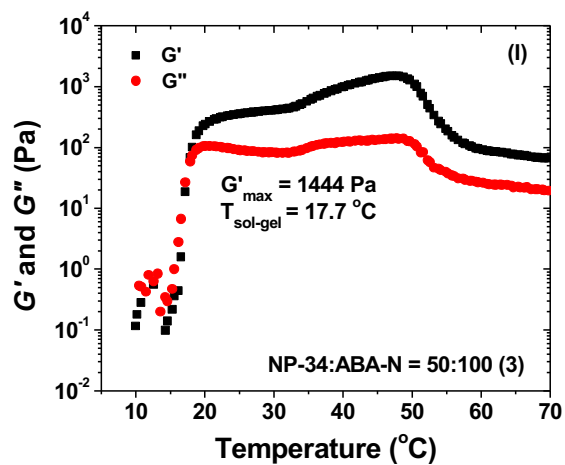
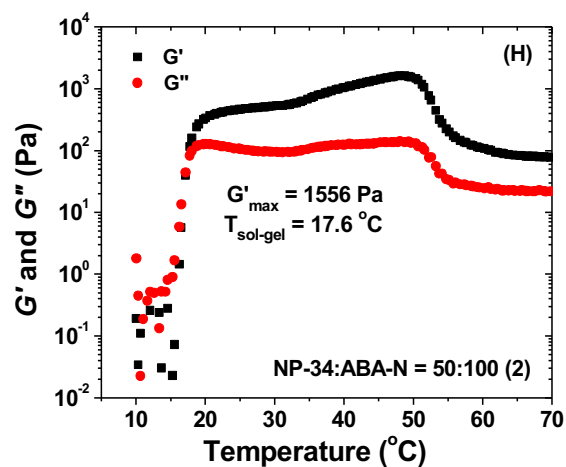
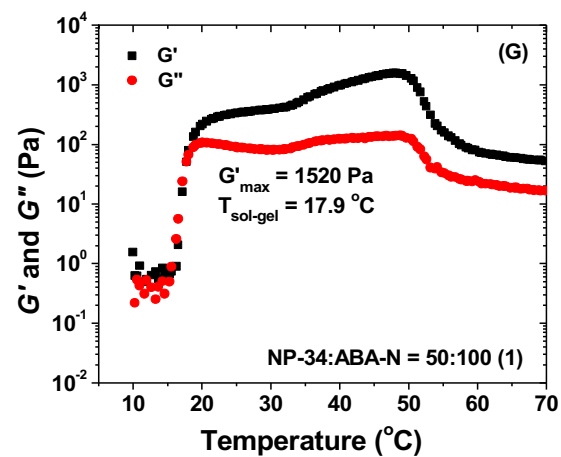


(Figure B13 continued)

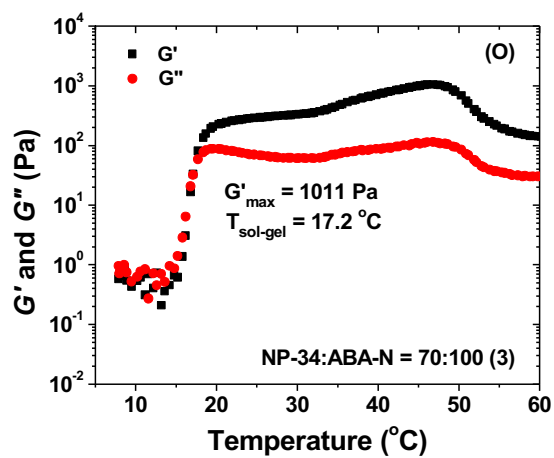
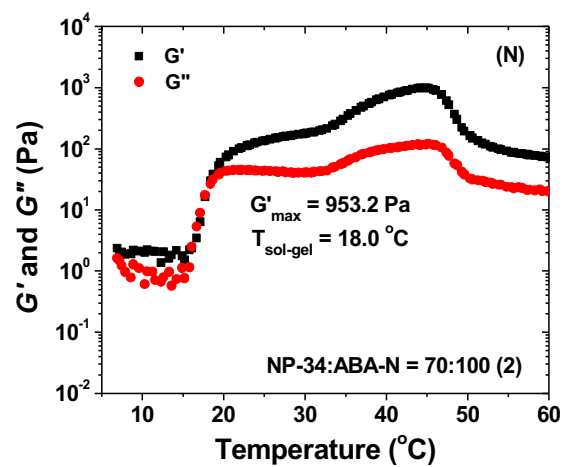
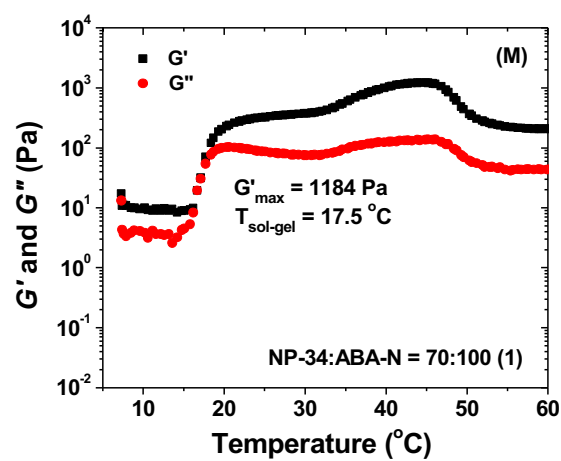


(Figure B13 continued)

Figure B14: Plots of dynamic storage modulus G' and loss modulus G'' of aqueous mixtures of ABA-N with a concentration of 10 wt% and NP-44 with various NP-to-polymer mass ratios versus temperature. The rheological data were collected from heating ramp experiments performed by using a frequency of 1 Hz, a strain amplitude of 1 %, and a heating rate of 3 °C/min. For each NP-to-ABA-N mass ratio, three rheological measurements were taken.

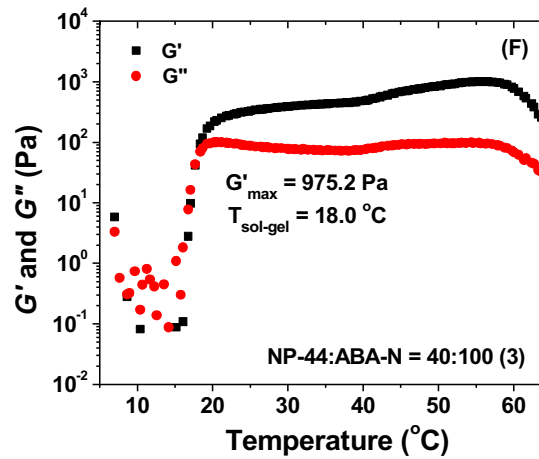
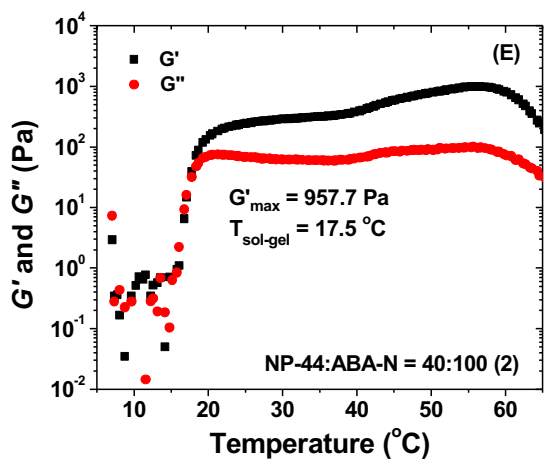
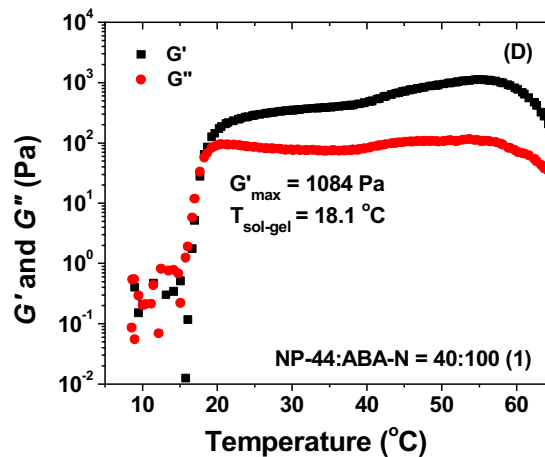
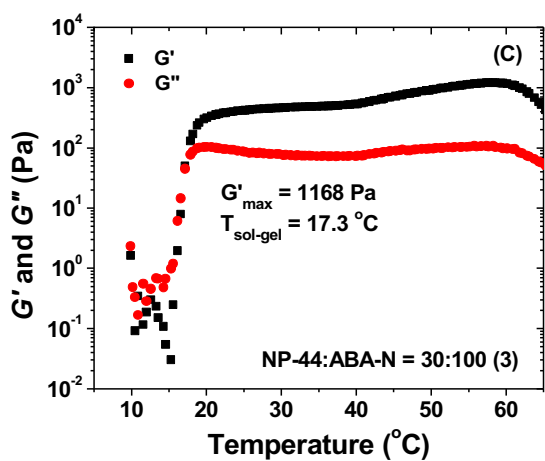
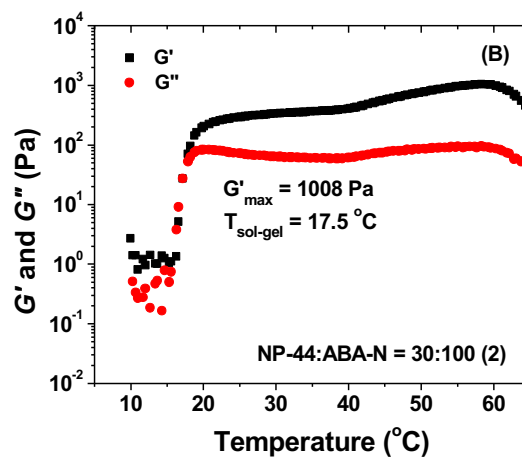
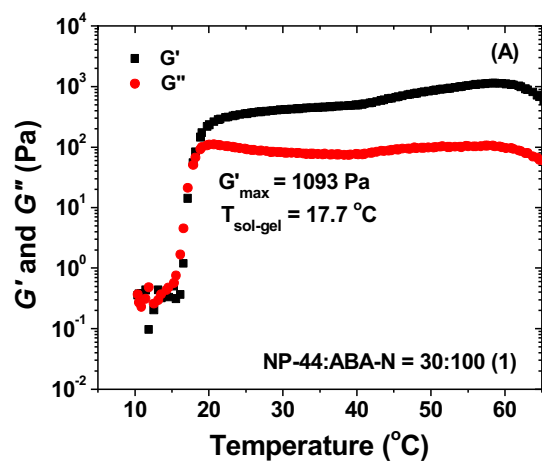


(Figure B14 continued)

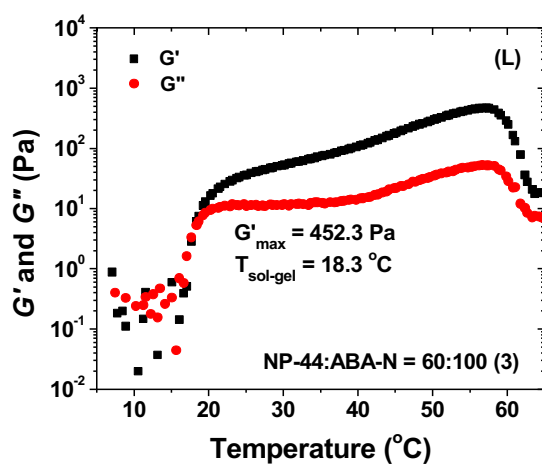
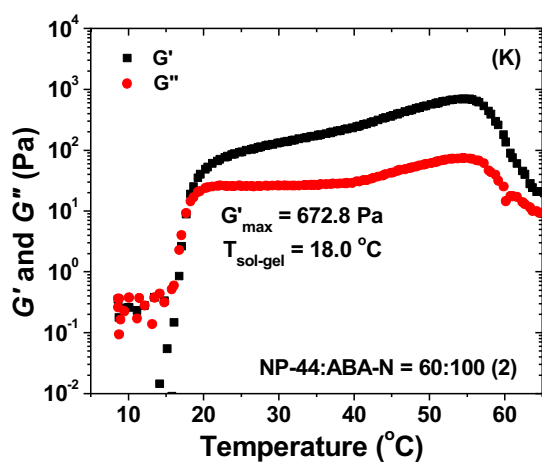
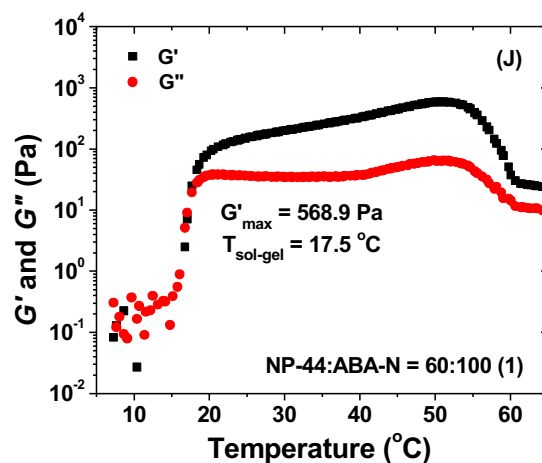
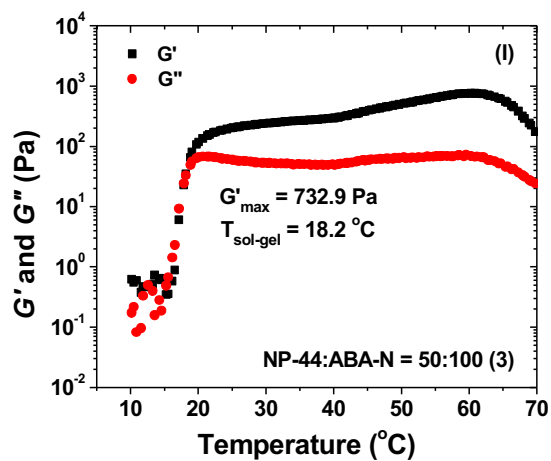
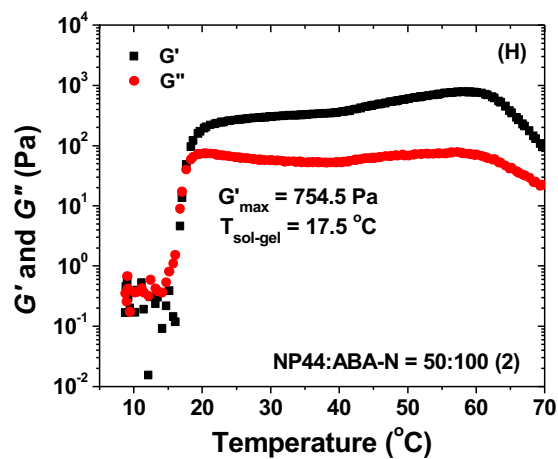
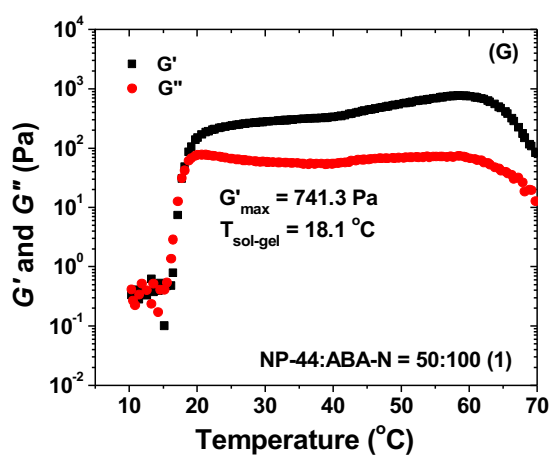


(Figure B14 continued)

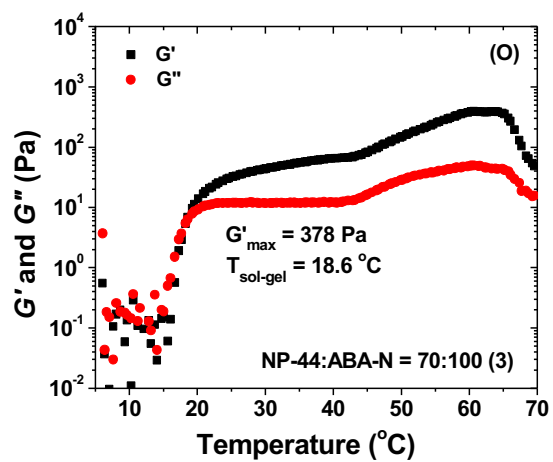
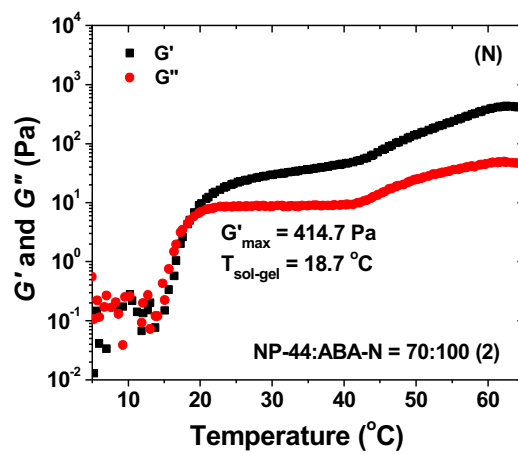
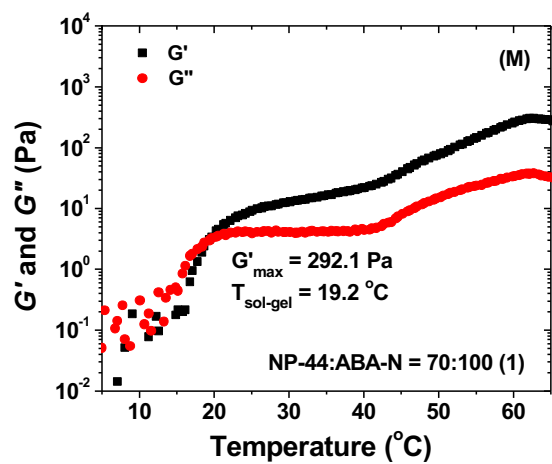


(Figure B14 continued)

Figure B15: Plots of dynamic storage modulus G' and loss modulus G'' of aqueous mixtures of ABA-N with a concentration of 10 wt% and NP-51 with various NP-to-polymer mass ratios versus temperature. The rheological data were collected from heating ramp experiments performed by using a frequency of 1 Hz, a strain amplitude of 1 %, and a heating rate of 3 °C/min. For each NP-to-ABA-N mass ratio, three rheological measurements were taken.

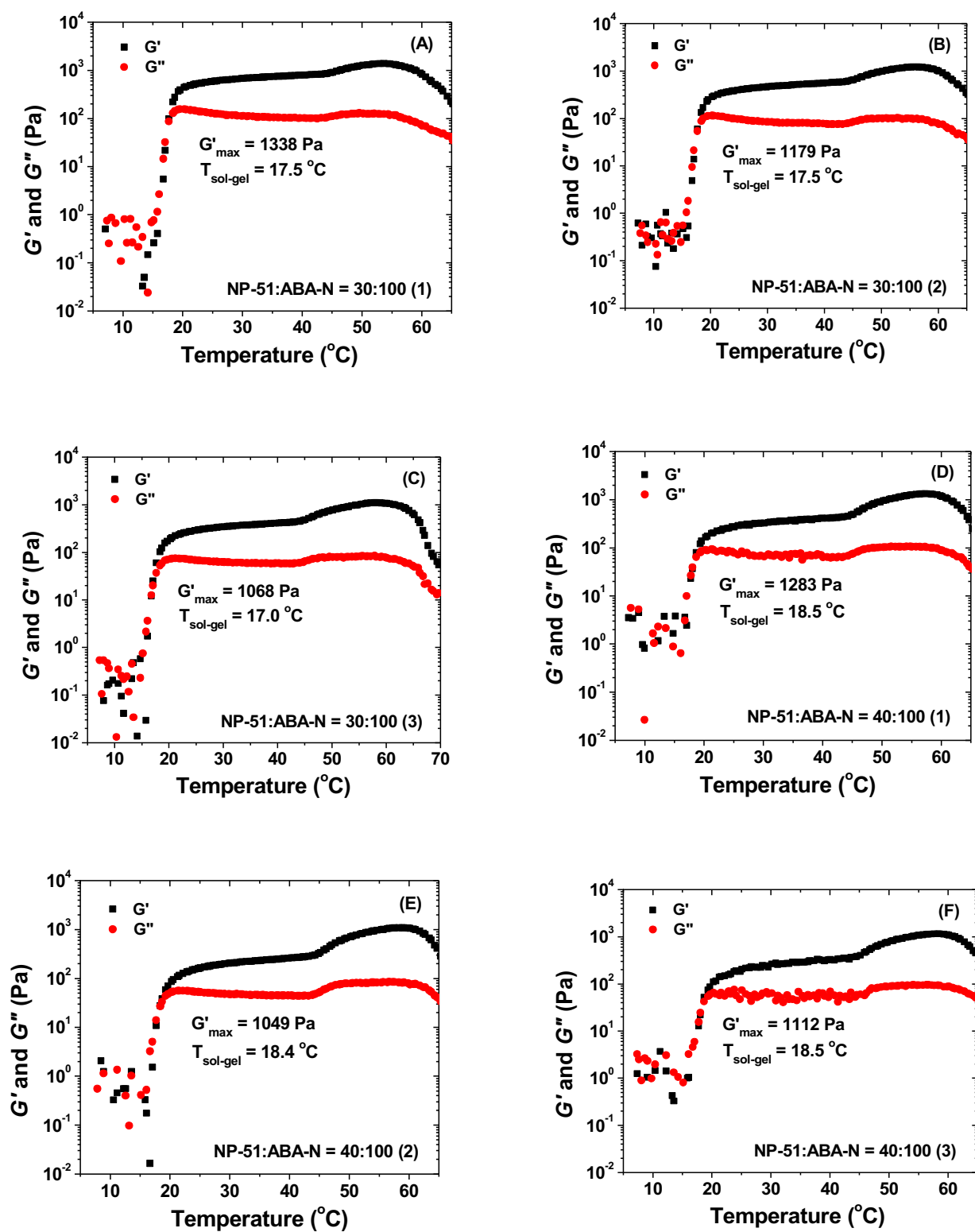


(Figure B15 continued)

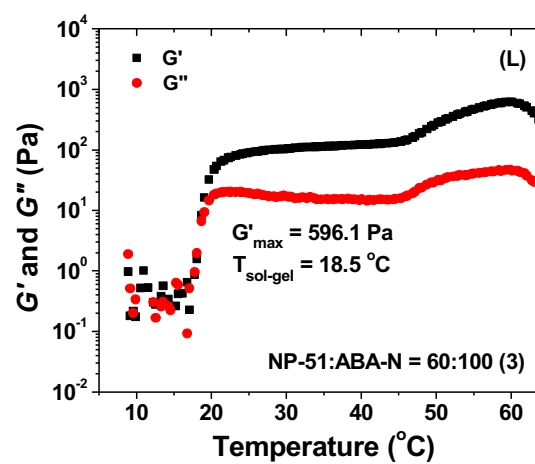
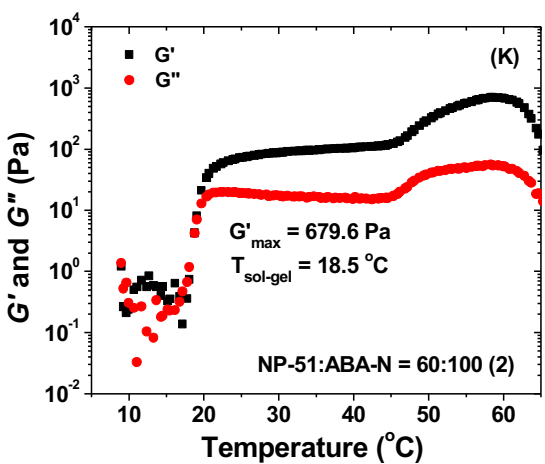
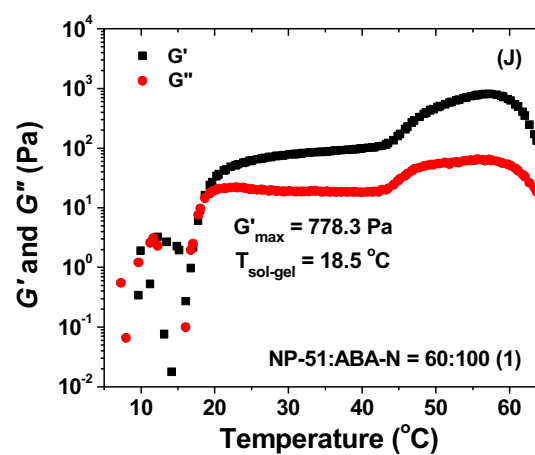
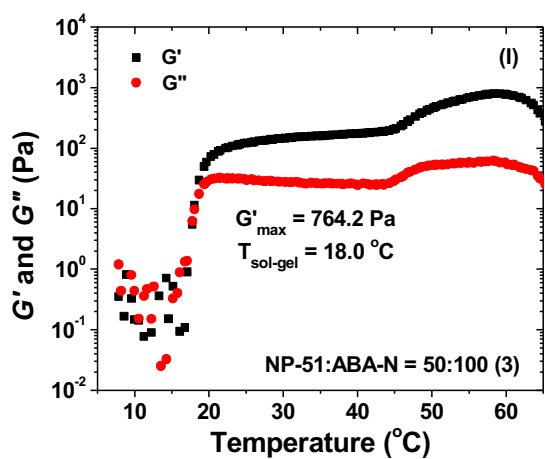
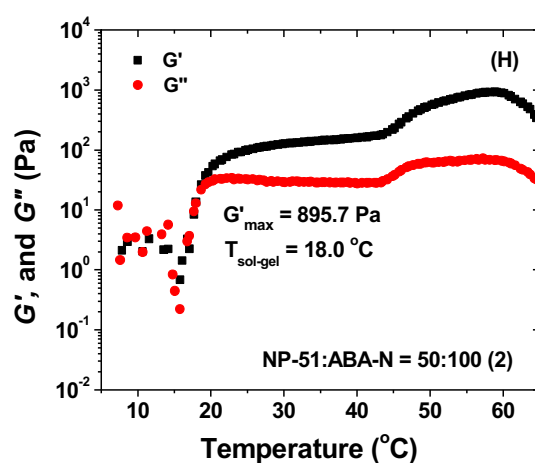
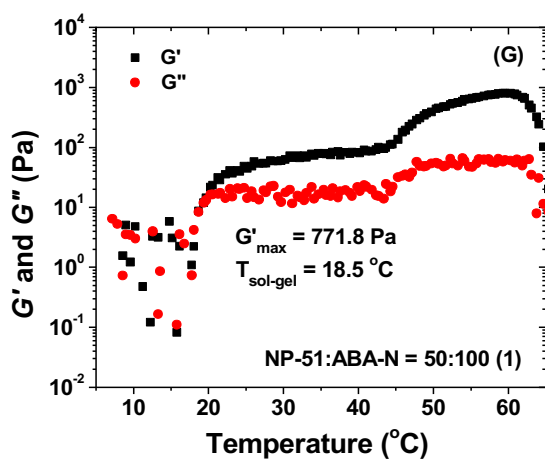


(Figure B15 continued)

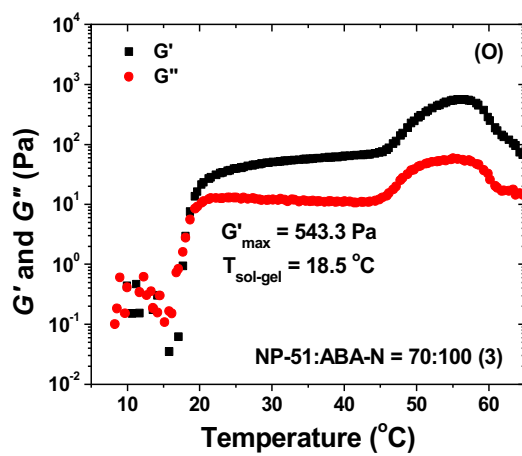
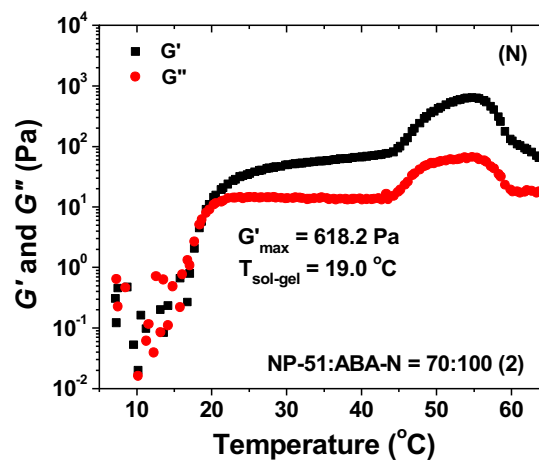
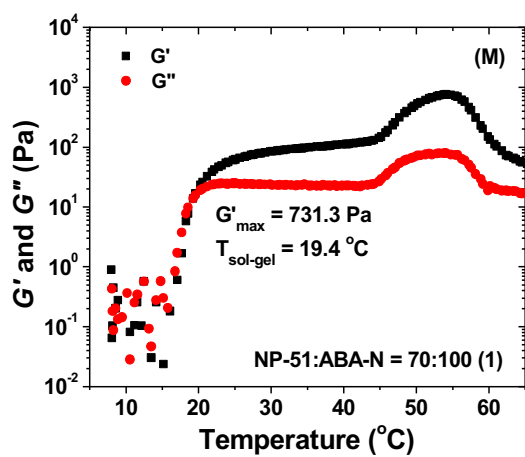


(Figure B15 continued)

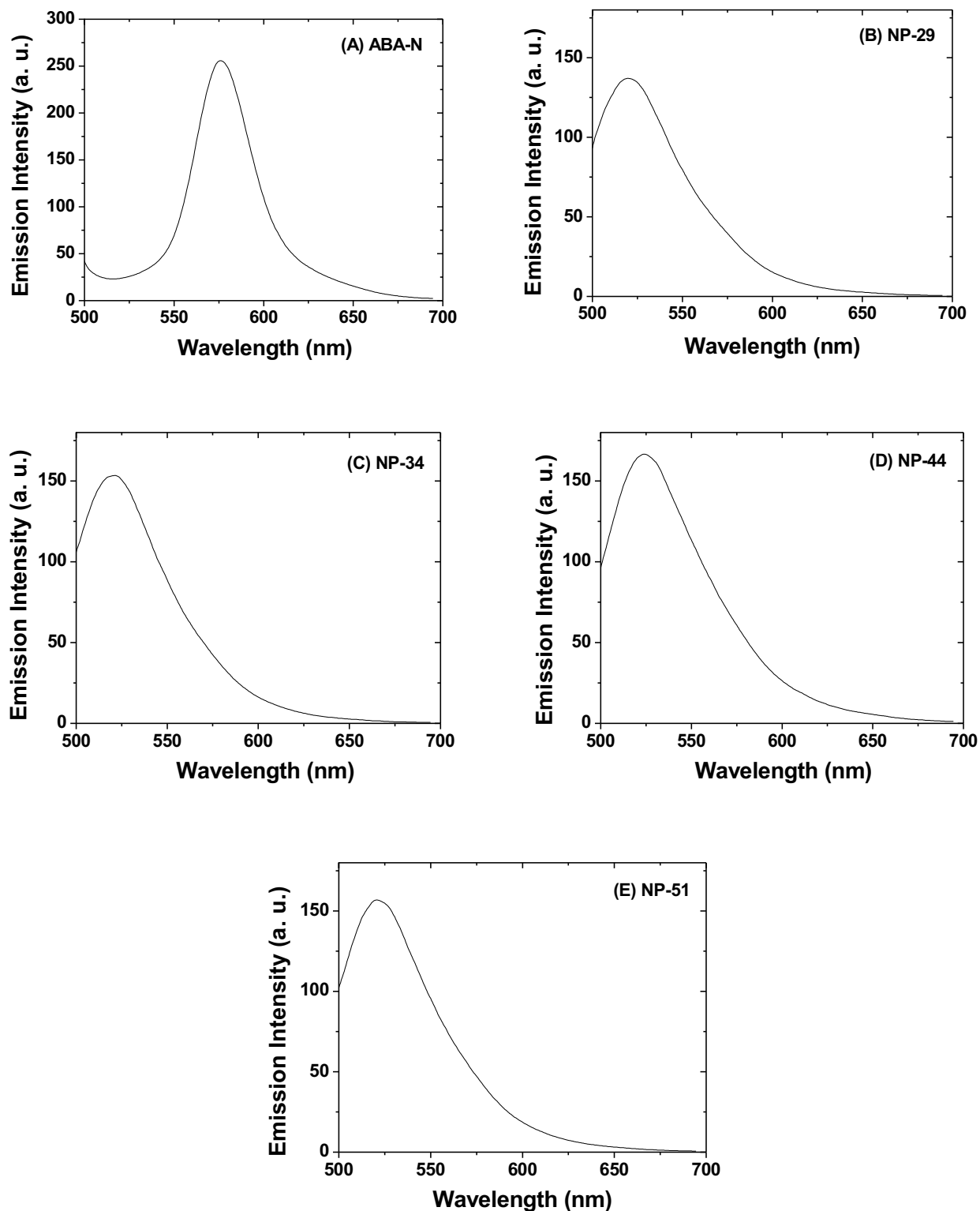


Figure B16. Fluorescence emission spectra at room temperature ($\sim 20^\circ\text{C}$) of an aqueous solution of (A) ABA-N with a concentration of 0.208 mg/g, (B) NP-29 with a concentration of 0.010 mg/g, (C) NP-34 with a concentration of 0.012 mg/g, (D) NP-44 with a concentration of 0.011 mg/g, (E) NP-51 with a concentration of 0.012 mg/g.

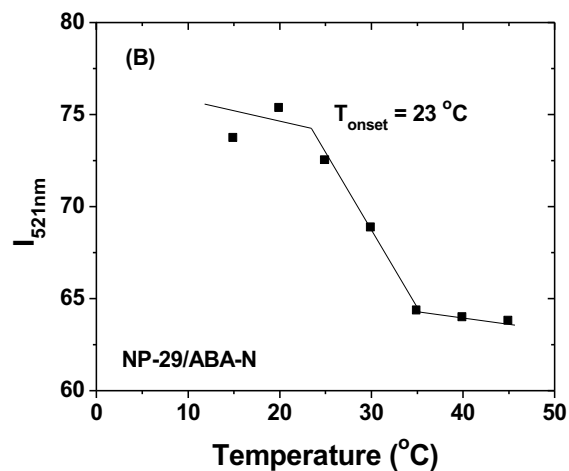
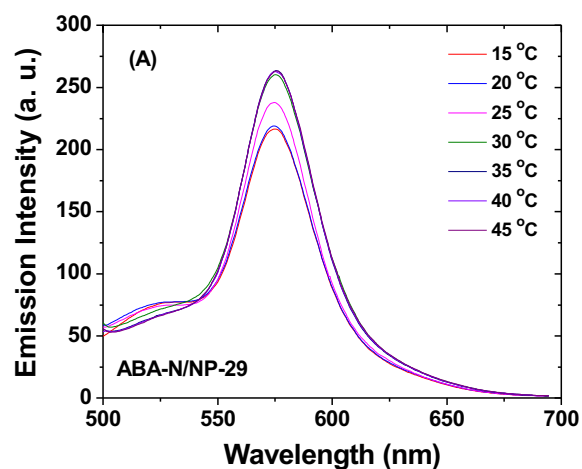


Figure B17. (A) Fluorescence emission spectra of an aqueous solution of ABA-N with a concentration of 0.208 mg/g and NP-29 with a concentration of 0.010 mg/g at various temperatures. (B) Plot of fluorescence emission intensity at 521 nm versus temperature.

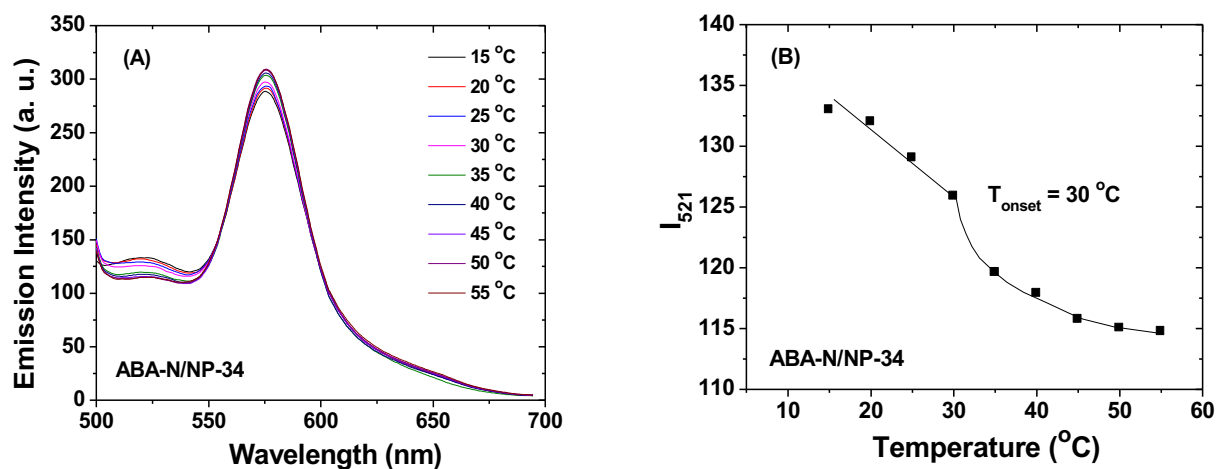


Figure B18. (A) Fluorescence spectra of an aqueous solution of ABA-N with a concentration of 0.208 mg/g and NP-34 with a concentration of 0.011 mg/g at various temperatures. (B) Plot of fluorescence emission intensity at 521 nm (I_{521}) versus temperature.

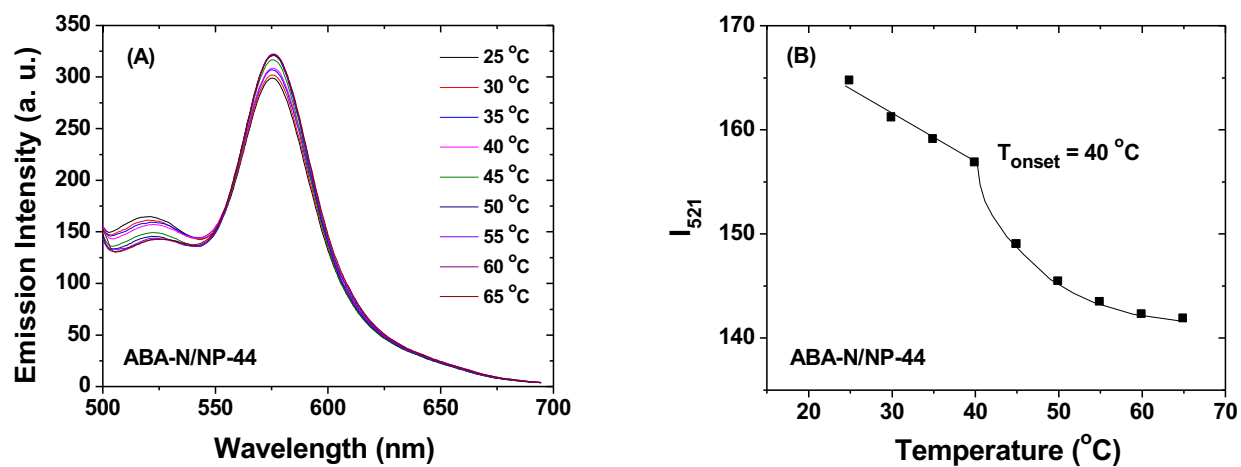


Figure B19. (A) Fluorescence emission spectra of an aqueous solution of ABA-N with a concentration of 0.206 mg/g and NP-44 with a concentration of 0.010 mg/g at various temperatures. (B) Plot of fluorescence emission intensity at 521 nm (I_{521}) versus temperature.

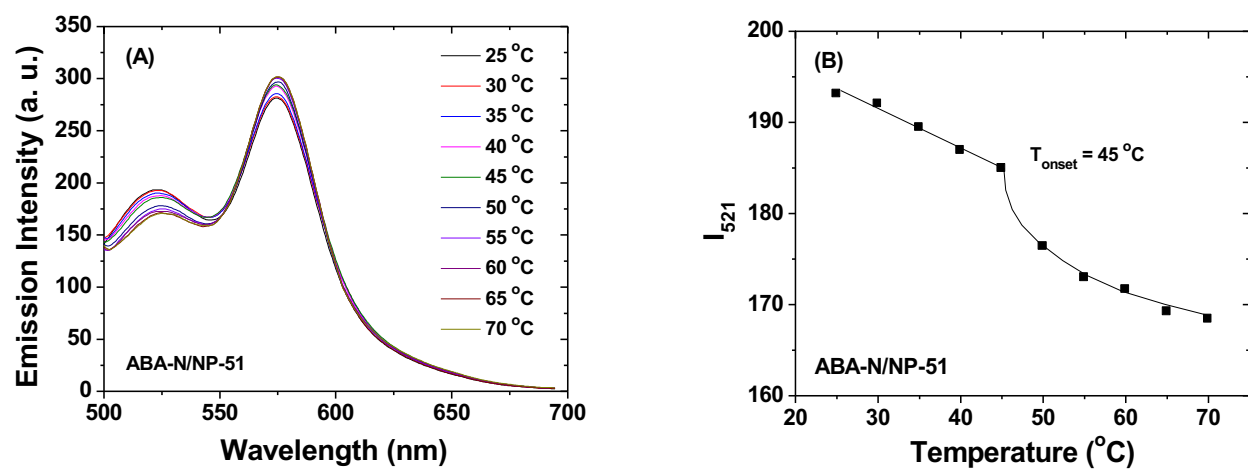


Figure B20. (A) Fluorescence emission spectra of an aqueous solution of ABA-N with a concentration of 0.205 mg/g and NP-51 with a concentration of 0.013 mg/g at various temperatures. (B) Plot of fluorescence emission intensity at 521 nm (I_{521}) versus temperature.

**Chapter 4. Enhancing Gelation Efficiency of A Doubly Thermosensitive
Hydrophilic Linear ABC Triblock Copolymer in Water by Thermoresponsive
Hairy Nanoparticles**

Abstract

This chapter describes a method to enhance the gelation efficiency of a doubly thermosensitive hydrophilic linear ABC triblock copolymer in water using thermoresponsive polymer brush-grafted nanoparticles (hairy NPs) with an appropriate lower critical solution temperature (LCST). A linear ABC triblock copolymer (ABC-Q) composed of a permanently hydrophilic, charged central block and two thermosensitive outer blocks with different LCSTs, $LCST_L$ (lower LCST) and $LCST_H$ (higher LCST), and two thermoresponsive hairy silica NPs with different LCSTs were synthesized. When the temperature was raised to above $LCST_L$, ABC-Q self-assembled into micelles with the lower LCST block forming the core; further increasing temperature to above $LCST_H$ triggered the collapse of the higher LCST block, producing 3-dimensional micellar network hydrogels. Rheological studies showed that adding thermoresponsive hairy NPs with a LCST similar to $LCST_H$ led to a significant increase in dynamic storage modulus (G'). The maximum value of G' (G'_{max}) increased with increasing amount of hairy NPs; for hybrid hydrogels formed from 6 wt % aqueous solutions of ABC-Q with hairy NPs, a 45% increase in G'_{max} was observed at the NP-to-polymer ratio of 60 : 100 compared with the sample with no NPs. Correspondingly, the calculated fraction of bridging chains increased from 65.0 % for the pure 6 wt% polymer sample to 94.6 % at the ratio of 60 : 100. This is because the hairy NPs with a LCST similar to the $LCST_H$ of ABC-Q can act as “seeds” to adsorb the collapsed higher LCST block of ABC-Q, promoting the formation of bridges among micellar cores and thus enhancing the gelation. In contrast, no benefit was observed when adding hairy NPs with a LCST significantly higher than $LCST_H$ of ABC-Q; the G'_{max} exhibited little change with increasing NP-to-polymer mass ratio. The observations from rheological measurements were supported by the results from fluorescence resonance energy transfer studies.

4.1. Introduction

Micellar hydrogels of thermosensitive hydrophilic block copolymers have been intensively studied in the past years.¹⁻⁵ Due to the thermoresponsive properties, the physical hydrogels made from these block copolymers can exhibit reversible sol-gel transitions in response to temperature changes. They have great potential in a variety of applications, such as controlled release of drugs and tissue engineering.⁶⁻⁸ In general, there are two types of stimuli-responsive block copolymer hydrogels: (i) hydrogels formed by packing of discrete micelles of, e.g., thermosensitive diblock copolymers and poly(ethylene oxide)-*b*-poly(propylene oxide)-*b*-poly(ethylene oxide) (PEO-*b*-PPO-*b*-PEO),^{2, 9-10} and (ii) physically crosslinked, 3-dimensional network hydrogels where micellar cores are linked by bridging chains.¹¹⁻¹⁵

ABA triblock copolymers composed of a permanently hydrophilic middle block and two thermosensitive outer blocks can self-assemble into 3-D network hydrogels when the polymer concentration is above the critical gelation concentration (CGC) and the temperature is above the lower critical solution temperature (LCST) of the outer blocks. The physically crosslinked ABA triblock copolymer hydrogels are often preferred over the first type of packing-based micellar hydrogels because the CGC can be significantly lower. For example, our group previously reported a doubly responsive ABA triblock copolymer with a CGC of < 5 wt%, while the CGC for thermosensitive hydrophilic diblock copolymers is usually around 20 wt%.¹⁶⁻¹⁷ However, during the network self-assembly of thermosensitive ABA triblock copolymers in water, the two outer blocks from the same block copolymer molecules could be assembled into the same hydrophobic core, i.e., loops are formed.¹⁸⁻¹⁹ It is known that loops do not contribute to the elastic property of the network and decrease the moduli of the hydrogels.

It should be noted here that the temperature-induced micellization and gelation of thermosensitive hydrophilic ABA triblock copolymers in water occur simultaneously, which has been considered as one reason that a significant portion of block copolymer molecules form loops in the gelation. This has prompted the investigation of thermoresponsive ABC linear triblock copolymers as gelators, where the micellization and gelation can be separate, stepwise processes.²⁰⁻

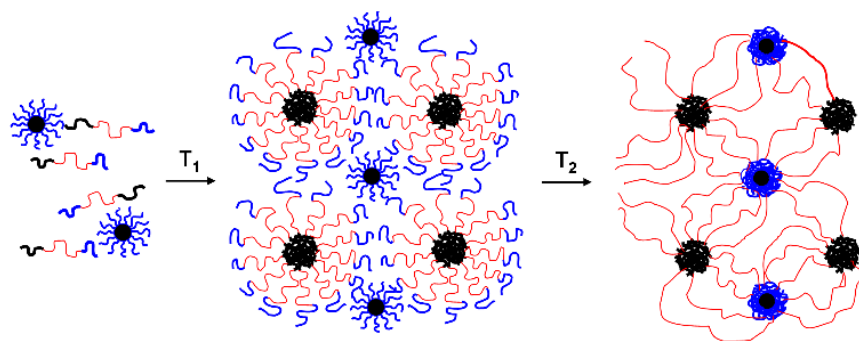
²⁵ Armes and coworkers synthesized doubly thermosensitive ABC linear triblock copolymers with different LCSTs for the outer blocks.²⁰ They found that these triblock copolymers were rather inefficient gelators with a minimum concentration of 20 wt% for gelation; the gelation efficiency was even worse than that of ABA triblock copolymers. They attributed the inefficient gelation of ABC triblock copolymers in water to the separation of micellar self-assembly from gel network formation; the intramicellar collapse of the outer block occurs prior to the development of the intermicellar hydrophobic interactions. Later, Zhou et al. used thermosensitive amphiphilic ABC linear triblock copolymers composed of a hydrophobic A block, a hydrophilic PEO block, and a thermosensitive poly(*N*-isopropylacrylamide) (PNIPAM) block to make multi-compartment hydrogels.^{21, 23} The triblock copolymer self-assembled to form spherical micelles at room temperature, and upon heating above the LCST of the PNIPAM block, the polymer micellar aqueous solutions turned into two-compartment micellar hydrogels, which were confirmed by cryo-TEM study. A free-standing hydrogel can be formed at a concentration of 5 wt%, indicating that these ABC triblock copolymers are good gelators, different from what Armes et al. reported. Reinicke et al. prepared hybrid micelles of ABC triblock copolymers with the C block being thermoresponsive and maghemite nanoparticles (NPs) in water by exploiting the electrostatic interaction between the charged NPs and the oppositely charged A block of the ABC triblock copolymer.²⁶ At a sufficiently high concentration, the aqueous solutions of such hybrid micelles

exhibited reversible sol-gel transitions upon magnetic inductive heating. Note that here the magnetic NPs were already located in the core of micelles before the gelation caused by the collapse of the thermosensitive C block.

We previously studied hybrid micellar network hydrogels of thermosensitive ABA triblock copolymers and thermoresponsive polymer brush-grafted nanoparticles (hairy NPs).²⁷⁻²⁸ We found that when the LCST of hairy NPs was similar to that of the outer blocks of the ABA copolymer, co-micellization occurred and the hairy NPs were located in the core of micelles; the rheological properties of micellar hydrogels were not affected much by the incorporation of hairy NPs. Differently, when the LCST was significantly higher than that of the ABA, the hairy NPs were located in the interstitial space of micelles. The dynamic storage modulus G' decreased significantly with the increase of the NP-to-polymer mass ratio, suggesting that the incorporation of higher LCST hairy NPs adversely affected the formation of 3-D network hydrogels and promoted the formation of polymers loops.

Here we reported a method to improve the gelation efficiency of a doubly thermosensitive hydrophilic ABC triblock copolymer with different LCSTs for the two outer blocks by using thermoresponsive hairy NPs with an appropriate LCST transition temperature. Our hypothesis is that hairy NPs with a LCST similar to that of the higher LCST block of the ABC copolymer could act as “seeds” to promote physical crosslinking by adsorbing the collapsed thermosensitive C blocks and thus reduce the formation of loops (Scheme 4.1). As such, the gelation efficiency is enhanced, making the formed 3-D network hydrogels stronger via the two-compartment micellar network mechanism.

The doubly thermosensitive hydrophilic ABC triblock copolymer is PDEGEMA-*b*-P(TMAEMA-I)-*b*-(PDEGMMA-*co*-RhBMA) (ABC-Q), which was synthesized by reversible



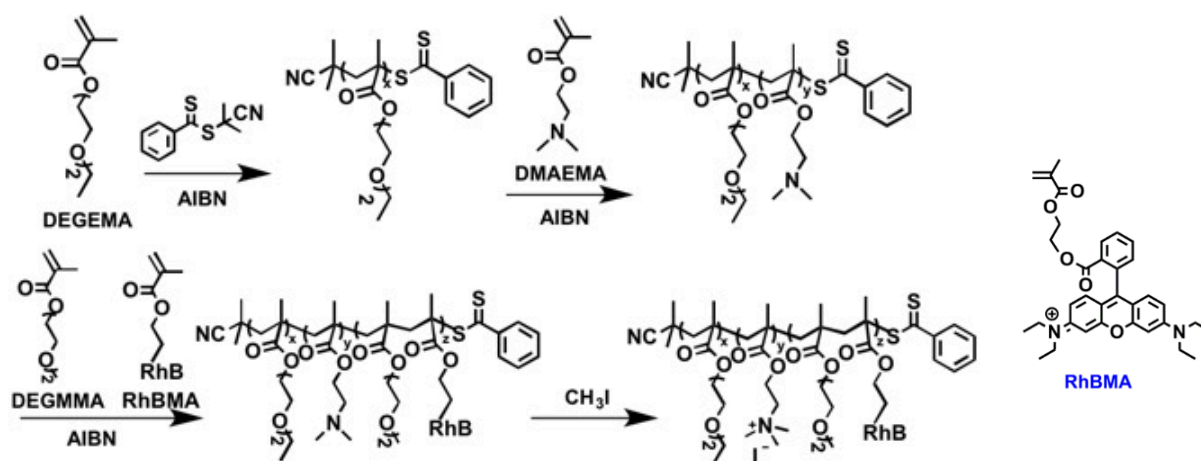
Scheme 4.1. Schematic Illustration of the Formation of a 3-D Network Hydrogel by ABC Triblock Copolymer Composed of a Lower LCST A Block, a Permanently Hydrophilic B Block, and a Higher LCST C Block in the Presence of Hairy NPs with a LCST Similar to that of the Thermosensitive C Block of the ABC Triblock Copolymer

addition-fragmentation chain transfer (RAFT) polymerization and subsequent post-polymerization modification (Scheme 4.2). Note that PDEGEMA and PDEGMMA exhibit a cloud point in water at 4 and 26 °C, respectively, according to the literature.²⁹⁻³⁰ Two batches of thermosensitive hairy NPs with different LCST transitions were prepared by surface-initiated atom transfer radical polymerization (SI-ATRP, Scheme 4.3); one batch (NP-29.5) had a LCST transition similar to that of the P(DEGMMA-*co*-RhBMA) block of ABC-Q and another one had a significantly higher LCST (NP-51). To study the interactions between thermosensitive ABC triblock copolymer micelles and hairy NPs, fluorescence energy resonance transfer (FRET) was employed.^{27-28, 31} We copolymerized NBDMA, a FRET donor, into the thermoresponsive polymer brushes of hairy NPs, and incorporated RhBMA, a FRET acceptor, into the PDEGMMA block of the ABC triblock copolymer (Schemes 4.2 and 4.3). Rheological measurements were employed to study the effect of incorporating hairy NPs into the hydrogels of ABC-Q at various NP-to-polymer mass ratios.

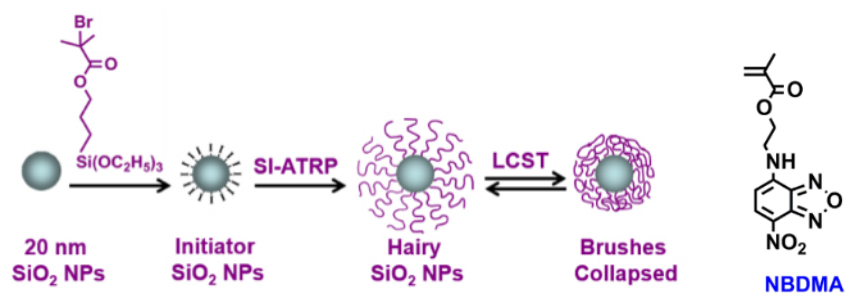
4.2. Experimental Section

4.2.1. Materials

MIBK-ST (a 30-31 wt% dispersion of SiO₂ nanoparticles in methyl isobutyl ketone) was donated by Nissan Chemical as a gift; according to the website of Nissan Chemical, the size of silica NPs in this dispersion is 10-15 nm. Triethoxysilane (95%) and iodomethane (stabilized, 99%) were purchased from Acros Organics and used as received. The platinum-divinyltetramethyldisiloxane complex in xylene (2.1-2.4% platinum, Gelest, Inc.) was used as received. CuBr (98%, Aldrich) was purified according to a procedure described in the literature.³² *N,N,N',N',N''*-Pentamethyldiethylenetriamine (PMDETA, 99%, Aldrich), ethyl 2-



Scheme 4.2. Synthesis of Doubly Thermosensitive ABC Linear Triblock Copolymer PDEGEMA-*b*-P(TMAEMA-I)-*b*-P(DEGMMA-co-RhBMA) by Reversible Addition-Fragmentation Chain Transfer (RAFT) Polymerization and Subsequent Quaternization, and Molecular Structure of RhBMA



Scheme 4.3. Synthesis of Thermoresponsive Hairy Nanoparticles by Surface-Initiated Atom Transfer Radical Polymerization (SI-ATRP) from Initiator Functionalized, 20 nm Silica Nanoparticles (NP) and Molecular Structure of NBDMA

2-bromoisobutyrate (EBiB, 98%, Aldrich), di(ethylene glycol) methyl ether methacrylate (DEGMMA, 97%, TCI America), and 2-(dimethylamino)ethyl methacrylate (DMAEMA, 98.5%, TCI America) were each stirred with CaH_2 , distilled under reduced pressure, and stored in a refrigerator. Di(ethylene glycol) ethyl ether methacrylate (DEGEMA), tri(ethylene glycol) methyl ether methacrylate (TEGMMA), rhodamine B-containing methacrylate (RhBMA, Scheme 4.2) and NBD-containing methacrylate (NBDMA, Scheme 4.3) were synthesized according to the procedures in the literature.^{15, 27, 33-34} 2-(2-Cyanopropyl)dithiobenzoate (CPDB) was made according to a slightly modified literature procedure,³⁵ and the molecular structure was verified by ^1H NMR spectroscopy. All other chemical reagents were purchased from either Fisher Scientific/Acros or Aldrich and used without further purification unless otherwise noted.

4.2.2. General Characterization

NMR spectra were recorded on a Varian Mercury 300 NMR spectrometer or a Varian VNMRs 500 MHz spectrometer, and the residual solvent proton signal was used as the reference peak. Size exclusion chromatography (SEC) of the PDEGEMA macro CTA, PDEGEMA-*b*-PDMAEMA macro-CTA, ABC triblock copolymer (before quaternization), and the free polymers formed in the synthesis of hairy NPs was carried out at room temperature using PL-GPC 20 (Polymer Laboratories, Inc.) equipped with a refractive index detector, one PLgel 5 μm guard column (50×7.5 mm), and two PLgel 5 μm mixed-C columns (each 300×7.5 mm, linear range of molecular weight from 200 to 2 000 000 Da). THF was used as the solvent and the flow rate was 1.0 mL/min; the SEC system was calibrated with narrow-dispersed polystyrene standards. The SEC data were processed using Cirrus GPC/SEC software (Polymer Laboratories, Inc.). Thermogravimetric analysis (TGA) of hairy silica nanoparticles was performed in air at a heating rate of 20 $^\circ\text{C}/\text{min}$ from room temperature to 800 $^\circ\text{C}$ using a TA Discovery TGA-MS.

4.2.3. Synthesis of Doubly Thermosensitive ABC Triblock Copolymer PDEGEMA-*b*-PDMAEMA-*b*-P(DEGMMA-*co*-RhBMA)

DEGEMA (3.273 g, 16.2 mmol), 2-(2-cyanopropyl)dithiobenzoate (CPDB, 22.2 mg, 0.100 mmol), 2,2'-azobis(2-methylpropionitrile) (AIBN, 0.145 g of a solution of AIBN in anisole with a concentration of 1.34 wt %, 0.012 mmol), and anisole (3.053 g) were added into a 25 mL two-necked round-bottom flask. The mixture was degassed by three freeze-pump-thaw cycles and then the flask was immersed in a 70 °C oil bath. ¹H NMR spectroscopy and SEC were used to follow the progress of the RAFT polymerization. The flask was removed from the oil bath after 4 h and 55 min, and a sample was taken immediately for the determination of the monomer conversion by ¹H NMR spectroscopy analysis. The polymerization mixture was diluted with THF (~5 mL) and then precipitated in hexane and diethyl ether (9:1, v/v) three times. The polymer was dried under high vacuum and analyzed by ¹H NMR spectroscopy to ensure that the monomer and solvents were completely removed. SEC analysis results (relative to polystyrene standards): $M_{n,SEC} = 14.1$ kDa; polydispersity index (PDI): 1.15. The degree of polymerization (DP) was 75, calculated from the monomer conversion and the molar ratio of monomer to RAFT chain transfer agent (CTA).

The obtained PDEGEMA macro-CTA ($M_{n,SEC} = 14.1$ kDa, 0.534 g), AIBN (0.085 g of a solution of AIBN in anisole with a concentration of 1.34 %, 0.0069 mmol), DMAEMA (3.208 g, 20.4 mmol), and toluene (5.987 g) were added into a 50 mL two-necked flask. The mixture was stirred under a nitrogen atmosphere to dissolve the polymer. After the solution was degassed by three freeze-pump-thaw cycles, the flask was placed into an oil bath with a preset temperature of 70 °C. The polymerization was monitored by SEC. After 22 h, the flask was removed from the oil bath, and the mixture was diluted with THF and precipitated in a mixture of hexanes and ethyl

ether (8:2, v/v) three times. The purified diblock copolymer was dried under high vacuum, and analyzed by ^1H NMR spectroscopy and SEC. SEC results: $M_{n,\text{SEC}} = 66.6$ kDa; PDI = 1.19.

The obtained PDEGEMA-*b*-PDMAEMA macro-CTA ($M_{n,\text{SEC}} = 66.6$ kDa, 1.492 g), AIBN (0.056 g of a solution of AIBN in anisole with a concentration of 1.34 %, 0.0046 mmol), DEGMMA (2.086 g, 11.1 mmol), RhBMA (3.7 mg, 6.7 μmol), and toluene (5.719 g) were added into a 50 mL two-necked flask. The mixture was stirred under a nitrogen atmosphere to dissolve the polymer. After the solution was degassed by three freeze-pump-thaw cycles, the flask was placed into an oil bath with a preset temperature of 70 °C. The polymerization was monitored by SEC. After 5 h 40 min, the molecular weight of the triblock copolymer was found to reach the desired value. The flask was removed from the oil bath, and the mixture was diluted with THF. The reaction mixture was precipitated three times in a mixture of hexanes and ethyl ether (8 : 2, v/v), and the polymer was dried under high vacuum. The obtained ABC triblock copolymer was analyzed by ^1H NMR spectroscopy and SEC. SEC results: $M_{n,\text{SEC}} = 84.5$ kDa; PDI = 1.31.

4.2.4. Quaternization Reaction of PDEGEMA-*b*-PDMAEMA-*b*-P(DEGMMA-*co*-RhBMA) with CH_3I to Yield PDEGEMA-*b*-poly(2-(methacryloyloxy)ethyltrimethylammonium iodide)-*b*-P(DEGMMA-*co*-RhBMA) (PDEGEMA-*b*-P(TMAEMA-I)-*b*-P(DEGMMA-*co*-RhBMA), ABC-Q)

Iodomethane (CH_3I) was used for the quaternization of DMAEMA units of ABC triblock copolymer PDEGEMA-*b*-PDMAEMA-*b*-P(DEGMMA-*co*-RhBMA), producing PDEGEMA-*b*-P(TMAEMA-I)-*b*-P(DEGMMA-*co*-RhBMA) with the middle block being charged and thus more hydrophilic.³⁶ PDEGEMA-*b*-PDMAEMA-*b*-P(DEGMMA-*co*-RhBMA) (0.995 g, 2.90 mmol DMAEMA units) was added into a 100 mL three-necked flask and dissolved in dry THF (25.4 g) under N_2 . The flask was then completely wrapped with aluminum foil to protect the reaction

mixture from exposure to light. CH₃I (2 mL) was added into the polymer solution, and the reaction mixture was stirred at ambient temperature overnight. The volatile components were then removed under high vacuum, yielding the quaternized polymer, ABC-Q, as a pale pink solid.

4.2.5. Synthesis of Thermosensitive Polymer Brush-Grafted Silica Nanoparticles

The P(DEGMMA-*co*-TEGMMA-*co*-NBDMA) hairy NPs (NP-29.5) was synthesized using the same procedure as described in Chapter 3.²⁸ Briefly, silica NPs (MIBK-ST, Nissan Chemical) were surface-functionalized with 3-(triethoxysilyl)propyl 2-bromo-2-methylpropanoate with ammonia as catalyst. The ATRP initiator-functionalized NPs were purified by multiple rounds of ultracentrifugation and re-dispersion, and finally dispersed in DMF to form an NP dispersion with a concentration of 16.3 wt% (determined by gravimetric analysis). To make NP-29.5, CuBr (19.6 mg, 137 μ mol), CuBr₂ (4.5 mg, 20.1 μ mol), the ATRP initiator-functionalized NPs in DMF (2.243 g solution, corresponding to 366 mg initiator NPs), and DMF (13.72 g) were added into a 50 mL two-necked flask. DEGMMA (2.833 g, 15.1 mmol), TEGMMA (1.497 g, 6.45 mmol), NBDMA (12.1 mg, 41.4 μ mol), ethyl 2-bromoisobutyrate (28.6 mg, 147 μ mol) and PMDETA (32.5 mg, 188 μ mol) were then added into the flask. After the mixture was degassed by three freeze-pump-thaw cycles, the flask was placed in a 45 °C oil bath, and the polymerization progress was monitored by ¹H NMR spectroscopy analysis. After 2 h and 5 min, the monomer conversion reached 42.5 %, and the flask was taken out from the oil bath and opened to air. The hairy NPs were purified by ultracentrifugation. The P(TEGMMA-*co*-tetra(ethylene glycol) methyl ether methacrylate) (PTEGMMA-*co*-TrEGMMA) brush-grafted silica NPs (NP-51) used in the present work was the same batch of hairy NPs from the previous work (NP-51);²⁸ the synthesis and characterization can be found in Chapter 3.

4.2.6. Dynamic Light Scattering Studies of LCST Transitions of Thermosensitive Hairy NPs NP-29.5 and PDEGEMA-*b*-P(TMAEMA-I)-*b*-P(DEGMMA-*co*-RhBMA) in Water

DLS studies of the LCST transitions in water of NP-29.5 at a concentration of 1.0 mg/g and PDEGEMA-*b*-P(TMAEMA-I)-*b*-P(DEGMMA-*co*-RhBMA) at a concentration of 2.0 mg/g were conducted using a Brookhaven Instruments BI-200SM goniometer equipped with a PCI BI-9000 AT digital correlator, a temperature controller, and a solid state laser (model 25-LHP-928-249, $\lambda = 633$ nm) at a scattering angle of 90° . The samples were filtered using Corning hydrophilic PTFE filters (0.45 μm pore size), and the DLS tubes were sealed with PE stoppers. The temperature was gradually increased, and at each selected temperature the solution was equilibrated for 20 min before the measurements were made. The DLS data were analyzed with a Laplace inversion program (CONTIN).

4.2.7. Fluorescence Spectroscopy Study of Aqueous Solutions of Thermosensitive Hairy NPs and PDEGEMA-*b*-P(TMAEMA-I)-*b*-P(DEGMMA-*co*-RhBMA)

A 0.414 mg/g aqueous solution of PDEGEMA-*b*-P(TMAEMA-I)-*b*-P(DEGMMA-*co*-RhBMA), a 0.013 mg/g aqueous dispersion of NP-29.5, a 0.011 mg/g aqueous dispersion of NP-51, an aqueous mixture of PDEGEMA-*b*-P(TMAEMA-I)-*b*-P(DEGMMA-*co*-RhBMA) with a concentration of 0.431 mg/g and NP-29.5 with a concentration of 0.013 mg/g, and an aqueous mixture of PDEGEMA-*b*-P(TMAEMA-I)-*b*-P(DEGMMA-*co*-RhBMA) with a concentration of 0.376 mg/g and NP-51 with a concentration of 0.012 mg/g were prepared. All the samples were kept in a refrigerator overnight. After being ultrasonicated in an ice/water bath for 15 min, the samples were heated to 15°C and kept at that temperature for 30 min. The samples were used immediately for fluorescence spectroscopy measurements. The samples were then heated to the

40 °C and maintained at that temperature for 30 min before the next fluorescence spectroscopy measurement.

To investigate the possibility of the formation of loops in the micelles of PDEGEMA-*b*-P(TMAEMA-I)-*b*-P(DEGMMA-*co*-RhBMA) at temperatures higher than the LCST of the P(DEGMMA-*co*-RhBMA) block, 4-chloro-7-nitro-2,1,3-benzoxadiazole (NBD-Cl) was loaded into the micelles in water as detailed below. A stock solution of NBD-Cl in acetone with a concentration of 0.049 mg/mL (10 µL) was added into an empty vial via a microsyringe, which was then dried under high vacuum for 5 h to remove the solvent. A 0.40 mg/g aqueous solution of PDEGEMA-*b*-P(TMAEMA-I)-*b*-P(DEGMMA-*co*-RhBMA) (2.009 g) was then transferred into the vial. The mixture was kept in a fridge overnight, and then equilibrated at 15 °C for 3 h to induce the formation of micelles. After the sample was further stirred at room temperature for 1 day, the fluorescence emission spectra of the sample at various temperatures were recorded.

All fluorescence spectroscopy studies were conducted on a PerkinElmer LS 55 luminescence spectrometer with the slit widths set at 10 nm for both excitation and emission and a scan speed of 100 nm/min. The excitation wavelength was 480 nm, and fluorescence emission spectra were collected from 500 to 700 nm.

4.2.8. Rheological Measurements

A typical procedure for the preparation of an aqueous mixture of ABC-Q and NP-29.5 is described below. The other hybrid samples with different NP-to-polymer mass ratios were prepared via similar procedures. ABC-Q was dried in a vial under high vacuum and weighed (314.3 mg), and water (4.925 g) was added into the vial. The sample was stored in a refrigerator overnight and then ultrasonicated in an ice/water bath for about 15 min to ensure the mixture was homogeneous with a polymer concentration of 6 wt %. After the rheological measurement was

taken, an aqueous solution of NP-29.5 with a concentration of 8.925 mg/g (2.629 g) was added into 1.955 g of the 6 wt % polymer solution to obtain the NP-to-polymer weight ratio of 20 : 100. For the aqueous mixtures of ABC-Q and NP-29.5, the polymer concentration was defined as $[\text{polymer mass}/(\text{polymer mass} + \text{water mass})] \times 100\%$. The mixture was ultrasonicated in ice/water bath for 15 min, and then a gentle air stream was used to evaporate water to keep the polymer concentration at 6 wt %, followed by the rheological experiment. A similar procedure was employed to increase the NP-to-polymer ratio to 30 : 100, 40 : 100, 50 : 100, and 60 : 100.

Rheological experiments were performed using a rheometer from TA Instruments (Model TA AR 2000ex) in a cone-plate geometry with a cone diameter of 20 mm and an angle of 2° (truncation 52 μm). The temperature was controlled by the bottom Peltier plate. For each rheological measurement, a micropipette was used to load 90 μL of the sample onto the plate. To minimize water evaporation during rheological study, the solvent trap was filled with water, and a solvent trap cover was used. Dynamic storage modulus G' and loss modulus G'' of a sample at various temperatures were measured by oscillatory shear experiments performed at a fixed frequency of 1 Hz in a heating ramp at a heating rate of 3 $^\circ\text{C}/\text{min}$. A strain amplitude of $\gamma = 1.0\%$ was used in all dynamic viscoelastic measurements. For each rheology study, three measurements were taken and the average value was used.

4.3. Results

4.3.1. Synthesis and Thermoresponsive Properties of ABC Triblock Copolymer P(DEGEMA)-*b*-P(TMAEMA-I)-*b*-P(DEGMMA-co-RhBMA)

The precursor ABC triblock copolymer, PDEGEMA-*b*-PDMAEMA-*b*-P(DEGMMA-co-RhBMA), was prepared by a sequential, three-step reversible addition-fragmentation chain

transfer (RAFT) polymerization process (Scheme 4.2). The synthesis of the first block PDEGEMA was carried out in anisole at 70 °C using 2-(2-cyanopropyl)dithiobenzoate (CPDB) as chain transfer agent (CTA) and AIBN as initiator; the molar ratios of DEGEMA : CTA : AIBN were 162 : 1 : 0.12. After the monomer conversion reached 46.3%, corresponding to a degree of polymerization (DP) of 75, the polymerization was stopped. SEC analysis showed that the obtained polymer had a unimodal peak with the $M_{n,SEC}$ of 14.1 kDa and PDI of 1.15 relative to polystyrene standards (Figure 4.1). The obtained PDEGEMA was then used as macro-CTA to grow the second block PDMAEMA in toluene at 70 °C with the DMAEMA-to-macro-CTA molar ratio of 539 : 1, yielding PDEGEMA-*b*-PDMAEMA with the $M_{n,SEC}$ of 66.6 kDa and PDI of 1.19. Based on the DP = 75 of the first block PDEGEMA, we calculated the block length of the second block PDMAEMA from the 1H NMR spectrum of the purified and dried polymer. The DP of the middle block PDMAEMA was found to be 345, obtained by using the integrals of the peak at 1.22 ppm from $-CH_2CH_3$ of PDEGEMA and the peak at 2.56 ppm from $-OCH_2CH_2N(CH_3)_2$ of PDMAEMA (Figure 4.2A). The PDEGEMA-*b*-PDMAEMA-*b*-P(DEGMMA-*co*-RhBMA) was then synthesized using the diblock copolymer as macro-CTA to polymerize DEGMMA with a small amount of RhBMA in the molar ratio of 1 : 6.3×10^{-4} . From the SEC analysis, the unimodal peak shifted to the high molecular weight side and remained relatively narrow (Figure 4.1), and the values of $M_{n,SEC}$ and PDI were 84.5 kDa and 1.31, respectively. The DP of the third PDEGMMA block was calculated to be 142 using the integrals of the peak at 1.22 ppm from the $-CH_2CH_3$ of PDEGEMA and the peak at 3.40 ppm from $-OCH_3$ group of PDEGMMA (Figure 4.2B).

It is known that PDMAEMA is a thermo- and pH-responsive polymer. To make the middle block permanently hydrophilic, we converted it to P(TMAEMA-I) by reacting the ABC triblock

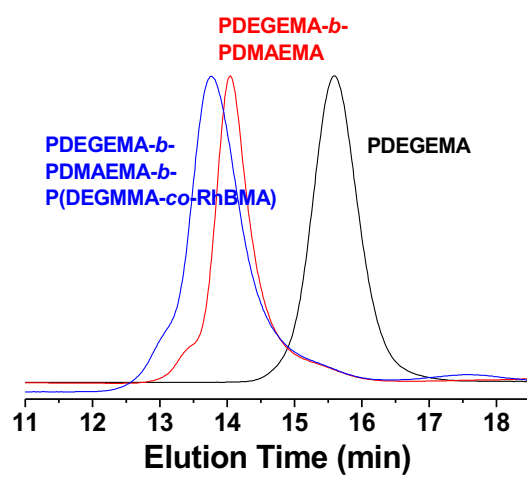


Figure 4.1. Size exclusion chromatography traces of PDEGEMA, PDEGEMA-*b*-PDMAEMA, and PDEGEMA-*b*-PDMAEMA-*b*-P(DEGMMA-*co*-RhBMA).

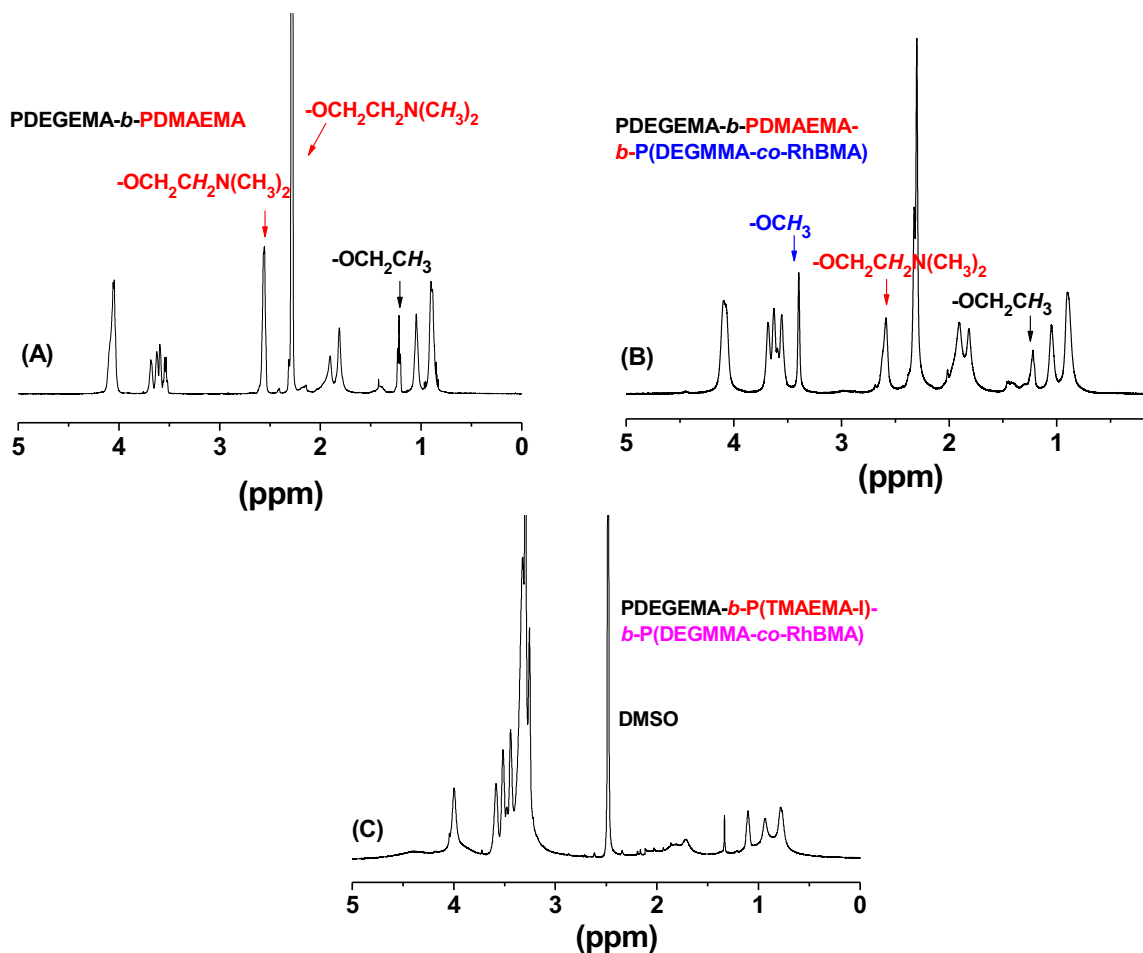


Figure 4.2. ^1H NMR spectrum of PDEGEMA-*b*-PDMAEMA macro-CTA in CDCl_3 (A), PDEGEMA-*b*-PDMAEMA-*b*-P(DEGMMA-*co*-RhBMA) in CDCl_3 (B) and PDEGEMA-*b*-P(TMAEMA-I)-*b*-P(DEGMMA-*co*-RhBMA) in DMSO-d_6 (C).

copolymer with excess iodomethane (CH_3I). The disappearance of the peak from the $-\text{OCH}_2\text{CH}_2\text{N}(\text{CH}_3)_2$ of PDMAEMA (Figure 4.2C), indicated that the quaternization was complete, yielding the targeted ABC triblock copolymer PDEGEMA-*b*-P(TMAEMA-I)-*b*-P(DEGMMA-*co*-RhBMA) (ABC-Q).

The quaternized ABC triblock copolymer contained two thermosensitive hydrophilic blocks, PDEGEMA and PDEGMMA with cloud points of 4 and 26 °C. To study the LCST transitions of PDEGEMA-*b*-P(TMAEMA-I)-*b*-P(DEGMMA-*co*-RhBMA) in water, dynamic light scattering (DLS) was employed. Figure 4.3 shows the plots of scattering intensity and hydrodynamic size (D_h) versus temperature for the quaternized ABC triblock copolymer in water at a concentration of 2.0 mg/g. Clearly, the block copolymer underwent two transitions. Below ~ 14 °C, both scattering intensity and hydrodynamic size increased significantly with increasing temperature. This can be attributed to the thermally induced micellization as the LCST of PDEGEMA in water is 4 °C. Because the transition temperature of PDEGEMA is very close to the freezing point of water, the plateau zone was not observed from both plots of scattering intensity and D_h in the low temperature range and thus we could not locate the critical micellization temperature (CMT). It is very likely the CMT is slightly higher than 4 °C due to the attachment to the more hydrophilic P(TMAEMA-I) block. Note that the hydrodynamic size of micelles is relatively large, which might result from the more extended conformations of the polyelectrolyte P(TMAEMA-I) block in addition to the weak association of micelles or molecules caused by the long range electrostatic interactions. In the temperature range from ~ 14 to ~ 28 °C, both scattering intensity and D_h leveled off, after which they started to increase again, indicating the second transition from the collapse of the outer P(DEGMMA-*co*-RhBMA) block. The onset temperature was 31 °C from the scattering intensity plot (Figure 4.3A) and 27 °C from the hydrodynamic size plot (Figure 4.3B).

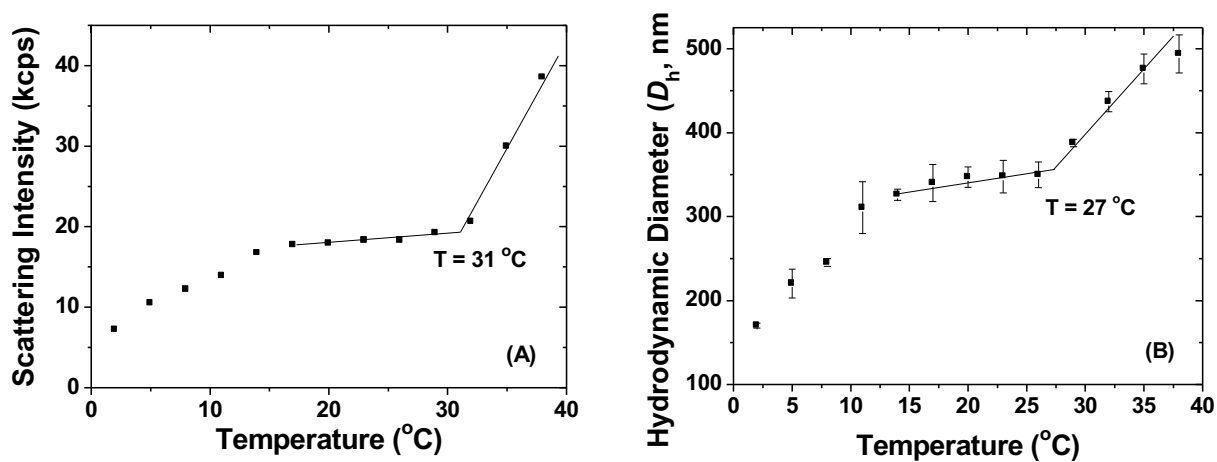
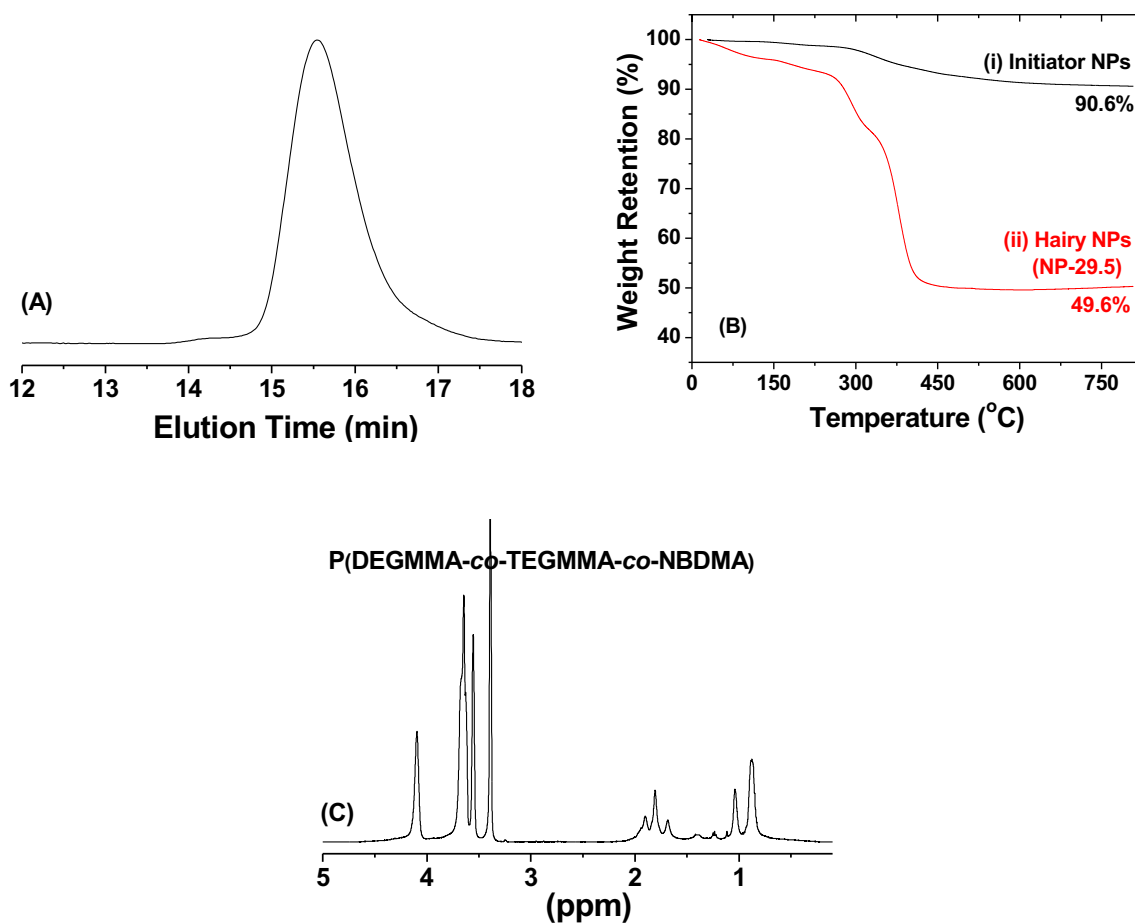


Figure 4.3. Plot of scattering intensity at scattering angle of 90° (A) and average apparent hydrodynamic diameter D_h (B), obtained from CONTIN, versus temperature from a dynamic light scattering study of a 2.0 mg/g solution of PDEGEMA-*b*-P(TMAEMA-I)-*b*-P(DEGMMA-co-RhBMA) in pure water.

Note that the cloud point of PDEGMMA in water is 26 °C. The slightly higher transition temperature can be attributed to the presence of the more hydrophilic, charged P(TMAEMA-I) block.

4.3.2. Synthesis of Thermosensitive Hairy NPs with Different LCST Transitions

To explore the possibility of enhancing gelation efficiency of doubly thermosensitive ABC triblock copolymer in water, we needed to use thermoresponsive hairy NPs with the LCST transition similar to that of the P(DEGMMA-*co*-RhBMA) block of the triblock copolymer. We previously reported the synthesis of P(DEGMMA-*co*-TEGMMA-*co*-NBDMA) brush-grafted silica NPs (NP-29), which showed a LCST transition in water with onset temperature (LCST_{onset}), end temperature (LCST_{end}), and middle point (LCST_{mid}) of 25, 32, and 29 °C, a perfect candidate for the current work. Note that the very small amount of NBDMA was incorporated into the brushes for fluorescence resonance energy transfer (FRET) study. Therefore, we made a new sample, designated as NP-29.5, using the same procedure. The $M_{n,SEC}$ and PDI of free P(DEGMMA-*co*-TEGMMA-*co*-NBDMA) were 12.3 kDa with PDI of 1.23, according to the SEC analysis (Figure 4.4A). TGA showed that the weight retention of NP-29.5 was 49.6 %, in contrast to 90.6 % of the initiator NPs (Figure 4.4B). The DP of the polymer was found to be 50, calculated using the monomer conversion and the molar ratio of monomer-to-sum of free and surface initiators; the numbers of DEGMMA and TEGMMA monomer units were 34 and 16, respectively, calculated from the ¹H NMR spectrum of free polymer P(DEGMMA-*co*-TEGMMA-*co*-NBDMA) (Figure 4.4C). Based on the TGA data, the DP of the polymer, and the size of core silica NPs (20 nm), the grafting density of NP-29.5 was calculated to be 0.36 chains/nm², similar to that of NP-29 we reported previously (0.42 chains/nm²).



Figures 4.4. (A) Size exclusion chromatography of the free copolymer formed from the free initiator in the synthesis of P(DEGMMA-*co*-TEGMMA-*co*-NBDMA) brush-grafted silica nanoparticles (NP-29.5). (B) Thermogravimetric analysis (TGA) of (i) the ATRP initiator-functionalized silica nanoparticles and (ii) P(DEGMMA-*co*-TEGMMA-*co*-NBDMA) brush-grafted silica nanoparticles (NP-29.5). (C) ¹H NMR spectroscopy analysis of the free copolymer formed from the free initiator in the synthesis of NP-29.5.

The thermosensitive property of NP-29.5 in water was studied by DLS (Figure 4.5). The $LCST_{onset}$, $LCST_{end}$, and $LCST_{mid}$ of the LCST transition were 27 °C, 32 °C, and 29.5 °C, respectively, which are essentially the same as those for NP-29. Thus, the LCST transition of NP-29.5 was similar to the second transition temperature of ABC-Q (Figure 4.3). Therefore, one can imagine that when the temperature is increased to above the LCST of NP-29.5 and the P(DEGMMA-*co*-RhBMA) block of the quaternized ABC triblock copolymer, the collapsed brushes of NP-29.5 will act as a “glue” to enhance the formation of bridging chains in the network gel and thus the gel’s mechanical strength. For comparison, NP-51, a batch of thermoresponsive hairy NPs with much higher LCST transition (the $LCST_{onset}$, $LCST_{end}$, and $LCST_{mid}$ were 45, 56, and 51 °C, respectively), was employed in the study of hybrid block copolymer hydrogels. The synthesis and characterization of NP-51 can be found in Chapter 3. Thus, when P(DEGMMA-*co*-RhBMA) block of the quaternized ABC undergoes a LCST transition, NP-51 is still hydrophilic and will be located outside the core of micelles and thus cannot function as a crosslinking promoter.

4.3.3. Rheology Study of Hybrid 3-D Network Hydrogels of ABC-Q and NP-29.5 with a Polymer Concentration of 6 wt% and Various Polymer-to-NP Mass Ratios

A 6 wt% solution of ABC-Q in water was prepared, which was found to undergo a sol-to-gel transition upon heating from ~ 0 to 40 °C. The gelation behavior of this sample was further studied by oscillatory shear experiments conducted in heating ramps using a constant frequency of 1 Hz, a strain amplitude of 1 %, and a heating rate of 3 °C/min. Figure 4.6A shows the plots of dynamic storage modulus G' and loss modulus G'' versus temperature. When the temperature was below 17 °C, the values of both G' and G'' are small, and $G' < G''$. This indicates a free-flowing liquid state of the sample.

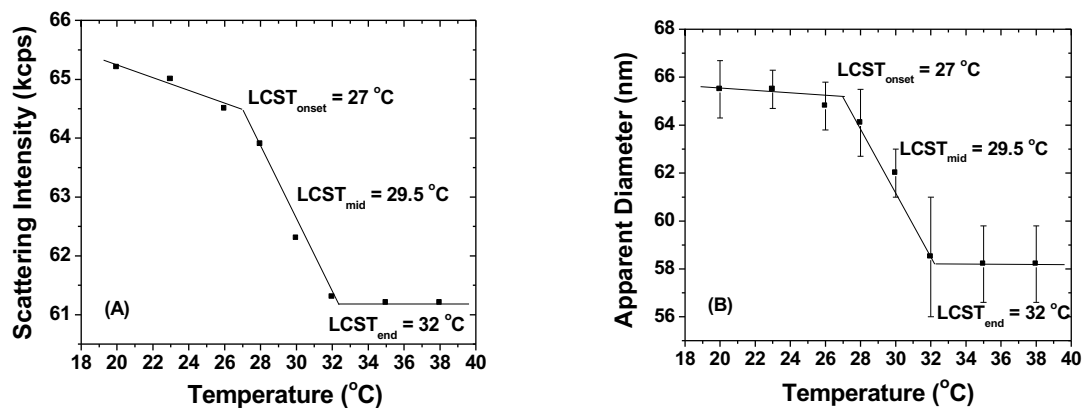


Figure 4.5. Plot of scattering intensity at scattering angle of 90° (A) and average apparent hydrodynamic size D_h (B), obtained from CONTIN analysis, as a function of temperature from a dynamic light scattering study of a 1.0 mg/g aqueous dispersion of P(DEGMMA-co-TEGMMA-co-NBDMA) brush-grafted silica nanoparticles (NP-29.5).

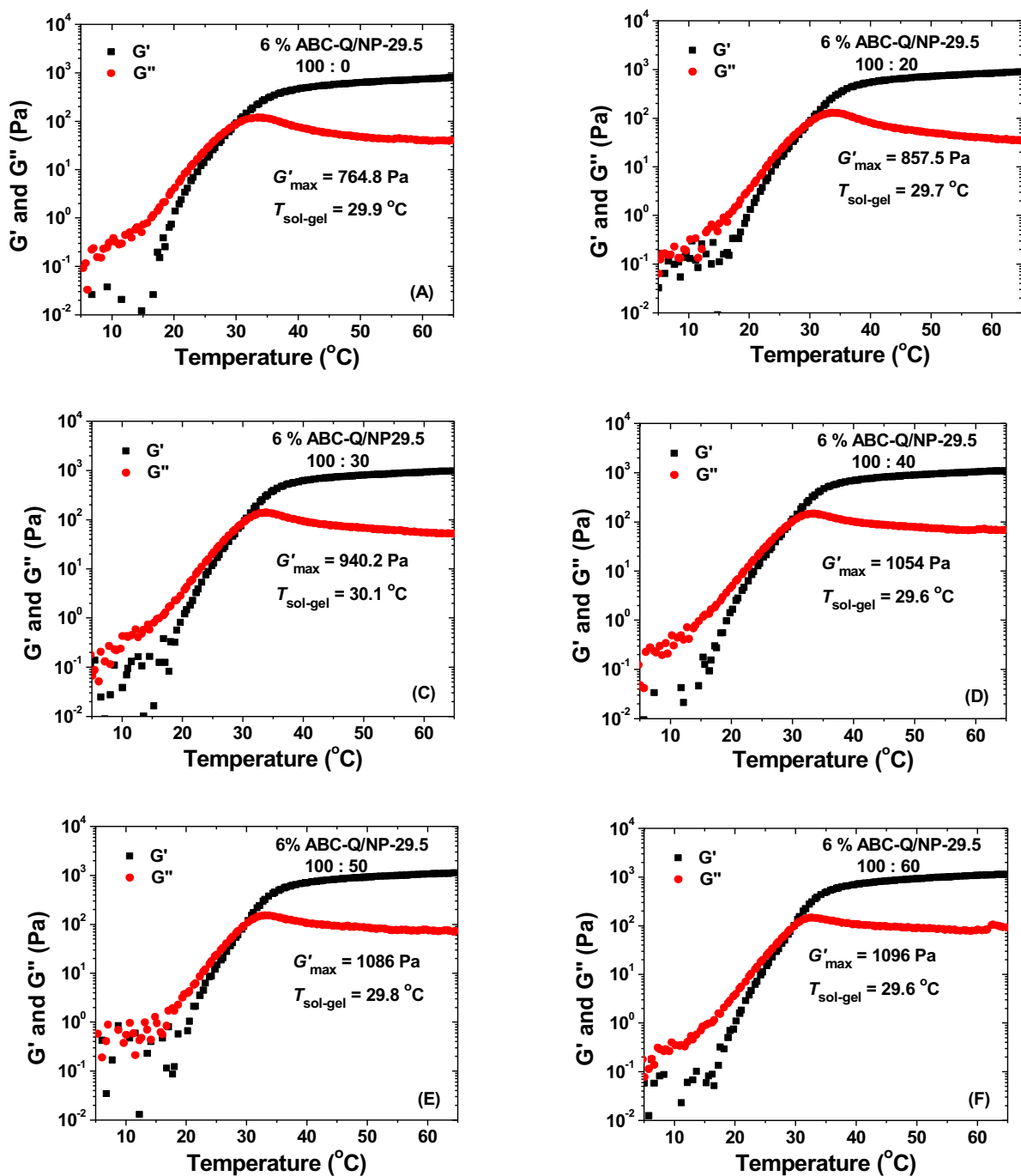


Figure 4.6. Representative plots of dynamic storage modulus G' and loss modulus G'' of aqueous mixtures of PDEGEMA-*b*-P(TMAEMA-*I*)-*b*-P(DEGMMA-*co*-RhBMA) with a concentration of 6 wt% and NP-29.5 with various polymer-to-NP mass ratio versus temperature. The rheological data were collected from oscillatory shear experiments conducted in heating ramps using a frequency of 1 Hz, a strain amplitude of 1 %, and a heating rate of 3 °C/min.

Upon further heating, G' and G'' increased abruptly, and G' increased faster than G'' ; the crossover of the two curves occurred at 29.5 °C, at which $G' = G''$, which is commonly identified as the sol-gel transition temperature ($T_{\text{sol-gel}}$). Above the $T_{\text{sol-gel}}$, the increase of G' slowed down, and G'' gradually decreased; the fact that G' was significantly higher than G'' indicated a solid-like behavior (gel state). This can be attributed to the LCST transition of the outer P(DEGMMA-*co*-RhBMA) block, triggering the association of the collapsed P(DEGMMA-*co*-RhBMA) blocks into micellar cores and formation of crosslinking points.

To examine the effect of incorporating NP-29.5 into the thermosensitive micellar hydrogels of PDEGEMA-*b*-P(TMAEMA-*I*)-*b*-P(DEGMMA-*co*-RhBMA), an aqueous dispersion of NP-29.5 was added into the 6 wt% aqueous solution of the quaternized ABC triblock copolymer, and the NP-to-polymer mass ratio was gradually increased from 20 : 100, 30 : 100, 40 : 100, 50 : 100 to 60 : 100. The concentration of the ABC triblock copolymer, which is defined as $[(\text{polymer mass})/(\text{polymer mass} + \text{water mass})] \times 100\%$, was maintained at 6 wt% by evaporating a calculated amount of water from the sample. For each sample, three rheology measurements were conducted, and the representative heating ramp curves are shown in Figure 4.6; the other two rheological curves are included in the Appendix C.

For each rheological curve, the G'_{max} , which is normally observed at 65 °C because G' keeps increasing gradually at high temperatures, and the sol-gel transition temperature ($T_{\text{sol-gel}}$) are recorded and shown in each plot. As can be seen from Figure 4.6, $T_{\text{sol-gel}}$ remained nearly constant, around 29.8 °C with variations of ≤ 0.3 °C, with the increase of NP-to-polymer mass ratio, indicating the presence of NP-29 did not affect the ABC-Q to form a 3-D network hydrogel, even when the NP-to-polymer mass ratio reached 60 : 100. Differently, the G'_{max} value increased significantly when the NP-to-polymer mass ratio was increased from 0 : 100 to 40 : 100. After that,

the G'_{\max} changed only slightly. To better appreciate the increase of G'_{\max} with the addition of NP-29, we replotted G' versus temperature for all six samples on a linear scale (Figure 4.7A); the average of G'_{\max} values from three measurements as a function of NP-to-ABC-Q mass ratio is shown in Figure 4.7C. For the pure 6 wt% aqueous solution of ABC-Q, the average G'_{\max} was 756 Pa; the average G'_{\max} increased to 866 Pa, 940 Pa, and 1075 Pa, respectively, when the NP-to-polymer mass ratio was increased from 20 : 100, to 30 : 100, and 40 : 100. With further addition of NP-29.5, the average G'_{\max} changed only slightly, 1069 Pa for the mass ratio of 50 : 100 and 1099 Pa for the ratio of 60 : 100. Thus, the G'_{\max} increased by 45% at the NP-to-polymer ratio of 60 : 100 compared with that of the sample with no NPs added, suggesting that the addition of NP-29.5 significantly improved the mechanical property of the ABC 3-D network hydrogels.

Similar results were obtained from frequency sweeps conducted at 40 °C for all samples. (The data can be found in the Appendix C.) Figure 4.7D shows the plots of the average value of G' at 1 Hz ($G'_{1\text{Hz}}$) from three runs versus the NP-to-ABC-Q mass ratio. $G'_{1\text{Hz}}$ increased with the increase of NP-29.5-to-polymer mass ratio; at the ratio of 60 : 100, the $G'_{1\text{Hz}}$ value increased by 48% compared with the sample without any hairy NPs. This again showed that adding NP-29.5 significantly increased the mechanical strength of the physically cross-linked micellar hydrogels of ABC-Q.

4.3.4. Rheology Study of Hybrid Micellar Hydrogels of ABC-Q and NP-51 with a Polymer Concentration of 6 wt% and Various NP-to-Polymer Mass Ratios

For comparison, the gel properties of hybrid 3-D network micellar hydrogels of ABC-Q and NP-51 with a polymer concentration of 6 wt% and various NP-to-polymer mass ratios were also studied by rheological measurements using the same conditions. Similarly, for each sample,

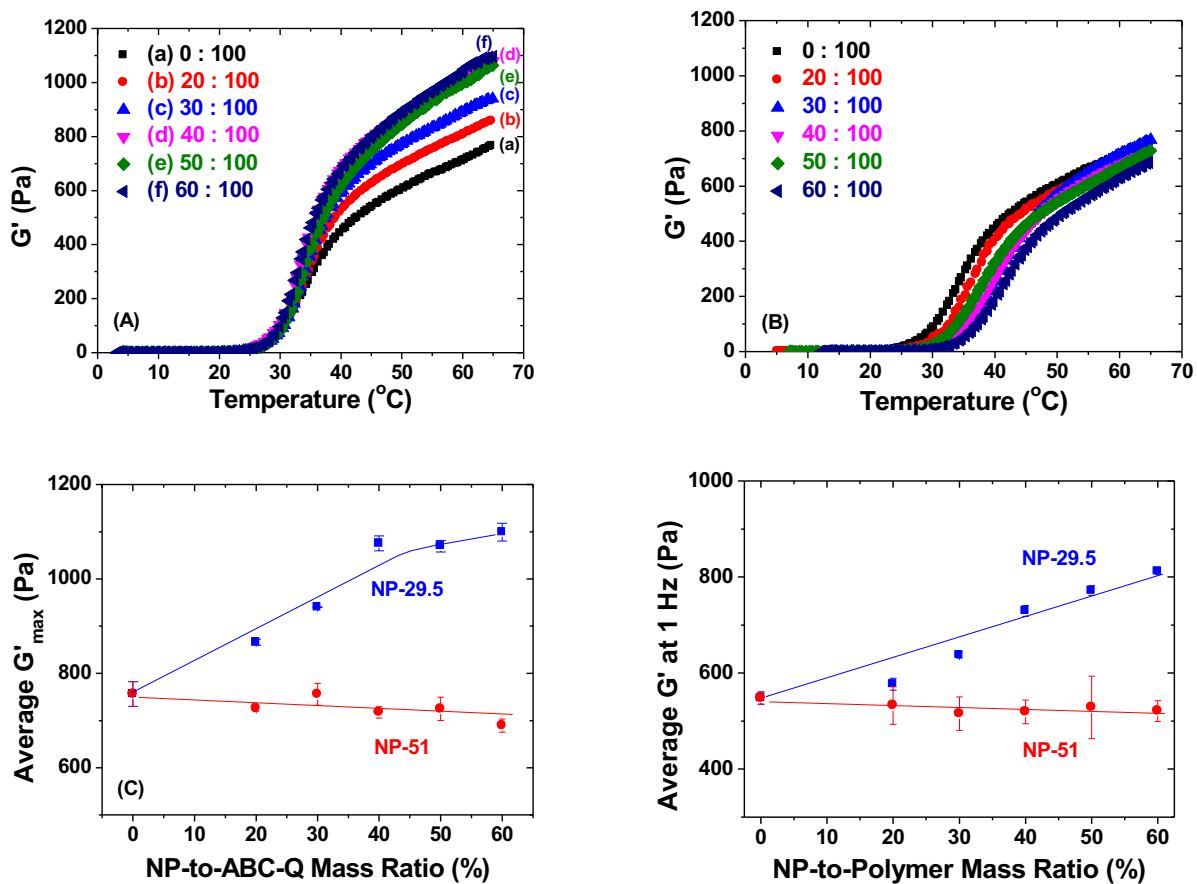


Figure 4.7. Plots of dynamic storage modulus G' versus temperature for aqueous mixtures of ABC-Q and NP-29.5 (A) and NP-51 (B) at various NP-to-polymer mass ratios (replotted from Figures 4.6 and 4.8); (C) plots of average G'_{\max} versus NP-to-polymer mass ratio for NP-29.5 and NP-51; (D) plots of average $G'_{1\text{Hz}}$ versus NP-to-polymer mass ratio for NP-29.5 and NP-51.

three rheological measurements were taken, and frequency sweeps were conducted at 40 °C at a 1 wt% strain amplitude. Figure 4.8 shows the representative rheological curves of five samples with the mass ratio of NP-51 to ABC-Q ranging from 20 : 100, to 30 : 100, 40 : 100, 50 : 100, and 60 : 100; the G'_{\max} is replotted against NP-to-polymer mass ratio (Figure 4.7B). Other heating ramp curves and frequency sweeps can be found in the Appendix C. Similar to the samples of NP-29.5 and ABC-Q, the $T_{\text{sol-gel}}$ remained almost the same, varying from 29.5 to 30 °C with addition of NP-51 into the 6 wt% aqueous solution of ABC-Q. Figure 4.7C and D shows the plots of average G'_{\max} from three heating ramps and average $G'_{1\text{Hz}}$ from three frequency sweeps versus NP-51-to-ABC-Q mass ratio. Both G'_{\max} and $G'_{1\text{Hz}}$ exhibited little change with increasing NP-to-ABC-Q mass ratio. The average G'_{\max} decreased from 756 Pa at a ratio of 0 : 100 to 689 Pa at the mass ratio of 60 : 100, while $G'_{1\text{Hz}}$ decreased from 548 to 527 Pa.

4.4. Discussion

Although the sol-gel transition temperatures of hybrid hydrogels of ABC-Q with addition of either NP-29.5 or NP-51 at various mass ratios stayed almost unchanged, the G'_{\max} exhibited different trends for NP-29.5 and NP-51 as shown in Figure 4.7. For NP-29.5, G'_{\max} was found to increase significantly with the addition of NP-29 up to a NP-to-polymer mass ratio of 40 : 100 and leveled off above that. For hybrid hydrogels of ABC-Q and NP-51, we observed a trend that G'_{\max} decreased very slightly with increasing amount of NP-51. ABC-Q is a doubly thermosensitive hydrophilic triblock copolymer composed of a PDEGEMA block, a permanently hydrophilic, charged middle block, and a P(DEGMMA-*co*-RhBMA) block. From the DLS study, the LCST of the PDEGMMA block was essentially the same as that of NP-29.5. Thus, upon heating from 0 °C in an ice/water bath, ABC-Q exhibited stepwise transitions; above the LCST of the first block

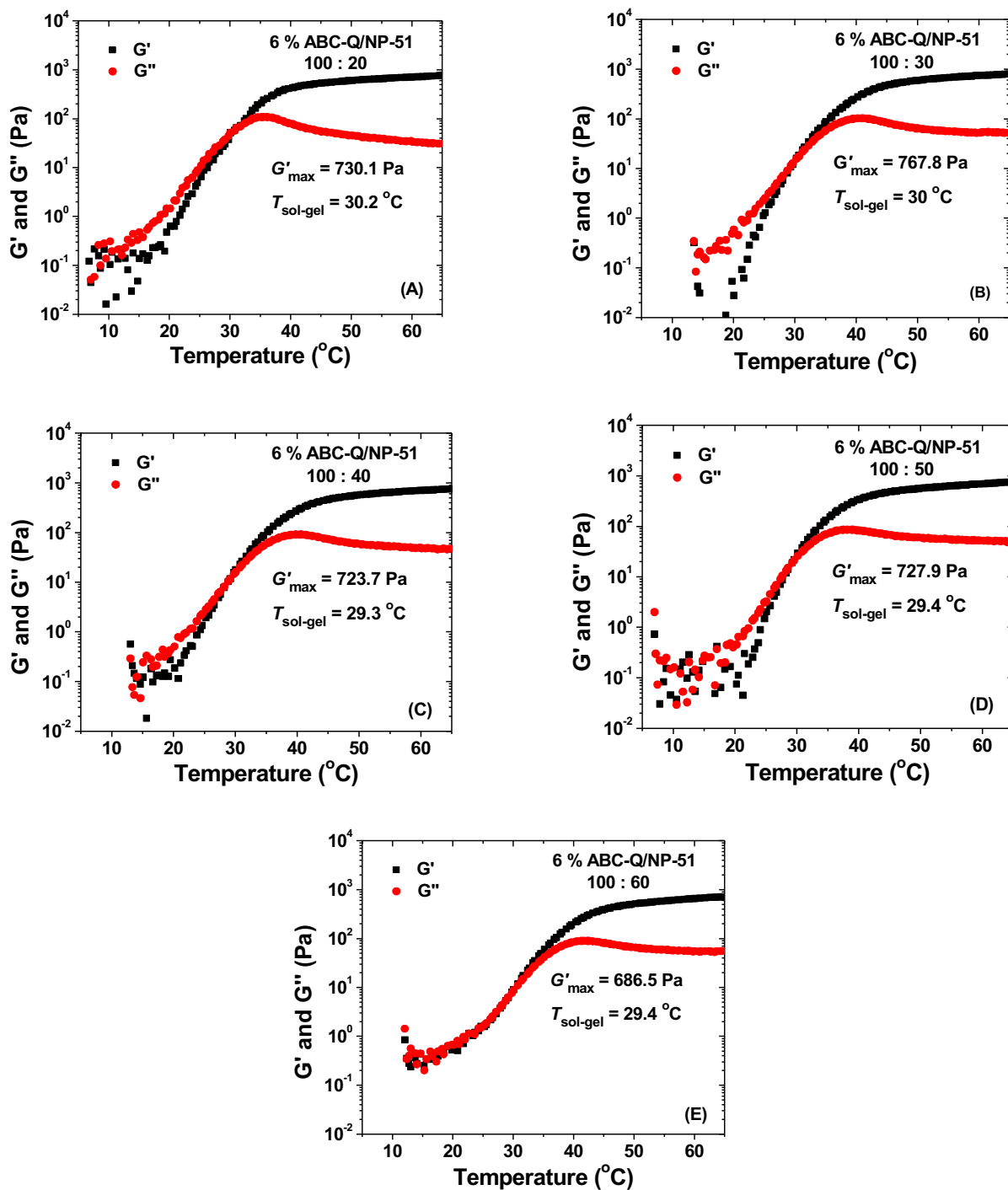


Figure 4.8. Representative plots of dynamic storage modulus G' and loss modulus G'' of aqueous mixtures of PDEGEMA-*b*-P(TMAEMA-*I*)-*b*-P(DEGMMA-*co*-RhBMA) with a concentration of 6 wt% and NP-51 with various polymer-to-NP mass ratio versus temperature. The rheological data were collected from oscillatory shear experiments conducted in heating ramps using a frequency of 1 Hz, a strain amplitude of 1 %, and a heating rate of 3 °C/min.

PDEGEMA, the triblock copolymer molecules began to self-assemble into micelles. Considering the small DP for PDEGEMA (DP = 75) and the much larger DPs for the blocks of P(TMAEMA-I) (DP = 345) and PDEGMMA (DP = 142), the block copolymer micelles should be spherical micelles. At a sufficiently high concentration (e.g., 6 wt% in our study), when the temperature reached the LCST of the third block, the P(DEGMMA-*co*-RhBMA) block collapsed and self-associated into hydrophobic micellar cores, which acted as physically crosslinked points (Scheme 4.1), resulting in the formation of 3-dimensional network hydrogels. As mentioned in the Introduction, loop formation is unavoidable in thermosensitive ABA and ABC triblock copolymers, which leads to a gel with a weak mechanical property.

The G' of a transient physically crosslinked hydrogel is a measure of the number density of elastically active polymer chains (i.e., bridging chains among micellar cores) and can be described by $G' = \nu k_B T$, where ν is the number density of elastically active/bridging polymer chains per unit volume, k_B is Boltzmann constant, and T is the absolute temperature.³⁷⁻³⁸ If every middle block of ABC-Q is elastically effective, then $\nu = cN_A/M$, where c is the concentration of the polymer solution, N_A is the Avogadro's number, and M is the molecular weight of ABC-Q.^{32,39} The fraction of bridging chains is calculated as the G' observed from the temperature ramp curves divided by the calculated G' at a specific temperature $\times 100\%$. Calculations showed that for the pure 6 wt % aqueous solution of ABC-Q, the fraction of bridging chains was 54.2 % at 50 °C and 65.0 % at 65 °C, indicating that a significant portion of ABC-Q molecules did not function as elastically active chains in the network hydrogel; one possibility is that the third PDEGMMA block loops back to the PDEGEMA core. To confirm this, a fluorescence resonance energy transfer (FRET) study was conducted. Note that a very small amount of Rhodamine B was copolymerized into the outer PDEGMMA block in the synthesis of the ABC triblock copolymer. We loaded NBD-Cl, a FRET

donor for acceptor Rhodamine B, into the core of ABC-Q micelles at 15 °C. When the temperature was raised to 40 °C, the peak intensity at 574 nm (from RhBMA) increased, while the intensity of the peak at 533 nm (from NBD-Cl) decreased upon excitation with 480 nm light (Figure C6 in Appendix C). This indicates that the two dye molecules NBDMA and RhBMA were in close proximity (within 1-10 nm) and caused the FRET to occur, which suggested that the PDEGMMA block looped back to the micellar core of PDEGEMA. Note that if NBD-Cl is absent, the emission intensity from RhBMA in ABC-Q at 578 nm decreased with increasing temperature from 15 to 40 °C (see Appendix C).

We hypothesized that adding thermosensitive hairy NPs with a LCST similar to that of the outer block PDEGMMA could improve the gelation efficiency, for these hairy NPs could act as “seeds” for the formation of hydrophobic PDEGMMA micellar cores (i.e., physical crosslinking points). This is exactly what we observed when NP-29.5, which had a very similar LCST to that of the P(DEGMMA-*co*-RhBMA) block of ABC-Q, was added into the 6 wt% aqueous solution of ABC-Q; the G'_{\max} increased with increasing amount of hairy NPs (Figure 4.7). Evidently, the hairy NPs served as “glue” to absorb the collapsed PDEGMMA block of ABC-Q when the temperature is raised to above the LCST transition, resulting in the formation of more bridging chains under the same conditions and thus an increase in G' (Scheme 4.1). On the other hand, the LCST of NP-51 is higher than $LCST_{PDEGMMA}$ by ~ 20 °C. Thus, when the PDEGMMA block self-assembled into hydrophilic micellar cores, NP-51 was still fully hydrated and thus was excluded from the core of micelles. From our previous study of hybrid micellar hydrogels of thermosensitive ABA triblock copolymers and hairy NPs, the presence of hairy NPs in the interstitial space adversely affected the formation of the network and decreased the mechanical strength of the gels.

Using the aforementioned method, we calculated the fractions of bridging chains in hybrid hydrogels of 6 wt% aqueous solutions of ABC-Q with various amounts of NP-29.5, and of 6 wt% aqueous solutions of ABC-Q and NP-51 with various NP-to-polymer mass ratios at 50 and 65 °C (Figure 4.9). With addition of NP-29.5, at 65°C, the fraction of bridging chains increased from 65.0 % for the pure 6 wt% aqueous solution of ABC-Q, to 74 % at the NP-to-polymer mass ratio of 20 : 100, to 94.6 % at the ratio of 60 : 100, which indicated that there were more bridging chains formed when NP-29 was added into the polymer solution. Similar to G'_{\max} in Figure 4.7, the fraction of bridging chains also leveled off at mass ratios above 40 : 100. For hybrid hydrogels of ABC-Q and NP-51, the fraction of bridging chains decreased slightly from 65.0 % for the pure 6 wt% aqueous solution of ABC-Q, to 62.5 % at the mass ratio of 20 : 100, and 59.3 % at the ratio of 60 : 100. Apparently, when the P(DEGMMA-co-RhBMA) block undergoes the LCST transition, NP-51 is still highly hydrophilic and cannot effectively “glue” the collapsed PDEGMMA blocks together. Because the hydrophilic NP-51 hairy NPs were located in the interstitial space of micelles, they interfered the formation of bridging chains among the micellar cores, causing the fraction of bridging chains to decrease slightly with addition of NP-51.

To experimentally confirm the different locations of NP-29.5 and NP-51 in the 3-D network micellar hydrogels of ABC-Q, FRET studies were conducted for dilute aqueous mixtures of ABC-Q and NP-29.5 or NP-51 at 15 °C and 40 °C. Note that a FRET donor, NBDMA (a NBD-containing methacrylate monomer, Scheme 4.2), was incorporated into the thermosensitive polymer brushes of both NP-29.5 and NP-51, and a FRET acceptor, RhBMA (a Rhodamine B-containing methacrylate monomer), was copolymerized into the thermosensitive PDEGMMA block of ABC and thus ABC-Q. If the two dye molecules NBDMA and RhBMA are in close proximity (within 1-10 nm), FRET would occur, resulting in a decrease in the fluorescence emission intensity at 521

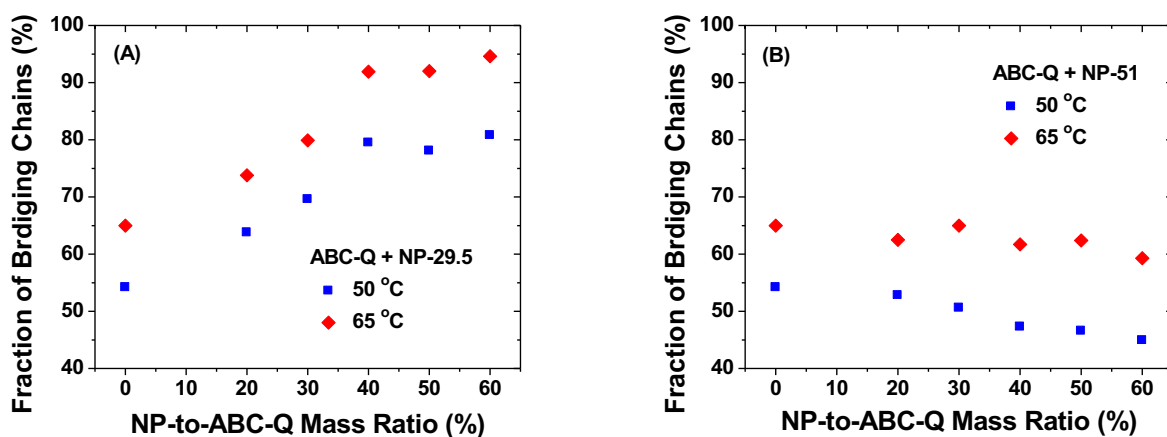


Figure 4.9. Plots of calculated fractions of bridging chains versus NP-to-polymer mass ratio for hybrid hydrogels of (A) 6 wt% ABC-Q solution with various amounts of NP-29.5 and (B) 6 wt% aqueous solution of ABC-Q with various NP-51-to-ABC-Q mass ratios at 50 and 65 °C. Average G' values from three heating ramps at 50 and 65 °C were used in the calculations.

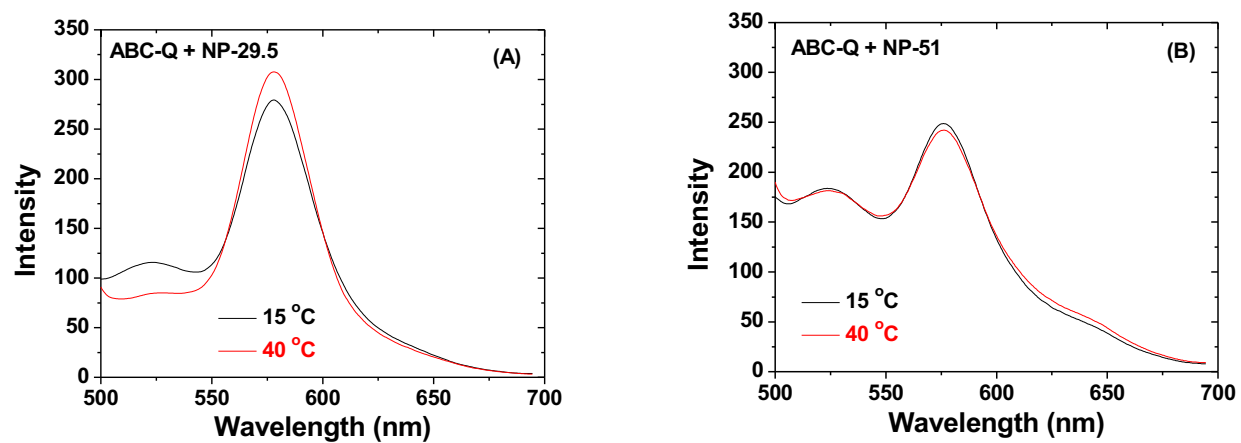


Figure 4.10. Fluorescence spectra of aqueous solutions of (A) ABC-Q with a concentration of 0.431 mg/g and NP-29.5 with a concentration of 0.013 mg/g and of (B) ABC-Q with a concentration of 0.376 mg/g and NP-51 with a concentration of 0.012 mg/g at 15 (black curves) and 40 °C (red curves).

nm and in increase in the intensity at 578 nm. Two aqueous mixtures of ABC-Q and hairy NPs were prepared for FRET experiments, one with an ABC-Q concentration of 0.431 mg/g and an NP-29.5 concentration of 0.013 mg/g, and the other with an ABC-Q concentration of 0.376 mg/g and an NP-51 concentration of 0.012 mg/g. The fluorescence emission spectra of the two samples at 15 and 40 °C are shown in Figure 4.10. For the mixture of ABC-Q and NP-29.5, the NBDMA peak at 521 nm decreased from 115 to 84 a.u.), while the RhBMA peak at 578 nm increased from 279 to 308 a.u. when the temperature was raised from 15 to 40 °C. The FRET occurred because when the temperature was increased to 40 °C, above the LCSTs of the PDEGMMA block of ABC-Q and NP-29.5, the collapsed P(DEGMMA-*co*-RhBMA) block interacted strongly with the collapsed brushes on the NPs, and thus the FRET pairs were within 1-10 nm range. For the mixture of ABC-Q and NP-51, the intensity of the peak at 521 nm remained unchanged, while the peak at 578 nm decreased slightly, which was caused by the increase of temperature. This confirmed that there was no or little interaction at 40 °C between NP-51 and the collapsed P(DEGMMA-*co*-RhBMA) block of the ABC-Q micelles, consistent with what we expected.

4.5. Conclusions

A doubly thermosensitive ABC triblock copolymer ABC-Q composed of a lower LCST A block, a permanently hydrophilic middle B block, and a higher LCST C block and two thermoresponsive hairy NPs with LCSTs of 29.5 and 51 °C in water were prepared for studying the effect of adding hairy NPs into aqueous solutions of ABC-Q on gel properties. When the LCST of hairy NPs was similar to that of the C block of ABC-Q, the G'_{\max} and the fraction of bridging chains increase significantly when the hairy NPs were added into the aqueous solutions of ABC-Q. We believe that this is because the collapsed hairy NPs acted as “seeds” adsorbing the collapsed

C block of ABC-Q when the temperature was above their LCSTs as confirmed by a FRET study, which promoted the formation of bridging chains among micellar cores and increased the number of elastically active chains in the polymer network. In contrast, for hybrid hydrogels of ABC-Q and NP-51, G'_{\max} and thus the fraction of bridging chains decrease slightly, for the brushes in NP-51 were still highly hydrated when the thermosensitive C block of ABC-Q began to collapse and associate into micellar cores. The results reported in this work could provide a guideline for design of hybrid hydrogels with enhanced mechanical properties, and the method introduced here could be used to increase the hydrogel property and simultaneously introduce new functions through the use of NPs.⁴⁰⁻⁴⁶

4.6. References

1. Hamley, I. W., *The Physics of Block Copolymers*. Oxford University Press: Oxford, 1998.
2. Hamley, I., *Block Copolymers in Solution: Fundamentals and Applications*. John Wiley & Sons: Chichester, 2005.
3. Jeong, B.; Kim, S. W.; Bae, Y. H. *Adv. Drug Deliver. Rev* **2002**, *54*, 37-51.
4. Gil, E. S.; Hudson, S. M. *Prog. Polym. Sci.* **2004**, *29*, 1173-1222.
5. Madsen, J.; Armes, S. P.; Lewis, A. L. *Macromolecules* **2006**, *39*, 7455-7457.
6. He, C.; Kim, S. W.; Lee, D. S. *J. Control Release.* **2008**, *127*, 189-207.
7. Yu, L.; Ding, J. *Chem. Soc. Rev.* **2008**, *37*, 1473-1481.
8. Park, M. H.; Joo, M. K.; Choi, B. G.; Jeong, B. *Accounts. Chem. Res.* **2012**, *45*, 424-433.
9. Sugihara, S.; Kanaoka, S.; Aoshima, S. *Macromolecules* **2005**, *38*, 1919-1927.
10. Jin, N.; Woodcock, J. W.; Xue, C.; O'Lenick, T. G.; Jiang, X.; Jin, S.; Dadmun, M. D.; Zhao, B. *Macromolecules* **2011**, *44*, 3556-3566.
11. Li, C.; Tang, Y.; Armes, S. P.; Morris, C. J.; Rose, S. F.; Lloyd, A. W.; Lewis, A. L. *Biomacromolecules* **2005**, *6*, 994-999.
12. Kirkland, S. E.; Hensarling, R. M.; McConaughy, S. D.; Guo, Y.; Jarrett, W. L.; McCormick, C. L. *Biomacromolecules* **2008**, *9*, 481-486.
13. O'Lenick, T. G.; Jiang, X.; Zhao, B. *Langmuir* **2010**, *26*, 8787-8796.
14. Woodcock, J. W.; Jiang, X.; Wright, R. A. E.; Zhao, B. *Macromolecules* **2011**, *44*, 5764-5775.
15. Henn, D. M.; Wright, R. A. E.; Woodcock, J. W.; Hu, B.; Zhao, B. *Langmuir* **2014**, *30*, 2541-2550.

16. Woodcock, J. W.; Wright, R. A. E.; Jiang, X.; O'Lenick, T. G.; Zhao, B. *Soft Matter* **2010**, *6*, 3325-3336.
17. Jin, N.; Zhang, H.; Jin, S.; Dadmun, M. D.; Zhao, B. *Macromolecules* **2012**, *45*, 4790-4800.
18. Balsara, N. P.; Tirrell, M.; Lodge, T. P. *Macromolecules* **1991**, *24*, 1975-1986.
19. Yamaguchi, D.; Cloitre, M.; Panine, P.; Leibler, L. *Macromolecules* **2005**, *38*, 7798-7806.
20. Li, C.; Buurma, N. J.; Haq, I.; Turner, C.; Armes, S. P.; Castelletto, V.; Hamley, I. W.; Lewis, A. L. *Langmuir* **2005**, *21*, 11026-11033.
21. Zhou, C.; Hillmyer, M. A.; Lodge, T. P. *J. Am. Chem. Soc.* **2012**, *134*, 10365-10368.
22. Koonar, I.; Zhou, C.; Hillmyer, M. A.; Lodge, T. P.; Siegel, R. A. *Langmuir* **2012**, *28*, 17785-17794.
23. Zhou, C.; Toombes, G. E. S.; Wasbrough, M. J.; Hillmyer, M. A.; Lodge, T. P. *Macromolecules* **2015**, *48*, 5934-5943.
24. Xuan, S.; Lee, C.-U.; Chen, C.; Doyle, A. B.; Zhang, Y.; Guo, L.; John, V. T.; Hayes, D.; Zhang, D. *Chem. Mater.* **2016**, *28*, 727-737.
25. Kitazawa, Y.; Ueki, T.; McIntosh, L. D.; Tamura, S.; Niitsuma, K.; Imaizumi, S.; Lodge, T. P.; Watanabe, M. *Macromolecules* **2016**, *49*, 1414-1423.
26. Reinicke, S.; Dohler, S.; Tea, S.; Krekhova, M.; Messing, R.; Schmidt, A. M.; Schmalz, H. *Soft Matter* **2010**, *6*, 2760-2773.
27. Hu, B.; Henn, D. M.; Wright, R. A. E.; Zhao, B. *Langmuir* **2014**, *30*, 11212-11224.
28. Hu, B.; Wright, R. A. E.; Jiang, S.; Henn, D. M.; Zhao, B. *Polymer* **2016**, *82*, 206-216.
29. Ishizone, T.; Seki, A.; Hagiwara, M.; Han, S.; Yokoyama, H.; Oyane, A.; Deffieux, A.; Carloti, S. *Macromolecules* **2008**, *41*, 2963-2967.
30. Han, S.; Hagiwara, M.; Ishizone, T. *Macromolecules* **2003**, *36*, 8312-8319.

31. Wu, T.; Zou, G.; Hu, J.; Liu, S. *Chem. Mater.* **2009**, *21*, 3788-3798.
32. O'Lenick, T. G.; Jin, N.; Woodcock, J. W.; Zhao, B. *J. Phys. Chem. B* **2011**, *115*, 2870-2881.
33. Horton, J. M.; Bao, C.; Bai, Z.; Lodge, T. P.; Zhao, B. *Langmuir* **2011**, *27*, 13324-13334.
34. Li, D.; Jones, G. L.; Dunlap, J. R.; Hua, F.; Zhao, B. *Langmuir* **2006**, *22*, 3344-3351.
35. Mitsukami, Y.; Donovan, M. S.; Lowe, A. B.; McCormick, C. L. *Macromolecules* **2001**, *34*, 2248-2256.
36. Wright, R. A. E.; Hu, B.; Henn, D. M.; Zhao, B. *Soft Matter* **2015**, *11*, 6808-6820.
37. Yoshida, T.; Kanaoka, S.; Watanabe, H.; Aoshima, S. *J. Polym. Sci. A Polym. Chem.* **2005**, *43*, 2712-2722.
38. He, Y.; Boswell, P. G.; Bühlmann, P.; Lodge, T. P. *J. Phys. Chem. B* **2007**, *111*, 4645-4652.
39. Noro, A.; Matsushita, Y.; Lodge, T. P. *Macromolecules* **2009**, *42*, 5802-5810.
40. Balazs, A. C.; Emrick, T.; Russell, T. P. *Science* **2006**, *314*, 1107-1110.
41. Schexnailder, P.; Schmidt, G. *Colloid Polym. Sci.* **2009**, *287*, 1-11.
42. Pozzo, D. C.; Walker, L. M. *Macromol. Symp.* **2005**, *227*, 203-210.
43. Ilg, P. *Soft Matter* **2013**, *9*, 3465-3468.
44. Nambam, J. S.; Philip, J. *Langmuir* **2012**, *28*, 12044-12053.
45. Qin, J.; Asempah, I.; Laurent, S.; Fornara, A.; Muller, R. N.; Muhammed, M. *Adv. Mater.* **2009**, *21*, 1354-1357.
46. Roeder, L.; Bender, P.; Kundt, M.; Tschöpe, A.; Schmidt, A. M. *Phys. Chem. Chem. Phys.* **2015**, *17*, 1290-1298.
47. The work presented in this Chapter has been accepted for publication on *Macromolecules* as an article.

Appendix C

for

Chapter 4. Enhancing Gelation Efficiency of A Doubly Thermosensitive

Hydrophilic Linear ABC Triblock Copolymer in Water by Thermoresponsive

Hairy Nanoparticles

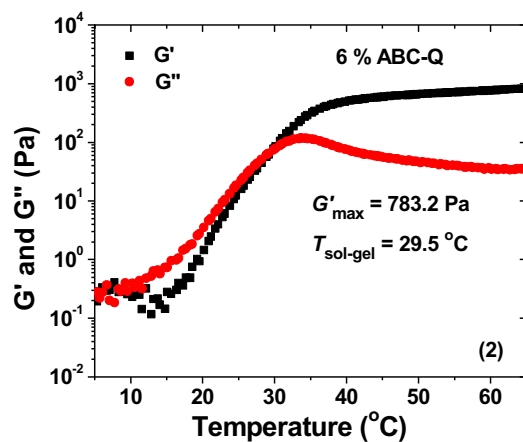
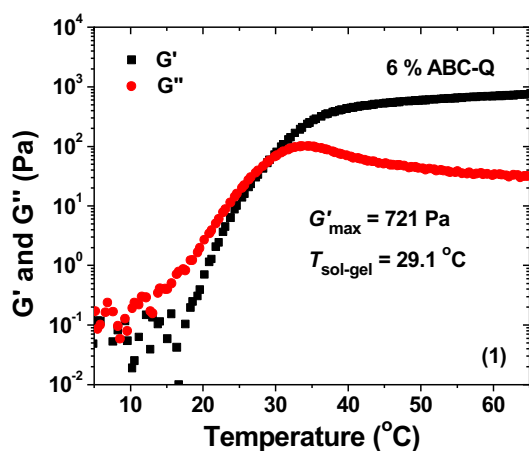
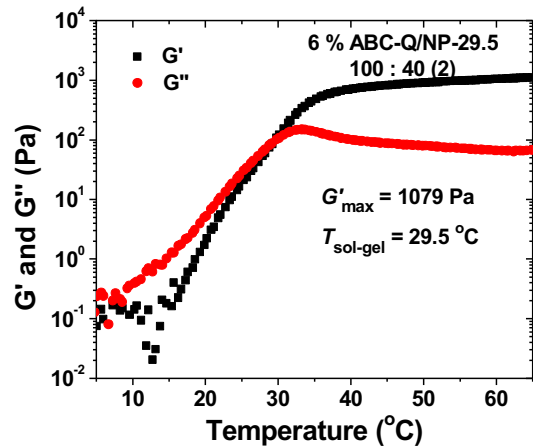
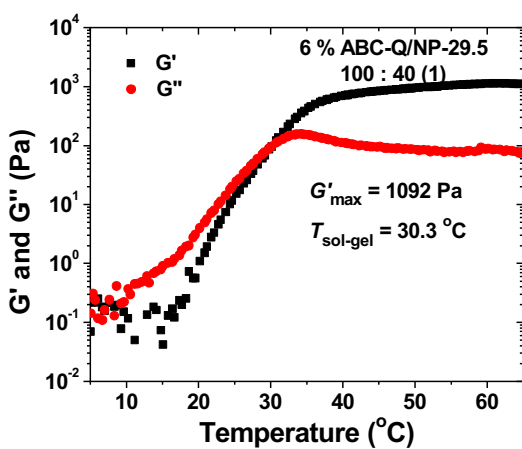
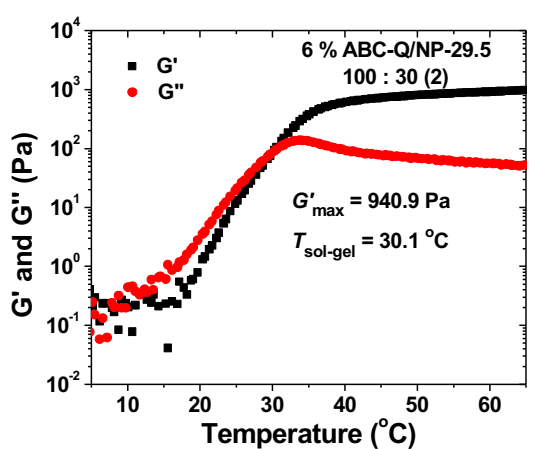
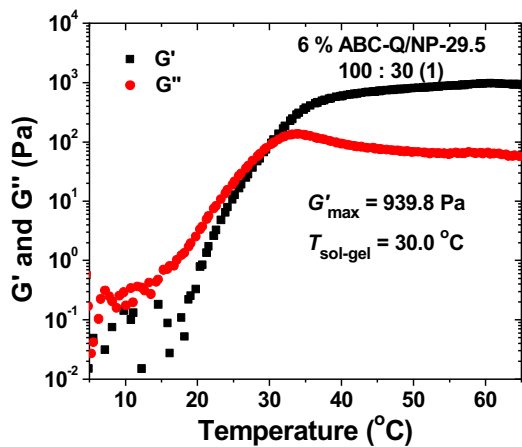
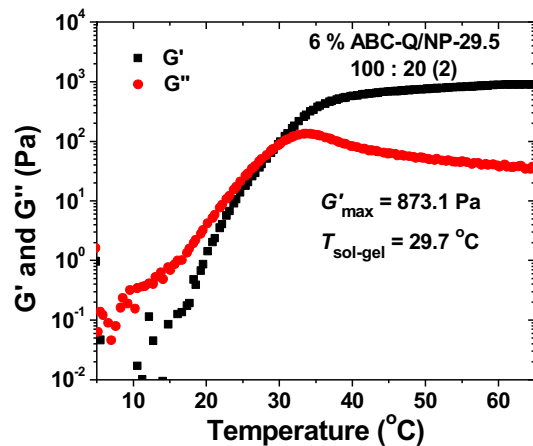
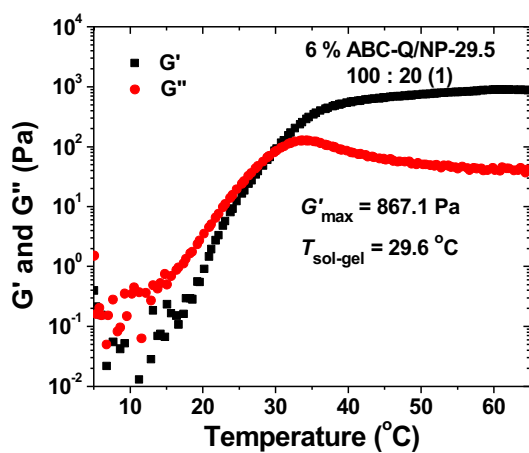
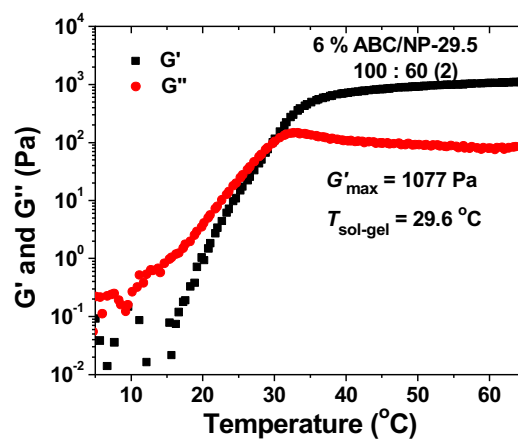
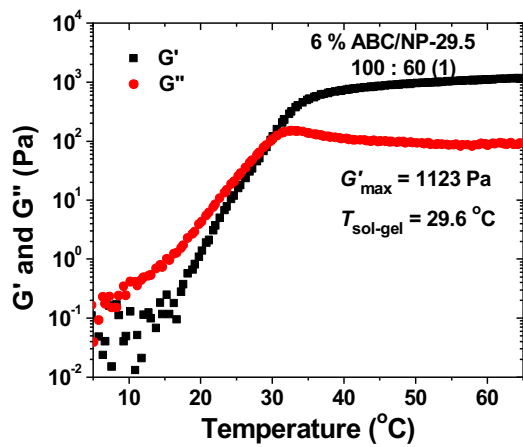
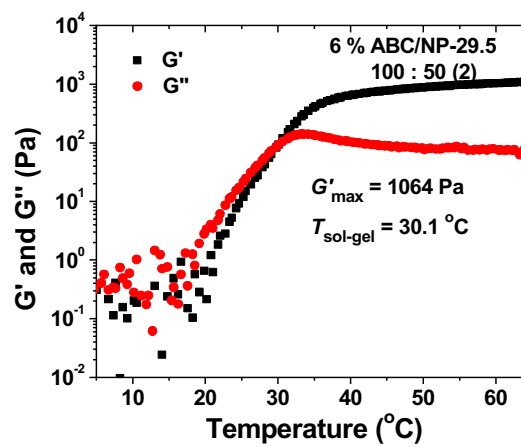
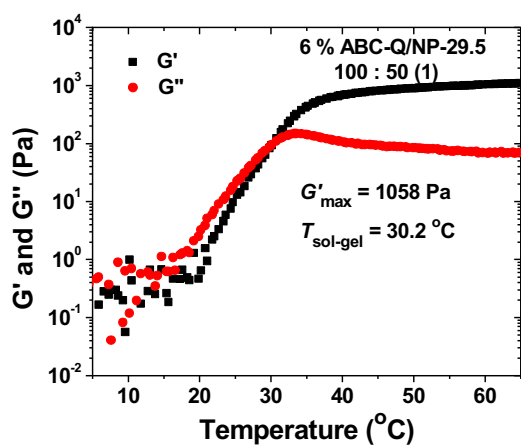


Figure C1. Plots of dynamic storage modulus G' and loss modulus G'' of an aqueous solution of PDEGEMA-*b*-P(TMAEMA-*I*)-*b*-P(DEGMMA-*co*-RhBMA) with a concentration of 6 wt%. The rheological data were collected from heating ramp experiments performed by using a frequency of 1 Hz, a strain amplitude of 1 %, and a heating rate of 3 $^{\circ}\text{C}/\text{min}$.

Figure C2. Plots of dynamic storage modulus G' and loss modulus G'' of aqueous mixtures of ABC-Q with a concentration of 6 wt% and NP-29.5 with various polymer-to-NP mass ratios versus temperature. The rheological data were collected from oscillatory shear experiments conducted in heating ramps using a frequency of 1 Hz, a strain amplitude of 1 %, and a heating rate of 3 °C/min.



(Figure C2 continued)



(Figure C2 continued)

Figure C3: Plots of dynamic storage modulus G' and loss modulus G'' of aqueous mixtures of ABC-Q with a concentration of 6 wt% and NP-51 with various polymer-to-NP mass ratio versus temperature. The rheological data were collected from heating ramp experiments performed by using a frequency of 1 Hz, a strain amplitude of 1 %, and a heating rate of 3 °C/min.

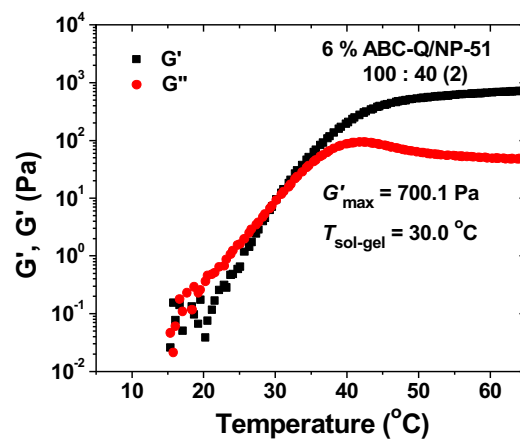
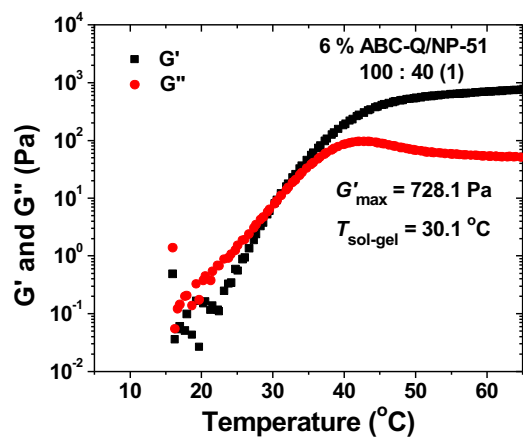
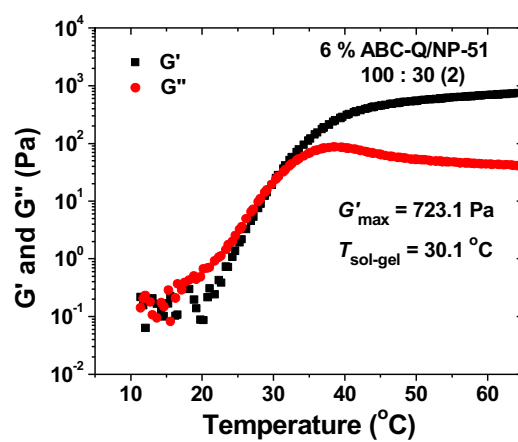
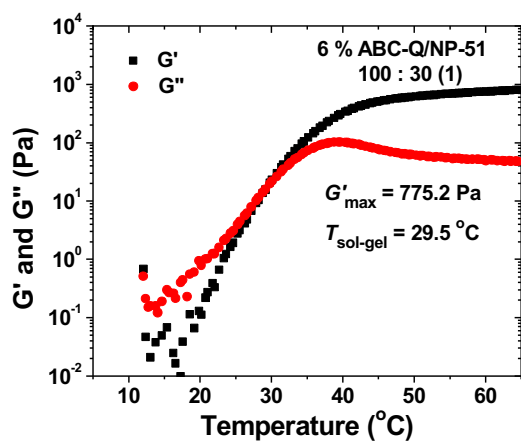
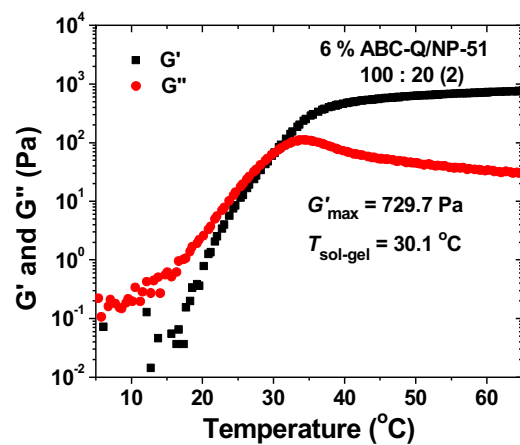
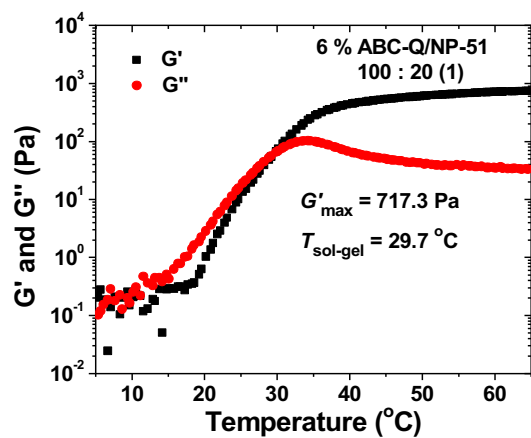


(Figure C3 continued)

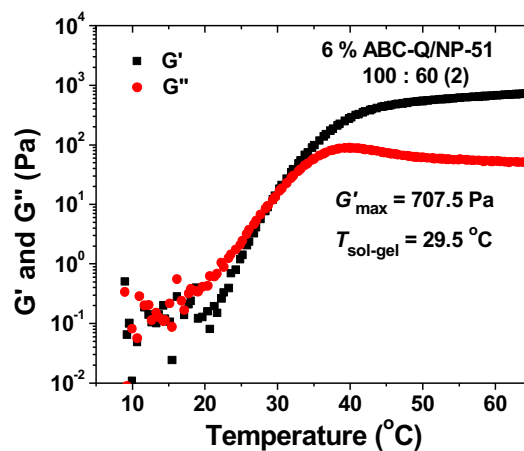
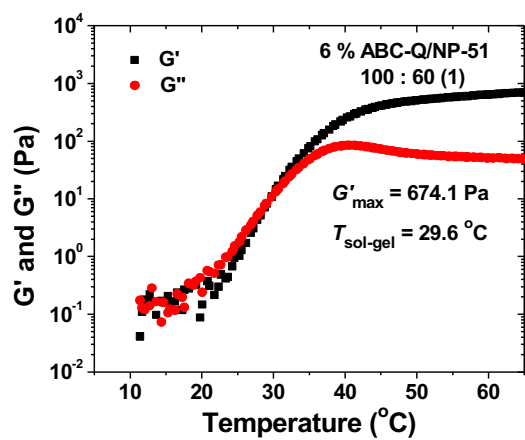
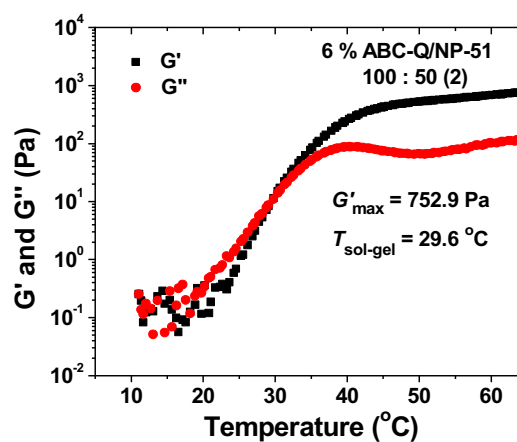
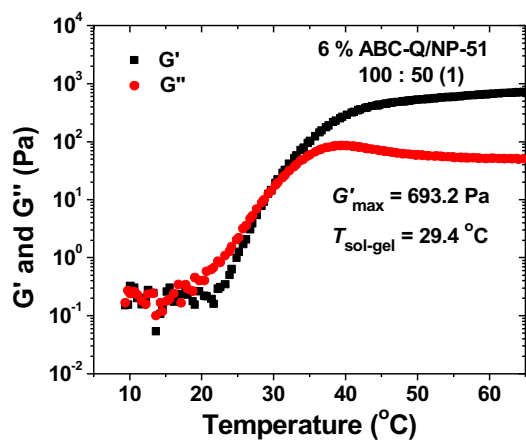


(Figure C3 continued)

Figure C4. Frequency dependences of dynamic storage modulus G' (black square) and loss modulus G'' (red circle) at 40 °C of hybrid 3-D network micellar hydrogels of ABC-Q and NP-29.5 NPs with various NP-to-polymer mass ratios and a polymer concentration of 6 wt % defined as $[(\text{polymer mass})/(\text{polymer mass} + \text{water mass})] \times 100\%$. A strain amplitude of 1.0% was used in the frequency sweep experiments.

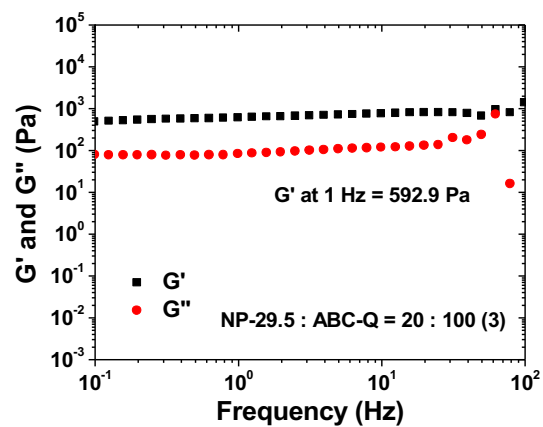
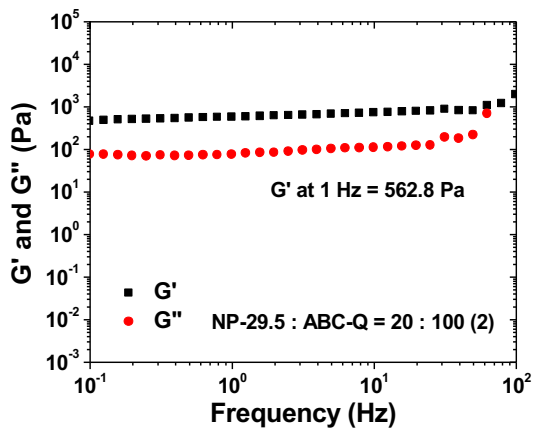
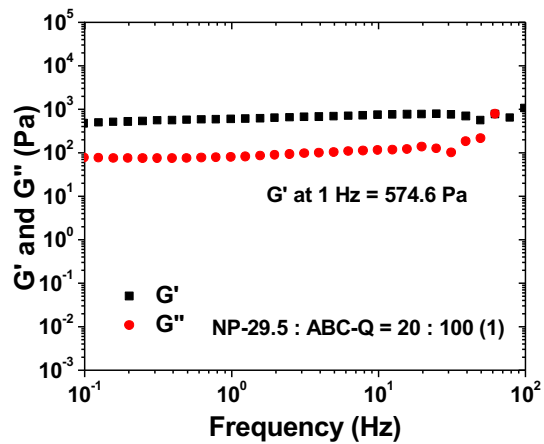
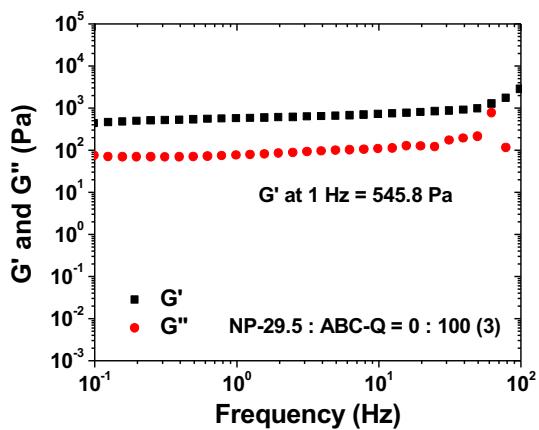
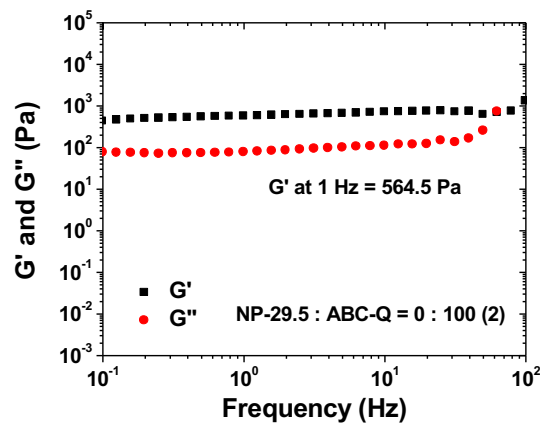
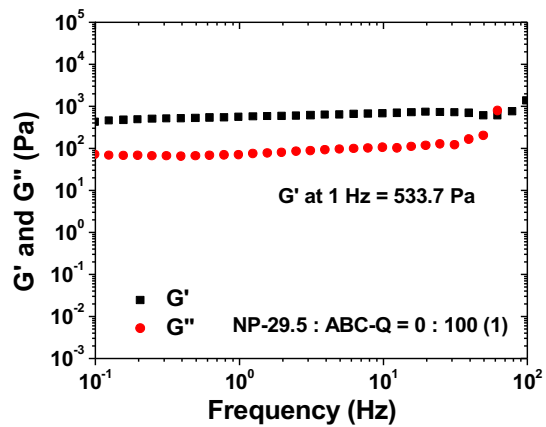


(Figure C4 continued)

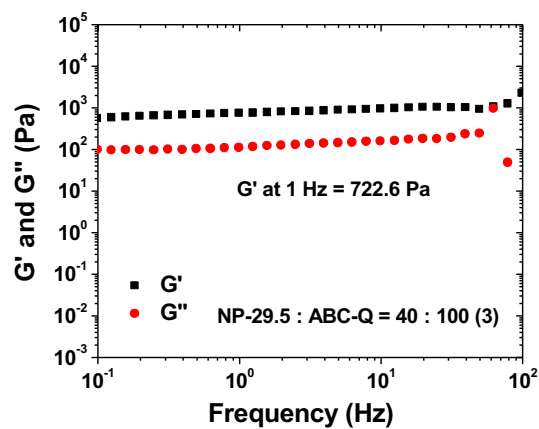
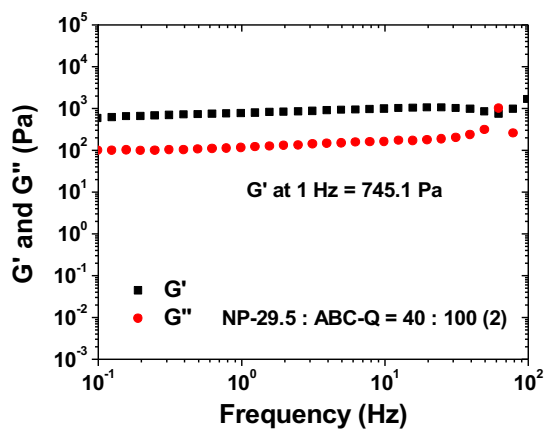
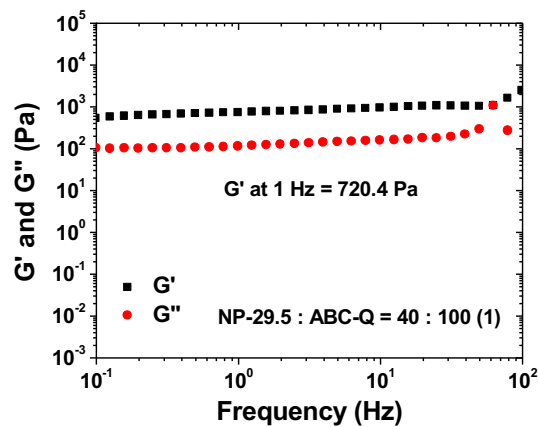
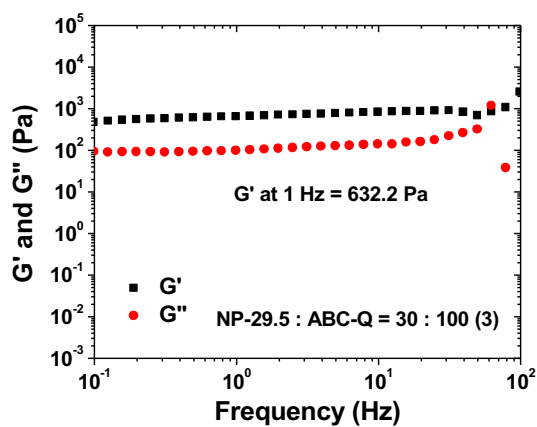
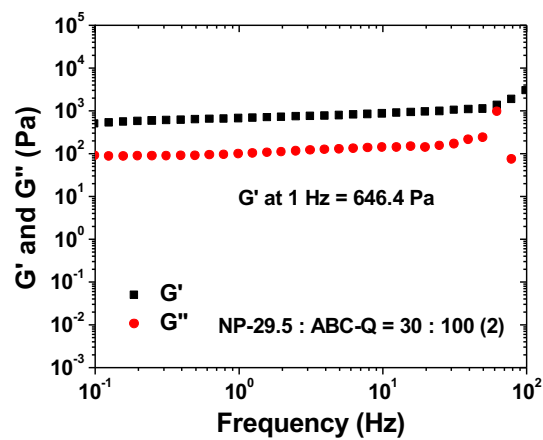
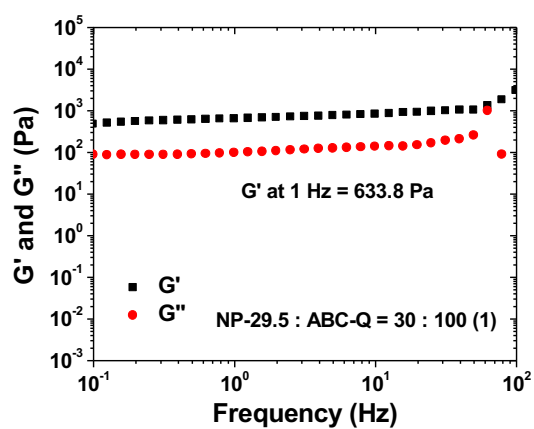


(Figure C4 continued)

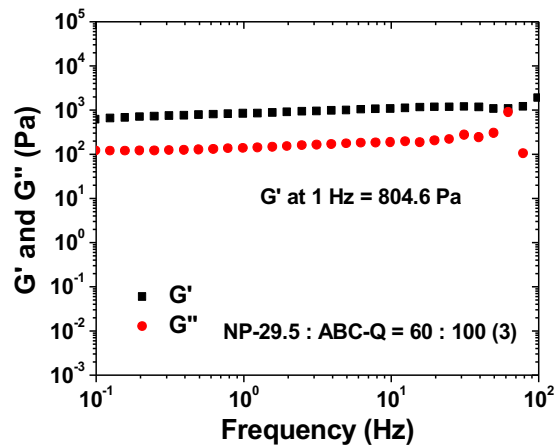
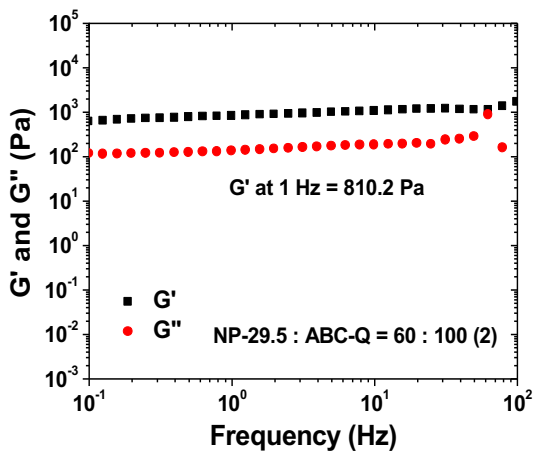
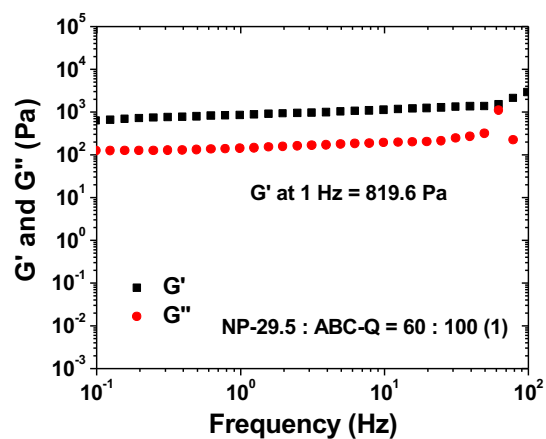
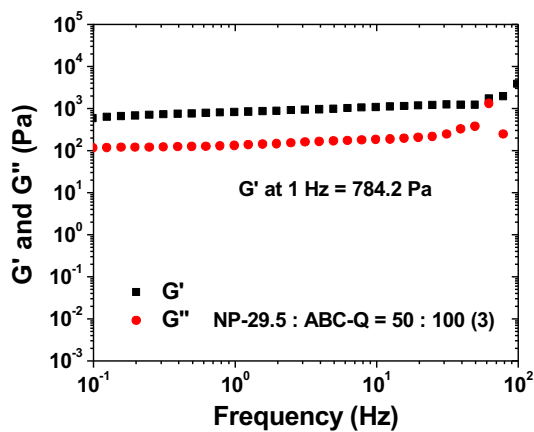
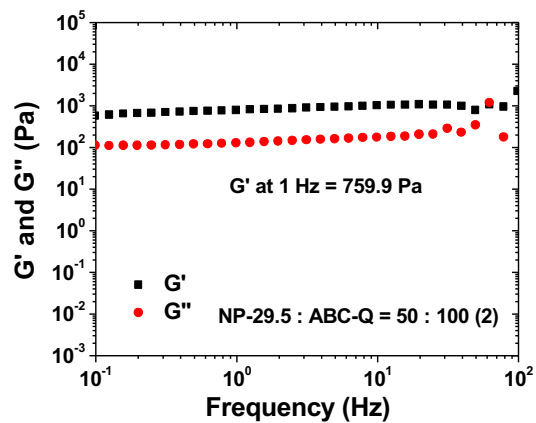
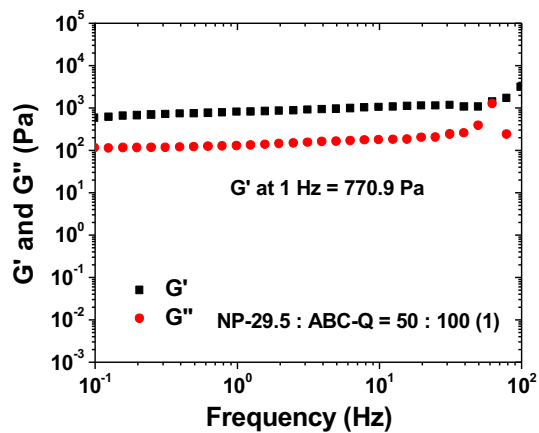


(Figure C4 continued)

Figure C5. Frequency dependences of dynamic storage modulus G' (black square) and loss modulus G'' (red circle) at 40 °C of hybrid 3-D network micellar hydrogels of ABC-Q and NP-51 NPs with various NP-to-polymer mass ratios and a polymer concentration of 6 wt % defined as $[(\text{polymer mass})/(\text{polymer mass} + \text{water mass})] \times 100\%$. A strain amplitude of 1.0% was used in the frequency sweep experiments.

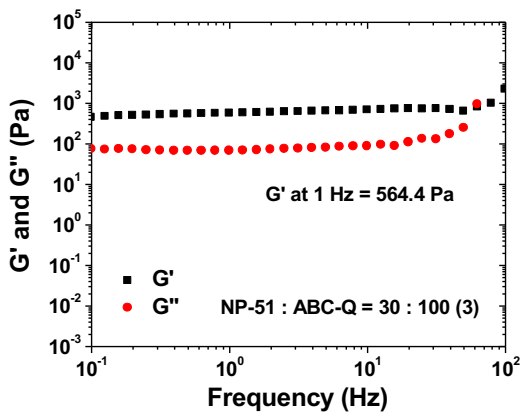
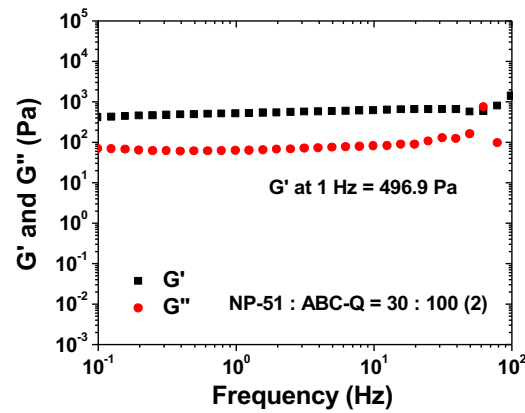
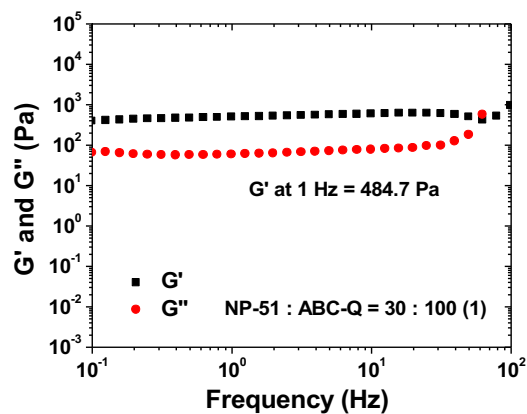
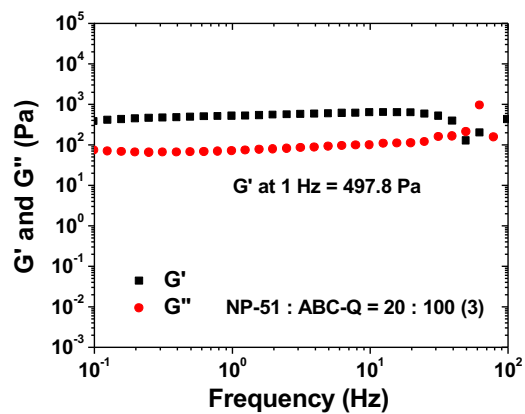
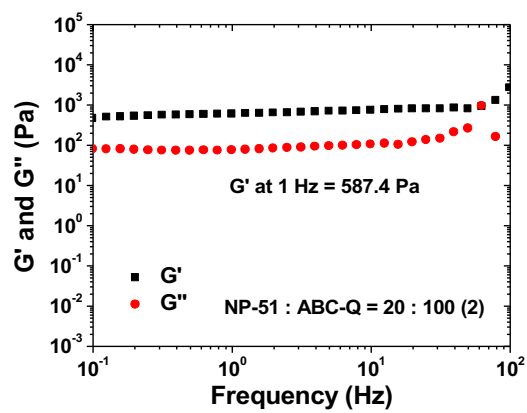
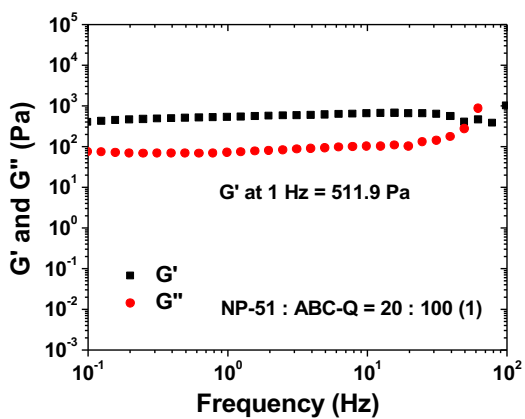


(Figure C5 continued)

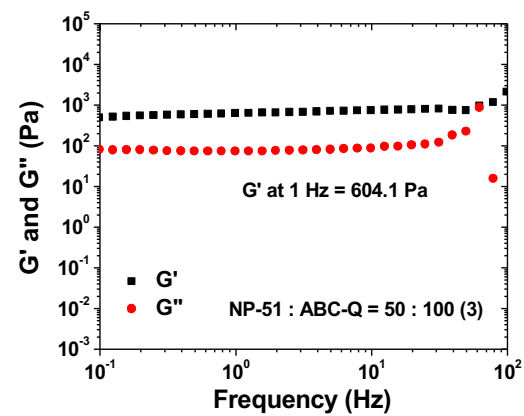
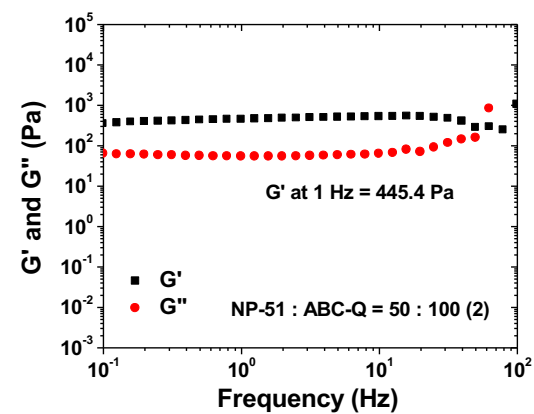
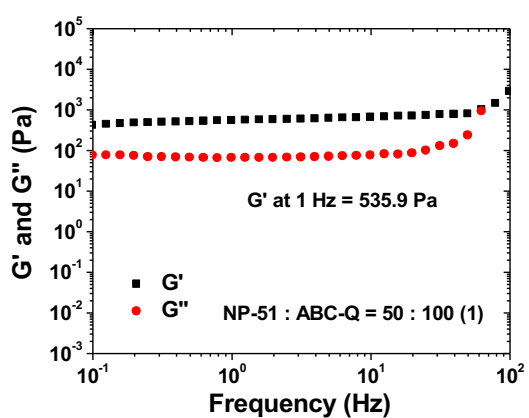
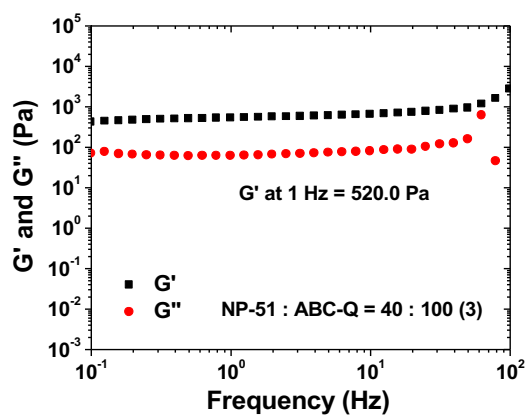
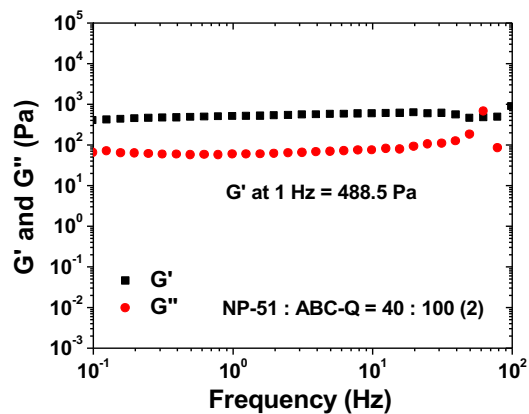
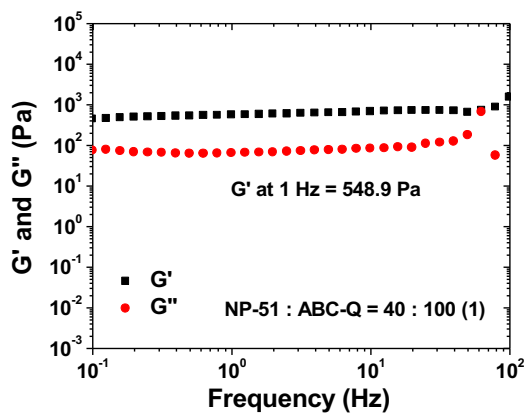


(Figure C5 continued)

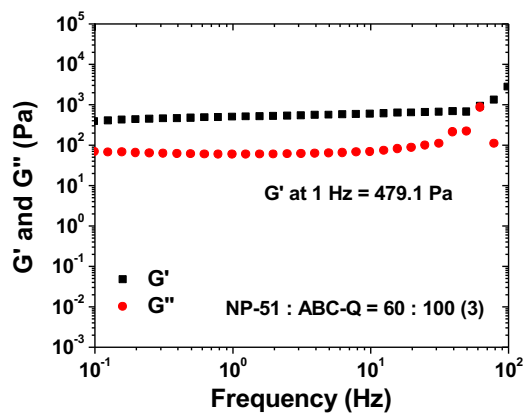
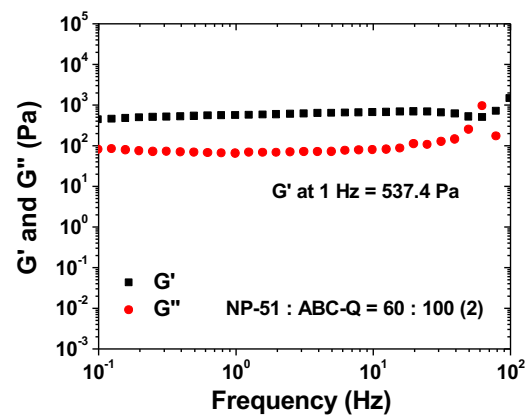
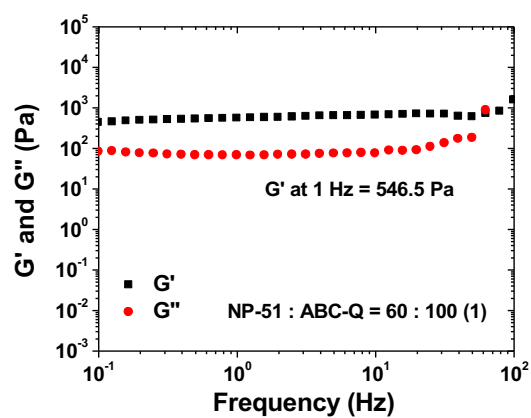


(Figure C5 continued)

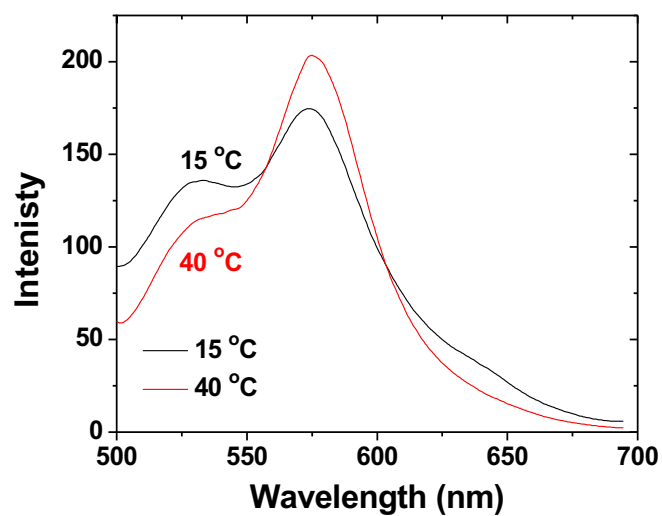


Figure C6. Fluorescence spectra of an aqueous solution at 15 (black curve) and 40 °C (red curve) of ABC-Q with a concentration of 0.40 mg/g loaded with 2.44×10^{-4} mg/g NBD-Cl. NBD-Cl was loaded into the PDEGEMA micelle core at 15 °C.

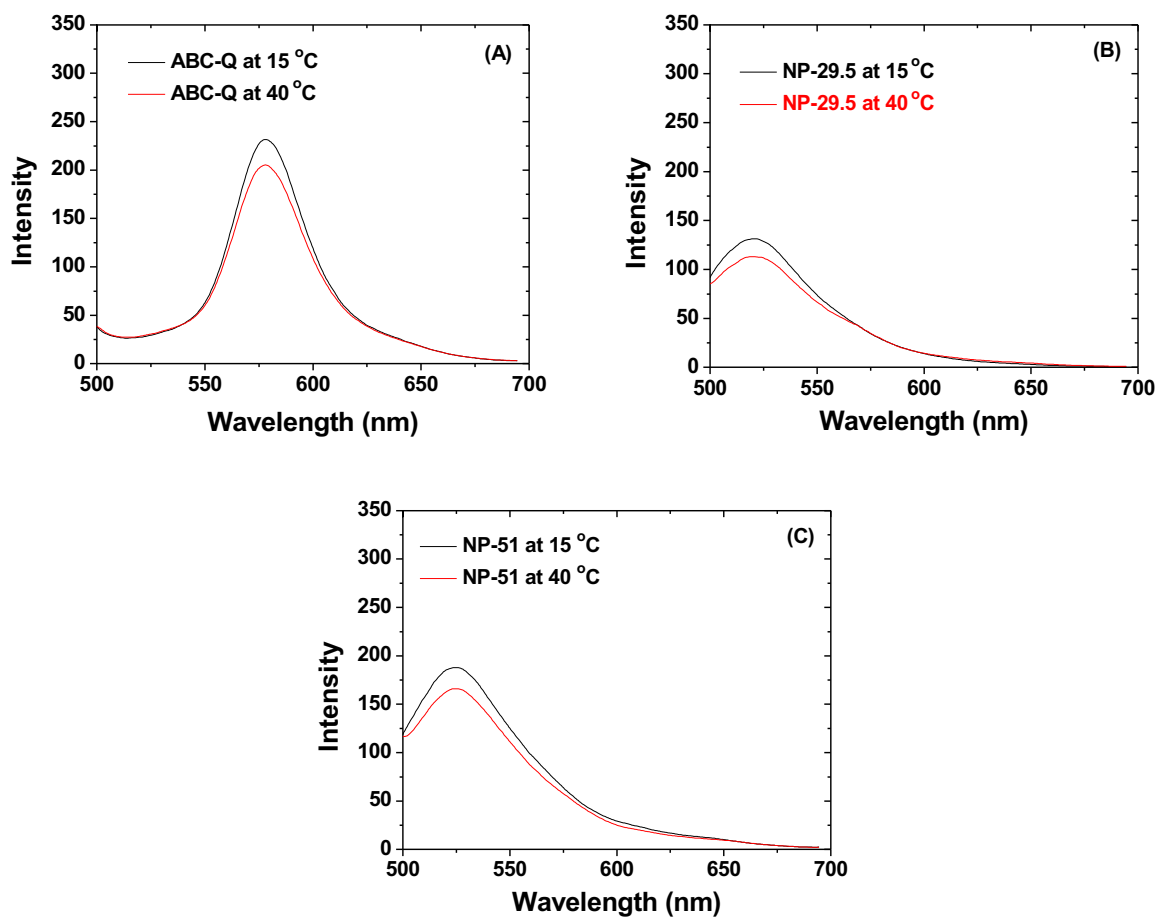


Figure C7. Fluorescence emission spectra of an aqueous solution of (A) ABC-Q with a concentration of 0.414 mg/g, (B) NP-29.5 with a concentration of 0.013 mg/g, (C) NP-51 with a concentration of 0.011 mg/g at both 15 °C and 40 °C.

Chapter 5. Thermosensitive Polymer Brush-Grafted Mesoporous Silica Nanoparticles

Abstract

This chapter describes the synthesis of mesoporous silica nanoparticles (MSNs) with a size of 30-40 nm, the functionalization of MSNs with a bulky chlorodimethylsilane-terminated atom transfer radical polymerization (ATRP) initiator, and the growth of thermoresponsive polymer brushes on MSNs by surface-initiated ATRP. The surface areas of the bare MSNs and poly(di(ethylene glycol) methyl ether methacrylate) (PDEGMMA)-grafted MSNs were measured by Brunauer-Emmett-Teller (BET) method, which were 890 and 4.4 m²/g, respectively. Thermogravimetric analysis (TGA) showed that the weight retentions at 800 °C of the initiator MSNs and PDEGMMA-grafted MSNs were 78.0 % and 45.8 %, respectively. Dynamic light scattering (DLS) studies showed a decrease of hydrodynamic size (D_h) of PDEGMMA-grafted MSNs in water upon heating, from 131 nm at 21 °C to 100 nm at 30 °C. These data indicated that PDEGMMA was confirmed to be grown on the MSNs by surface-initiated ATRP.

5.1. Introduction

In the past years, mesoporous silica nanoparticles (MSNs) were used as potential carriers for drug delivery due to their high surface areas, high drug loading capacity, good biocompatibility and excellent mechanical and chemical stability.¹⁻³ The distinctive properties of MSNs, such as high surface area, high pore volume and tunable pore sizes, allow for an excellent loading capacity and efficient encapsulation of a variety of molecules.

Researchers have taken the advantage of the biodegradability of the nanoparticles in vivo to release the drug from the MSNs, but it is difficult to control the degradation of MSNs, and thus the therapeutic efficiency is compromised. One alternative that has been developed recently is the MSN-based stimuli-responsive drug delivery systems, which allow for triggered release of therapeutic drugs at the diseased site by external stimuli, such as temperature, pH, light, magnetic fields and ultrasounds.⁴⁻⁹ In addition, the poor dispersibility of MSNs in water limits their potential in vivo biomedical applications. Therefore, there is a need to design and synthesize MSNs with a good dispersibility and a capability of controlling drug release, which will improve the efficiency of drug delivery.

A simple delivery system is based on a combination of MSNs with temperature-responsive polymers in which the access to mesopores is controlled by temperature. Temperature-responsive polymers that exhibit a lower critical solution temperature (LCST) in water, such as poly(*N*-isopropylacrylamide) (PNIPAM) with a LCST at $\sim 32\text{ }^{\circ}\text{C}$, can be used and grafted onto the MSNs. At temperatures below the LCST, these polymers are in the hydrated state with coil conformations; above the LCST, the polymers are in the collapsed state.

Generally there are two methods to graft polymers onto the mesoporous silica nanoparticle surface: “grafting to” and “grafting from”. For the “grafting to” method, the preformed, end-

functionalized polymers are grafted onto the nanoparticles. For example, Oupicky and coworkers used the thiol-functionalized MSNs with sizes of 80-90 nm to react with pyridyl disulfide-terminated PNIPAM.¹⁰ Sugawaka et al. made PNIPAM-grafted mesoporous silica composites by using azide-functionalized MSNs and alkynyl-terminated PNIPAM.¹¹ However, it is usually hard to achieve high grafting densities by “grafting to”. For the “grafting from” method, an initiator is immobilized onto the surface of nanoparticles, followed by surface-initiated polymerization to grow polymer brushes. In recent years, “living”/controlled polymerization techniques, e.g., atom transfer radical polymerization (ATRP) and reversible addition-fragmentation chain transfer polymerization (RAFT), have been widely employed because they allow for the synthesis of polymer brushes with predetermined molecular weights, narrow polydispersities and high and controllable grafting densities.¹²⁻¹³ For ATRP, an ATRP initiator is first fixed on the MSNs, followed by surface-initiated ATRP (SI-ATRP) to grow polymers from the MSNs.¹⁴⁻¹⁷ Similarly, for RAFT, a CTA is immobilized onto the MSNs first.¹⁸⁻¹⁹

Here we presented the synthesis of thermoresponsive polymer-grafted MSNs. Bare MSNs were prepared using a literature method,²⁰ and surface functionalized with a bulky chlorodimethylsilane-terminated ATRP initiator which is anchored by a maleimide-anthracene cycloadduct, followed by the surface-initiated ATRP of di(ethylene glycol) methyl ether methacrylate to make thermosensitive polymer-modified MSNs.

5.2. Experimental Section

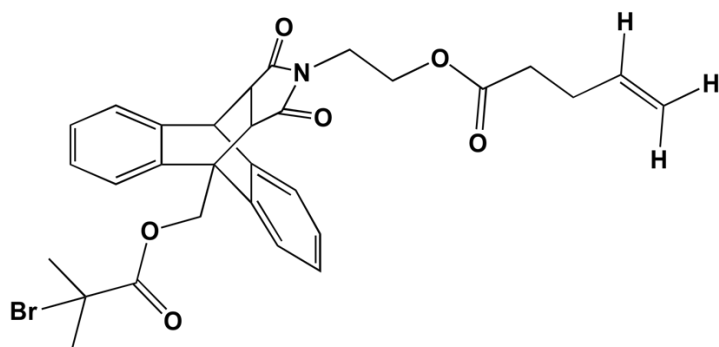
5.2.1. Materials

Triethanolamine (99.5 %, Sigma-Aldrich), cetyltrimethylammonium bromide (CTAB, 99 %, Fisher Scientific), tetraethyl orthosilicate (TEOS, 98 %, Acros) and chlorodimethylsilane (96 %, Acros)

Fisher Scientific) were used as received. The platinum-divinyltetramethyldisiloxane complex in xylene with a Pt concentration of 2.1 – 2.4 % was purchased from Gelest, Inc. CuBr (98 %, Aldrich) was purified via a procedure described previously.²¹ *N,N,N',N',N''*-Pentamethyldiethylenetriamine (PMDETA, 99%, Aldrich), ethyl 2-bromoisobutyrate (EBiB, 98%, Aldrich), and di(ethylene glycol) methyl ether methacrylate (DEGMMA, 97%, TCI America) were each stirred with CaH₂, distilled under reduced pressure, and stored in a refrigerator. The ATRP initiator, anchored by a maleimide-anthracene cycloadduct, 2-(9-(((2-bromo-2-methylpropanoyl)oxy)methyl)-12,14-dioxo-11,12,14,15-tetrahydro-9*H*-9,10-[3,4] epipyrroloanthracen-13(10*H*)-yl)ethyl pent-4-enoate (MA=, Scheme 5.1) was provided by Dr. Jun Li as a gift.²² All other chemical reagents were purchased from either Fisher Scientific/Acros or Aldrich and used without further purification unless otherwise noted.

5.2.2. General Characterization

NMR spectra were recorded on a Varian Mercury 300 NMR spectrometer or a Varian VNMR 500 MHz spectrometer, and the residual solvent proton signal was used as reference. Size exclusion chromatography (SEC) of the PDEGMMA free polymers formed in the synthesis of mesoporous silica NPs was carried out at room temperature using PL-GPC 20 (Polymer Laboratories, Inc.) equipped with a refractive index detector, one PLgel 5 μ m guard column (50 \times 7.5 mm), and two PLgel 5 μ m mixed-C columns (each 300 \times 7.5 mm, linear range of molecular weight from 200 to 2 000 000 Da). THF was used as the solvent and the flow rate was 1.0 mL/min. The SEC system was calibrated with narrow-dispersed polystyrene standards, and the SEC data were processed using Cirrus GPC/SEC software. The DLS measurements were performed on a Malvern Zetasizer Nano ZS equipped with a He-Ne 633 nm laser and a temperature controller at a scattering angle of 173°. Thermogravimetric analysis (TGA) of nanoparticles was performed in



Scheme 5.1. Molecular Structure of the ATRP Initiator, 2-(9-(((2-Bromo-2-Methylpropanoyl)Oxy)Methyl)-12,14-Dioxo-11,12,14,15-Tetrahydro-9H-9,10-[3,4]Epipyrroloanthracen-13(10H)-yl)Ethyl Pent-4-Enoate (MA=)

air at a heating rate of 20 °C/min from room temperature to 800 using a TA Discovery TGA-MS. Transmission electron microscopy (TEM) of initiator-functionalized and PDEGMMA-grafted mesoporous silica NPs was performed using a Zeiss Libra 200 HT FE MC microscope with an accelerating voltage of 200 kV, and bright field images were taken with a bottom-mounted Gatan UltraScan US100XP CCD camera. Samples were drop-cast from dispersions in THF with a concentration of 1 mg/mL onto a carbon-coated, copper TEM grid using a glass pipette and were allowed to dry at ambient conditions. The BET surface area was determined by Brunauer-Emmett-Teller (BET) theory.

5.2.3. Synthesis of Mesoporous Silica Nanoparticles (MSNs) with Sizes of 30-40 nm

Mesoporous silica nanoparticles with sizes of 30-40 nm were synthesized according to a literature procedures with slight modifications.²⁰ Triethanolamine (0.411 g, 2.75 mmol) and CTAB (2.084 g, 5.72 mmol) were added to 120 mL of water, and the solution was stirred at 80 °C for 30 min. TEOS (2.343 g, 11.2 mmol) was then added to the CTAB solution, and the mixture was stirred vigorously at 80 °C for 6 h until a colloidal state was achieved. The synthesized nanoparticles were centrifuged and washed thoroughly with methanol. The size of the colloidal mesostructured silica nanoparticles was 36.2 nm according to DLS. The surface area of the mesoporous silica nanoparticles was measured by BET, which was 890 m²/g.

To remove the surfactant template, mesoporous silica nanoparticles (210 mg) were dispersed in methanol (100 mL), mixed with concentrated HCl (12 M, 5.0 mL), refluxed overnight under N₂, and then washed extensively with methanol and water.

5.2.4. Synthesis of PDEGMMA-Grafted Mesoporous Silica Nanoparticles (PDEGMMA-MSNs)

A bulky ATRP initiator silane was synthesized by the hydrosilylation reaction between MA= (Scheme 5.1) and chlorodimethylsilane. MA= (521.9 mg, 0.700 mmol), chlorodimethylsilane (2 mL), and the platinum-divinyltetramethyldisiloxane complex in xylenes (2.1-2.4 % platinum concentration, 100 μ L) were added into a 50 mL two-necked flask, followed by adding 6 mL dry THF. The mixture was stirred at room temperature under N₂, and ¹H NMR spectroscopy analysis was used to monitor the reaction. After the reaction was complete, THF and excess chlorodimethylsilane was removed under vacuum, yielding the bulky ATRP initiator silane (MA-CDMS).

To immobilize the chlorodimethylsilane-terminated bulky ATRP initiator (MA-CDMS) onto the mesoporous silica nanoparticles, mesoporous silica nanoparticles (518 mg) was added into a 50 mL two-necked round bottom flask along with dry THF (20 mL), and MA-CDMS (506.8 mg, 0.604 mmol). The flask was placed in an oil bath with a preset temperature of 70 °C, and the reaction was run over a period of 3 days. The initiator nanoparticles were then dispersed in DMF and separated by ultracentrifugation (Beckman Optima L-90K Ultracentrifuge with type 60 Ti rotor, 35,000 rpm, 60 min). This dispersion-centrifugation cycle was repeated three more times. The initiator NPs were then dried under a nitrogen flow overnight.

To synthesize PDEGMMA-grafted mesoporous silica nanoparticles, CuBr (16.6 mg, 115 μ mol), initiator MSNs (98.4 mg), and DMF (12.82 g) were added into a two-necked flask. The mixture was sonicated in an ultrasonic water bath to form a homogeneous dispersion. DEGMMA (4.284 g, 22.8 mmol) and ethyl 2-bromoisobutyrate (19.5 mg, 100 μ mol) were then added into the flask. After the mixture was degassed by three freeze-pump-thaw cycles, PMDETA (20.1 mg, 116

μmol) was injected into the flask at the thawing point of the frozen mixture by using a microsyringe. The flask was then placed in an oil bath with a preset temperature of 45 °C, and the progress of the polymerization was monitored by ^1H NMR spectroscopy analysis. After 3 h and 5 min, the flask was taken out from the oil bath and opened to air, and an aliquot was withdrawn immediately for ^1H NMR spectroscopy analysis to determine the monomer conversion. The mixture was diluted with THF (20 mL), and the polymer-grafted MSNs were isolated by ultracentrifugation at 35 k rpm for 60 min. The NPs were then dispersed in THF and separated again by centrifugation. This dispersion-centrifugation washing process was repeated for a total of 5 times. The free polymer PDEGMMA was analyzed by SEC relative to polystyrene standards. The values of $M_{n,\text{SEC}}$ and PDI were 25.1 k and 1.24, respectively. The monomer conversion was 54.1 %, determined by ^1H NMR spectroscopy analysis. The degree of polymerization (DP) of the polymer was 123, which was calculated from the monomer conversion and free initiator. The surface area of the mesoporous silica nanoparticles was measured by BET, which was 4.4 m^2/g .

5.3. Results and Discussion

5.3.1. Synthesis of Mesoporous Silica Nanoparticles (MSNs)

The bare mesoporous silica NPs (MSNs) were prepared by using CTAB as surfactant templates and TEOS as silica source according to the method reported by Yamada et al.²⁰ After the reaction, the surfactant template was extracted by using concentrated HCl. Both DLS and TEM were used to characterize MSNs. The size of the colloidal mesostructured silica nanoparticles was 36.2 nm. Figure 5.1A showed that the MSNs have a spherical shape. Brunauer-Emmett-Teller (BET) method was also used to characterize the MSNs' BET surface area, which was found to be 890 m^2/g . These results indicate that the obtained MSNs were suitable for further modification to grow

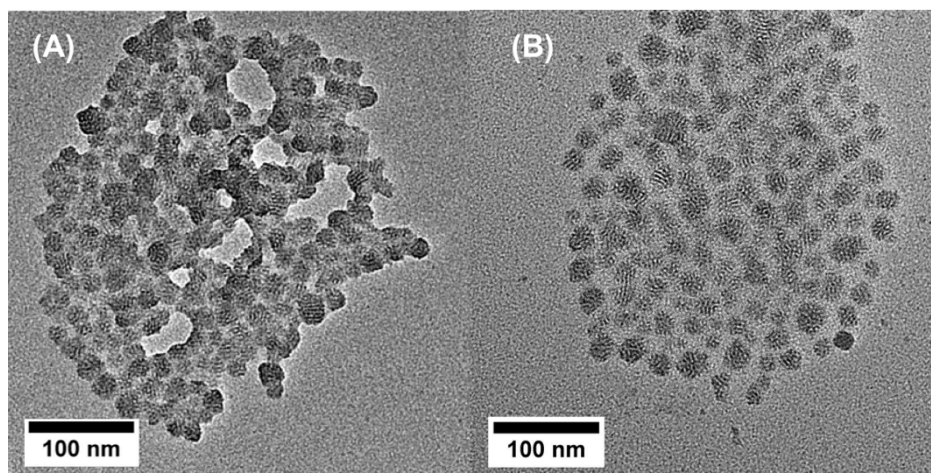


Figure 5.1. TEM pictures of (A) ATRP initiator-functionalized MSNs and (B) PDEGMMA-grafted MSNs (PDEGMMA-MSNs).

polymer brushes.

The size of bare MSNs can be tuned by using different types of tetraalkoxysilane. According to Yamada et al., the mean nanoparticle diameter increases in the order tetramethoxysilane (TMOS), tetraethoxysilane (TEOS), tetrapropoxysilane (TPOS), and tetrabutoxysilane (TBOS) from 19 ± 10 nm, to 30 ± 20 nm, 43 ± 25 nm and 78 ± 50 nm, respectively.²⁰

5.3.2. Synthesis of PDEGMMA-Grafted Mesoporous Silica Nanoparticles (PDEGMMA-MSNs)

A bulky chlorodimethylsilane-terminated ATRP initiator (MA-CDMS) was synthesized via a hydrosilylation reaction between MA= \equiv and chlorodimethylsilane. Since chlorodimethylsilane is very sensitive to water moisture, dry THF was used as medium for the immobilization reaction. The mass ratio of the initiator silane and MSNs used here was 1.02 : 1.00, and the immobilization reaction was carried out at 70 °C under N₂ for over three days. The initiator MSNs were purified by ultracentrifugation.

PDEGMMA were then grown from the initiator MSNs by surface-initiated ATRP of DEGMMA at 45 °C using CuBr/PMDETA as catalyst in the presence of free initiator EBiB. After a desired monomer conversion was reached, the polymerization was stopped and the obtained PDEGMMA-grafted MSNs were purified by repetitive dispersion in THF and ultracentrifugation. The number average molecular weight and the PDI of free polymer PDEGMMA were 25.1 kDa and 1.24 (Figure 5.2), respectively, relative to polystyrene standards, indicating that the polymerization was controlled. The ¹H NMR spectrum of the PDEGMMA-MSNs dispersion in CDCl₃ was recorded and is shown in Figure 5.3. The broad peak at 4.1 ppm corresponds to the –COOCH₂ of PDEGMMA, indicating the PDEGMMA was successfully grafted onto the MSNs. The degree of polymerization (DP) of the polymer was 123, which was calculated from the

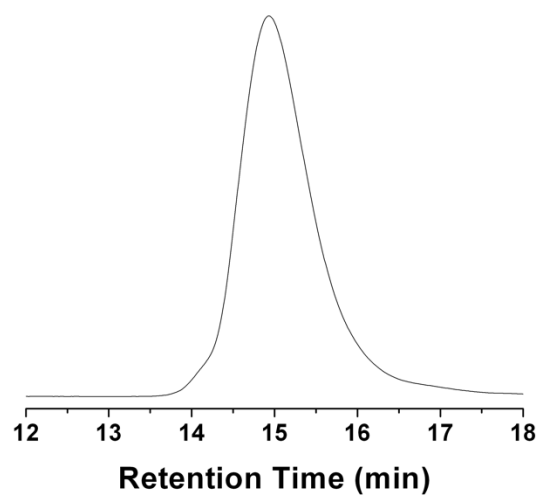


Figure 5.2. SEC trace of the free polymer PDEGMMA formed from the free initiator in the synthesis of PDEGMMA-grafted MSNs by surface-initiated atom transfer radical polymerization.

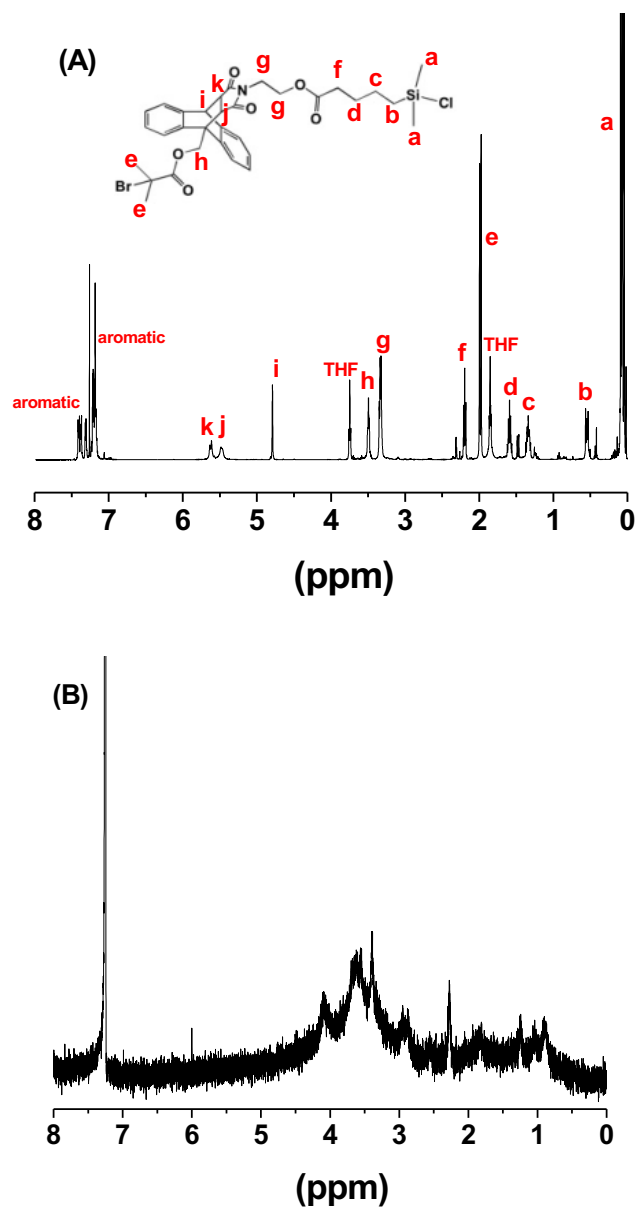


Figure 5.3. ^1H NMR spectra of (A) chlorodimethylsilane-terminated ATRP initiator (MA-CDMS) and (B) PDEGMMA grafted MSNs (in CDCl_3).

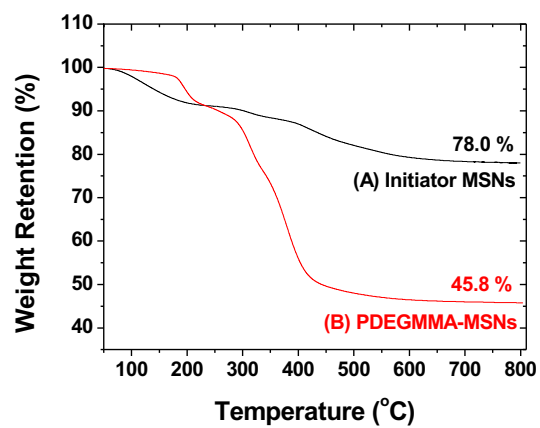


Figure 5.4. TGA data of ATRP initiator-functionalized MSNs and PDEGMMA-grafted mesoporous silica NPs.

monomer conversion and free initiator. Figure 5.4 shows the TGA curves of the ATRP initiator-functionalized MSNs and PDEGMMA-grafted MSNs. Clearly, PDEGMMA was successfully grown from the NPs as indicated by a weight retention of 45.8 % at 800 °C, in contrast to 78.0 % for the initiator MSNs. The nitrogen adsorption experiment also showed that the surface area of PDEGMMA-grafted MSNs was only 4.4 m²/g, in contrast to 890 m²/g. The BET data suggest that the pore accessibility and specific surface areas were sacrificed to a large extent. This might be caused by the PDEGMMA brushes grafted inside the pore of the nanoparticles. To prevent this, the surfactant template can be removed after the surface initiated polymerization under mild conditions. Figure 5.1B shows a typical TEM micrograph of PDEGMMA-grafted MSNs. The spherical morphology of MSNs remained after the PDEGMMA polymer was grown, and the mesopores can be clearly seen. Different from initiator MSNs, the interparticle distance is larger, indicating the presence of the grafted PDEGMMA polymer. DLS was employed to study the thermoresponsive property of PDEGMMA-grafted MSNs in water. Figure 5.5 shows the average apparent hydrodynamic size (D_h) of PDEGMMA-MSNs in water at a concentration of 1.0 mg/g as a function of temperature. The D_h gradually decreased with increasing temperature, from 131 nm in the temperature range of 14 – 20 °C to 100 nm at 30 °C. The onset temperature of the LCST transition was 21 °C, and the LCST transition continued over a temperature range of 7 °C. The lower LCST of PDEGMMA grafted on nanoparticles in accordance with our group's previous observations that the LCST of polymer brushes is lower by a few degrees than that of the corresponding free polymer in water.²³⁻²⁴

5.4. Conclusions

Thermoresponsive PDEGMMA-grafted MSNs have been prepared from initiator-functionalized MSNs by SI-ATRP. TEM, NMR, TGA and DLS studies confirmed the grafting of

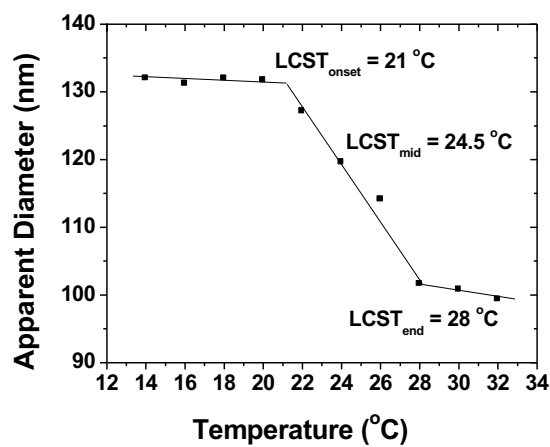


Figure 5.5. Plot of the average apparent hydrodynamic size D_h , obtained from CONTIN analysis, as a function of temperature from a dynamic light scattering study of a 1.0 mg/g aqueous dispersion of PDEGMMA brush-grafted mesoporous silica nanoparticles (PDEGMMA-MSNs).

PDEGMMA on MSNs. The thermosensitive hairy MSNs can be used as drug delivery vehicles and can be incorporated into injectable hydrogels, however the synthesis needs to be optimized. The preliminary work described in this Chapter serves as a starting point for future work on hybrid injectable hydrogels of thermosensitive triblock copolymers and mesoporous silica nanoparticles.

5.5. References

1. Slowing, I. I.; Vivero-Escoto, J. L.; Trewyn, B. G.; Lin, V. S. Y. *J. Mater. Chem.* **2010**, *20*, 7924-7937.
2. Singh, N.; Karambelkar, A.; Gu, L.; Lin, K.; Miller, J. S.; Chen, C. S.; Sailor, M. J.; Bhatia, S. N. *J. Am. Chem. Soc.* **2011**, *133*, 19582-19585.
3. Li, Z.; Barnes, J. C.; Bosoy, A.; Stoddart, J. F.; Zink, J. I. *Chem. Soc. Rev.* **2012**, *41*, 2590-2605.
4. Gao, Q.; Xu, Y.; Wu, D.; Sun, Y.; Li, X. *J. Phys. Chem. C* **2009**, *113*, 12753-12758.
5. Baeza, A.; Guisasola, E.; Ruiz-Hernández, E.; Vallet-Regí, M. *Chem. Mater.* **2012**, *24*, 517-524.
6. Lai, J.; Mu, X.; Xu, Y.; Wu, X.; Wu, C.; Li, C.; Chen, J.; Zhao, Y. *Chem. Commun.* **2010**, *46*, 7370-7372.
7. Ruiz-Hernández, E.; Baeza, A.; Vallet-Regí, M. *ACS Nano* **2011**, *5*, 1259-1266.
8. Paris, J. L.; Cabañas, M. V.; Manzano, M.; Vallet-Regí, M. *ACS Nano* **2015**, *9*, 11023-11033.
9. Baeza, A.; Colilla, M.; Vallet-Regí, M. *Expert Opin. Drug Deliv.* **2015**, *12*, 319-337.
10. You, Y.-Z.; Kalebaila, K. K.; Brock, S. L.; Oupický, D. *Chem. Mater.* **2008**, *20*, 3354-3359.
11. Murakami, K.; Watanabe, S.; Kato, T.; Sugawara, K. *J. Colloid Interface Sci.* **2013**, *419*, 223-227.
12. Qu, Z.; Xu, H.; Gu, H. *ACS Appl. Mater. Interfaces* **2015**, *7*, 14537-14551.
13. Huang, X.; Hauptmann, N.; Appelhans, D.; Formanek, P.; Frank, S.; Kaskel, S.; Temme, A.; Voit, B. *Small* **2012**, *8*, 3579-3583.
14. Yang, Y.; Yan, X.; Cui, Y.; He, Q.; Li, D.; Wang, A.; Fei, J.; Li, J. *J. Mater. Chem.* **2008**, *18*, 5731-5737.

15. Yang, J.; Shen, D.; Zhou, L.; Li, W.; Li, X.; Yao, C.; Wang, R.; El-Toni, A. M.; Zhang, F.; Zhao, D. *Chem. Mater.* **2013**, *25*, 3030-3037.
16. Mai, W.; Sun, B.; Chen, L.; Xu, F.; Liu, H.; Liang, Y.; Fu, R.; Wu, D.; Matyjaszewski, K. *J. Am. Chem. Soc.* **2015**, *137*, 13256-13259.
17. Sun, J.-T.; Hong, C.-Y.; Pan, C.-Y. *J. Phys. Chem. C* **2010**, *114*, 12481-12486.
18. Hong, C.-Y.; Li, X.; Pan, C.-Y. *J. Phys. Chem. C* **2008**, *112*, 15320-15324.
19. Wan, X.; Wang, D.; Liu, S. *Langmuir* **2010**, *26*, 15574-15579.
20. Yamada, H.; Urata, C.; Aoyama, Y.; Osada, S.; Yamauchi, Y.; Kuroda, K. *Chem. Mater.* **2012**, *24*, 1462-1471.
21. O'Lenick, T. G.; Jin, N.; Woodcock, J. W.; Zhao, B. *J. Phys. Chem. B* **2011**, *115*, 2870-2881.
22. Li, J.; Shiraki, T.; Hu, B.; Wright, R. A. E.; Zhao, B.; Moore, J. S. *J. Am. Chem. Soc.* **2014**, *136*, 15925-15928.
23. Hu, B.; Henn, D. M.; Wright, R. A. E.; Zhao, B. *Langmuir* **2014**, *30*, 11212-11224.
24. Hu, B.; Wright, R. A. E.; Jiang, S.; Henn, D. M.; Zhao, B. *Polymer* **2016**, *82*, 206-216.

Chapter 6. Conclusions and Future Work

The hybrid hydrogels investigated in this dissertation work consist of thermosensitive triblock copolymers and thermoresponsive polymer brush-grafted nanoparticles (hairy NPs). The thermosensitive hydrophilic ABA triblock copolymers, P(DEGMMA-*co*-DEGEMA-*co*-RhBMA)-*b*-PEO-*b*-P(DEGMMA-*co*-DEGEMA-*co*-RhBMA), used in Chapter 2 and 3 were synthesized by atom transfer radical polymerization (ATRP) from a difunctional PEO macroinitiator with a molecular weight of 20 kDa. ATRP is a “living”/controlled radical polymerization technique that is widely used for the synthesis of ABA triblock copolymers and AB diblock copolymers.^{1,2} The ABC triblock copolymer, PDEGEMA-*b*-P(TMAEMA-I)-*b*-(PDEGMMA-*co*-RhBMA), used in Chapter 4 was synthesized by reversible addition-fragmentation chain transfer (RAFT) polymerization and subsequent post-polymerization modification. Thermoresponsive polymer-grafted silica NPs with different LCSTs were synthesized via surface-initiated atom transfer radical polymerization (SI-ATRP) technique, which is widely used for the synthesis of hairy silica NPs with different sizes.³⁻⁶ Different monomers were used for each hairy NP sample to tune their LCSTs. Rheological measurements were employed to study the properties of hybrid network hydrogels.

Chapter 2 presents a method to control and tune the locations of thermoresponsive hairy NPs in the thermosensitive polymer network hydrogels. The different locations of NPs, either inside or outside micellar cores, were realized by controlling the LCST of hairy NPs ($LCST_{NP}$) relative to that of the thermosensitive outer blocks of ABA ($LCST_{ABA}$).⁷ When the $LCST_{NP}$ was similar to $LCST_{ABA}$, the NPs were located in the core of micelles upon heating above their LCSTs. When the $LCST_{NP}$ was much higher than $LCST_{ABA}$, the NPs were located in the interstitial space of micelles. The locations of NPs in the ABA polymer networks were confirmed by fluorescent resonance energy transfer (FRET) at dilute concentrations, while the effects of different locations

of hairy NPs of hybrid network hydrogels formed from 10 wt% ABA aqueous solutions were studied by rheological measurements. When the NPs were inside the core of micelles, the dynamic storage modulus G' of the gels and the sol-gel transition temperature ($T_{\text{sol-gel}}$) exhibited little change with increasing NP-to-polymer mass ratio. On the other hand, the hairy NPs in the interstitial space affected the formation of polymer networks and increased the fraction of polymer loops, resulting in lower G' and slightly higher $T_{\text{sol-gel}}$. In addition, for gels with NPs in the interstitial space, a noticeable increase in G' was observed in the heating ramps around LCST_{NP} , which was caused by the collapsed hairy NPs adsorbing polymer chains in the dangling and loop forms, increasing the density of bridging chains.

As a follow up work of Chapter 2, Chapter 3 presents a study of the effect of LCST transition of hairy NPs initially located in the interstitial space on properties of hybrid micellar network hydrogels.⁸ Four batches of thermoresponsive polymer-grafted NPs with different LCSTs but all higher than the LCST of the ABA triblock copolymer were synthesized. Rheological measurements were conducted to study the effects of LCST transition of hairy NPs on hybrid micellar network hydrogels of ABA with a concentration of 10 wt%. The dynamic storage modulus G' exhibited a sharp increase in the heating ramp at a temperature corresponding to the LCST transition of hairy NPs for all hybrid hydrogels. This phenomenon was caused by the collapse of the brushes on NPs triggering the absorption of thermosensitive outer blocks of ABA in the dangling and loop forms and the reorganization of the 3-D network structure, which increased the density of bridging chains and thus the G' . This explanation was supported by the results from FRET studies.

For hydrophilic ABA triblock copolymers composed of thermosensitive outer blocks, the temperature-induced micellization and gelation in water occur simultaneously, which has been

considered as one main reason that a significant portion of block copolymer molecules form loops during the gelation process. Differently, for doubly thermoresponsive linear ABC triblock copolymers with different LCSTs for the two outer blocks, the micellization and gelation can be separate, stepwise processes. Chapter 4 describes a method to enhance the gelation efficiency of a doubly thermosensitive hydrophilic linear ABC triblock copolymer in water using thermoresponsive polymer-grafted NPs with a LCST that is similar to LCST of the C block.⁹ The rheological studies showed that there was a 45 % increase in G' when the hairy NPs were added into the aqueous solution of the ABC triblock copolymer with a concentration of 6 wt% at the NP-to-polymer ratio of 60 :100. This is because the hairy NPs can act as “seeds” to adsorb the collapsed higher LCST block of the ABC copolymer, promoting the formation of bridging chains among micellar cores and thus enhancing the gelation efficiency. In contrast, when the LCST of hairy NPs were significantly higher than the LCST of the C block, no benefit was observed from the rheological studies.

The results from the previous chapters provide methods to design and prepare injectable hybrid hydrogels with tunable hydrogel properties and possible new functions introduced through the use of NPs. The hybrid hydrogels could be more useful if the mesoporous silica nanoparticles (MSNs) were used since they are widely used as potential carriers for drug delivery due to their high surface areas and high drug loading capacity. Chapter 5 describes the preliminary synthesis of thermoresponsive polymer brush-grafted MSNs with a size of 30-40 nm from initiator-functionalized MSNs by using SI-ATRP. TEM, NMR, TGA and DLS studies confirmed the successful grafting of PDEGMMA on MSNs. However, the synthetic route needs to be optimized to solve the problem of the reduced surface area after the SI-ATRP, which is likely caused by the growth of polymer chains inside the pores of MSNs.

A possible research project for further investigation of hybrid hydrogels is the hybrid injectable hydrogels of thermosensitive triblock copolymers and thermoresponsive polymer-grafted MSNs. Aqueous solutions of thermosensitive triblock copolymers make the hydrogels injectable, and thermoresponsive hairy MSNs can be used as carriers for drug delivery because the mesopores can be closed and opened by changing temperature. By tuning the LCST of the triblock copolymers and hairy MSNs, the mechanical properties of the hybrid hydrogels can be increased as described in Chapter 4. In addition to the mechanical properties of hydrogels studied by rheological measurements, biomedical applications can also be explored, such as the controlled release and delivery studies as well as the biocompatibility studies. Besides hairy MSNs, some other hairy NPs with specific functions can also be used to prepare the hybrid hydrogels, such as magnetic nanoparticles or magnetic mesoporous nanoparticles.

6.1. References

1. Henn, D. M.; Wright, R. A. E.; Woodcock, J. W.; Hu, B.; Zhao, B. *Langmuir* **2014**, *30*, 2541-2550.
2. He, L.; Hu, B.; Henn, D. M.; Zhao, B. Submitted.
3. Tian, C.; Bao, C.; Binder, A.; Zhu, Z.; Hu, B.; Guo, Y.; Zhao, B.; Dai, S. *Chem. Commun.* **2013**, *49*, 8668-8670.
4. Li, J.; Shiraki, T.; Hu, B.; Wright, R. A. E.; Zhao, B.; Moore, J. S. *J. Am. Chem. Soc.* **2014**, *136*, 15925-15928.
5. Li, J.; Hu, B.; Yang, K.; Zhao, B.; Moore, J. S. *ACS Macro Lett.*, **2016**, *5*, 819-822.
6. Wright, R. A. E.; Hu, B.; Henn, D. M.; Zhao, B. *Soft Matter* **2015**, *11*, 6808-6820.
7. Hu, B.; Henn, D. M.; Wright, R. A. E.; Zhao, B. *Langmuir* **2014**, *30*, 11212-11224.
8. Hu, B.; Wright, R. A. E.; Jiang, S.; Henn, D. M.; Zhao, B. *Polymer* **2016**, *82*, 206-216.
9. Hu, B.; Fu, W.; Zhao, B. *Macromolecules* Accepted.

Vita

Bin Hu was born in Shanghai, China. He attended Fudan University from 2007 to 2011, where he received his B.S. degree in Macromolecular Materials and Engineering. After graduation, he enrolled as a graduate student in the Department of Chemistry at the University of Tennessee, Knoxville. He joined Professor Bin Zhao's research group in December, 2011, and worked on hybrid micellar network hydrogels of thermosensitive hydrophilic triblock copolymers and thermosensitive hairy nanoparticles. Bin Hu received a Doctor of Philosophy Degree in Chemistry from the University of Tennessee, Knoxville in August, 2016.